



UNIVERSIDADE D
COIMBRA

Cristiana Lages Pires

IMPROVING THE ACCURACY OF PERMEABILITY
DATA TO GAIN PREDICTIVE POWER:
ASSESSING SOURCES OF VARIABILITY IN ASSAYS
USING CELL MONOLAYERS

Tese no âmbito do Doutoramento em Química, ramo de Química Biológica, orientada pela Professora Doutora Maria João Pedrosa Ferreira Moreno Silvestre, coorientada pela Professora Doutora Ana Cristina Bairrada Fortuna e apresentada ao Departamento de Química da Faculdade de Ciências e Tecnologia da Universidade de Coimbra.

Abril de 2024

Faculdade de Ciências e Tecnologia
da Universidade de Coimbra

Improving the Accuracy of Permeability Data to Gain Predictive Power: Assessing Sources of Variability in Assays using Cell Monolayers

Cristiana Lages Pires

Doctoral thesis in Chemistry in the field of Biological Chemistry, supervised by Professor Doctor Maria João Pedrosa Ferreira Moreno Silvestre, co-supervised by Professor Doctor Ana Cristina Bairrada Fortuna and presented to the Department of Chemistry of the Faculty of Sciences and Technology of the University of Coimbra.

Abril de 2024



UNIVERSIDADE D
COIMBRA

The study presented in this dissertation was supported by Portuguese Foundation for Science and Technology (FCT) through the PhD Grant SFRH/BD/138873/2018. Other Portuguese, European and institutional funds, within the scope of several projects also contributed with financial support.



REPÚBLICA
PORTUGUESA

CIÊNCIA, TECNOLOGIA
E ENSINO SUPERIOR



COMPETE
2020

PORTUGAL
2020



Agradecimentos

Gostaria de expressar a minha profunda gratidão ao conjunto de pessoas que me acompanharam ao longo deste estudo:

Em especial, quero dedicar palavras de sincero apreço à minha orientadora, a Professora Maria João Moreno, por ser uma fonte constante de apoio e motivação ao longo deste percurso. Admiro imensamente o seu entusiasmo incansável pela investigação científica, a sua conduta profissional e a sua capacidade inesgotável de gerar novas e cativantes ideias para solucionar os mais diversos desafios. Não posso deixar de expressar um caloroso agradecimento por todas as discussões valiosas que compartilhámos ao longo destes anos, em relação à tese e para além disso. A sua dedicação e orientação foram fundamentais para o meu crescimento pessoal e profissional.

Foi uma honra e um privilégio ter tido a oportunidade de contar com a coorientação e apoio da Professora Ana Fortuna. Tenho a agradecer pela sua colaboração científica, conselhos e incentivos.

Gostaria de expressar o meu sincero agradecimento à Zaida Almeida, com quem tive o privilégio de partilhar este percurso. Foi gratificante ter alguém que não só nos desafia, mas também nos incentiva a ambicionar por objetivos superiores. Quero estender os meus agradecimentos à equipa incrível do laboratório de Química Biológica, aos colegas e ex-colegas com quem tive a oportunidade de trabalhar e partilhar momentos de lazer: Patrícia Martins, Filipe Gomes, Hugo Filipe, Daniela Vaz, Pedro Cruz, Inês Silva, Margarida, Cristiana, Andreia, Nícia, Alexandre. Também gostaria de agradecer aos co-autores das publicações e a todos com quem tive o privilégio de colaborar: Catarina Almeida, Ana Lúcia Carvalho, Joana Bicker, Susana Rosa.

Guardo os meus mais profundos e calorosos agradecimentos para a minha família e amigos. Aos meus pais e irmã, não há palavras para expressar o quanto sou sinceramente grata por todo o amor e apoio que sempre me proporcionaram ao longo da vida. Aos meus sogros, agradeço do fundo do coração pelo acolhimento, carinho e apoio. Finalmente, sou infinitamente grata ao meu companheiro David, obrigada por trazeres tanta felicidade e amor para a minha vida.

Table of contents

Abbreviations	ix
Abstract	xi
Resumo	xiii
Chapter I. General introduction	1
I.1 – The impact of ADME profiling in the drug discovery process.....	3
I.2 – The role of membrane permeability in ADME.....	4
I.3 – Mechanisms of drug’s permeation through biological membranes	6
(1) Passive diffusion.....	7
(2) Carrier-mediated transport.....	9
(3) Transcytosis	11
I.4 – The need to quantitatively predict the permeability of NCEs from its chemical structure.....	12
I.5 – Construction and performance evaluation of QSPRs models for permeability predictions	14
I.6 – QSPRs derived from <i>in vivo</i> permeability datasets.....	17
I.7 – QSPRs derived from <i>in vitro</i> permeability datasets.....	18
I.7.1 – Caco-2 monolayers	21
I.7.2 – How is the performance of QSPRs in predicting Caco-2 P_{app} values?	23
I.7.3 – How Caco-2 P_{app} data is selected and compiled to construct the QSPRs models	25
I.8 – Experimental variability of Caco-2 P_{app} values within-laboratory and between-laboratories	29
I.8.1 – Assessing the magnitude of variability within laboratories.....	30
I.8.2 – Assessing the magnitude of variability between laboratories	31
I.9 – Analysis of the sources of variability and their impact on P_{app} values ...	33
I.9.1 – Sources of variability related to cell culture.....	33
I.9.1.1 – Heterogeneity of the Caco-2 cells.....	36
I.9.1.1.1 – Cell source.....	36
I.9.1.2 – Variations in cell culture protocols	37

I.9.1.2.1 – Culture media composition.....	37
I.9.1.2.2 – Number of passages	39
I.9.1.2.3 – Seeding density	40
I.9.1.2.4 – Days post-seeding on inserts	41
I.9.1.2.5. – Characteristics of the membrane support	42
I.9.2 – Sources of variability related to the permeability experiments	44
I.9.2.1 – Composition of the transport media.....	46
I.9.2.1.2 – Addition of surfactants, amphiphilic polymers and co- solvents	48
I.9.2.1.3 – Addition of bovine serum albumin (BSA)	49
I.9.2.2 – Selection of the transport media pH value	53
I.9.2.3. – Unstirred water layer (UWL) and stirring conditions	54
I.10 – Strategies to reduce the variability of Caco-2 permeability data.....	55
I.10.1 – Standardization of cell culture and permeability assays protocols	55
I.10.2 – Normalization of P_{app} data to a reference compound.....	56
I.10.3 – Normalization of P_{app} data to a well-defined experimental condition.....	57
I.11 – Re-use of Caco-2 monolayers in permeability assays	58
I.12. – Use of an alternative cell line with faster implementation: MDCK monolayers.....	59
Chapter II. Aims of this thesis	63
II.1 – Aims	65
Chapter III. Materials and Methods	69
III.1 – Reagents and materials	71
III.2 – Cell culture and seeding	71
III.2.1 – Caco-2 cell line	72
III.2.2 – MDCK cell lines.....	72
III.3 – Structure and general properties of the tested compounds	73
III.3.1 – Preparation of test compound solutions.....	74
III.4 – Permeability assays	76
III.4.1 – TEER measurements.....	76
III.4.2 – Transport in Apical to Basolateral direction	77
III.4.3 – Transport in Basolateral to Apical direction	77

III.5 – Experimental procedure for the re-use of the Caco-2 monolayers in permeability assays.....	78
III.6 – Analytical methods for the quantification of the tested compounds...	78
III.7 – Data analysis.....	84
III.7.1 – Calculation of mass balance.....	84
III.7.2 – Calculation of P_{app}	84
III.8 – Confocal laser scanning microscopy and image analysis.....	85
III.9 – Flow cytometry analysis of P-gp expression	86
Chapter IV. Re-use of Caco-2 monolayers in permeability assays –	
Validation regarding cell monolayer integrity	89
IV.1 – Abstract	91
IV.2 – Introduction.....	91
IV.3 – Methods.....	94
IV.4 – Results and discussion	96
IV.4.1 – Effect of re-use on the cell monolayer integrity after single-time sampling permeability assays.	96
IV.4.2 – Effect of multiple sampling time points on the paracellular permeability through Caco-2 monolayers.....	101
IV.4.3 – Morphological features and integrity of the cell monolayer	104
IV.4.4. – Multivariate analysis	107
IV.5 – Conclusions	108
IV.6 – Supplementary material	110
IV.6.1 – Effect of a single-time point permeability assay (60 min) on the cell monolayer TEER values	110
IV.6.2 – Effect of single and multiple sampling on the cell monolayer TEER values	113
IV.6.3 – Effect of cell monolayer re-use on LY P_{app} for a single time point sampling (60 min).....	114
IV.6.4 – Effect of cell monolayer re-use and multiple time sampling on LY transport	115
IV.6.5 – Effect of the day post-seeding and re-use on morphological features and integrity of the cell monolayer	118
IV.6.6 – Effect of cell batch, passage number and day post-seeding on TEER and LY transport	120

IV.6.6.1 – Multivariate analysis.....	122
IV.6.7 – Quantitative analysis of the monolayer images obtained by confocal microscopy	124
Chapter V. Re-use of Caco-2 monolayers for a higher throughput assessment of compounds permeability – initial validation regarding cell properties	134
V.1 – Abstract.....	136
V.2 – Introduction	136
V.3 – Methods.....	139
V.4 – Results and discussion	141
V.4.1 – Effect of re-use on the passive permeation of reference compounds after single-time and multi-time sampling permeability assays.....	141
V.4.1.1 – Low passive permeability – Lucifer Yellow, Sodium fluorescein and atenolol	142
V.4.1.2 – High passive permeability – Propranolol and salicylic acid ...	144
V.4.2 – Effect of re-use on the permeability of a fluorescent glucose derivative (2-NBDG).....	145
V.4.3 – Effect of re-use on the permeability of rhodamine 123 and P-glycoprotein expression	148
V.4.4 –Additional validation studies and advantages of the re-use methodology	152
V.5 – Conclusions.....	153
V.6 – Supplementary material.....	133
V.6.1 – Effect of Caco-2 monolayer re-use on passive permeation	154
V.6.1.1 – Low permeation reference compounds – Lucifer yellow, Fluorescein and Atenolol.....	154
V.6.1.2 – High permeation reference compounds – Propranolol and salicylic acid.....	157
V.6.2 – Effect of Caco-2 monolayer re-use on transport of 2-NBDG	159
V.6.3 – Effect of Caco-2 monolayer re-use on transport of Rho.....	161
V.6.4 – Effect of Caco-2 monolayer re-use on P-gp expression	164
Chapter VI. Quantitative comparison of the distinct permeation pathways using MDCK-II, MDCK-MDR1 and Caco-2 monolayers	167
VI.1 – Abstract	169
VI.2 – Introduction.....	169

VI.3 – Methods.....	172
VI.4 – Results and discussion	174
VI.4.1 – Quantitative comparison of permeation pathways in MDCK monolayers.....	174
VI.4.1.1 – Characterization of paracellular permeability	174
VI.4.1.1.1 – TEER values.....	174
VI.4.1.1.2 – Morphological features and staining of tight junction protein ZO-1.....	175
VI.4.1.1.3 – Paracellular markers: Lucifer yellow, fluorescein and atenolol	177
VI.4.1.2 – Characterization of the transcellular permeability	180
VI.4.1.3 – Characterization of the active efflux by P-gp	181
VI.4.2 – Quantitative comparison of permeation pathways between Caco-2 and MDCK monolayers.....	186
VI.4.2.1 – Morphological features and tight junctions staining	186
VI.4.2.2 – Compounds with low passive permeability.....	187
VI.4.2.3 – Compounds with high passive permeability	189
VI.4.2.4 – P-gp mediated efflux.....	190
VI.5 – Conclusions	192
VI.6 – Supplementary material	195
VI.6.1 – Characterization of paracellular tightness	195
VI.6.2 – Characterization of transcellular permeability.....	196
Chapter VII. Towards reducing Papp variability: understand and evaluate the effects of distinct methodologies used in permeability assays across cell monolayers	199
VII.1 – Abstract.....	201
VII.2 – Introduction	201
VII.3 – Methods	205
VII.4 – Results and discussion.....	208
VII.4.1 – Assessment of LY permeability simultaneously with test compounds.....	208
VII.4.1.1 – Assays with reference compounds	209
VII.4.1.2 – Assays with mixtures of compounds having unknown effects on cell monolayer integrity.....	210

VII.4.1.3 – Use of LY P_{app} values to reduce variability arising from changes in cell monolayer integrity	213
VII.4.2 – Effect of the sampling method.....	214
VII.4.2.1 – Slow passive permeation- Lucifer yellow.....	214
VII.4.2.2 – Fast passive permeation - Propranolol.....	216
VII.4.3 – Effect of BSA on the observed permeability	218
VII.4.3.1 – Effect of correcting of P_{app} value for unbound fraction of NBD-Cn to BSA: calculation of the P_{app}^{Unb} value.....	219
VII.5 – Conclusions	221
VII.6 – Supplementary material.....	224
Chapter VIII. General conclusions	229
References	237
Indexes	237
Index of figures	269
Index of figures in Supplementary Material.....	269
Index of tables	273
Index of tables in Supplementary Material.....	269

Abbreviations

A→B	Apical to basolateral transport direction
ADME	Absorption, distribution, metabolism and excretion
AI	Artificial intelligence
ATCC	American Type Culture Collection
ATP	Adenosine triphosphate
B→A	Basolateral to apical transport direction
BBB	Blood-brain barrier
BSA	Bovine serum albumin
CACO	Human colonic adenocarcinoma cancer cells
CI ₉₅	Confidence interval at 95%
DHE	Dehydroergosterol
DKFZ	German Cancer Research Center
DMEM	Dulbecco's modified eagle's medium
DMSO	Dimethyl sulfoxide
ECACC	European Collection of Authenticated Cell Cultures
EDTA	Ethylenediamine tetraacetic acid
FBS	Fetal bovine serum
FITC	Fluorescein-isothiocyanate
Flu	Sodium fluorescein
GCA	Glycocholic acid
GLUT	Glucose transporters
GTX-5	Gonyautoxin-5
HBBS	Hanks' balanced salt solution
HEPES	4-2-hydroxyethyl-1-piperazineethanesulfonic acid
HPLC	High performance liquid chromatography
HTS	High-throughput screening
LogD	Octanol-water distribution coefficient
LogP	Octanol-water partition coefficient
LY	Lucifer yellow
MDCK	Madin-Darby Canine Kidney

MDR	Multi-drug resistance
MFI	Median fluorescence intensity
MVA	Multivariate analysis
MW	Molecular weight
NBD-Cn	7-nitrobenz-2-oxa-1,3-diazol-4-yl -labeled alkyl chain
NBDG	[N-(7-nitrobenz-2-oxa-1,3-diazol-4-yl) amino]-2-deoxy-D-glucose
P_{app}	Apparent permeability coefficient
P_{app}^{AE}	Apparent permeability coefficient through passive pathway
P_{app}^{PP}	Apparent permeability coefficient through active efflux pathway
P_{app}^{Unb}	Apparent permeability coefficient corrected for unbound fraction
PBS	Phosphate-buffered saline solution
PC	Polycarbonate
PE	Polystyrene
PEPT	Peptide transporter
PET	Polyethylene terephthalate
P-gp	P-glycoprotein
PK	Pharmacokinetics
POPC	Phosphatidylcholine
PROP	Propranolol
Q_A	Amount of compound reaching the acceptor compartment
QSPR	Quantitative structure-property relationships
r^2	Coefficient of determination
Rho	Rhodamine 123
RMSE	Root-mean-squared error
SA	Salicylic acid
SD	Standard deviation
SLS	Sodium lauryl sulfate
TEER	Transepithelial electrical resistance
UWL	Unstirred water layer
ZO	Zonula occludens

Abstract

The ability to predict the rate of permeation of new chemical entities across biological membranes is of high importance for their success as drugs, as it determines their potential efficacy, pharmacokinetics and safety profile. *In vitro* permeability assays, particularly using the Caco-2 cell line, are commonly used to predict the permeability of compounds across the intestinal epithelium and oral absorption in humans. There is an extensive amount of P_{app} values generated from these assays available in literature and a significant fraction is collected in databases. The compilation of these P_{app} values for large datasets allows the application of artificial intelligence tools for establishing quantitative structure-permeability relationships (QSPRs) to predict the permeability of compounds from their structural properties. One of the main challenges that hinders the development of accurate predictions is the existence of multiple P_{app} values for the same compound, caused by differences in the experimental protocols employed. The present work aims to contribute to increase the throughput of this important assay and to decrease the variability in P_{app} data, the later by quantitatively characterizing the effect on P_{app} values for common experimental alterations in the protocols.

The reference protocol involves seeding Caco-2 cells on permeable membranes for at least 21 days to establish a cohesive monolayer of differentiated cells, which is used in a single permeability assay between days 21 and 30. In this work, a methodology was developed to allow the re-use of Caco-2 monolayers in at least two additional permeability assays, and implemented for assays on days 22, 25 and 28. The proposed re-use protocol was validated regarding i) maintenance of cohesion and integrity of the cell monolayer (using TEER measurements, permeability assays with paracellular markers and microscopic visualization of morphology and tight junctions staining after labeling with fluorescent antibodies), ii) passive permeation through the transcellular route (using permeability assays of several reference compounds). Preliminary results were obtained indicating that active transport through glucose transporters and the efflux protein P-glycoprotein is also maintained.

In addition, studies were pursued to critically assess the use of the faster-growing epithelial MDCK cells as a potential replacement for Caco-2 cells. Monolayers derived from MDCK-II, MDCK-MDR1 (overexpressing P-gp), and

Caco-2 cells were systematically compared regarding morphology, tightness and permeation of several model drugs. The goal of this quantitative comparison was to evaluate the possible extension of the amount of P_{app} data available for QSPR studies by including data from MDCK monolayers. As expected, MDCK-MDR1 showed a higher efflux activity. The results obtained also revealed significant differences in cell and tight-junction density, which could justify the differences observed on the paracellular permeability.

Finally, studies were conducted to evaluate the impact on P_{app} values of passive permeating compounds for some variable procedures commonly followed in permeation assays. First, the evaluation of Lucifer yellow permeability alongside with test compounds was validated as a quality control measure of cell monolayer integrity. This approach contributes to decrease the variability associated with monolayer integrity, particularly relevant when evaluating compound or mixtures with unknown effects on cell properties. Second, the use of transfer and replacement as sampling methods in multi-time assays showed to affect the measured P_{app} values. Insufficient homogenization of the acceptor solution in replacement assays emerged as a major cause of variability in P_{app} data. Third, the impact of including BSA in the transport media was assessed for a homologous series of amphiphiles with known interactions with BSA and lipid membranes. It was shown that the P_{app} values are affected to an extent that may revert the ranking order of the amphiphiles permeability. This may however be corrected by considering the unbound fraction of the amphiphile. This allows calculating the P_{app}^{Unb} which captures the permeability ranking order expected for the amphiphiles. It is mandatory that this correction is performed when compiling P_{app} values obtained in the presence of BSA, to reduce variability and improve data consistency, allowing the establishment of realistic QSPRs with predictive ability.

Keywords: Permeability assays, drug bioavailability, Caco-2 monolayers, high-throughput, re-use, MDCK monolayers, experimental variability

Resumo

A capacidade de prever a velocidade de permeação de novas entidades químicas através das membranas biológicas é de grande importância para o seu sucesso como fármacos, uma vez que esta determina a sua eficácia, farmacocinética e segurança. Os ensaios de permeabilidade *in vitro*, em particular os que usam monocamadas da linha celular Caco-2, são usualmente utilizados para prever a absorção por via oral em humanos. Existe disponível na literatura uma grande quantidade de valores de permeabilidade (P_{app}) através de monocamada de Caco-2, estando uma fração significativa reunida em bases de dados. A compilação do P_{app} para grandes conjuntos de compostos permite a aplicação de ferramentas de inteligência artificial para estabelecer relações quantitativas de estrutura-permeabilidade (QSPRs) com o objetivo de prever a permeabilidade de novos compostos a partir das suas propriedades estruturais. Um dos principais desafios que dificulta a construção de previsões precisas é a existência de múltiplos valores de P_{app} para o mesmo composto, causada por diferenças nos protocolos experimentais utilizados. O presente trabalho tem como objetivo contribuir para o aumento do rendimento deste importante ensaio e para a diminuição da variabilidade nos dados de P_{app} , este último objetivo através da caracterização quantitativa do efeito de algumas das alterações experimentais mais comuns.

O protocolo de referência requer o cultivo das células Caco-2 sobre membranas permeáveis durante pelo menos 21 dias para estabelecer uma monocamada coesa de células diferenciadas, que é usada num único ensaio de permeabilidade entre os dias 21 e 30. Neste trabalho, foi desenvolvida e uma metodologia para permitir a reutilização das monocamadas Caco-2 em pelo menos mais dois ensaios de permeabilidade, tendo sido implementada para ensaios aos dias 22, 25 e 28. O protocolo de re-utilização proposto foi validado relativamente i) à manutenção da coesão e integridade da monocamada de células (usando medições de TEER, ensaios de permeabilidade com marcadores da via paracelular e visualização microscópica da morfologia e abundância das junções apertadas após marcação com anticorpos fluorescentes), ii) à permeação passiva através da via transcelular (usando ensaios de permeabilidade para vários compostos de referência). Foram obtidos resultados preliminares que

indicam que a permeação ativa através dos transportadores de glucose e da proteína de efluxo glicoproteína-P é também mantida.

Foram também realizados estudos para avaliar criticamente o uso da linha celular epitelial de crescimento rápido, MDCK como um potencial substituto das células Caco-2. Monocamadas derivadas de células MDCK-II, MDCK-MDR1 (que sobre-expressam P-gp) e Caco-2 foram comparados sistematicamente em relação à sua morfologia, coesão e permeação de vários fármacos modelo. O objetivo desta comparação quantitativa foi avaliar a possível extensão da quantidade de dados de P_{app} disponíveis para estudos QSPR ao incluir os dados das monocamadas de MDCK. Como esperado, a MDCK-MDR1 mostrou uma atividade de efluxo maior. Os resultados obtidos também revelaram diferenças significativas na densidade celular e das junções apertadas.

Finalmente, foram realizados estudos para avaliar o impacto nos valores de P_{app} de compostos que permeiam passivamente para alguns dos procedimentos variáveis que são comumente usados em ensaios de permeabilidade. Primeiramente, a avaliação da permeabilidade da Lucifer Yellow em conjunto com os compostos de teste foi validada como uma medida de controlo de qualidade da integridade da monocamada celular. Esta abordagem contribuiu para diminuir a variabilidade associada à integridade da monocamada, com particular relevância quando se avaliam compostos ou misturas de compostos com efeitos desconhecidos sobre as propriedades celulares. Foi também avaliado o impacto do método de amostragem (transferência ou reposição) nos valores de P_{app} medidos em ensaios com amostragem a vários tempos. A homogeneização insuficiente da solução aceitante nos ensaios de reposição executados na direção apical-basolateral emergiu como a principal causa da variabilidade nos dados de P_{app} . Por fim, o impacto da inclusão de BSA no meio de transporte foi avaliado para uma série homóloga de anfifilas em que as interações com a BSA e com membranas lipídicas são bem conhecidas. Foi demonstrado que os valores de P_{app} são afetados a ponto de poderem reverter a ordem de classificação da permeabilidade das anfifilas. No entanto, isto pode ser corrigido ao considerar a fração não ligada da anfifila à BSA. Este método permite calcular o valor da P_{app}^{Unb} , que captura a ordem de classificação de permeabilidade esperada para as anfifilas. É obrigatório que esta correção seja realizada ao compilar os valores de

P_{app} obtidos na presença de BSA, de modo a reduzir a variabilidade e a melhorar a consistência dos dados, permitindo o estabelecimento de QSPRs realistas com capacidade preditiva.

Palavras-chave: Ensaios de permeabilidade, biodisponibilidade de fármacos, monocamadas Caco-2, alto rendimento, reutilização, monocamadas MDCK, variabilidade experimental

Chapter I

General introduction

I.1 – The impact of ADME profiling in the drug discovery process

The research for new drugs is a scientifically changing mission, owing to the numerous properties that need to be simultaneously optimized to arrive at a safe and efficacious drug. The assessment of absorption, distribution, metabolism, and excretion (ADME) properties that determine the pharmacokinetics (PK) profile of molecules is a necessary part of these optimization processes. The reason for this is because molecules can only produce a desired *in vivo* therapeutic effect if they are able to reach the target site from the point at which they are administered to the patient. This ability is governed by physicochemical characteristics of molecules and their relationships with several ADME processes. In addition to the importance of PK profiles, the toxicity of molecules is also crucial during the processes of optimizing their properties. Prior assessment of safety attributes ensures that an appropriate concentration of the molecule can circulate in the body over the length of time to achieve the desired effect with minimal adverse effects. Thus, besides activity and selectivity to the molecular target, the drug candidates must also possess good ADME and safety properties to ensure a sufficient and safe drug concentration at the site of action [1].

The implementation of ADME and toxicity profiling of new chemical entities in parallel with the pharmacological activity is now well-established in the early stages of the drug discovery processes. [2]. Testing new molecules for their potency against the therapeutic target is easier and faster compared to evaluating their ADME properties, which involves multiple assays. Thus, the traditional approach to drug development placed a strong focus on potency and the properties of ADME were not intensively considered until the molecules were on the brink of a costly clinical trial phase. However, this approach was not being very effective, as optimizing for affinity often resulted in chemical classes where further ADME improvement were not possible. Consequently, this has led to a remarkable proportion of drugs that failed reaching the market. In 1990, around 40% of all drug failures were due to the lack of appropriated PK properties of compounds entering in clinical development phases. As a response to the recognition of this issue and because failing in late-stage clinical phases causes significant economic losses, investments across the pharmaceutical companies were made to address ADME profiling in early steps of the drug discovery phase.

General introduction

This has driven the development of a variety of medium to high-throughput *in vitro* models, that make the ADME screening of NCEs more accessible [3,4].

The overall goal of early ADME studies is to evaluate the potential of the NCEs to display desirable properties. In that regard, those identified with ADME liabilities could be rejected or redesigned to modify specific chemical functionalities for appropriate optimization. This avoid those drug candidates with lower chances of success from going to more expensive and time-consuming development phases. In fact, it has been proven that the effort to incorporate early ADME profiling has succeed in reducing the percentage of drugs not entering in clinical phases due to PK issues, that lowered to about 10 % in 2000 [3].

In recent years, the major causes of drug failures in clinical trials have shifted toward the lack of efficacy and uncontrolled toxicity. Both issues are related in part to PK profiles. An analysis conducted over a 7-year period from 2013 to 2015 revealed that attrition in central nervous system (CNS) drug research was consistently high, with only 14-17% of drugs receiving market approval. Reducing high attrition rates in clinical trials is still a challenge for the pharmaceutical industry [5].

When determining the ADME profiles of molecules, it is important to account that there are several factors that contribute to their ADME behaviour. These factors include permeability across membranes, but also other parameters such as binding to plasma protein, binding to metabolic enzymes and elimination. The work developed for this dissertation focuses only on membrane permeation. This aspect will be the central point of the following sections.

I.2 – The role of membrane permeability in ADME

The compartmentalization of biological content and functions is an essential feature of biological systems. These complex systems have developed multiple levels of compartmentalization. The plasma membrane delimits each cell and defines the boundary between its external environment. The organelles of eukaryotic cells where different functions are organized in different compartments are delimited by biomembranes. In complex multicellular organisms there are other levels of compartmentalization, namely the epithelium, delimiting the living being from its exterior, and the endothelium, delimiting the different tissues and organs. Biomembranes are the structures

responsible for delineating the distinct compartments, as a single membrane in the case of delimiting cells and intracellular organelles, and as a monolayer of cells in the case of endothelia and epithelia.

Drugs are administered by different routes: oral, intravenous, transdermal, intramuscular, inhalation, sublingual and topical. With very few exceptions, drugs must permeate biological membranes before reaching their site of action. Oral route is usually the most preferred way to administer drugs because of its high levels of patient acceptance and long-term compliance. For a successful oral therapy, after the intake, a drug must reach the bloodstream, from where it can be distributed to the tissues and reach its site of action for the desired therapeutic effect. The extent to which an administered dose reaches unchanged to the systemic circulation is defined as its oral bioavailability. This PK property is mathematically defined by Equation I.1:

$$F = F_a \cdot F_g \cdot F_h \quad \text{I.1}$$

where F is the oral bioavailability, F_a is the fraction of the dose that is absorbed, F_g and F_h are the fraction of the dose that escapes as a result of metabolism by the gut and/or liver, respectively [6]. The primary barrier towards good bioavailability of drugs is absorption. The process of absorption occurs mostly at the gastrointestinal tract and requires transport through the membrane of enterocytes in the intestinal epithelium. The rate of absorption of a drug can be expressed applying the Fick's first law, Equation I.2:

$$J = P_{eff} \cdot C \cdot SA \quad \text{I.2}$$

where J is the mass transport across the barrier *per* unit time and surface area (mass/cm²/s), P_{eff} is the effective permeability coefficient (cm/s), ΔC is the concentration gradient at both sides of the barrier, which depends on the amount of drug solubilized in the intestinal luminal fluid (mass/cm³) and SA is the intestinal surface area available for transport (cm²) [6]. This equation highlights the drugs' physicochemical properties that influence the most its oral absorption, namely their aqueous solubility and permeability.

Along with being a pre-requisite for good oral absorption, the permeability is crucial for the distribution of the drug towards the pharmaceutical target organs (e.g., tumors, central nervous system) and cells. Also, the route for drug

General introduction

excretion that includes elimination and reabsorption involves crossing multiple tissue and cells layers at the liver and kidney, respectively. Hence, the permeability of a drug shapes its ADME behavior in the body by affecting not only its absorption but also its distribution, and excretion [7].

Accordingly, the evaluation of the permeability of NCEs through biological membranes is fundamental in ADME profiling during drug discovery.

I.3 – Mechanisms of drug's permeation through biological membranes

Biological membranes form the thin (~5 nm) boundaries of cell and internal organelles by separating the aqueous compartments. The basic structure of the membranes is a two-dimensional bilayer of phospholipid molecules that self-assemble with their hydrophilic heads oriented towards the outer surfaces of the bilayer in contact with the water, and the inside being composed of the hydrophobic chains. Proteins are also present in biomembranes, inserted into or adsorbed to this lipid matrix, as well as cholesterol and carbohydrates (glycoproteins and glycolipids). Different cell membranes throughout the body contain a distinct composition of lipids and proteins that confer them distinct structural, metabolic and functional properties. Despite these differences, they all serve as highly selective permeability barriers controlling which molecules enter and leave [8]. The biological barriers that are more important in drug ADME are the epithelial and endothelial cell monolayers lining the intestinal tract and blood capillaries, respectively.

Drugs permeate across a cell monolayer by several mechanisms, as shown in Figure I.1. These pathways are distinct, and the molecular properties of the drug that influence its transport by these routes are also different and will be discussed herein [7,9,10].

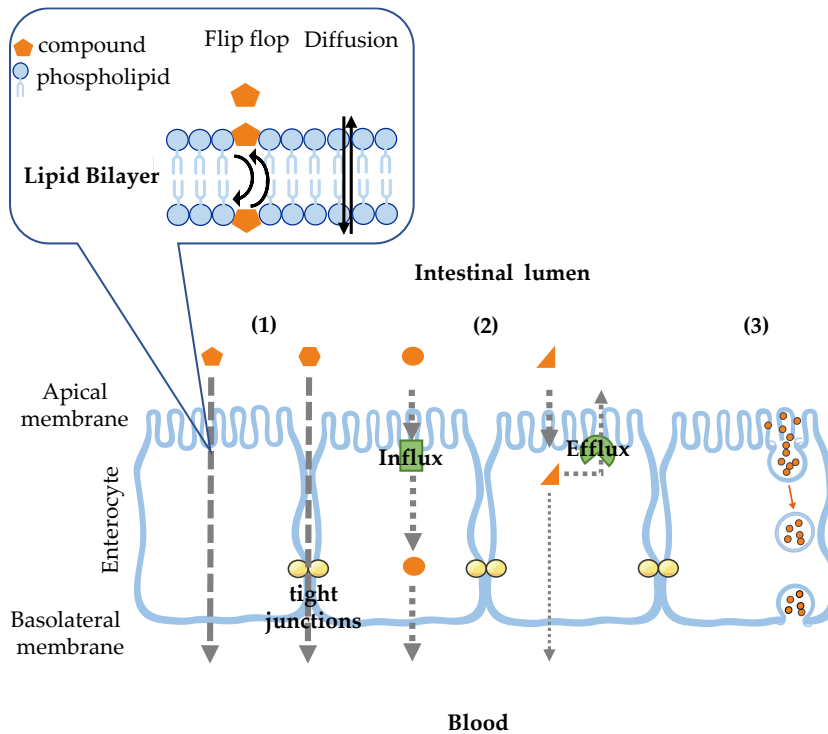


Figure I. 1 Mechanisms of drugs permeation through a cell monolayer, exemplified for the case of the intestinal epithelium. (1) Passive diffusion occurs through the cell's membrane (inset) or via the paracellular pathway between adjacent cells; (2) Carrier-mediated transport occurs for molecules that are recognized by transport proteins at the membrane. Depending on the direction of the transport, it may enhance (identified as Influx) or reduce (identified as Efflux) the cellular uptake of molecules; (3) Transcytosis occurs when large volumes of the aqueous medium outside the cell monolayer are moved through the cell inside of vesicles. This figure was produced in Microsoft PowerPoint using Servier Medical Art templates licensed under a Creative Commons Attribution 3.0 Unported License (<https://smart.servier.com>).

(1) Passive diffusion

This mechanism defines the movement of molecules in response to their concentration gradient between the water regions on both sides of the barrier. This transport may occur by two pathways - either the solute moves through the cell (transcellular transport) or passes through the spaces between adjacent cells (paracellular transport).

To cross cell membranes, the molecule partitions into the outer lipid leaflet of the bilayer and depending on the molecule structural features it diffuses or

General introduction

translocate (flip-flop) from the outer to the inner lipid leaflet. From there, the molecule equilibrates with the aqueous media inside the cell, thus permeating the cell cytoplasmic membrane [11]. In the case of permeation through cell monolayers, the molecule has to permeate through both the apical and the basolateral side of the cell monolayer. This may be done via the cell cytoplasm (fully permeating both membrane sides), or may occur by lateral diffusion in the cytoplasmic membrane to reach the other side without partitioning into the cytoplasm. In the case of tight cell monolayers, the outer leaflet of the cytoplasmic membrane of adjacent cells is connected by tight junctions that hinders the diffusion of membrane material between the apical and basolateral sides. Molecules may nevertheless equilibrate between both membrane sides by lateral diffusion in the membrane inner leaflet where the barrier imposed by the tight junctions is much less effective [12].

Lipophilicity is a property that reflects the affinity for the whole membranes. These supramolecular aggregates are, however, very heterogeneous, with a polar membrane/water interface and a highly hydrophobic center. While polar molecules may associate efficiently with the polar membrane interface, the solubility of the molecule in the non-polar center is the major determinant of permeation through lipid membranes. Therefore, molecules with a lower polarity are expected to show a higher permeability [13]. In practice, lipophilicity is usually characterized by the logarithm of the partition coefficient of a molecule between a lipidic phase (e.g., octanol) and an aqueous phase, defined as LogP for the partition of the neutral form of the molecule, or by the distribution coefficient of all species of the molecule that exist at a certain pH (LogD).

In current models for membrane permeation, it is assumed that the permeating molecule diffuses through the non-polar center of the lipid bilayer. In this respect, because larger solutes (with higher molecular weights, MW) have lower diffusion coefficients they are expected to permeate slower through the membranes.

In the case of molecules with ionizable groups, changes in their ionization state will also influence the rate of permeation, as uncharged species are usually more permeable. The charge state of a molecule depends on the environment pH value (at the aqueous medium and membrane surface) and on the pK_a values of their ionizable groups (acid/base character).

The passive diffusion is also responsible for the passage of solutes with tendency to follow the water extracellular route. This is most relevant in the case of solutes with high hydrophilicity and low MW (e.g., <200 Da for intestine) [7]. The membranes of adjacent cells are continuously connected by lateral strands of membrane proteins called tight junctions (zonula occludens and claudins). They form narrow pores filled with water that restricts the transport of molecules on the basis of their size. Additionally, this paracellular space presents a negative electrostatic potential due to the negatively charged residues of tight junction proteins, which favor the transport of cations [14].

The permeation through the paracellular route is usually less efficient than through transcellular routes because of the much lower surface area of the paracellular space compared to the membrane surface area. In the case of the intestinal epithelia, the paracellular space represents only 0.01 to 0.1% of the total surface area [9]. This is even smaller in the case of tight endothelia such as the Blood-brain barrier (BBB), and is significantly larger for fenestrated and/or sinusoidal endothelia such as those found in the liver [7].

(2) Carrier-mediated transport

This mechanism defines the translocation of molecules across membranes using specialized proteins embedded in the lipid bilayer for which the molecules are ligands. The transport starts with the binding of the molecule to the carrier site that is facing one side of the membrane. The carrier undergoes a conformational change, which lead to the exposure of the substrate-binding site to the opposite side of the membrane. Finally, the molecule dissociates from the transporter and is released. The carrier proteins can be localized in the apical and basolateral side of the cell monolayer leading to transport through the cell monolayer, or be located only in one of the sides leading to transport into the cell (influx) or out of the cell (efflux).

The uptake or influx transport is responsible for enhancing the permeation of compounds that are too polar to permeate via passive transcellular diffusion (polar nutrients e.g., amino acids, glucose, and some drugs). Such transport process is denominated as active if it requires energy consumption, directly or indirectly by adenosine triphosphate (ATP) hydrolysis. In this case, the transport

General introduction

may be done against a concentration gradient. When is not energy driven, it is defined as a facilitated diffusion transport. In addition to its direction down a concentration gradient, transport through this pathway is generally regulated by other factors. For example, transporters that facilitate glucose transport in mammalian cells are regulated by insulin and other hormones, whose signaling promotes glucose uptake into cells [15].

In contrast to the carrier-mediated uptake, efflux proteins actively pump out molecules from the inside to the outside of cells, thus reducing their concentration in the cells and consequently their effective transcellular flux. The most studied and well-known efflux transporters belong to the ATP binding cassette (ABC) family, which includes the P-glycoprotein (P-gp) encoded by the Multi-drug Resistance (MDR1) gene. The apical surface of capillary endothelial cells in the brain is among the human endothelial cells with the highest expression of P-gp. It was also found that P-gp is significantly expressed in the apical membrane of epithelial cells with secretory/excretory functions, such as colon, jejunum, kidney, liver and pancreas [16]. Thus, the localization and function of P-gp may suggest that these transporter acts to keep harmful xenobiotics out of the body by facilitating their excretion and thereby preventing the accumulation of such substances in critical organs such as the brain [17]. P-gp exhibits a very broad substrate specificity, interacting with molecules with a wide range of structural properties. Hydrophobicity is known to play an important role in the interaction of molecules with the P-gp binding site, with moderate to high lipophilicity being required. This suggests that P-gp binding site is preferentially accessed by ligands associated with the lipid bilayer [18,19]. A striking observation is that ligands with moderate lipophilicity are substrates of P-gp, while very lipophilic molecules usually behave as P-gp inhibitors [20-22]. This behavior may be interpreted as competition by the lipid membrane and P-gp for ligand binding, and the higher polarity of P-gp's binding pocket when compared with the lipid bilayer. Additionally, amphiphilic ligands with a high global lipophilicity may bind simultaneously to the lipid membrane and P-gp, hindering the conformational transitions required for P-gp's transport activity [23].

Unlike passive transport, the carrier-mediated process is saturable. This occurs when the carrier protein is faced with a high ligand concentration such that the total ligand molecules exceed the number of binding sites available for

transport. Consequently, the transport rate of the carrier will be maximal. Other differences of these mechanism are the stereospecificity (e.g., L-glucose and D-glucose) and the existence of competition, since molecules with similar structures can compete for the binding site (e.g., D-glucose and D-galactose).

(3) Transcytosis

This mechanism defines the cellular internalization and trafficking process of a molecule associated with membrane vesicles. The overall process involves the formation of endocytic vesicles on one side of the cell monolayer, vesicle transport through the cell, and their exocytosis on the opposite side. In endocytosis, the cell membrane folds onto itself to engulf portions of the extracellular fluids into intracellular membrane vesicles. The fate of the vesicles depends on their properties and on the endocytotic mechanism, fusing with lysosomes for the digestion of molecules present in the engulfed extracellular fluid, with the cell endoplasmic reticulum, or being transported through the cell towards the other side [24-27]. The later leads to transcytosis, with the final step being the fusion of the vesicle with the target membrane and the release of the cargo on the other side of cell by exocytosis. This is a significant route for the uptake of large macromolecules, such as proteins and peptides (> 1kDa) that are too large for passive diffusion or carried-mediated transport. Transcytosis is an energy requiring transport. The step of endocytosis may be driven by two pathways: non-specific adsorption to the membrane surface (adsorptive-mediated); or specific interaction with membrane proteins (receptor-mediated). Large plasma proteins, such as albumin are poorly transported through membranes, but cationization can increase their uptake by adsorptive-mediated endocytosis [28]. Among the common macromolecules that cells internalized by receptor-mediated transcytosis are transferrin [29] and low-density lipoproteins [30].

It is generally accepted that passive diffusion is the major route of membrane permeation for low molecular weight drugs. However, there is ample evidence that both the transcellular diffusion and carrier mediated are relevant for permeation [7,10,31]. The extent of contributions from each process to the transport depends on the properties of the drugs and biological membranes. For

General introduction

example, the transport of a drug by active efflux will not lead to a significant decrease in drug's net transport if passive permeation occurs faster than active efflux [31]. Also, due to the saturation behavior of carrier-mediated transport systems, the relative contribution of passive and active transport will depend on drug's concentration.

Drugs based on nucleic acids, as well as proteins and peptides, are emerging as future therapeutics for the treatment of several diseases, such as cancer and Parkinson [32,33]. For the delivery of these macromolecular drugs into cells, transcytosis is the most relevant route. Growing research has been undertaken to explore the use of endogenous receptors (e.g. transferrin) as targets to enhance the delivery of these therapeutics [34].

Within the scope of the work developed for this dissertation, in the following sections only the case of small molecules (<~1kDa) will be considered.

I.4 – The need to quantitatively predict the permeability of NCEs from its chemical structure

The constant demand for more effective drugs by the pharmaceutical market has resulted in an exponential increase in the number of NCEs generated at the early stage of drug discovery. The use of combinatorial chemical synthesis and high-throughput screening (HTS) technologies is having some impact on this, since once a promising molecule has been identified, larger series of molecules can be designed and synthesized. However, this scaling up in the order of thousands of NCEs have also increased the amount of experimental permeability *in vitro* and *in vivo* tests that need to be performed. Besides multiplying the costs involved, the many design-synthesize-test cycles can significantly slow down the discovery process. This has raised the need to create tools capable of screen virtually the permeability properties of NCEs even before being synthesized [35,36]. At this stage, computational tools (*in silico*) are the only option to get this information. To be able to generate such predictive models, it is necessary to know what are the rules that govern the permeation behavior of the molecules. It is the chemical structure of a molecule that determines its physicochemical properties such as lipophilicity, which in turn directly affect its ADME profile in the body. Hence, the most relevant molecular

properties to be used to predict permeability are those that can be readily determined based on the chemical structure.

The first effort to identify relevant molecular structural features, also known as molecular descriptors, and correlate them to oral bioavailability was pioneered by Lipinski and coworkers in 1970 [37]. In doing so, the authors created a model based on simple rules related with easily calculated molecular descriptors, well-known as Lipinski's rule of 5. According to those rules, poor absorption and permeability are more likely to occur when molecules fulfill two or more of the following criteria: MW > 500 Da; water-octanol partition coefficient (LogP) > 5, number of hydrogen bond donors (sum of O-Hs and N-Hs) > 5, and number of hydrogen bond acceptors (sum of N and O atoms) > 10. Those simple rules have been very useful in the screening of libraries of compounds. It should, however, be noted that they are a qualitative predictor of whether oral absorption is good or bad. Furthermore, there are exceptions to these rules. Several molecules with structural features outside the limits of rule parameters are absorbed after oral administration (e.g. several antibiotics) [31].

Alongside with the continuous increase of computing power and growth of experimental data for many compounds, *in silico* modelling has evolved into more robust approaches aimed at quantitatively predicting the permeability. Several mathematical rules denominated quantitative structure-property relationships (QSPRs) were attempted to relate the molecular structure of compounds with their properties [38]. The attractiveness of this strategy is undisputable. The property's values of new compounds could be predicted, even those not synthesized or experimentally measured.

But what are the expectations of a QSPR model applied in early discovery? This *in silico* tool will facilitate the drug discovery process in two ways. First, at the design stage of NCEs and compound libraries. Having the ability to predict the effect of a given structural modification on permeability, these *in silico* models can be used to guide the rational design of molecules with improved properties from the beginning of the process. Also, smaller and more focused combinatorial libraries can be created to contain subsets of molecules with desirable properties and structural diversity. Second, to optimize the screening and testing of NCEs. By filtering the molecules, the QSPRs models can lead to a rational selection of the most promising compounds for synthesis and enables the prioritization of the molecules that are tested both *in vitro* and *in vivo* [36].

General introduction

QSPRs models are not the only approach to predict ADME properties using *in silico* tools. Today, great emphasis has been placed on the application of more complex methods that use artificial intelligence (AI) techniques, namely machine learning to generate predictive models of properties through the use of molecular descriptors. These AI-based models analyzed large volumes of data to identify patterns and relationships in the data [39]. As for their performance, the models can predict the property impressively. However, the interpretation of the structural characteristics of the molecules that determine the property is not yet possible using these models. This makes them a kind of “black box” and makes their use difficult to optimize molecules with undesirable properties [40,41]. Furthermore, predictions from AI-based models are generally qualitative, either a molecule is predicted to pass through the barrier or not [42].

I.5 – Construction and performance evaluation of QSPRs models for permeability predictions

In an ideal application of a QSPR model, the users submit a structure of a new molecule as input and the software automatically calculates a numerical value for its permeability as output. The main challenge in the construction of QSPRs is to find an optimal quantitative relationship that link one or more molecular descriptors encoding information on the molecular structures to their permeability by employing a mathematical function (F) (Equation 3) [43,44]:

$$\text{permeability} = F(\text{molecular descriptors}) \quad \text{I.3}$$

Hence, the building of a model requires having both quantitative structural descriptors that are mostly calculated computationally (or experimentally in some cases), and quantitative permeability data, which must always be experimentally obtained. Then, the mathematical model fitted from the dataset is applied to predict the permeability of new compounds [45].

The permeability dataset of compounds used in QSPRs modeling are generally divided into a training set and a test set. The training set is used to develop the model. Afterwards, an external test set is used to validate the model before its use on predictions for new compounds. The performance accuracy of the QSPR model on the test set is crucial for assessing its ability of prediction for

external compounds. The model fitting performance is evaluated through comparison of the experimental and model prediction permeability values and is properly described in terms of regression-based statistic measures. Some of the metrics commonly used are the root-mean-squared error (RMSE) and coefficient of determination (r^2) calculated on training and test set according to Equations I.4 and I.5, respectively [45-47]:

$$\text{RMSE} = \sqrt{\frac{\sum_{i=1}^n (\hat{y}_i - y_i)^2}{n}} \quad \text{I.4}$$

$$R^2 = 1 - \frac{\sum_{i=1}^n (\hat{y}_i - y_i)^2}{\sum_{i=1}^n (\bar{y}_i - y_i)^2} \quad \text{I.5}$$

where \hat{y}_i is the predicted permeability value for the i th test compound; y_i is the observed value; \bar{y}_i is the average and n the total number of compounds in the set. The RMSE measures the error associated with the model's predictions. Larger RMSE values reflect a lower ability of the model to accurately predict the permeability. The R^2 measures the deviation between the observed values and the best fit values. R^2 values ranges from 0 to 1 and the closer the R^2 values are to unity, the better is the model predictions.

The accuracy of the model prediction is strongly dependent on the quality of the dataset used in the training and validation steps [38]. Thus, the process of selection of only high quality experimental data is a first key step for developing more robust QSPRs models. The quality of a dataset is assessed by at least three factors: diversity, size, and accuracy [48].

The structural diversity of a dataset is often analyzed within the concept of chemical space. Chemical space describes the set of all possible molecular structures and is estimated to contain more than 10^{60} molecules below 500 Da. Even the set of all organic compounds ever synthesized number up to 10^8 [49]. The concept of chemical space also refers to the property spaces in which these molecules are placed. In such spaces, the dimensions are defined by molecular descriptors and each molecule is assigned at the coordinates corresponding to the numerical values of its descriptors. The distance between two molecules measures their similarity. Thus, the diversity of the data can be assessed by the way molecules are distributed in this property space (e.g. Tanimoto similarity

General introduction

index) [49]. In practice, this leads to the existence of homogenous and diverse compounds sets. It is generally accepted that QSPRs models can only make reliable predictions for molecules contained in a very similar chemical space to those of the training set, defined as its applicability domain [50-52]. Because of that, the applicability of QSPRs developed on homogeneous datasets is limited to a particular subset of the structural space. The construction of models with heterogeneous datasets might find wider applicability in the prediction of more structurally diverse molecules. However, high diversity datasets imply a broad coverage of the chemical space, and for that larger data sizes are required.

The incorporation of large datasets in QSPRs modeling is also important to avoid overfitting. When the input training set is too small, it does not give sufficient information for the model generalization to new data, and the model is incapable of make predictions for molecules that are different from the training set [52]. Additionally, large quantities of data are necessary to ensure that after developing the model, a sufficient large number of new data is still available to be used for external validation [51].

The datasets used for QSPRs modeling are generated by experimental researchers and available in public databases and literature works. The collection of accurate and consistent permeability values is essential to obtain reliable datasets. Such data should have low experimental errors, and ideally should be measured under the same or identical experimental conditions, especially when compiled from a variety of sources [48]. Most of the quantitative experimental permeability measurements are obtained from *in vivo* and *in vitro* assays.

In addition to the availability of quality datasets, the accuracy of QSPRs models also depends on the property being modeled. Specifically, it is important to consider whether a QSPR concerns the prediction of a property that depends on just one process or whether it is the result of multiple processes. It is reasonable to expect that an accurate QSPR can be constructed for the prediction of the partitioning of small molecules into membranes. This will only depend on two processes, which are the interactions established between the molecule and the two media, aqueous medium and membrane. In relation to permeability across membranes, the possibility of arriving at a precise QSPR, capable of predicting it, may be more difficult. This arises because permeability can occur according to several mechanisms each with several steps which depend

differently on the distinct molecular descriptors. For instance, an increase in LogP is expected to contribute to an increase in permeability if the step of translocation through the membrane non-polar center is the rate limiting step, but contributes negatively if the rate limiting step is desorption from the membrane into the aqueous medium [12]. When considering the prediction of drug absorption after oral administration, it is even more challenging and less likely to arrive at simple but accurate QSPR models. This is because drug absorption is a process that involves several steps, including drug solubility, stability, and permeation through several biological barriers.

Many QSPRs have been developed and published over the last decades, based on either *in vivo* or *in vitro* data. Some examples will be described in the next section.

I.6 – QSPRs derived from *in vivo* permeability datasets

In vivo methods provide the most reliable measurements for assessing compound's permeability. Nevertheless, *in vivo* data based relationships are difficult to establish owing to the many steps and processes involved and the complexity of the biological mechanisms. Particularly, permeability through the intestinal barrier may occur by several mechanisms, including passive, facilitated and active mechanisms. Additionally, the collection of *in vivo* data is experimentally demanding and expensive and thus is limited to only a small number of compounds. The dataset is also usually biased towards compounds that show the expected properties. As a consequence of their limited size and poor representativity, the datasets publicly available generate difficulties in the training and validation of reliable models [53].

QSPRs models developed from *in vivo* datasets of human intestinal absorption [54] and oral bioavailability [55] can be found in literature. Klopman et al. [54] developed a model using experimental human intestinal absorption values obtained for a diverse set of 417 drugs. A correlation with a R^2 of 0.79 was achieved between the calculated and experimental values for the external dataset (n=50). The number of H-bond donors was found to be the most relevant molecular descriptor, showing a negative correlation with human intestinal absorption. Surprisingly, LogP was not statistically relevant as a descriptor and was not included in the model. An important factor to be accounted in this work,

General introduction

is the fact that the dataset used for modeling, although large, was significantly biased towards high absorption values. This was due to the existence of little experimental data in literature of drugs with low intestinal absorption.

In another work, Turner et al. [55] used oral bioavailability data of 159 structurally diverse drugs to develop a QSPR. A correlation value of 0.72 was achieved when the model was applied to the test set (n=10). Among the relevant descriptors are LogP, polar surface area, both with a negative contribution, and also H-bonding capacity with a positive contribution in the QSPR model. For compounds with low oral bioavailability, the values predicted by the model were not so accurate. These compounds would either be poorly absorbed or metabolized prior to reach the systemic circulation. Enzymatic metabolism is a complex and diverse range of processes, therefore compounds with low bioavailability in this study may not have been well predicted due to this additional complexity.

It is important to note that the two studies reached contradictory conclusions regarding the relevance of the descriptor LogP. This reflects the diversity and the limited size of the dataset considered, as well as the enormous complexity of the *in vivo* systems. To achieve better prediction ability, it is important to use larger datasets and simpler systems such as *in vitro* permeability assays.

I.7 – QSPRs derived from *in vitro* permeability datasets

In vitro models mimicking the biomembranes barrier properties have been introduced to predict *in vivo* permeation of compounds. They provide a higher throughput and cheaper alternative to the *in vivo* human experiments and particularly they offer benefits in terms of ethical considerations.

There are a high variety of experimental *in vitro* assays which measure the permeability of compounds through artificial lipid membranes and cell monolayers. The use of cell monolayers as models for the biological barriers has the advantage of capturing much of the complexity of the *in vivo* membrane permeation processes, rather than account for only the interaction of the molecule with the lipid bilayer. This complexity reflects the high similarity in cell morphology and the barrier to be model, the expression of tight junctions and various membrane transport systems as well as metabolic enzymes [56].

Cell-based models are mainly composed of immortalized cells with an intrinsic ability to grow into confluent monolayers and initiate spontaneous differentiation when seeded onto permeable membranes, such is the case of Transwell™ inserts. This apparatus consists of a polymer membrane of $\approx 10 \mu\text{m}$ in thickness that contains a high density of pores [57]. The inserts are fitted into the wells of a culture plate, dividing the system into two compartments: the apical side (insert) and the basolateral side (well), simulating respectively the intestinal lumen and blood circulation in the case of cell monolayers representative of the intestinal epithelium, as schematically represented in Figure I.2-A. The microporous membrane allows the exchange of culture medium components and small molecules while prevents the migration of cells between the two compartments. Furthermore, the configuration of such inserts is practical to perform assays to measure the permeation of compounds across the cell monolayer. The transport can be measured in two directions: from the apical to the basolateral compartment and from the basolateral to the apical compartment (Figure I.2-B). The test compound dissolved in transport medium is added to one of the sides of the cell monolayer (donor compartment) and after incubation for various time intervals, aliquots of the solution in the opposite side are taken (receiver compartment). The amount of compound in both sides is usually quantified by liquid chromatography (Figure I.2-C). Measuring the rate of transport ($\Delta Q^A/\Delta t$, mol/time) of a compound across a defined surface area of the barrier (A , cm^2) allows the calculation of an apparent permeability coefficient (P_{app} , cm/s), taking into account the amount of compound initially in the donor compartment (Q_0^D , mol), and the volume of this compartment (V^D , cm^3), Equation I.6 [58]:

$$P_{app} = \frac{\frac{\Delta Q^A}{\Delta t} V^D}{A Q_0^D} \quad \text{I.6}$$

General introduction

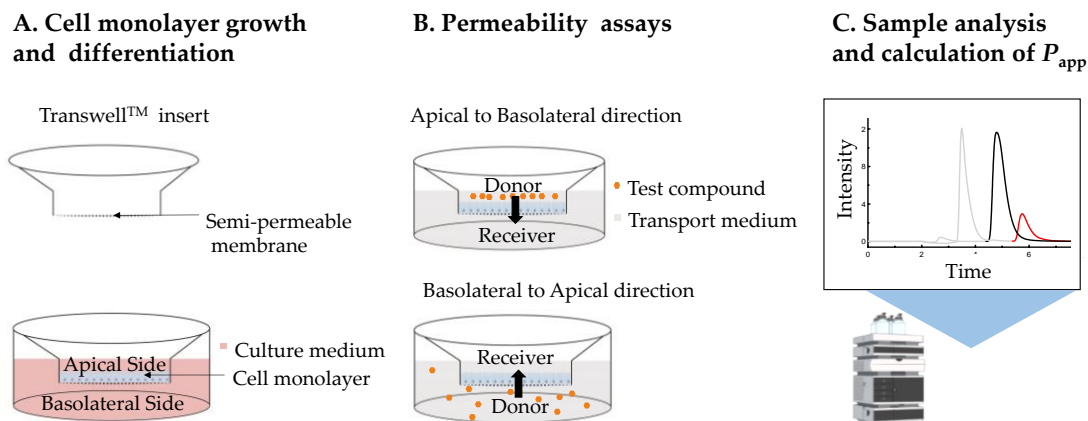


Figure I. 2 Schematic representation of the experimental procedure for the use of cell monolayers to assess the permeability of compounds, consisting of three major steps: cell culture, permeability assay, and data analysis. (A) The cell culture step consists of seeding the cells on microporous membranes and allow them to divide to form a confluent and differentiated monolayer. (B) In the permeability assay, the flow of the test compound through the monolayer is evaluated, which may be done in the apical-to-basolateral or basolateral-to-apical directions. (C) Lastly, the data analysis step includes quantifying the amount of compound in the samples collected from the assay and the calculation of the corresponding *in vitro* P_{app} . This figure was produced using Microsoft PowerPoint.

The unidirectional assays only inform about the overall permeability. Conversely, the assessment of transport in both directions can help to identify if some form of active carrier-mediated transport is involved in permeation (efflux or influx). If there is a significant difference between the P_{app} values in both directions, this suggest that the compound may be a transporter substrate. Additional incubation assays with known inhibitors may then be carried out to assess the contribution of a specific transporter [59].

Several cell lines from different tissues or species have been established as tools to predict the membrane permeability properties of compounds. The most well-characterized and validated cell-based model is the culture of monolayers of Caco-2 cells. The popularity of this model comes out from its good compromise between relevance and simplicity, and is widely used across the pharmaceutical industry and academia [60,61]. For this reason, a large number of P_{app} values for different molecules have been obtained using this model that in principle could be used to derive QSPRs.

I.7.1 – Caco-2 monolayers

The Caco-2 cell line was first isolated from a colorectal carcinoma of a 72-year-old male in 1977. From the beginning of the studies on this cell line, the Caco-2 cells showed a spontaneous differentiation pathway when cultured for long-term[62]. Despite its colonic epithelial origin, the cells demonstrated a closer morphological and functional resemblance to the small intestine enterocytes [63,64]. Caco-2 cells display undifferentiated characteristics at the early 3 or 4 days of culture. However, after 20-30 days of post-confluence, the Caco-2 cells form a monolayer of columnar and polarized cells with brush border microvilli in the apical side, villi, formation of domes and tight intercellular junctions [65,66].

The tight junction's formation and integrity is a critical parameter when evaluating the cell monolayer barrier properties, as it allows discriminating between a well-differentiated and tight barrier and a roughly associated barrier. The measurement of the transepithelial electrical resistance (TEER) is a direct measure of the resistance to ion flux through the paracellular pathway. This is a simple technique that provides information in real time about the ionic conductance of the paracellular route and, indirectly, reflects the integrity of the cell monolayer. A voltage-measuring electrode pair is placed in each compartment of the insert. The resistance measured is then corrected for blank filter resistance (cell free filter), multiplied by the filter surface area, and expressed in $\Omega\cdot\text{cm}^2$ [67]. Typically, the Caco-2 monolayers exhibit high TEER values ($250\text{--}2500 \Omega\cdot\text{cm}^2$) [68]. In this respect, the monolayers reflect more closely their colonic origin than the small intestine (TEER of human jejunum: $34 \pm 12 \Omega\cdot\text{cm}^2$ [69] and human colon: $120 \pm 43 \Omega\cdot\text{cm}^2$ [69] and $119 \pm 9 \Omega\cdot\text{cm}^2$ [70]; TEER of mouse jejunum: $40\text{--}70 \Omega\cdot\text{cm}^2$ [71] and rat colon: $111 \pm 5 \Omega\cdot\text{cm}^2$ [70]). It is also relevant to note that low TEER values do not necessarily reflect the formation of non-confluent cell monolayers, as the high ion conductivity may reflect active and/or facilitated ion transport through the cell membranes [72].

A more reliable method to access tight junction's integrity is through the evaluation of the permeability of hydrophilic molecules that are known to permeate mainly through the paracellular route. Examples of hydrophilic markers used include sodium fluorescein (376 Da), lucifer yellow (444 Da), fluorescein-isothiocyanate (FITC)-labeled dextran (MW 4000) as well as

General introduction

radiolabeled mannitol (180 Da). Low P_{app} values for these specific markers is an indication of the presence and integrity of tight junctions in the cell monolayer. The obtained P_{app} values for these markers of paracellular permeability across Caco-2 monolayers were reported to be in the order of 10^{-7} cm/s [73,74].

Caco-2 monolayers also expressed a variety of transporters that are present in various epithelial and endothelial barriers of the body. Intestinal transport systems for the uptake of peptides, amino acids, sugars and monocarboxylic acids have been identified in these cells. With regard to efflux transporters, the most important is P-gp, which was found to be significantly expressed in the apical membrane of these cell monolayers [59,75,76].

Caco-2 monolayers were used for the first time to model human intestinal absorption by Hidalgo and co-workers in 1980s [63]. These scientists were pioneering on the optimization and characterization of Caco-2 monolayer in order to carry out drug permeability assays. In 1990, the potential use of these cells in predicting intestinal permeability was first demonstrated by the group of Artursson et al. [77]. The P_{app} values measured across Caco-2 monolayers correlated well with the permeability values across rat ileum for most of the drugs tested, except for the case of the very hydrophilic drug atenolol that showed a relatively slower permeation through the Caco-2 monolayer. At that time, this study was a turning point towards the phenomenal explosion of the use of Caco-2 permeability assays to evaluate drug absorption after oral administration.

From the early 1990s, several studies were published in which Caco-2 P_{app} data of compounds with different physicochemical properties were compared with the corresponding human absorption fraction. Good correlations between *in vitro* and *in vivo* values have been obtained, especially for those compounds that are transported by passive transcellular route [78-80]. Generally, a sigmoidal relationship is obtained between the logarithm of apparent permeability ($\text{Log}P_{app}$) and the extent of human intestinal absorption. Caco-2 model is able to categorize the compounds with i) complete absorption in humans when the P_{app} are $> 1 \times 10^{-6}$ cm/s; and ii) absorption $< 100\%$ when P_{app} are $< 1 \times 10^{-6}$ cm/s. Compounds with moderate absorption, $> 1\%$ but $< 100\%$, lead to P_{app} between 0.1×10^{-6} and 1.0×10^{-6} cm/s [58].

As a result of these favorable predictive properties, the Caco-2 permeability assay has become a standard *in vitro* tool to screen compounds for their intestinal permeability and oral absorption. It has been, by far, the most used cell model for predicting the permeability properties of compounds across biological barriers [60,61]. Caco-2 monolayers has also been investigated in comparative studies as a surrogate model for a preliminary prediction of BBB permeability [81,82].

A survey of the literature between the years of 2015 and 2020 shows the widespread use of this permeability assay, with 80% of the published studies on the evaluation of intestinal absorption using Caco-2 monolayers. During recent decades, permeability assays with Caco-2 monolayers have been also used to elucidate the transport mechanism of nanosystems designed for oral drug delivery [83]. In addition to its well-established application in pharmacology, this methodology has currently been extended to a broad range of scientific areas. Of particular relevance are the studies related to human nutrition, which account for over 30% of the publications. In these area, Caco-2 assays have been used to study the absorption mechanisms of bioactive compounds from natural plant extracts [84].

1.7.2 – How is the performance of QSPRs in predicting Caco-2 P_{app} values?

Although also presenting some complexity, *in vitro* cell-based systems are more focused on a single physicochemical process compared to *in vivo* models, which is membrane permeability. It is expected, therefore, that more predictive QSPRs can be developed using *in vitro* P_{app} datasets.

There are various examples of publications in the literature of QSPRs studies that aimed at the quantitative prediction of *in vitro* P_{app} values established with Caco-2 monolayers datasets. The first attempt to find a correlation function between P_{app} values measured across Caco-2 monolayers and simple molecular properties appeared in 1996. Waterbeemd et al. [85] used a dataset of 17 drugs that varied in their MW and lipophilicity. For this dataset, a good correlation was

General introduction

achieved ($R^2 = 0.89$) considering two molecular descriptors, where a positive correlation was obtained with MW, and a negative correlation with the H-bonding potential. Of particular relevance is the unexpected positive contribution of MW to the QSPR equation, which may reflect correlations between the MW and lipophilicity for the considered dataset. However, the permeability coefficient for the drugs in the dataset did not correlate with the MW descriptor alone ($R^2 = 0.16$), not even for a small homologous series of 5 beta-blockers drugs. One explanation for the lack of correlation may be the narrow MW range of analyzed drugs (138 - 398 Da for all drugs and 249 - 267 Da for beta-blockers drugs).

Over the last decades, several QSPRs models for Caco-2 permeability predictions have been published, applying more sophisticated and computationally demanding modeling techniques, a wider range of descriptor types and larger datasets. Table I.1 present some examples of developed QSPRs approaches during the last 10 years. The analysis of their performances reveals large uncertainties (RMSE) in predictions of P_{app} values of sets of molecules independent from the training set. Thus, some caution should be exercised when applying any of the models for quantitative predictions, as they can produce misleading information regarding the molecule's ability to permeate biological membrane barriers.

Although the more recently constructed QSPRs models have becoming more and more sophisticated and use larger and more heterogeneous databases, their predictive ability capacity has not been significantly improved relatively to the models previously published.

Table I. 1 Overview of some examples of in silico contributions to the quantitative prediction of P_{app} values across Caco-2 monolayers. The analyzed research studies were published between 2012 and 2022. The information regarding the dataset sizes, the range of P_{app} values of the compounds included in datasets and the relevant procedures related to their collection are indicated for each study. The predictive performance of the best model obtained in each study is reported for the test set and when applied for an external test set. The most relevant molecular descriptors found in each model are also summarized.

Prediction model		Data collection			Performance	Molecular descriptors
Author, year	Size of training set (tr) test set (t) external test set (ext-t)	Log P_{app} range	Available online and free	Data sources	Best model	Most important
Sherer et al. [86] 2012	tr: 15,791 t: 1536 ext-t: 313	[-7.5; -4.3]	no	In house ^a literature publications	R ² _t : 0.52 RMSE _t : 0.20 R ² _{ext-t} : 0.41 RMSE _{ext-t} : 0.91	LogD Polar surface area H-bond potential
Singh et al. [87] 2015	Tr: 508 t: 70 ext-t: 100	[-7.8; -3.4]	yes	> 250 literature publications	RMSE _{test} : 0.27 RMSE _{ext-t} : 0.24	Polar surface area LogP
Wang et al. [88] 2016	tr: 1017 t: 255	[-7.8; -3.5]	yes	2 public databases ^b 23 literature publications	R ² _{test} : 0.81 RMSE _{test} : 0.31 R ² _{ext-t} : 0.75 RMSE _{ext-t} : 0.36	H-bond donors Polar volume LogP
Wang and Chen [89] 2020	tr: 1458 t: 369	[-7.9; -3.7]	yes	1 public database ^c Literature publications of Wang et al. 2016	R ² _{test} : 0.76 RMSE _{test} : 0.39	H-bond potential

^a Proprietary P_{app} data was obtained across different cell lines in the pharmaceutical Merck databases. The majority of P_{app} data was from LLC-PK1 cell line, which is a renal epithelial cell line derived from porcine kidney cells. The external test set include only Caco-2 P_{app} values gathered from literature.

^b ChEMBL (<https://www.ebi.ac.uk/chembl>) and online chemical data set (<https://ochem.eu/>) public database

^c ChEMBL public database

1.7.3 – How Caco-2 P_{app} data is selected and compiled to construct the QSPRs models

The procedures related with the collection of P_{app} experimental data are crucial to ensure data quality for the development of more robust QSPRs models. Regarding the reported models in Table I.1, with the exception of the dataset used by Sherer et al. [86] that comprises a huge amount of in-house/proprietary data

General introduction

and some public data, in all the other studies the dataset was collected from public sources and is available online. The utilization of large public datasets implies that its collection had been made from more than one source. This way of compiling P_{app} data is particularly problematic because it introduces interlaboratory variability into the correlations derived from these datasets. This is due to the existence of variability in Caco-2 P_{app} values for the same compound when they are measured in different laboratories and sometimes even in the same laboratory. The variability factor is a recognized limitation of the Caco-2 permeability assays, and issues related with that have been addressed since 1990s [90-92]. Sherer et al. [86] performed a detailed analysis of the variation in P_{app} values for the same compound that was measured twice on separate dates. The authors obtained a $R^2 = 0.66$ for the two P_{app} datasets. In point of fact, the low accuracy of their QSPR model ($R^2 = 0.52$) is in agreement with the experimental uncertainty of the P_{app} values from which the model was obtained.

In the process of selecting the P_{app} dataset to construct the model, some authors have explained their criteria when they were confronted with different reported P_{app} values for the same molecule. Wang and Chen [89] described that when the P_{app} values were not significantly different, their arithmetic mean was considered as the final value to be included in the dataset. When they found large differences in the P_{app} values, the data for this molecule was eliminated from the final dataset.

The selection of particular P_{app} measurements from multiple studies will tend to minimize the variability and increase the accuracy of the QSPR approach. But it has also a drawback, which is the potential bias that can be introduced into the correlations obtained. If applied to compound datasets obtained using the same procedures, the correlations tend to work well. Limitations for these models are likely to arise, however, if the biased correlations are extended to compound datasets obtained by different procedures. This precludes the use of this data to develop QSPRs that may be reliably applied [93]. The alternative is using experimental P_{app} values that are consistent across different research groups and available to the public in a database that represents a physicochemical permeability space as large as possible.

The collection of quantitative P_{app} data for permeation across Caco-2 monolayers can be performed from internal databases of pharmaceutical companies or literature sources as well as from commercial and publicly accessible data compilations. Sherer et al. [86] developed a QSPR model using the most extensive dataset ever reported, including over 15,700 P_{app} values of compounds. Unfortunately, the permeability data belongs to a big pharmaceutical company and is not available to the scientific community, limiting its use for additional QSPRs studies. The literature is considered the primary source for collection of Caco-2 P_{app} values. Yet, building a large enough dataset to be used for *in silico* applications from literature sources requires a significant investment of time and effort. The amount of available data is sparsely published throughout a large number of journals articles, and it is usually demanding to manually search and extract information since each article needs to be considered on its own. For that reason, compilations and reviews of literature data already published are a much more convenient source of Caco-2 assay data, in particular that ones that were compiled by experts in the field and include primary reference for all data [94].

In an attempt to assist the construction of QSPRs by providing easy, free, and open access to the literature information, a variety of publicly available databases have been developed on the Web. The databases PerMM [95] (**Permeability of Molecules across Membranes**, 2019) and MolMeDB [96] (**Molecules on Membranes Database**, 2019) are the most recent efforts towards the compilation of experimental Caco-2 P_{app} data extracted from literature studies. The comparison between the two databases is present in Table I.2.

The PerMM (https://permm.phar.umich.edu/membrane_systems/9) database contains a set of 186 molecules with experimentally determined permeability coefficients for assays performed in Caco-2 monolayers. The molecules are divided into different chemical classes (organic acids, alkaloids, etc.) and groups with different ionization properties (neutral, bases, etc.). The permeability values were collected from a compilation of measurements published in a book chapter written by Alex Avdeef (2012) [97]. Published studies by this author investigating the membrane permeability of compounds are highly cited according to the platform Web of Science, and thus it is considered skilled in the field. Regarding the data compiled by Avdeef for the database, it

General introduction

was first collected from 55 literature studies performed in different laboratories. Then, the collected P_{app} permeability values were pre-treated to correct for all non-transcellular effects by removing the contributions of the aqueous boundary layer, filter and paracellular permeability. When the values of each permeability component could not be determined from the original works, it was necessary to calculate estimates for their values. Finally, the parameter reported for molecules in the database is the transcellular permeability coefficient ($\log P_c$) at pH 6.5 [95]. Note, that the use of this parameter and pH makes the comparison with other research experimental data much more difficult. Another disadvantage is that the values reported in the chapter book by the author are not directly linked to the primary literature reference. Instead, as exemplified for the drug propranolol, Avdeef provides nine literature references for the indicated permeability. Analyzing all the references cited, it is observed that only six include permeability assays across Caco-2 monolayers with the reported P_{app} values varying by almost two orders of magnitude, $\text{Log}P_{app}$ from -5.4 to -3.7 (Table I.2). The value considered in the database is -4.2, which is within the range of the reported values but does not correspond to any specific result nor to the average of all. In addition to the lack of information regarding the source of the data selected for inclusion in the database, the corresponding experimental conditions of the assay(s) and the corrections introduced are also not available. This significantly lowers the confidence in the dataset and limits its use to the specific conditions considered.

The MolMeDB (<https://docs.molmedb.upol.cz>) database contains 637 compounds with Caco-2 permeability values. The $\text{Log}P_{app}$ data was obtained from *in silico* methodologies or experimental assays. For some compounds, such as propranolol, only data from *in silico* studies is reported. For some others, the reported $\text{Log}P_{app}$ values includes experimental and *in silico* data and varies by several orders of magnitude (e.g., salicylic acid with values from -3.4 to -5.5, Table I.2). One positive point of this database is that all entries include the reference to the primary source of data. Also, the database can be easily downloaded to give access to the parameters in an organized manner. Although this simplifies the initial curation of data, a secondary curation is still necessary since the detailed description about the experimental conditions of the assays is not documented.

Another major problem of the two databases discussed above is their relatively small size.

For the mentioned reasons, the information available in these databases cannot be straightforwardly used for the development of better QSPRs models for Caco-2 monolayer permeation.

Table I. 2 Performance comparison of two online databases containing experimental data of drug permeability across Caco-2 monolayers: PerMM and MolMeDB. The databases are compared relative to the amount of data, the parameter chosen to report permeability, the sources from which the data were collected and the values reported for two reference drugs. The level of organization and interpretation of the databases are also evaluated.

Database	Number of compounds	Parameter	Data collection			Include primary reference	Organization level after download	Interpretation level
			Experimental work	<i>In silico</i> work	Values reported for Salicylic Acid			
PerMM [95] 2019	186	^a Log P_c	✓		-4.57	-4.20	medium	hard
			✓		-5.47			
			✓		-4.89			
			✓		-4.66			
MolMeDB [96] 2019	637	Log P_{app}	✓		-4.78			
			✓		-4.73	✓	good	easy
				✓	-4.66			
				✓	-4.23			
				✓	-3.39			

^a log P_c is the transcellular permeability at pH 6.5. It is extracted from Log P_{app} values obtained in the assays by removing the contributions of the aqueous boundary layer, support filter and paracellular permeability from the P_{app} term.

I.8 – Experimental variability of Caco-2 P_{app} values within-laboratory and between-laboratories

When aiming at quantitative prediction of Caco-2 permeability using QSPRs approaches, the variability associated with the P_{app} data is one of the most important issues to be addressed. The experimental variability occurring

General introduction

between laboratories, and even within the same laboratory, is conditioning the creation of large and consistent databases of P_{app} values to be used for *in silico* works. To help understand the impact of this variability on QSPRs modelling tasks, it is important to first address its dimension.

I.8.1 – Assessing the magnitude of variability within laboratories

In many cases, each laboratory sets up and follows its in-house experimental protocols to determine the P_{app} values of compounds across Caco-2 monolayers. The protocols are generally optimized and standardized within the laboratory, starting at the earliest cell culture procedures to the transport assays and data analysis.

To assess the extent of variability within laboratories, Egan et al [98] collected the mean and standard deviation (SD) of P_{app} values from a set of compounds assayed in five randomly selected permeability studies published in the literature [58,99-102]. The datasets included compounds with diverse physicochemical properties and permeating through distinct pathways. The coefficient of variation (%SD) was calculated for the replicate measurements of each compound in each publication. The mean of the coefficients of variation from the entire dataset in each study varied from 5.6 % to 28.3 % (left side, Table I.3). Although there are some differences in the internal variability in each laboratory, the coefficients of variation were small or moderate. A direct correlation between the number of replicates and the coefficients of variation may be observed, suggesting that in some of the studies the number of replicates may be insufficient.

The extent of the variability is evaluated individually for some reference compounds included in the datasets (right side, Table I.3). The P_{app} values of the hydrophilic marker mannitol showed variations of 20 to 30 % among assays performed in the same laboratory. A smaller internal variability is observed in all laboratories for propranolol (4 to 14 %), while for amoxicillin a larger variability was observed. These compounds were selected due to the distinct permeation pathways, with mannitol permeating paracellularly, propranolol permeating transcellularly by passive diffusion, while amoxicillin is a substrate of the PepT1 transporter. The distinct internal variability obtained for the three compounds suggests that the paracellular pathway and transporter expression

can be more sensitive to small variations within a given laboratory. Yazdanian et al. [100] carried out 102 permeability assays with mannitol over 22 months in its laboratory. The observation that the variability for P_{app} values of mannitol is among the highest, reinforces the concern that in some cases the small variability observed is due to an insufficient number of independent replicates.

Table I. 3 Magnitude of the variability in Caco-2 P_{app} values obtained in experiments carried out in the same laboratory. The five studies analyzed were selected from Egan et al. [98]. Coefficient of variation relative to the mean (%SD) for replicates of P_{app} values obtained within a given laboratory. The variability is shown for the entire dataset and for some selected reference compounds.

Study	All compounds			Mannitol		Propranolol		Amoxicillin	
	Number	Replicates per compound	%SD ^b	n	%SD	n	%SD	n	%SD
Irvine et al. [99]	55	6	28.3	6	33.3	6	11.8	6	47.6
Yazdanian et al. [100]	51	3-9 ^a	12.7	102	31.6	6	14.2		
Artursson et al. [58]	20	3	< 10						
Chong et al. [101]	10	3	10.3	3	20.0	3	6.8	3	25.0
Pade et al. [102]	9	3	5.6	12	20.0	3	4.0		

^a with exception of mannitol, that included 102 assays performed over 22 months

^b %SD = 100 × standard deviation/mean

I.8.2 – Assessing the magnitude of variability between laboratories

The variability in P_{app} values measured in different laboratories have been highlighted and discussed in several publications. Early in 1996, Artursson et al [90], showed that the results obtained for a set of reference compounds in four different laboratories, lead to four different sigmoidal relationships between Caco-2 P_{app} and the fraction absorbed in humans. The deviation obtained between the distinct laboratories reached 1.75 $\log P_{app}$ units, an interval larger than the width of the transition between poorly to fully absorbed drugs. This inter-laboratory variability has severe consequences in the classification of compounds according to their P_{app} values. More recently, Lee et al. [103] reported the quantitative differences found in the P_{app} values of 10 compounds determined in seven distinct laboratories, including that of the authors. The majority of compounds analyzed showed variations lower than 10-fold in the P_{app} values

General introduction

obtained across the independent laboratories. However, variations as high as 30-fold and 60-fold were found for two of the compounds in the set (propranolol and metoprolol, respectively).

The variability inter-laboratories is not limited to compounds that permeate through a specific transport route, in contrast to what was identified in the analysis within a given laboratory (Table I.3). This is highlighted in the scatter plot constructed from P_{app} values obtained in 7 distinct laboratories for three reference compounds permeating through distinct routes (Figure I.3).

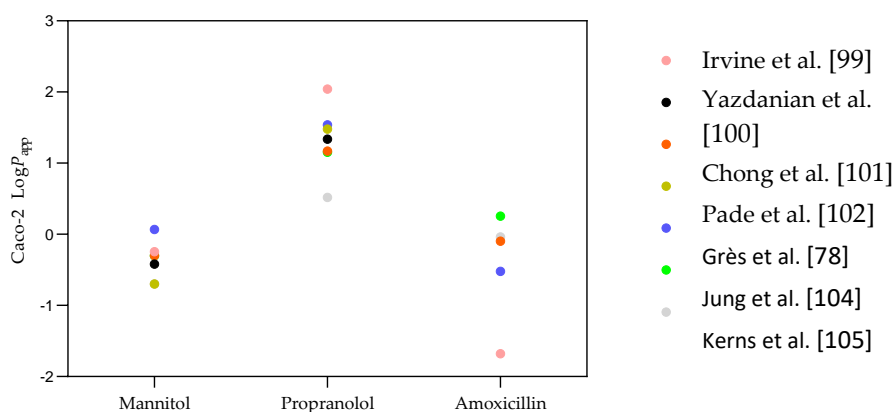


Figure I. 3 Variability in Caco-2 P_{app} values obtained in experiments carried out in 7 different laboratories. The plot includes values for mannitol (a marker for paracellular passive permeation), propranolol (a reference drug for transcellular passive permeation), and amoxicillin (mainly transported by PepT1). The P_{app} values were taken from the indicated references and plotted using GraphPad version 8.4.2. The analyzed studies include those presented in Table I.3 and other studies selected from references cited in [103,106].

Interestingly, a smaller variability was observed for the paracellular marker mannitol, in contrast with the larger variability observed within each laboratory. This may reflect the use of mannitol as an internal control for the selection of properly formed Caco-2 monolayers, with those monolayers showing P_{app} values outside the expected range being discarded. The $\text{Log } P_{app}$ values for mannitol ranged from -0.70 to 0.07, corresponding to a variation of 6-fold in P_{app} , while that of propranolol varied between 0.52 and 2.04, corresponding to a 30-fold variation in P_{app} . The largest inter-laboratory variability was observed for amoxicillin, with experimental values ranging from -1.68 to 0.26 (85-fold variation in P_{app}). These results show that a direct quantitative comparison of inter-laboratory P_{app} values is very difficult or even impossible. To narrow the

inter-laboratory variability and allow the quantitative analysis required for the establishment of QSPRs, the sources of variability must be identified and taken into account. This is discussed below, in section I.9.

I.9 – Analysis of the sources of variability and their impact on P_{app} values

The Caco-2 model has been the focus of several studies addressing the probable causes of variability for permeability data obtained within and between laboratories [75,92,107,108]. The factors encountered to explain the variability were mainly of two types: (i) heterogeneity of the Caco-2 cell line and (ii) variations in protocols followed for cell culture and permeability assays.

The most common sources of variability and their impact on permeability values are analyzed in greater depth in the following sections. To facilitate the analysis, the sources of variability for the two main phases of the Caco-2 assays, cell culture and the permeability experiments, are analyzed separately. For each aspect, the analysis is conducted in two steps. In the first stage, a global analysis of several protocols from the literature is carried out to identify the most relevant experimental factors that may contribute to variability. In the second stage, a detailed analysis is carried out for each of the experimental variables identified in the previous step regarding their variation in the protocols and their impact on P_{app} values.

I.9.1 – Sources of variability related to cell culture

To better identify the differences in the methodologies followed to grow Caco-2 monolayers, a literature survey of Caco-2 permeability studies published between 2015 and 2020 was carried out, yielding a total of 221 works. These works were thoroughly reviewed to extract the information on the experimental procedures followed during the culture of Caco-2 cells pre- and post-seeding on Transwells™. The outcome of this global analysis is summarized in Table I.4. Based on variations in experimental conditions between protocols, it is possible to identify the most relevant factors that could be potential causes of variability.

General introduction

Table I. 4 Analysis of the experimental factors related with cell culture that are potential causes of variability in Caco-2 permeability data, obtained from a survey of the literature published between 2015 and 2020 (221 papers) The distinct experimental variables identified and their frequency is shown, as well as some of the cell properties that may be affected.

Variability sources	Experimental variables		Effect on cell properties
Cell supplier	ATCC	48 %	selection of subclones [109,110]
	ECACC	10 %	
	China	10 %	
	NCSS	5 %	
	DSMZ	3 %	
	other cell banks or labs	7 %	
	not described or gift	17 %	
Passage number	Low (5-70)	44 %	proliferation rate and selection of subclones [111-114], morphology [112,113], differentiation [111,113], transporters [111,112], enzymatic activity [111,113,114]
	High (70-120)	3 %	
	not described	53 %	
Interval of passages	Without interval	11 %	proliferation rate, time to reach confluency, morphology, differentiation, expression of transporters [115]
	1-10	56 %	
	>10	33 %	
Seeding density (cells/cm ²)	(0.4-9) × 10 ⁴	30 %	proliferation rate, time to reach confluency, morphology, differentiation, expression of transporters [115]
	(0.1-1) × 10 ⁶	41 %	
	Not described	29 %	
Days post seeding	0-7	4%	morphology and differentiation [115], expression of transporters [115,116]
	7-20	17%	
	21-28	74%	
	Not described	5%	
Membrane diameter (mm)	24	13%	differentiation [117]
	12	41%	
	6.5	34%	
	4.3	2%	
	Not described	10%	

ATCC: American Type Culture Collection; ECACC: European Collection of Authenticated Cell Cultures - UK; NCSS: National Centre for Cell Science - India; DSMZ: German Collection of Microorganisms and Cell Cultures GmbH – Germany; China: include several cell banks and institutes.

To evaluate the impact of each variable on the measured permeability, the P_{app} values obtained under the distinct experimental conditions were compared. A quantitative analysis can only be done when systematic studies were performed where the variable under evaluation is the only change in the protocol. Whenever this information exists, this analysis was performed for compounds permeating through distinct pathways. The results obtained from this systematic analysis are collected in Table I.5. The effect of the variables

identified in Tables I.4 and I.5 are discussed in detail in the following sub-sections.

Table I. 5 Analysis of the impact of several sources of variability related with cell culture protocols (pre- and post-seeding in the Transwell™ inserts) on the P_{app} values across Caco-2 monolayers. For each variable evaluated, the permeability assays were carried out by the same research group and that experimental condition was the only change in the protocol.

Non-bold compounds permeate by passive diffusion, mostly transcellular. **Bold** compounds permeate through the paracellular pathway. **Bold italic** compounds are known substrates of transporters (peptide transporter PepT1 or P-gp).

The symbols - and + indicate the absence or presence of glutamine.

The numbers in bold indicate statistically significant differences with at least one of the conditions in the variable analyzed, from the statistical analysis performed in the respective reference.

Compound	Variability sources				Reference
P_{app} (10^{-6} cm/s) A →B					
Cell supplier					
	ATCC	DKFZ ^a			
Mannitol	5.23 ± 0.24	0.187 ± 0.007			Walter and Kissel [109]
Acetylsalicylic acid	20.6 ± 0.7	22.7 ± 1.3			
<i>Cephadrine</i>	1.36	1.45			Behrens et al. [110]
Culture media composition					
	5.5 mM Glucose	25 mM Glucose	- glutamine	+ 0.6mM glutamine	
	0.43 ± 0.05	0.71 ± 0.01			D'Souza et al. [118]
Mannitol			3.9	1.0	DeMarco et al. [119]
			- serum	+ 10% (v/v) serum	
			3.0	0.87 ± 0.16	Ranaldi et al. [120]
Hydrocortisone	20.4 ± 0.64	25.2 ± 0.25			D'Souza et al. [118]
<i>Digoxin</i>	0.99 ± 0.05	1.27 ± 0.05			
Passage number					
	Low (28-47)	High (93-112)			
Mannitol	3.4	2.2			Yu et al. [111]
	5	5			Lu et al. [112]
Hydrocortisone	40	50			
Progesterone	650	900			Yu et al. [111]
<i>Cephadrine</i>	9.49±0.47	2.05±0.01			
<i>Glycylsarcosine</i>	8	9			Lu et al. [112]
Seeding density (cells/cm²)					
	Low (1x10 ⁴)	Intermediate (6x10 ⁴)	High (1x10 ⁵)		
FITC-dextran (Mw 4000)	0.07	0.05	0.05		
<i>Cephadrine</i>	1.6	2.1	2.5	Behrens et al. [115]	
Day post-seeding					

General introduction

	7	14	21	28	
FITC-dextran (Mw 4000)	0.05	0.25	0.04	0.02	Behrens et al. [115]
<i>Cephradine</i>	1.1	1.3	2.03 ± 0.6	1.8	
<i>Cyclosporin</i> ^b	8	9	11	18	Hosoya et al. [116]
Membrane material and coating					
	PC	PE	PET	PC+Collagen	
FITC-dextran (Mw 4000)	0.03	0.022 ± 0.0066	0.012 ± 0.0038	0.05	Behrens et al. [115]
Mannitol	22.1 ± 0.09		7.44 ± 0.33		Walter and Kissel [109]
<i>Cephradine</i>	2.0	0.75	0.25	3.79 ± 1.48	Behrens et al. [115]
Membrane diameter (mm)					
	6.5 (24-well plate)	12 (12-well plate)	24 (6-well plate)		
Mannitol	1.4 ± 0.2	1.3 ± 0.1	0.90 ± 0.1		Markowska et al. [117]
Propranolol	38.9 ± 1.9	36.6 ± 0.9	24.2 ± 0.3		Markowska et al. [117]

^a DKFZ: German Cancer Research Center ^b P_{app} in B → A direction

1.9.1.1 – Heterogeneity of the Caco-2 cells

The Caco-2 cell line is itself a source of variability due to its heterogeneous and unstable nature. Their cultures are characterized by the presence of different subpopulations of cells. Those changes may occur in the differentiation phase of the cell monolayer [65] and even in the stationary phase of growth [107]. The inherent heterogeneity of the Caco-2 populations was identified as the source of variations in cultures regarding cell morphology [109,110,121], paracellular transport across cell monolayers [109,110], enzyme expression [109], and transporters expression and function [110,122].

1.9.1.1.1 – Cell source

The variability of the Caco-2 cell characteristics could be related to the cell line origin. Cell vials can be purchased from commercial suppliers (cells banks) or obtained from cultures developed in other laboratories. Cells from the ATCC supplier are the most commonly used (Table I.4).

For a comparative study, Walter and Kissel [109] have grown under identical culture conditions two different Caco-2 cell lines obtained from the American Type Cell Culture (ATCC) and the German Cancer Research Center (DKFZ). Dissimilarities between the cells from the two sources were found regarding

several parameters, namely in their morphology, density, enzymatic activity, and paracellular permeability. Heterogeneity was also observed within the cells from each supplier. Caco-2 monolayers obtained from cells acquired to ATCC displayed a more heterogenous morphology, exhibiting patches of cells with larger and smaller diameter. The P_{app} values of the paracellular marker mannitol varied by 28-fold between the two sources, whereas the P_{app} values of the highly permeable acetylsalicylic acid was similar. Additionally, a follow up study of Behrens et al. [110] revealed that ATCC cell monolayers were composed of subpopulations with high expression of the peptide transporter PepT1 and subpopulations with no expression. Contrarily, the transporter PepT1 was homogeneously distributed in monolayers prepared from cells acquired from DKFZ. In these cells, PepT1 expression levels were about two times higher than in monolayers prepared from ATCC cells.

I.9.1.2 – Variations in cell culture protocols

The heterogeneity of Caco-2 cells and the exposure to selection pressure promoted by the respective culture conditions can give rise to different cell subpopulations, in a phenomenon referred to as phenotypic drift. Therefore, the maintenance of defined and consistent culture conditions has an important role in establishing reproducible experiments with Caco-2 monolayers [75]. Unfortunately, many discrepancies in culturing protocols can be identified in the literature (Table I.4). The experimental factors that vary often among the protocols from distinct laboratories include the culture media composition, cell passage number, density at which cells are seeded on inserts, time for differentiation of the cell monolayer and the characteristics of the membrane supports.

I.9.1.2.1 – Culture media composition

The components included in the culture media can influence the phenotype and grow of Caco-2 cells, thus modulating their morphological and functional properties such as differentiation, permeability, and transporters activity.

General introduction

In the study of D'Souza et al. [118], Caco-2 monolayers were cultured in media containing physiological (5.5 mM) or high (25 mM) glucose concentrations. The authors reported that higher glucose concentrations significantly affected the cell's monolayers integrity and permeability. The cell monolayers obtained from cells cultured at 25 mM glucose showed higher P_{app} values for both mannitol (an increase of 65%) and hydrocortisone (an increase of 24%), which permeate by passive paracellular and transcellular diffusion respectively. This reflects a decrease in the cell monolayer tightness (also supported by a decrease in TEER), and a decrease in the barrier properties of the cells' membrane (also supported by an increase in the membrane fluidity has evaluated by fluorescence anisotropy). In the case of digoxin (a P-gp substrate), the P_{app} values increased by about 20% in both A-B and B-A directions, while the efflux ratio was not significantly affected, in agreement with a higher passive permeability and no effect on the activity of the efflux transporter. The activity of PepT1 on the transport of the peptide Gly-Sar was also shown to be influenced by the high concentration of glucose, with a decrease in the maximum transport capacity without alterations in the substrate affinity (Table I.5). Collectively, the results were interpreted in light of an increased oxidative stress at the higher glucose concentrations, which has been shown to influence the barrier properties of the cell membranes [123,124], the development of tight junctions [125,126], and the properties of some transporters [127].

DeMarco et al. [119] removed glutamine from the cells' monolayer culture media, which is known to be an essential nutrient for the maintenance of intestinal mucosal integrity, and the result was an increase of the P_{app} values of mannitol.

Ranaldi et al. [120] observed that the P_{app} values of mannitol were higher in Caco-2 cells cultured with serum-free medium as compared to serum-supplemented medium. The deprivation of serum components in the culture medium was found to affect the maturation of tight junctions during the differentiation period, leading to an increase of the paracellular permeability of cell monolayers growing under these conditions.

Behrens et al [115] showed that the supplementation of culture media with peptone, increased the expression of PepT1 by 1.5 to 2-fold leading to an increase in the transport of its substrate cephradine. Although this could be an expected result due to the induction of transporter expression when cells are cultured in

the presence of a transporter substrate, it is relevant to note that it was not observed with the supplementation with other PepT1 substrates such as penicillin or streptomycin.

I.9.1.2.2 – Number of passages

It is now well established that Caco-2 cell properties vary as the number of passages increase. The explanation for such effect has been ascribed to the heterogeneity of Caco-2 populations which have different rates of proliferation. The cells population thus become enriched in the subpopulations with faster grow which possess different characteristics [111].

Due to the propagation of the Caco-2 cell line across laboratories worldwide, the stocks of Caco-2 cells may differ by dozens and even hundreds in the number of passages. In the publications where this variable is reported, the cells have been used in permeability studies at passage numbers from 5 to 120 (Table I.4). Yu et al. [111] and Lu et al. [112] compared the properties of Caco-2 cells from early (28-36 and 35-47) and late passages (93-108 and 87-112). Briske-Anderson et al. [113] examined cells that were serially passaged 90 times from the 19 to 109 passage numbers. The three studies reported changes in morphology, proliferation, differentiation, and permeability of the cells at different passage numbers.

The most prominent difference regarding the cell's morphology was the detection of regions composed of multiple layers of cells in passage numbers above 87, while those at passages between 35 and 47 grew as monolayers [112]. However, the grow of multiple cell layers may be also due to other factors since the formation of cell monolayers at passages higher than 87 has been shown by several authors [128-130]. Furthermore, the cells proliferation rate before reaching confluency was found to be higher in cells with higher passage numbers [111-113]. An increase in the TEER values of cells at these higher passages was also observed by all the authors. At early stages of monolayers culture, the increment in TEER values was explained by the faster rate of growth and higher cell density of the cells at later passages. Nevertheless, after the confluence was reached, cells at higher passages still displayed higher values of TEER [111,112]. At this later stage of culture, the TEER is a reflection not only of the cell density but also the

General introduction

integrity of the developed tight junctions. In agreement with this, in the study by Yu et al. [111] the increment of TEER values was accompanied by a decrease in the paracellular diffusion of mannitol. However, this was not the case in the study by Lu et al. [112] where cell passage number increased TEER values but had no effect on mannitol permeability. [112] Conflicting evidence among studies has also been presented for the influence of cell passage number in carrier-mediated transport. The PepT1 activity was tested with the substrate glycylsarcosine, which P_{app} value remained unaltered in late and early passages [112]. Contrarily, the P_{app} value of the PepT1 substrate cephradine was found to diminish 5-fold in late passages in a study by Yu et al. [111] (Table I.5). These studies exemplify the high variability observed in the results from this assay, and point towards contributions from other factors.

Given the variation of the cell's characteristics with the passage number, the use of the same batches of cells is recommended to avoid the selection of sub-populations and thus reduce cell-to-cell variations. This means that cells with close passage numbers should be used for related experiments. Artursson et al. [128] recommend using a window of 10 passages, and cells at passage numbers from 95 to 105 where recommended to perform the permeability assays. The variety in the interval of passage numbers used in several literature studies can be seen in Table I.4.

I.9.1.2.3 – Seeding density

The initial density of cells seeded on the membrane support influences the time needed to reach cell confluence, which must be attained before cell differentiation can occur. Therefore, different seeding densities may result in variations in the differentiation stage, even though the monolayers have the same age in terms of number of days in culture [107]. The seeding densities reported on literature studies may differ by almost 3 orders of magnitude, ranging from 10^3 to values up 10^6 cells/cm² (Table I.4).

Behrens et al. [115] compared the properties of cell monolayers 21 days after being seeded at a low, intermediate, and high cell density. The lowest seeding density (1×10^4 cells/cm²) led to thinner cell monolayers which also presented alterations on the organization of tight junctions. Multiple cell layers were

observed only for the highest seeding density (1×10^5 cells/cm²). Nevertheless, the paracellular permeability remained unaltered between the distinct seeding densities as confirmed by the P_{app} values of FITC-Dextran. An identical result was obtained for the carrier-mediated transport of cephradine by PepT1 that was not affected by the seeding density, nor was the level of PepT1 expression. However, the expression levels of P-gp were significantly higher in the intermediated cell density (6×10^4 cells/cm²) (Table I.5). This was interpreted as a sign of decreased cell monolayer differentiation when using too high and too low cell densities.

I.9.1.2.4 – Days post-seeding on inserts

The number of days that Caco-2 cells are allowed to stay in the porous membrane support is a crucial parameter in cell differentiation. Already from the early studies, it has become clear that at least 21 days after seeding are required to obtain a confluent and differentiated cell monolayer for use in transport assays [63,65,77]. In fact, this is the most common procedure, that is followed in 74% of studies reported in the literature. Nevertheless, in a significant number of publications (21%) the permeability assays were performed with cell monolayers at less than 21 days after seeding (Table I.4).

The time of cell culture in the inserts was shown to influence their morphology, differentiation, tightness, and expression of transporters [115,116].

Behrens et al [115] analyzed the cell monolayers properties after 7, 14, 21 and 28 days post seeding at a density of 6×10^4 cells/cm². Through the visualization of actin filaments and nucleus by confocal microscopy, the authors found significant changes in cell morphology and cytoskeleton maturation (actin staining). During the first two weeks (days 7 and 14), the monolayers were not fully differentiated as demonstrated by a thin and flat monolayer with weak actin staining and many small nuclei, indicating that a large number of cells are in the process of division. On the third week (day 21), they found columnar shaped cells with well-established brush border. The paracellular permeability was evaluated with FITC-dextran MW 4000, being low at day 7, increasing at day 14, and continuously decreased for longer periods reaching the lowest value at day 28. The expression levels of PepT1 transporter continuously increased from day 7 reaching a maximum between the day 21 and 28. Accordingly, the transport of its substrate, cephradine also increased with cell monolayer age. In this work it

General introduction

was also shown that P-gp expression levels reached a peak at day 21 and then declined at day 28. The effect of day post-seeding on P-gp expression was also evaluated by Hosoya et al. [116]. In contrast with the previous study, it is shown that P-gp expression is significant along the entire culture period of 27 days, with a maximum at day 27. However, the P_{app} values of the P-gp substrate cyclosporin A were enhanced in the B→A direction only after day 17, reaching a maximum at day 27. This suggests that although present, P-gp may not be fully functional until day 17 (Table I.5).

I.9.1.2.5. – Characteristics of the membrane support

Different types of permeable membrane are commercially available to grow Caco-2 monolayers, presenting specific physical properties regarding the type of material, the diameter, and the size of the pores. Aimed at improving cell growth and differentiation, some authors have also proposed to coat the filters with hydrogels prepared from the proteins usually found on the extracellular matrix *in vivo*, such as collagen, before cell seeding.

The cultivation of the cells on membranes with distinct characteristics was found to influence the cells morphology [115], selection of subclones [109], proliferation rate [131] and differentiation [109,115,117].

Membrane material and coating

Polycarbonate (PC) membranes are the most frequently used, but other materials such as polyethylene terephthalate (PET), and polystyrene (PE) are also used due to some specific advantageous properties. For example, PET membranes are translucent, enabling microscopic visualizations of the cell monolayers during the culture time [75].

Behrens et al [115] cultivated Caco-2 cells on PC, PET and PE membranes and found that the cell morphology was significantly altered between the distinct materials. Caco-2 cells grown on PET and PE membranes formed flat monolayers, indicative of poor differentiation. Moreover, PET membranes caused differences in the microvillus structure. In contrast, cell monolayers grown on PC membranes consisted of tall columnar-shaped cells with a thick

microvillus structure. No significant variations were observed between the membrane type and the expression of PepT1 and P-gp transporters. However, PET membranes showed a small stimulating effect on the P-gp expression, whereas PepT1 expression was slightly decreased [115]. Cells grown on PET membranes also displayed lower P_{app} values for the paracellular marker FITC-Dextran (MW 4000) than cells grown on the other membrane materials. Among them, the highest FITC-Dextran P_{app} value was obtained for PC membranes. Accordingly, Walter and Kissel [109] also reported a higher P_{app} value of mannitol when cells were cultured on PC rather than PET filters (Table I.5). The decrease in paracellular permeability was explained based on an increase in tight junction's organization, indirectly supported by a stronger actin staining observed for cells grown on PET and PE relative to PC membranes. However, this is not direct evidence, since changes in actin organization could be caused by the different adherence of cells to the porous support membranes [132]. Tighter interactions between the cells' basolateral surface and the material of the porous membrane could also lead to a decrease in the access to the membrane pores and therefore to a decrease in the observed paracellular permeability. In agreement with this interpretation, increasing the space between the cell monolayer and the support membrane through the introduction of a gel matrix (e.g. collagen) was shown to lead to an increase in the observed paracellular permeability [115]. Coating has also shown to influence the properties of the cell monolayers. Behrens et al. [115] showed that coating PC filters with rat collagen resulted in an increased expression of PepT1 and P-gp transporters and produced a significant increase in the transport of cephadrine, a substrate of PepT1 (Table I.5).

Membrane diameter and pore size

There are commercially available Transwell™ inserts for use with culture plates of 6, 12 and 24 wells. The majority of studies in the literature have used the 12-well format, probably to achieve a balance between the number of assays per plate and surface/volume ratio (Table I.4).

Markowska et al. [117] determined the P_{app} values of mannitol and propranolol using PC membranes with the same pore size (0.4 μm) but different diameters (6.5, 12 and 24 mm, corresponding to plates with 24, 12 and 6 wells). The P_{app} values for both compounds had a tendency to decrease as the diameter

General introduction

of the membrane increased. The most significant variation was found for propranolol and larger diameter membranes (Table I.5). The authors attributed this decrease in P_{app} to the heterogeneous nature of Caco-2 cells, with monolayers having differences in passive transport caused by the variable development of actin rings and tight junctions. Nonetheless, it would also be interesting to evaluate the possibility of the cell monolayer being less cohesive at the membrane periphery when larger diameter membranes are used.

Regarding the pore size, Lechanteur et al. [131] analyzed the impact on monolayer integrity when Caco-2 cells were seeded on membranes with a pore size of 1 μm or 3 μm . The monolayers exhibited differences in their TEER values, with monolayers seeded on 3 μm membranes showing the lowest values. Visualization of the monolayers using microscopic techniques allowed the identification of two distinct characteristics in the monolayers seeded on 3 μm membranes. These monolayers showed gaps on the apical side and also the additional presence of cells on the basolateral side of the Transwell™, resulting in a loosely packed double cell layer. The authors conclude that Caco-2 cells were able to migrate across membranes with a pore size of 3 μm , but not through the 1 μm pores. Therefore, membranes with pore size inferior to 1 μm are recommended for permeability assays, and the most commonly used is 0.4 μm [128].

1.9.2 – Sources of variability related to the permeability experiments

Large differences in the experimental settings of the permeability assay protocols are commonly observed among research groups. An experimental variable that often varies between labs is the transport media used to perform the assay, which present variations on its pH and composition including the presence of additives and/or cosolvents. Also, the stirring rate, sampling methodology (replacement or transfer), number of sampling time points and total duration of the assay can differ.

The use of different protocols may have distinct effects on the properties of the cell monolayers and on molecules being tested (e.g. distinct ionization at the pH of the assay), which ultimately can lead to changes in P_{app} values for the same compound. To allow the comparison between the results obtained by distinct

laboratories it is crucial to quantitatively evaluate the impact that each experimental variables has on the P_{app} results. This is performed by assessing the P_{app} values of compounds obtained under the distinct variables, using systematic studies where only that experimental condition is changed. The analysis of P_{app} values of compounds originated from the use of distinct experimental variables in permeability assays protocols are collected in Table I.6. Each of the sources of variability included in Table I.6 will be discussed in detail in next sub-sections.

Table I. 6 Analysis of the impact of different protocols for the permeability assays on the P_{app} values of reference compounds across Caco-2 monolayers. For each source of variability evaluated, the permeability assays were carried out by the same research group where only that experimental condition is varied.

Non-bold compounds are transported by passive diffusion, mostly transcellular. **Bold** compounds are transported through the paracellular pathway. **Bold italic** compounds are known substrates of peptide transporter PepT1 or P-gp. The symbols: - and + indicate the absence or presence of the corresponding additives.

The numbers in bold indicate statistically significant differences with at least one of the conditions in the variable analyzed, from the statistical analysis performed in the respective reference.

Compound	Variability sources										Reference
P_{app} (10^{-6} cm/s) A \rightarrow B											
Addition of bile salts, surfactants, and co-solvents in the donor side											
	10mM taurocholate		10mM cholate		10mM SLS ^a		2 % (v/v) DMSO		2 % (v/v) ethanol		
	-	+	-	+	-	+	-	+	-	+	
Dexamethasone	1.7	2.1	1.4	1.4	1.6	1.0	1.4	1.0	1.4	1.4	Yamashita et al. [133]
			1 % (v/v) povidone		1 % (v/v) pluronic F68		1 % (v/v) gelucir 44/14				
	-		+		+		+				
Sch 56592 ^b	100		140		115		30				
Sch-X ^b	100		135		150		165				Saha et al. [134]
Sch-Y ^b	100		105		135		20				
Addition of BSA in the acceptor side											
	0		0.5		1		2		4% (w/v)		
Atenolol	0.68 \pm 0.04								0.53 \pm 0.04		
Warfarin	28.2 \pm 1.5								33.1 \pm 0.5		
Chlorpromazine	9.1 \pm 1.7								46.5 \pm 2.0		Aungst et al. [135]
Phenytoin	15.4 \pm 0.3								21.5 \pm 1.2		
Mannitol	0.3								0.3		Neuhoff et al. [136]
	1		2		2		2		1		
SCH-A ^c	4		11		15		18		19		Krishna et al. [137]
	8								9		
Propranolol	110								150		Neuhoff et al. [136]

General introduction

Metoprolol	100				110	
Progesterone	8.2				22.6	
SCH-B ^c	2.2				9.4	Krishna et al. [137]
SCH-E ^c	11				10	
<i>Digoxin</i>	3				4	Neuhoff et al. [136]
Addition of BSA % (w/v) in the donor side						
	0	0.1	0.5	1	4% (w/v)	
Mannitol	0.3				0.3	
Metoprolol	100 ^d				90 ^d	Neuhoff et al. [136]
Propranolol	100 ^d				60 ^d	
	36	35	32	28		Katneni et al. [138]
Diazepam	53	46	29	21		
Addition of BSA % (w/v) in the donor and acceptor sides						
	1% (v/v) DMSO/4				4/4	
Curcumin	7.1 ± 0.6				3.5 ± 0.3	Yu at al. [139]
pH (apical/basolateral)						
	5.0/7.4	6.0/7.4	7.4/7.4	8.0/7.4		
FITC-dextran		0.006 ± 0.001	0.003 ± 0.000			Yamashita et al. [133]
Atenolol		0.19 ± 0.02	0.40 ± 0.01			
	0.30 ± 0.08		1.26 ± 0.08	2.31 ± 0.09		Neuhoff et al. [140]
Dexamethasone		12.3 ± 0.2	12.1 ± 0.5			
Salicylic acid		87.5 ± 4.8	3.35 ± 0.12			Yamashita et al. [133]
<i>Ampicillin</i>		0.17 ± 0.01	0.081 ± 0.001			
Stirring rate						
	0	Low (135 rpm)	High (1090 rpm)			
Mannitol		0.22 ± 0.08	0.26 ± 0.11			Artursson et al. [141]
Testosterone	35.7 ± 3.3	51.8 ± 7.9	100.8 ± 7.9			
		Low (250 rpm)	High (420 rpm)			
Propranolol		75 ± 10	221 ± 13			
<i>Verapamil</i>		57 ± 6	174 ± 15			Korjamo et al. [142]
		64 ± 14 ^d	140 ± 11 ^d			

^aSLS: sodium lauryl sulfate ^bSch 56592 LogP= 2.4, Sch-X LogP not determined, Sch-Y LogP= 4.0. The values reported correspond to the amount of compound transported per time and are expressed as a percentage in relation to transport in the absence of surfactants (100%).

^cSCH-A LogP= 6.32, SCH-B LogP= 5.89, SCH-E LogP= 2.18. ^d P_{app} in the B→A direction.

1.9.2.1 – Composition of the transport media

Permeability assays are often performed with buffered salt solutions which are used to wash the cell monolayer, to prepare the solution of the test compounds, and finally as transport media in the assay. Hanks' Balanced Salt

Solution (HBSS) supplemented with D-glucose (5.5 mM) is the most frequently used media in assays. Its composition in salts and glucose guarantees cell viability and the maintenance of the ionic balance at the cell membrane during the experiments [143]. However, limitations can often arise on permeability assessments due to the high polarity of HBSS aqueous solutions that prevents the solubilization of non-polar compounds. This can give rise to their immediate precipitation and consequent turbidity of the buffer solution. Before being added to the donor compartment, pre-filtering the solution can help remove precipitates but result in uncertainty regarding the exact concentration of compound. If not filtered, poor reproducibility of permeability measurements may be observed as the suspensions are not homogenous [144]. In this regard, the addition of several solubilizing agents to the transport media in the donor compartment has been considered. Before analyzing in detail, the impact of specific solubilizing agents, it is important to systematize the distinct effects expected.

The first distinction is whether the solubilizing agent interacts with the cell monolayer (A) or not (B). Case **A** may lead to very distinct effects depending on the solubilizing agent and how it interacts with the cell monolayer. It may disrupt the tight junctions (**A1**) leading to an increase in the paracellular permeability. The solubilizing agents may partition to the cell membrane changing their fluidity, and therefore passive transcellular permeability (**A2**). Or they may interact with transporters (**A3**), in this case with many possible outcomes. Competition for transport by efflux proteins is one of the most common situations, leading to an increase of P_{app} in the A→B direction and a decrease of P_{app} in the B→A direction. When the solubilizing agent does not interact directly with the cell membrane, the effects mostly depend on how the test compound was present in solution. If large aggregates were present, the solubilizing agent will decrease the size of the aggregates leading to an increase in the amount of compound available to interact with the cell monolayer, and therefore to an increase in P_{app} (**B1**). However, if the test compound was not aggregated or if the aggregates were small and dynamic, the solubilizing agent will not necessarily increase the compound availability (**B2**). In this case, the outcome will depend strongly on the properties of the solubilizing agent. Association of the compound with large solubilizing agents such as large micelles, proteins or other polymers will decrease the compound availability, and therefore its permeability (**B2a**). If the solubilizing agent is very small, such as organic solvents, the effect will be

General introduction

mostly a decrease in the adsorption of the test compound to the apparatus, leading to an increase in P_{app} (**B2b**). The organic solvents may also lead to changes in the properties of the aqueous media, such as viscosity or osmolarity, with the outcome in the observed P_{app} being case specific and difficult to rationalize.

Solubilizing agents are occasionally added also to the acceptor compartment. In this case the most important objectives are to decrease the adsorption of the test compound to the apparatus, to decrease its retention in the cell monolayer, and to guarantee sink conditions. The effects on P_{app} depend on many factors and cannot be easily systematized.

The impact of some typical solubilizing agents on the P_{app} values of compounds are presented and discussed in sections bellow.

I.9.2.1.2 – Addition of surfactants, amphiphilic polymers and co-solvents

Bile salts, synthetic surfactants, amphiphilic polymers and small percentages of co-solvents are usually incorporated into the transport solution of the donor compartment, and occasionally also in the acceptor compartment.

The use of bile salts as solubilizers in permeability assays is a natural choice considering their bio-relevance in the small intestine, particularly during lipid digestion. Bile salts form small micelles above their critical micelle concentration which can solubilize poorly soluble molecules (e.g., cholesterol and liposoluble vitamins), enhancing their absorption at the intestine [145]. Yamashita et al. [133] showed that the presence of 10 mM of taurocholate or cholate bile salts on the donor side had no effect on the P_{app} values of the lipophilic drug dexamethasone ($\log D_{7.4} = 2.01$). In contrast, the P_{app} value decreased to half with the use of 10 mM of the synthetic surfactant sodium lauryl sulfate (SLS) (Table I.6). This result was interpreted on the basis of a decrease in the fraction of dexamethasone available for permeation due to its association with the large SLS micelles. Nevertheless, the presence of SLS also caused a decline in TEER values, indicating that the integrity of the cell monolayer was compromised. In addition, SLS interacts efficiently with cell membranes [146], increases their fluidity [147], and has been shown to modulate P-gp activity [148]. This solubilizing agent may therefore be included as case **A1**, **A2**, **A3**, each one with different outcomes in P_{app} . The overall result was a balance between all effects. The bile salts used in this study also interact with the cell membranes [149,150], influence their fluidity [150], and

modulate P-gp activity [151]. However, their lower lipophilicity leads to less significant effects at the concentrations used, and results in no effects on the observed permeability of dexamethasone.

Saha et al. [134] measured the permeability of three poorly soluble molecules, Sch 56592, Sch-X, and Sch-Y, in the presence of 1% (v/v) of various solubilizing agents, including the amphiphilic polymers povidone and pluronic F68, and the surfactant gelucir 44/14. As observed by Yamashita et al. [133], the presence of the surfactant has impact in many aspects. A key distinction in this study is the aggregation of test compounds in the absence of the surfactant, while in the previous study the test compound was at a concentration below its solubility in the aqueous medium. Therefore, in addition to the effects on the cell membrane, there is also an increase in the amount of test compound solubilized (Case B2). The solubility of Sch-X is increased by 133-fold in the presence of the surfactant and the value of P_{app} increased to 165%, indicating that the most important factor was B2b. A lower increase in solubility was observed in the case of Sch 56592 (12-fold) and Sch-Y (2-fold), and their P_{app} decreased to 30 and 20% respectively. This indicates that the decrease in the availability due to binding to the surfactant micelles was dominant for these test compounds (case B2a). The effect of the amphiphilic polymers was always an increase in P_{app} , more significant for Sch-X. Notably, the overall impact of the polymers is intricate, involving various aspects, and is difficult to rationalize.

Dimethyl sulfoxide (DMSO) and ethanol are some examples of organic solvents usually incorporated as solubilizers. At concentrations below 2% these solvents show little toxicity and lead to non-significant variations in P_{app} [152,153] in the case of test compounds that were already solubilized in the aqueous medium. For poorly soluble compounds, the addition of the organic solvent is expected to lead to an increase in P_{app} (Case **B2b**), although no direct support for this effect could be found in the literature. In contrast, Yamashita et al. [133] and Aungst et al. [135] observed a small decrease of P_{app} in the presence of 2% DMSO or dimethylacetamide, respectively. This effect points towards changes on the physical properties of transport media, such as an increase in viscosity.

I.9.2.1.3 – Addition of bovine serum albumin (BSA)

General introduction

Reaching the blood circulation, the molecules are to some extent bound to proteins and lipoproteins in the plasma or are dissolved in plasma aqueous medium (unbound). The main protein responsible for the binding in plasma is human serum albumin. The molecules with high lipophilicity typically have a high fraction bound to plasma proteins. Only the unbound fraction of the molecule is free to diffuse across the endothelial membranes into the tissues, which is a limiting factor for their permeation [154]. In general, bovine serum albumin (BSA) is used for *in vitro* assays due to its similarity with human serum protein [155,156] and much lower price.

The addition of BSA to the transport medium of Caco-2 assays has been suggested with the purpose of overcoming four main difficulties usually found in the permeability assessment of poorly water soluble and strongly lipophilic compounds. Depending on the problem, BSA can be added to the donor, acceptor, or both compartments. BSA is usually added to both sides to solve (i) the low solubility of the compound in the aqueous medium and/or (ii) the unspecific adsorption of the compound to apparatus. On the other hand, BSA is added only to the acceptor side, to reduce (iii) the accumulation of compounds inside the cells, and (iv) to guarantee sink conditions [144]. The inclusion of serum albumin in the acceptor compartment of Caco-2 permeability assays is also a natural choice that approaches the *in vivo* conditions. A BSA concentration of 4% (w/v) is typically used since it is the concentration of albumin when the lumen side is perfused with the blood. Some specific examples are included in Table I.6 and will be discussed below.

Regarding the addition of BSA to the acceptor compartment only, Aungst et al. [135] reported that 4% (w/v) BSA leads to a marked increase in the P_{app} values of chlorpromazine (5.4-fold), a moderate increase for phenytoin (1.4-fold), but no effect for atenolol or warfarin. The results correlated with the compounds lipophilicity, with their $cLogD_{7.4}$ ¹ varying from 2.74 for chlorpromazine to -1.80 for atenolol, with intermediate values for phenytoin and warfarin. In another study, Krishna et al. [137] evaluated the effect of 1% DMSO or 0.5 to 4% BSA on the recovery of the very lipophilic SCH-A (LogP= 6.32). The recovery was only 40% in the presence of 1% DMSO, and increased to 75% with 4% (w/v) BSA. This increase in recovery was mainly due to a decrease in the amount of SCH-A

¹ Calculated using the MarvinSketch software (version 22.9.0, <http://www.chemaxon.com>)

retained by the Caco-2 monolayer, which dropped from 54 to 26 % when 4 % (w/v) BSA was added. Also, the amount adsorbed to the apparatus in the donor side decreased from 8.5 to 0.2 %, in the presence of 1% DMSO or 4% BSA, respectively. As expected, the increase in the amount of SCH-A quantified in the acceptor compartment leads to an increase in its P_{app} values, 5-fold higher at 4% BSA relative to 1% DMSO. A similar trend was also observed for other lipophilic molecules SCH-B (LogP= 5.89) and progesterone (LogP= 3.87), with an increase of their P_{app} values by 4-fold and 3-fold. In contrast with the strong effect in the case of very lipophilic compounds, no significant effects were observed in the case of compounds with low or moderate lipophilicity, mannitol (LogP= - 2.5), SCH-E (LogP= 2.14), metoprolol (LogP=2.15), and propranolol (LogP= 2.5) [136,137].

The inclusion of serum albumin in both the donor and acceptor compartments is also a common approach followed in Caco-2 assays protocols. Yu et al. [139] studied the effect on the permeability of curcumin, which has a very low solubility in water, when using DMSO or 4% (w/v) BSA in the donor side as solubilizing agents, while the acceptor compartment always included 4% BSA. The results showed a 2-fold decrease in the P_{app} value of curcumin when BSA was added to the donor compared to the addition of DMSO.

It is not common to find studies where BSA is added only to the donor compartment because the assays are mainly to model absorption across the intestinal epithelium (A→B direction), where serum albumin is only present in the acceptor side. However, when studying the permeability in the secretory direction (B→A), the addition of BSA to the donor compartment is a natural choice. Neuhoff et al. [136] showed that the addition of 4% BSA to the basolateral compartment decrease the P_{app} in the B→A direction for metaprolol and propranolol, with no effects for mannitol. Katneni et al. [138] has systematically and quantitatively studied this effect using several compounds, observing a small decrease in P_{app} for propranolol and a larger decrease for diazepam. In both studies, the reduction in P_{app} was explained by a smaller amount of the compound being available to permeate, specifically the unbound fraction.

The studies discussed above show that the presence of BSA in the transport medium does not alter the P_{app} values for compounds with low lipophilicity [135-138]. That is, for compounds that do not significantly bind to BSA, that are not adsorb to the assay apparatus, and that are not sequestered in the cell monolayer.

General introduction

This result also shows that the presence of BSA does not influence the properties of the cell monolayer, which is in agreement with the absence of strong interactions between the protein and the cell membranes [157]. This stands in contrast with the effect of other commonly used solubilizing agents like surfactants, amphiphilic polymers, or organic solvents, which may interact with the cell monolayer and alter their properties.

The P_{app} measured for compounds that bind moderately or strongly to BSA decreases when the protein is added to the donor compartment [136,138,139], primarily because of a reduction in the fraction of unbound compound available for permeation. When this is the sole factor at play, it's possible to estimate the P_{app} value in the absence of BSA by reverse calculation, considering the binding affinity for BSA [136,138]. In some studies, the decrease observed in P_{app} is lower than that predicted by the fraction of unbound compound. This may reflect massive aggregation and/or significant adsorption to the apparatus in the absence of BSA in the transport medium. This is the case observed for curcumin, where the reported binding affinity is $2 \times 10^5 \text{ M}^{-1}$ [158], leading to less than 10% of unbound curcumin at 4% BSA. A decrease of at least 10-fold in P_{app} was expected while only a 2-fold decrease in P_{app} was observed [139].

The use of BSA as a solubilizing agent in the donor compartment need not, therefore, to be a factor of variability in the P_{app} reported in permeability assays. Even when the P_{app} corrected for the unbound fraction is not reported, it may be calculated from the observed P_{app} regarded that the concentration of BSA and the binding affinity are known. This is another advantage of using BSA in comparison with other solubilizing agents.

When BSA is added to the donor compartment, an equally efficient binding agent should also be added to the acceptor side. Otherwise, the equilibrium with the acceptor compartment would be achieved at a very small amount of compound transported, and sink conditions could not be guaranteed. In the studies discussed above, it was shown that adding BSA to the acceptor compartment leads to an increase in the observed P_{app} [135-137]. In this case, the P_{app} value to be considered is that in the presence of BSA, because in the absence of the solubilizing agent the conditions required for the assay were not verified. Namely: i) no significant sequestration in the cell monolayer, ii) no significant adsorption to the apparatus, and iii) less than 10% of the compound being

transported to the acceptor compartment relative to its equilibrium concentration in this compartment [128].

I.9.2.2 – Selection of the transport media pH value

The pH at the apical side of cell monolayer constitutes a very important factor for ionizable compounds. Depending on the pK_a , minimal variations in pH value can lead to significantly different fractions of ionized and unionized species and because the passive transcellular permeability of neutral species is usually significantly larger [159], lead to large variabilities in P_{app} values observed.

The permeability assays are often performed at a fixed pH of 7.4 in both the apical and basolateral compartments. To obtain this pH, the buffer media is supplemented with 4-(2-hydroxyethyl)-1-piperazineethanesulfonic acid (HEPES) at 10 or 25 mM. However, in a way to mimic the conditions found *in vivo* across the intestinal epithelium, a pH gradient can be established across the cell monolayer by using a pH of 5.5-6.5 in the apical compartment, and pH 7.4 in the basolateral compartment. This is particularly relevant in the case of active transport because the functionality of pH-dependent active carriers depends on the presence of a pH gradient acting as a driving force. To obtain the acidic pH, the buffer media is usually supplemented with 2-Morpholinoethanesulfonic acid (MES - 10 or 25 mM).

Yamashita et al. [133] compared the P_{app} values acquired in the absence and presence of a pH gradient, (7.4/ 7.4) versus (6.0/7.4). The results revealed that dexamethasone and FITC-dextran were not affected by the pH. However, changing the apical pH from 7.4 to 6.0, increased the P_{app} values of weak acids (salicylic acid) and PepT1 substrates (ampicillin), while the opposite occurs in the case of weak bases (atenolol) (Table I.6). The permeability results for salicylic acid and atenolol are explained based on the variation of the neutral form of the compounds. For ampicillin, this molecule at pH 7.4 is present in solution in the anionic (60 %) and zwitterionic (40 %) forms, and at pH 6 is mainly in the zwitterionic form (94 %)². The higher permeability observed at pH 6 is difficult to understand in terms of variations in the fractions of the different forms, since both the anionic and the zwitterionic forms have low passive permeability.

² Calculated using the MarvinSketch software (version 22.9.0, <http://www.chemaxon.com>)

General introduction

Therefore, the effect of pH points towards another mechanism of transport across Caco-2 monolayers. Ampicillin is in fact known to be a substrate of PepT1 transporter. The higher P_{app} values observed for ampicillin under the pH gradient can be explained due to its transport by the PepT1 transporter, which is driven by a transmembrane H^+ gradient [160].

The use of a pH gradient in permeability assays may lead to misleading results regarding the existence of efflux transport for weak bases. Neuhoff et al. [140] measured the bi-directional transport of atenolol when the apical pH was reduced from 8 to 5, and reported a decrease of P_{app} values in the A-B direction by a factor of 8 compared to no changes in the P_{app} values in the B-A direction (Table I.6). At the lower pH, the concentration of uncharged species decreased, resulting in a “false” efflux, even though atenolol permeates only by passive pathways. As expected, no difference in the transport of atenolol in both directions was found in the absence of a pH gradient.

I.9.2.3. – Unstirred water layer (UWL) and stirring conditions

Adjacent to the cell monolayer there is an unstirred layer of water (UWL) that acts as an additional barrier to the permeation of compounds through the cell monolayer. For fast permeating compounds (low resistance to transport through the cell monolayer), this additional barrier leads to a strong decrease in the overall P_{app} (a strong increase in the overall resistance), while for compounds that permeate very slowly the increase in the overall resistance may be negligible. The lipophilicity of the test compound is another factor that is determinant for the effect of the UWL on the observed P_{app} . This is due to the depletion of compound in the aqueous media close to the membrane caused by the extensive membrane partition of very lipophilic compounds, and the inefficient diffusion of compound from the bulk aqueous medium in the absence of agitation.

A small UWL is present in the intestinal epithelium *in vivo* [161], but in *in vitro* Transwell™ inserts the UWL can be remarkably thick. The apparent UWL thickness was estimated to be 1544 μm [141], whereas the cell monolayer is generally 17 to 30 μm thick [63]. Keeping the Transwell™ plates under stirring during the transport experiments reduce the UWL thickness. Applying an orbital agitation at 1090 rpm lowered the apparent thickness of the UWL to 128 μm [141]. However, stirring can also cause cell detachment from the porous membrane

compromising the cell monolayer integrity. The speed should therefore be kept as high as possible, but without affecting the cell monolayer integrity.

Conducting permeability assays at various stirring rates allows the determination of the impact of distinct UWL thickness on the P_{app} values for the test compounds. Artursson et al. [141] reported a variation in P_{app} values of testosterone between 36 to 101 (10^{-6} cm/s) when the applied stirring rate changed from 0 to 1090 rpm, respectively. Yet, there was no significant effect of agitation on the P_{app} value for mannitol, indicating that the monolayer integrity was not compromised. The effect on testosterone P_{app} but not on mannitol reflects the higher effect of the UWL in the case of fast permeating compounds. Similar results were obtained by Korjamo et al. [142] where the P_{app} values of propranolol and of verapamil increased 3-fold when the stirring rate changed from 250 to 420 rpm. In this study the effect of stirring was evaluated for both the A→B and B→A transport directions. It should be noted that the increase in P_{app} was greater for transport in the A→B direction, which could lead to incorrect interpretations regarding the contribution of active transport.

I.10 – Strategies to reduce the variability of Caco-2 permeability data

The development of highly predictive and widely applicable models to predict permeation through biological barriers is a difficult task, or even impossible, before serious efforts are done to generate consistent data. Of course, any expectation of obtaining a large, heterogeneous, public data base of Caco-2 P_{app} values that have been measured using the same cell population and experimental conditions, is presently unrealistic. This will involve the production of enormous new amounts of P_{app} data by the same researcher and laboratory. But can something be done to allow different researchers to obtain consistent data and to use the abundant P_{app} data already existing in the literature?

Motivated by the objective to improve the consistency of available P_{app} values, a few studies have evaluated possible solutions to overcome the variability problem.

I.10.1 – Standardization of cell culture and permeability assays protocols

General introduction

As long as the experimental conditions varies, Caco-2 P_{app} data will be inherently different. To achieve a reduction in the number of experimental conditions that are different among the studies, the standardization of Caco-2 assay procedures is imperative. The first step in this direction is the development and use of a uniform/common methodology. The culturing protocol, membrane support, cell passage numbers and experimental conditions used in the assays (pH, stirring rate, etc..) must be standardized. A common protocol will ensure the reproducibility of results over time and between laboratories [162].

With this objective in mind, attempts were made to create technical protocols that can be easily followed by the scientific community [67,128,163,164]. Of all of them, the protocol defined by Hubatsch et al in 2007 [128] is the most cited, accounting with more than 900 citations. It was published in the journal Nature Protocols and contain in detail all the procedures necessary for evaluating the permeability of compounds through Caco-2 monolayers, including some suggestions and troubleshooting. For this reason, throughout this thesis this protocol will be referred to as a reference or standard protocol for the use of Caco-2 monolayers in permeability assays.

Strictly following the conditions defined in a standard protocol may not always be easy for researchers. This is because not all laboratories have the same equipment or the same conditions so that the experimental protocol can be reproduced in a rigorous way. Sometimes some modifications may be necessary. The analysis of 221 studies published with Caco-2 assays reveals that only 17 % of the studies cited this protocol as the methodology followed to perform the experiments. Of these, only 20 % strictly followed the procedures described, with the remaining studies following them, but with some modifications.

I.10.2 – Normalization of P_{app} data to a reference compound

The routine measurement of reference compounds with known permeability characteristics has been proposed as a possible approach to standardize the results of Caco-2 assays. Ideally, marker molecules of monolayer integrity (e.g., mannitol) and high passive permeability (e.g., propranolol) should be used. This characterization of the model allows the establishment of acceptance criteria, such as for the tightness of the cell monolayer. By being

monitored regularly, the use of this standardized permeability cut-offs can reduce the variability within laboratories [162].

To address the issue of variability, one can also evaluate the P_{app} values of a test compound relative to a reference compound. This approach to normalization of P_{app} data was followed by some authors before assembling the various datasets that were compiled from different laboratories into a single larger dataset [106,165].

Larregieu et al [106] used the P_{app} value of the transcellular marker metoprolol that was measured in all datasets compiled from different sources as a reference value to normalize the P_{app} values of the other compounds. The authors showed that normalizing to metoprolol from each dataset can minimize inter-laboratory variability for lipophilic compounds (e.g., propranolol). However, this was unsuccessful for hydrophilic compounds (e.g., terbutaline) and transporter substrates (e.g., amoxicillin), whose resulting variability after normalizing was still high.

In a work on QSPRs, Paixão et al [165] used the P_{app} values measured in the study that included the largest number of reference compounds to normalize the P_{app} values of compounds collected in other studies. Using this procedure, the authors obtained a reduction in the experimental RMSE before and after normalization from 0.43 to 0.37. A reduction on the overall inter-laboratory variability was achieved, but the variability was still high regardless of normalization.

1.10.3 – Normalization of P_{app} data to a well-defined experimental condition

So far, the solutions proposed by researchers have not proven sufficiently effective in overcoming the variability problems associated with P_{app} data. Considering the different conditions frequently used in assays, normalizing data for the change of a particular experimental parameter between studies may be a promising method for standardizing P_{app} values. This approach has the advantage of using data that is already available, whether in the literature or databases.

Before applying this approach, it will be necessary to first carry out a quantitative characterization of the effect on P_{app} values of the most common alterations observed in experimental protocols among literature. With this aim, a

General introduction

systematic study must be performed by the same researcher, in the same laboratory and where only a single experimental condition is changed at a time in the permeability assay. After quantifying what are their effects on the P_{app} values of compounds, it would be possible to define correction factors. The application of these factors would allow converting the P_{app} values obtained under a distinct but well-defined condition to the P_{app} values that would be obtained if the standard condition was used. Therefore, this approach is only possible to be applied for studies that include a detailed description of the assay's parameters.

As would be expected, in order for P_{app} data to be normalized for all of the most common alterations in protocols, there are a large number of experimental variables that need to be measured. Furthermore, multiple compounds also need to be used when testing each variable due to its distinct effects on different permeation pathways (Table I.6). As consequences of this, it will be necessary to carry out a large number of permeability assays to apply this normalization method. This task, which will already consume a lot of time and labor, will be even more difficult given the low throughput of the Caco-2 model. Thus, alternatives must be found to improve the throughput of the Caco-2 assays in compound's permeability assessments. Two possible alternatives will be discussed in the next sections.

I.11 – Re-use of Caco-2 monolayers in permeability assays

When following the standard protocol procedures [128], the main limitation for using Caco-2 monolayers for high-throughput measurements is the 3-week implementation period and regular feeding requirements. As described in the previous sections, this period of time is necessary to attain a confluent and fully differentiated cell monolayer. However, after 21 days post- seeding, several studies have been shown that the Caco-2 monolayers maintain their morphological and functional properties until day 30 [65,112,113]. In point of fact, in the reference protocol, the authors described that cells were maintained in the inserts for a total of 21 to 29 days. Such an extended period is often used to provide flexibility in choosing the day to conduct the experiment, with cell monolayers always being used to perform a single assay. Although it has never been explored, this stability period can be used to investigate the possibility of

whether a Caco-2 monolayer, already used to perform a permeability assay may be suitable to be re-used for another assay(s). This approach of re-using Caco-2 monolayers is fully aligned with the 3 R's principles, as it reduces the resources needed for assays by using an already implemented cell monolayer. Furthermore, it has the advantage of being able to increase the throughput of the Caco-2 permeability assays while following the procedure proposed in the reference protocol.

The major concern regarding the re-use of a cell monolayer for consecutive permeability assays is the possible loss of properties of the cell monolayer due to use in previous assays, namely its integrity and functionality. Therefore, the development of methodologies for the re-use of cell monolayers must first guarantee a full recovery of the cell monolayer properties between assays.

I.12. – Use of an alternative cell line with faster implementation: MDCK monolayers

Another alternative to increase the throughput of permeability assays to evaluate the normalization method could be to replace the Caco-2 cells with a faster growing cell line with similar properties.

Madin-Darby Canine Kidney (MDCK) monolayers have been used as an alternative cell culture model to evaluate permeability through the intestinal epithelium [56,166]. MDCK cells were originally isolated from the distal tubular part of canine kidney tissue. Although they are of non-human origin, morphologically, these cells have been shown to be similar to Caco-2 cells in mimicking the intestinal phenotype *in vivo*. Specifically, they differentiate into columnar epithelial cells displaying apical microvilli and tight junctions. Distinctly from Caco-2, these cells monolayers only need to be cultured on inserts for a period of 3 to 7 days to achieve a differentiated and tight cell monolayer. This becomes a significant advantage considering the reduction of labor, costs, and risk of cell contamination [68,167].

Two types of MDCK strains with different electrical resistance properties have been described: MDCK-I (type I), which forms epithelial monolayers with high TEER values, above $1000 \Omega \text{ cm}^2$, and the MDCK-II (type II), which generates more permeable epithelia with TEER values of the order of $100 \Omega \text{ cm}^2$. The low resistance shown by the type II strain is lower than that of Caco-2 cells and, is

General introduction

closer to that observed for the small intestine, which is the reason for its common use [167,168]. Lucifer yellow P_{app} value across MDCK monolayers is expected to be somewhat higher than that in Caco-2 monolayers, consistent with their low resistance values. However, LY P_{app} in MDCK monolayers is of the order of 10^{-7} cm/s, comparable to that observed in Caco-2 monolayers and thus indicating that a tight barrier is established in spite of the lower TEER [99]. This apparent contradiction can be explained by the fact that physiologically the renal epithelium has a permissive role in the passage of ions, and TEER reflects the resistance to movement of ions not only through paracellular pathways but also via ion channels, transporters, and ion pores. The reason for the low TEER value of MDCK cells is the higher expression level of ion pores that facilitate the ionic movement. In spite of their low TEER values, the monolayers form a tight paracellular pathway for small marker molecules of low passive permeability [81].

The use of MDCK monolayers as a tool to assess the membrane permeability characteristics of compounds was discussed by Irvine et al in 1999 [99]. According to the study, the P_{app} values of several passively absorbed compounds were comparable between MDCK and Caco-2 monolayers, with a correlation of $r^2=0.79$ being obtained between both systems.

Regarding the expression levels of some transporters, particularly the P-gp, it appears that the MDCK model expressed P-gp at lower levels with respect to intestinal tissue and Caco-2 cells [56]. To address this lack, the MDR1 gene encoding human P-gp was transferred into MDCK-II cells. The resulting cell line, named MDCK-MDR1 overexpresses P-gp and has an enhanced efflux of known substrates compared to the parental cell line and Caco-2. Hence, MDCK-MDR1 monolayers are routinely used to conduct bidirectional assays to evaluate the influence of P-gp mediated efflux on compounds transport. In addition, they are also used as a surrogate model for predicting BBB permeability [81,82,169].

Like Caco-2 cells, the MDCK cell line also consists of heterogeneous cell populations that when combined with the use of distinct experimental protocols (see section I.9) can also give rise to variable P_{app} results for the same compound [92,170]. Although also widely used, the applicability of MDCK monolayers remains lower compared to Caco-2 monolayers [171].

A quantitative comparison between the Caco-2 and MDCK cell models is important to gain valuable knowledge on the use of the permeability data

obtained with them. First, to find out whether monolayers from MDCK cell lines can be used as an alternative to Caco-2 monolayers to characterize the effect of experimental variables on P_{app} values. And second, to evaluate whether the P_{app} data obtained in one and another cell line can be merged with the purpose of increasing the datasets applied in the construction of QSPRs. Regarding their properties and ability to predict the permeability of compounds, cell monolayers obtained from MDCK, transfected MDR1 and Caco-2 cells were compared in a few literature studies [81,82,172]. The comparison between P_{app} values obtained with the distinct cell models requires that the assays must be carried out under the same experimental conditions and preferably with the same researcher. For that reason, systematic studies of these types are very scarce in literature. In the works of Veszelka et al. [82] and Hellinger et al. [81], the comparison between cell lines is performed with systematic and detail procedures. They characterize morphology, gene expression and drug transport through passive and active pathways. However, these works do not cover a full evaluation of all permeation pathways and commonly used reference compounds. Some additional work within this objective, including systematic and quantitative studies is still needed to provide a quantitative comparison of the two cell models.

Chapter II

Aims of this thesis

II.1 – Aims

The ability to predict the rate of permeation across biological barriers from the compound chemical structure would greatly improve the success in the design and development of new pharmaceutical drugs with better ADME/tox profiles. However, for the reasons exposed in the general introduction of this thesis, this is not yet possible to predict accurately. To increase the predictive power of permeability data obtained using cell monolayers such as Caco-2, it is necessary to improve the consistency and quality of the data. Instead of attempting the impossible task of obtaining large amount of new data, all under the same conditions, it is more attainable to improve data collected from literature and/or databases. The general objective of this study is to explore the feasibility of applying corrective methods to convert P_{app} values determined under different experimental conditions to a selected standard condition. In order to systematically characterize the effect on P_{app} values for the common alterations in the protocols, it is also essential that Caco-2 permeability assessments can be performed in a higher throughput manner.

In line with the purpose of increasing the throughput of Caco-2 permeability assays, the specific aims of this study are as follows:

(1) Develop and implement a methodology to allow the re-use of Caco-2 monolayers in additional permeability assays. The initial phase involves assessing whether carrying out a permeability assay impacts the integrity of the cell monolayers, since this property is the primary pre-requisite for use of cell monolayers in permeability assays. The second phase requires evaluating whether incubating the cell monolayers with culture medium after an assay is sufficient for the recovery of possible losses of monolayer integrity. The results obtained are shown in Chapter IV.

Aims

(2) Validate the re-use of Caco-2 monolayers as a methodology to be applied for a higher throughput assessment of compounds permeability. The validation studies include evaluating the maintenance of distinct cell monolayers properties during the period of re-use. This is achieved by assessing and comparing the properties of cell monolayers used in a single assay and re-used in additional assays. In addition to the validation of the re-use regarding the cell monolayer integrity (goal 1), the full validation comprises the characterization of compounds that permeate through both passive and carried-mediated routes. The results obtained are shown in Chapter V.

(3) Evaluate the potential of using cell monolayers derived from the faster-growing MDCK-II and MDCK-MDR1 cells as an alternative to increase the throughput of permeability assays. To rationalize the permeability data obtained across MDCK-II, MDCK-MDR1 and Caco-2 monolayers it is essential to perform a quantitative comparison between the models. This work comprises a systematic evaluation of their properties, which is carried out by the same research under the same experimental conditions. The properties evaluated includes the morphology, tightness and permeability of compounds that permeate through both passive and carried-mediated routes. The results obtained are shown in Chapter VI.

Among the permeability studies performed across Caco-2 monolayers, it is common to find multiple experimental methodologies diverging from that used on the reference protocol. To reduce the variability in the P_{app} values reported, it is essential to quantify the impact of the distinct assay conditions. This work intends to contribute to reduce the variability in P_{app} data by quantitatively evaluating the effects on P_{app} for some specific methodologies used in the permeability assays. Within this goal, our specific aims are:

(4) Perform a systematic study to quantitatively characterize the effect on the P_{app} values of compounds following the passive permeation route of three experimental variables: (i) the possible effects of the tested compounds on cell monolayer integrity, through the simultaneous measurement of P_{app} for a paracellular marker (ii) the use of the transfer or replacement as sampling method, and (iii) the presence of BSA in the transport medium. The results obtained are shown in Chapter VII.

Chapter III

Materials and Methods

III.1 – Reagents and materials

The Caco-2 cell line was purchased from the European Collection of Authenticated Cell Cultures (ECACC 09042001, Salisbury, UK, received at passage 44) and kindly supplied by Professor Paula Marques.

The MDCK-II parent cells and MDCK-MDR1 transfected cells were purchased from the Netherlands Cancer Institute (NKI-AVL, Amsterdam, Netherlands) and kindly supplied by Professor Ana Fortuna.

Cell culture medium and supplements were all purchased from Merck S.A (Algés, Portugal), except fetal bovine serum (FBS) that was obtained from Gibco-Life Technologies (Porto, Portugal). Corning® Transwell™ 12-well plate polycarbonate membrane inserts (1.12 cm² surface area, 0.4 µm pore size) and 12-well culture plates were acquired from VWR (Lisboa, Portugal).

Rhodamine 123 and 2-[N-(7-nitrobenz-2-oxa-1,3-diazol-4-yl) amino]-2-deoxy-D-glucose (2-NBDG) were purchased from Setareh Biotech (Eugene, OR, USA). Ethylenediamine tetraacetic acid (EDTA), hank's balanced salt solution (HBSS), HEPES, Hoechst 33342, Triton X-100, DMSO, lucifer yellow CH dipotassium salt, (±)-propranolol hydrochloride, atenolol, sodium fluorescein and salicylic acid, (±)-verapamil hydrochloride were acquired from Merck S.A (Algés, Portugal). The fluorescent 7-nitrobenz-2-oxa-1,3-diazol-4-yl (NBD)-labeled alkyl chain amphiphiles (NBD-C_n, n = 4 to 8) were synthesized and purified, as previously reported by us [173], and the products were stored at -20 °C in the dry state or dissolved in MeOH.

Zonula occludens-1 (ZO-1) rabbit polyclonal primary antibody and Cy3 Goat anti-rabbit IgG secondary antibody used in immunostaining for confocal microscopy were purchased from Alfacene (Lisboa, Portugal), Dako fluorescence mounting medium from Agilent (Lisboa, Portugal), and bovine serum albumin from Applichem (Darmstadt, Germany). The FITC-conjugated mouse monoclonal antibody to human P-gp (CD243) used for flow cytometry was obtained from BD Pharmingen (San Diego, CA, USA).

Ammonium formate (≥99%), formic acid and methanol of High Performance Liquid Chromatography (HPLC) grade were supplied from Fisher Scientific (Lisboa, Portugal).

III.2 – Cell culture and seeding

Methods

III.2.1 – Caco-2 cell line

Caco-2 cells culture and monolayers preparation were as described in the reference protocol [128]. The cells were routinely grown in T75 cm² flasks with Dulbecco's modified Eagle's medium (DMEM) high glucose (4.5 g/L glucose with 4 mM L-glutamine) supplemented by 1.5 g/L sodium bicarbonate, 10% (v/v) heat-inactivated FBS and 1% (v/v) non-essential amino acids, in a humidified atmosphere of 5% CO₂ at 37 °C.

As recommended in the reference protocol, the permeability assays were performed using cells in high passage numbers within a defined interval of 10 passages, between 95 and 105. After reaching late passages of culture, mycoplasma free stocks of cells were frozen at passages 89 or 93 and stored in liquid nitrogen. At the time of the experiments, the cells were thawed and cultivated for at least two passages before their seeding on inserts. When reaching 80–90% confluence on the flasks, usually after 3–4 days, the cells were detached with 0.25% (w/v) trypsin-EDTA (5 min at 37 °C) and subcultured at a split ratio of 1:8.

To avoid seeding aggregated cells and the formation of multilayers in Transwell™ inserts, the cell clusters were disaggregated into single cells by passing them 3 times through a syringe needle of 23 gauges (BD Falcon) before cell counting. Caco-2 cells were seeded at 2.6×10^5 cells/cm² on 12-well membrane inserts and kept in culture with DMEM medium (containing 1 % (v/v) penicillin (Pen; 10,000 units/mL)–streptomycin (Strep, 10 mg/mL)) for 21 days. Medium was renewed 6h following seeding and then every 2–3 days thereafter during the time of culture. The medium was also changed 12-24 h before the use of cell monolayers in permeability experiments.

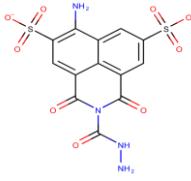
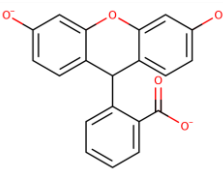
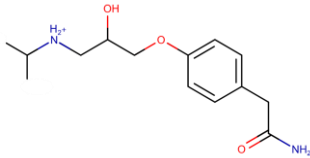
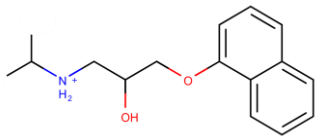
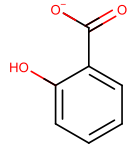
III.2.2 – MDCK cell lines

The parent and MDR1-transfected MDCK cells were cultured in high-glucose DMEM containing 3.7 g/L sodium bicarbonate and supplemented with 10% (v/v) heat-inactivated FBS and 1% (v/v) Pen/Strep. Cells were grown in T75 cm² flasks at 37 °C in 5% CO₂ and 95% relative humidity and passaged twice a week using 0.25% (w/v) trypsin-EDTA (5 min at 37 °C). The permeability assays were performed with MDCK-II cells from passage 11–18, MDCK-MDR1 from passage 15–23. The cells were seeded in 12-well Transwell™ membrane inserts

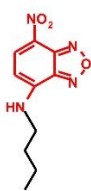
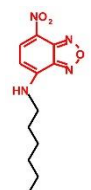
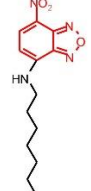
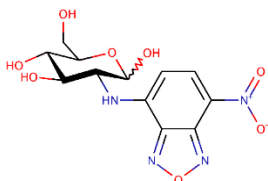
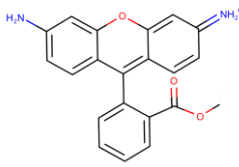
at a density of 5.4×10^5 cells/cm². Assays were conducted 7 days post-seeding and culture medium was changed every other day during culture and 12-24 h before the use of cell monolayers in permeability experiments.

III.3 – Structure and general properties of the tested compounds

Table III. 1 Molecular structure and some molecular descriptors calculated using the MarvinSketch software (version 22.9.0, <http://www.chemaxon.com>) for the compounds used in this work.

Permeation pathway	Name	Structure	Molecular descriptors
Paracellular	Lucifer Yellow (LY)		MW (g/mol) 428
			pK _a -3, -2, 3, 9.5
			Charge at pH 7.4 -2
			PSA (Å ²) 250
			cLogD _{7.4} -6.2
			cLogP -1.4
Passive permeation, mostly Paracellular	Fluorescein (Flu)		MW (g/mol) 332
			pK _a 3.8, 6.1 ^a
			Charge at pH 7.4 -2
			PSA (Å ²) 90
			cLogD _{7.4} 0.16
			cLogP 4.1
Paracellular	Atenolol		MW (g/mol) 266
			pK _a 9.7
			Charge at pH 7.4 +1
			PSA (Å ²) 89
			cLogD _{7.4} -1.8
			cLogP 0.4
Passive permeation, mostly Transcellular	Propranolol (Prop)		MW (g/mol) 260
			pK _a 9.7
			Charge at pH 7.4 +1
			PSA (Å ²) 46
			cLogD _{7.4} 0.4
			cLogP 2.6
Transcellular	Salicylic acid (SA)		MW (g/mol) 137
			pK _a 3
			Charge at pH 7.4 -1
			PSA (Å ²) 60
			cLogD _{7.4} -1.5
			cLogP 2.0

Methods

			MW (g/mol)	266	
			pK _a	12.3	
			Charge at pH 7.4	0	
			PSA (Å ²)		
			cLogD _{7.4}	2.06	
			cLogP	2.06	
Passive permeation, mostly Transcellular			MW (g/mol)	294	
			pK _a	12.3	
			Charge at pH 7.4	0	
			PSA (Å ²)		
				cLogD _{7.4}	2.95
			cLogP	2.95	
			MW (g/mol)	322	
			pK _a	12.3	
			Charge at pH 7.4	0	
			PSA (Å ²)		
			cLogD _{7.4}	3.84	
			cLogP	3.84	
Active and facilitated influx by glucose transporters			MW (g/mol)	342	
			pK _a ^a	-	
			Charge at pH 7.4	0	
			PSA (Å ²)	192	
				cLogD _{7.4}	-2.3
				cLogP	-2.3
Passive (transcellular) permeation, active efflux by P-gp			MW (g/mol)	345	
			pK _a	6.1 ^a	
			Charge at pH 7.4	+1	
			PSA (Å ²)	87	
				LogD _{7.4}	0.53 ^b
				cLogP	2.8

^a Experimentally determined pK_a values (from Ref. [1] and [2] for Flu and Rho, respectively),

^b LogD value from Ref. [2] PSA: polar surface area

III.3.1 – Preparation of test compound solutions

The preparation of test compound's solutions to be used in permeability assays is summarized in Table III.2. Stock solutions of the compounds were prepared independently in different solvents according to their solubility properties and stored at -20 °C. Donor solutions were prepared under aseptic conditions immediately before experiments, with the exception of the amphiphiles NBD-C_n which were prepared the day before. The concentration of compounds in stock solutions was determined by UV-vis spectrophotometry. For compounds whose stocks were prepared in DMSO and water, small aliquots

of the stocks were added directly to the HBSS solution. The volume fraction of DMSO in solution was less than 1 %. For the other compounds dissolved in methanol, the solutions were prepared by dropping the respective amount of the methanol stock solution into a glass tube. Methanol was evaporated under a gentle stream of nitrogen and heat, producing a film. Then, the film was dissolved in HBSS to obtain the desired concentration of the compound. In the case of NBD-Cn amphiphile solutions, their films were dissolved with a 100 μ M BSA solution previously prepared in HBSS. The resulting solutions were allowed to equilibrate overnight at 37 °C in a water bath with stirring at 100 rpm.

Table III. 2 Preparation of the donor solutions of test compounds evaluated in permeability assays.

Compound	Stock solutions		Quantification		Donor solutions	
	Concentration (mM)	solvent	Molar extinction coefficient ($M^{-1}cm^{-1}$)	λ (nm)	Concentration (μ M)	solvent
LY	5	sterile Milli-Q	1.2×10^4	430	20	HBSS
Flu	6	sterile Milli-Q	7.5×10^4	495	20	HBSS
Atenolol	2.5	DMSO	1.4×10^3	279	25	HBSS + 1% (v/v)
Propranolol	2	MeOH	7.1×10^3	290	25	HBSS
SA	2	MeOH	3.8×10^2	300	25	HBSS
NBD-Cn	0.5	MeOH	2.1×10^4	468	10	HBSS + 100 μ M BSA
2-NBDG	10	MeOH	2.1×10^4	468	250	HBSS
Rhodamine	0.1	MeOH	1.0×10^5	507	5	HBSS
Verapamil	100	DMSO			100	HBSS + 0.1% (v/v)

The cholesterol analogue dehydroergosterol (DHE) solutions emulsified by the bile salt glycocholic acid (GCA) were prepared in the absence and presence of coffee extracts. Arabica Brazil green grains were supplied by FEB company. The preparation of coffee extracts were performed by subjecting the coffee grains to distinct commercial roasting procedures, originating light (L) and dark (D) roasted coffee beans. Using a coffee grinder, the coffee beans were subsequently milled with two different grinding levels to obtain fine (1) and coarse (3) particle sizes. The final coffee beverages, denoted as L1 (light roast and fine grinding), D1, L3 and D3 were extracted in an espresso machine (Flama 10) operating at 15 bar in the proportion of 6 g per 40 mL of water. In order to have uniform extractions, a tamper of 51 mm was used to pressure the coffee powder in the

Methods

coffee portafilter basket previous to the extraction. The sample corresponding to 50 beverages was lyophilized at $-42\text{ }^{\circ}\text{C}$, 100 mT in a Kinetics Ez-Dry freeze dryer (Kinetics, Dresden, Germany) coupled to an Edwards 12 vacuum pump (Edwards, Burgess Hill, UK). The powders were weighed and the coffee concentration ranged from 32.7-34.9 mg/mL for the four samples, giving on average 1.0 g of coffee in 40 mL of an espresso like beverage. Coffee extracts solutions to be used in permeability assays were prepared by diluting 16 times the lyophilized coffee in HBSS plus the bile salt GCA (10 mM). Then, the mixtures were allowed to equilibrate overnight at $37\text{ }^{\circ}\text{C}$ in a water bath with stirring at 100 rpm. On the day of the experiment, DHE was added to the coffee/GCA mixture or to GCA only (Control) as an aliquot from a DMSO stock of 10 mM DHE. The addition was performed under vigorous vortex mixing to facilitate DHE interaction with the GCA micelles and prevent its precipitation. The final DHE concentration ranged from 10 to 100 μM , corresponding to $\leq 1\%$ (v/v) DMSO. LY was added to the final mixtures at a concentration of 20 μM .

III.4 – Permeability assays

III.4.1 – TEER measurements

On the day of the experiment, the integrity of the cell monolayers was examined by measuring the TEER values using a Millicell®ERS-2 voltmeter (Merck S.A, Algés, Portugal). Within the flow laminar hood, the electrodes were first sterilized by immersion in a solution of 70 % (v/v) ethanol in water for 15 min and allowed to air dry for a few seconds. The electrodes were then immersed in sterile HBSS buffer (supplemented with 25 mM HEPES, 0.35 g/L sodium bicarbonate, pH 7.4) to equilibrate for 15 min.

Before the measurements, the culture medium was decanted, and the cell monolayers were washed twice with HBSS pre-warmed at $37\text{ }^{\circ}\text{C}$ (0.5 mL in the apical and 1.5 mL in the basolateral sides). During the 8 min incubation required for the washing steps, the plate containing the inserts was placed with the lid-covered in an incubator (previously aseptic) without CO_2 at $37\text{ }^{\circ}\text{C}$ with a plate orbital shaker (IKA-Schüttler MTS4, JMGS, Lisboa, Portugal) set at 50 rpm. A filter insert without cells was included in each set of experiments for correction

of the TEER value for the background resistance. The net TEER values ($\Omega \text{ cm}^2$) were calculated by subtracting the cell-free filter resistance and multiplying by the filter area.

After the permeability assay, the remaining solutions of the inserts were decanted, pre-warmed HBSS (0.5 mL apical and 1.5 mL basolateral) was added to the cell monolayers, and their TEER values were measured again.

III.4.2 – Transport in Apical to Basolateral direction

Test compound solutions were pre-warmed at 37 °C. Before initiating the experiments, 1.2 mL of HBSS at 37 °C was added to the wells of a 12-well plate (acceptor compartment). Then, the HBSS on the apical side of the monolayers was decanted and the inserts were placed into new empty wells. The permeability assays were started immediately with the addition of 450 μL of the compound's solutions to the apical side (3-4 inserts were manipulated at the same time), from which a 50 μL sample was collected for the analysis of concentration at t_0 . The inserts were successively positioned in the pre-prepared 12-well plate containing HBSS, and the lid-covered plate was placed on the incubator (without CO_2 , 50 rpm and 37 °C). At defined time points of sampling, the plate was positioned into the laminar flow hood for transfer of the inserts into new wells containing fresh HBSS (transfer method). At the end of the assays, the inserts were transferred into empty wells and 50 μL was taken from the apical solution.

III.4.3 – Transport in Basolateral to Apical direction

The test compounds solutions at 37 °C were added to the wells of a 12 well-plate (1250 μL). The inserts with the cell monolayers were transferred into the plate, and the apical side of the cell monolayers was filled with 400 μL of pre-warmed HBSS (acceptor compartment). A 50 μL sample was immediately collected from the basolateral solutions (t_0). The lid-covered plate was placed on the incubator (without CO_2 , 50 rpm and 37 °C). At defined time points of sampling, aliquots of 200 μL were withdraw from the apical side. The solution was carefully mixed by pipetting up and down twice before being removed. A

Methods

200 μL of pre-warmed HBSS was added to replace the withdrawal volume (replacement method). At the end of the assays, the inserts were transferred into empty wells and 200 μL and 50 μL were taken from the apical and basolateral solutions, respectively.

For the collection of the samples in the permeability assays from B→A direction, taking and replacing an aliquot of the solution in the apical side was preferred over transferring all the solution to a new well. This was due to the fact that under the conditions of these assay, the sampling by transfer would require turning the insert upside down to decant the solution, which represented an aggressive way for handling the cell monolayers.

III.5 – Experimental procedure for the re-use of the Caco-2 monolayers in permeability assays

The manipulations of the cell monolayers during the TEER measurements, permeability assays, media renewals and solutions preparation were always carried out under aseptic conditions, in a laminar flow hood.

At the end of a permeability assay, after washing the cell monolayer with HBSS and measuring their TEER value (see above), HBSS was replaced by DMEM culture medium (0.5 mL apical and 1.5 mL basolateral). The inserts were maintained during two full days in a humidified atmosphere and 5% CO_2 at 37 $^\circ\text{C}$, with the culture medium being changed 24 h before the next permeability assay.

III.6 – Analytical methods for the quantification of the tested compounds

The samples collected from the permeability assays were stored at $-20\text{ }^\circ\text{C}$ until analysis.

The quantification of the test compounds on the samples (except for Flu and NBD-Cn) was performed by reverse phase HPLC using a Nucleosil C18 ODS column (150 \times 4.6 mm, 5 μm), preceded by a pre-column Zorbax ODS C18 column (12.5 mm \times 4.6 mm, 5 μm). The flow rate was maintained constant at 1 mL/min and the columns were equilibrated at 30 $^\circ\text{C}$. The elution of the compounds

included both isocratic and gradient elution steps comprising two eluents, eluent A consisted of 0.05 M ammonium formate adjusted with formic acid to pH 3.5, and eluent B was methanol. The quantitative analysis was carried out using a fluorescence detector. The samples from the acceptor compartment of the permeability assays were injected directly on the HPLC. In the case of compounds that permeated very slowly, with a very small amount being expected at the basolateral side, the injected volume was the maximum of the injection loop (900 μ L) to increase the sensitivity for their detection. The samples from the donor compartment were previously diluted 1:20 with 950 μ L of HBSS and a volume of 100 μ L was injected. The chromatograms obtained for the samples in the donor and acceptor compartments at the end of the multi-time sampling permeability assays are presented in Figure III.1. Due to the setup of the injection system, a larger volume of sample injected leads to a corresponding delay in the elution of the compounds. Apart from this, the comparison of the chromatograms for samples from the donor and acceptor compartments show that the elution profile was not affected by the 1 - 2 h incubation or transport through the cell monolayers.

Methods

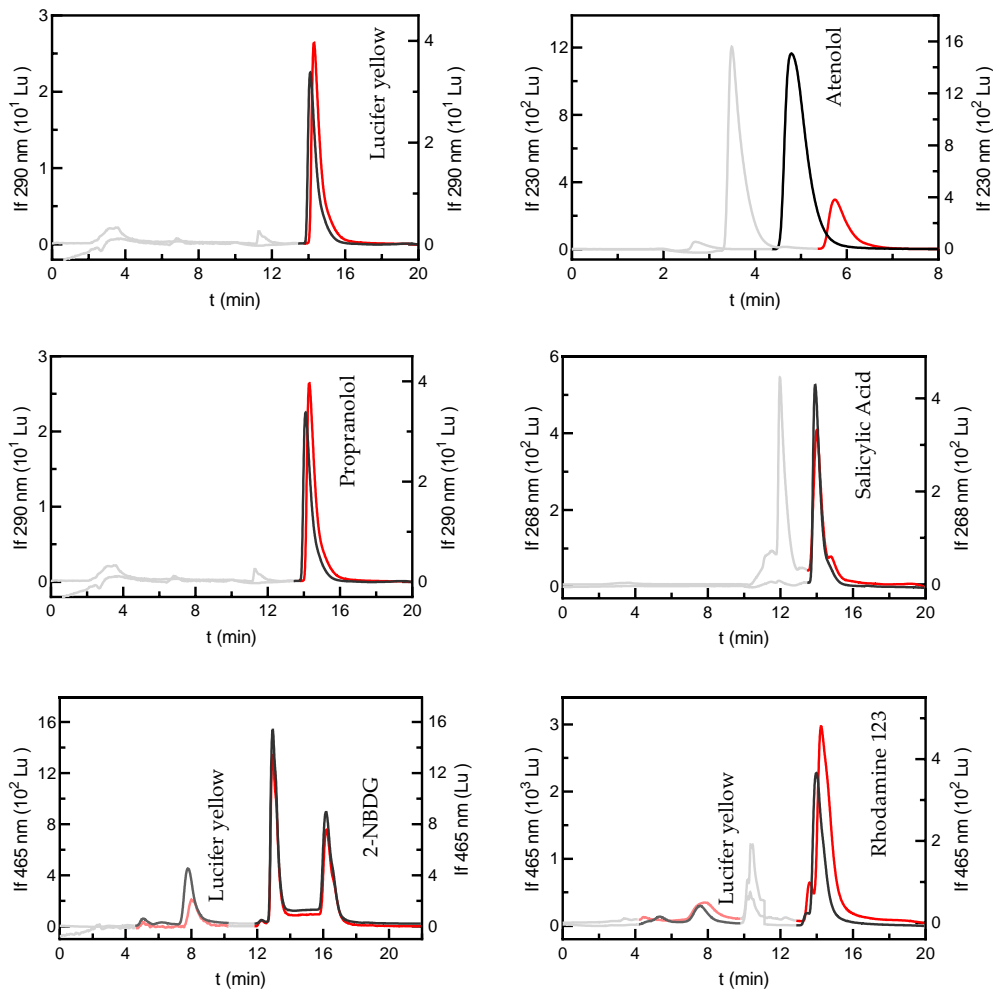


Figure III. 1. Typical HPLC chromatograms with fluorescence detection, for the compounds used in the permeability assays. The chromatograms of the samples collected from the donor compartment correspond to the left y-axis, and those from the acceptor compartment correspond to the right y-axis. The examples shown correspond to a typical sample at the end points of a multi-time sampling permeability assay. The concentration of the analytes was calculated from the integration of the chromatogram in the regions indicated in black or red, for samples collected from the donor or acceptor compartments, respectively. The chromatogram regions indicated in grey correspond to residual fluorescence from the mobile phase and/or HBBS. When the test compound and LY were in the same sample, LY concentration was calculated from the area between 4 and 10 min (light black and red).

The optimal chromatographic conditions applied for each compound are detailed in Table III.3. The optimized method for the paracellular marker LY consisted of 100 % eluent A (ammonium formate), and leads to a retention time of the major band around 8 min. To allow the analysis of the samples when both the control LY and the test compound were applied on the same cell monolayer, the developed methods for the other compounds always started with 100 % of eluent A (with the exception of Atenolol). Then, after 7 min, the eluent B (methanol) was added to allow the elution of the test compound. The simultaneous quantification of LY and 2-NBDG or Rho is illustrated in Figure III.1. For each compound, the calibration curves were built from 3 independent set of solutions, for the two injected volumes of 100 and 900 μ L. Data acquisition and integration of peak areas was done using the Chemstation software B.03.01 from Agilent (Lisboa, Portugal).

The concentration of Flu in the samples was determined from its fluorescence intensity at $\lambda_{ex/em}$ 485/530 nm in a black 96-wells plate (Costar®), using the SpectraMax iD5 Multi-Mode Microplate Reader (Molecular Devices Corporation Sunnyvale, CA, USA). Before the measurements, the pH of all samples was increased to 8.5-9 by adding a small aliquot of 10 M NaOH for the full ionization of Flu phenolic group, increasing its fluorescence quantum yield [174]. To guaranty that the samples analyzed are within the linear concentration range, the donor solutions were previously diluted 24-fold with HBSS.

The quantification of the amphiphiles NBD-C4, NBD-C6 and NBD-C8 was performed by transferring the samples collected from the assays to a black 96-well plate. The fluorescence intensity was measured at $\lambda_{ex/em}$ 450/530 nm using the microplate reader. The NBD fluorophore has low fluorescence quantum yields in polar environments such as water, which is markedly enhanced upon binding to BSA [175]. Thus, the presence of BSA was taken as an advantage to allow the direct quantification of the NBD-Cn samples above the sensitivity of this method. The donor solutions were previously diluted 10-fold with HBSS,

Methods

ensuring that the samples analyzed were within the linear concentration range. Quantification of NBD-Cn was performed using calibration curves prepared in HBSS with 10 μM of BSA or HBSS with 100 μM of BSA, for samples from the apical and basolateral compartments, respectively.

The performance of the analytical methods was validated through the determination of linearity (r^2 and linear range), method detection limit (MDL) and method quantification limit (MQL) over the concentration ranges of the used samples. The parameters obtained for the calibration curves are provided in Table III.3.

Table III. 3 Conditions and parameters of the calibration curves for the tested compounds used in the permeability assays.

Conditions						Calibration curve ^a			
HPLC with RP18 stationary phase and fluorescence detection									
Reference compounds	Mobile phase		Fluorescence detection wavelengths (nm)	Injection volume (μL)	Retention time (min)	r^2	Calibration range (μM)	MDL (μM) ^b	MQL (μM) ^c
	A : Ammonium formate 50 mM pH 3.5 (adjusted with formic acid)	B : Methanol time (min) % A							
LY	0 – 10	100	Ex: 430 Em: 530	100	5.1 & 7.8	0.9992	0.13 – 2.1	0.045	0.14
				900	5.1 & 8.0	0.9987	0.0011 – 0.038	0.0016	0.0047
Atenolol	0 – 8	80	Ex: 230 Em: 302	100	4.8	0.9999	0.043 – 2.7	0.019	0.056
				900	5.8	0.9998	0.0013 – 0.17	0.0023	0.0068
PROP	0 – 5	100	Ex: 290 Em: 340	100	14.2	0.9998	0.19 – 2.2	0.038	0.11
	5 – 7	40		900	14.2	0.9967	0.008 – 0.29	0.019	0.056
	7 – 15	40							
	15 – 18	100							
SA	0 – 5	100	Ex: 268 Em: 406	100	13.9	0.9989	0.088 – 2.6	0.11	0.33
	5 – 7	60		900	14.1	0.9991	0.0028 – 0.21	0.0076	0.023
	7 – 15	60							
	15 – 18	100							
2-NBDG	0 – 7	100	Ex: 465 Em: 530	100	13.1	0.9999	0.19 – 10.0	0.11	0.33
	7 – 7.5	85		100	13.1	0.9999	0.0046 – 0.26	0.0013	0.0039
	7.5 – 18	85							
	18 – 20	100							
Rho	0 – 5	100	Ex: 465 Em: 530	100	14.2	0.9995	0.012 – 0.20	0.0065	0.020
	5 – 7	40		900	14.3	0.9978	0.00077 – 0.024	0.0013	0.0040
	7 – 15	40							
	15 – 18	100							
Fluorescence detection in 96 well plate reader									
	Sample	Sample pre-treatment	Fluorescence wavelengths (nm)	Volume (μL)	r^2	Calibration range (μM)	MDL (μM) ^b	MQL (μM) ^c	
Flu	pH 7.4	pH 8.5-9 NaOH 10M	Ex: 485 Em: 530	200	0.9998	0.0019 – 0.95	0.0019	0.005	
	1200 μL	1.2 μL							
NBD-C4	10 μM BSA			200	0.9999	0.10 – 3.1	0.026	0.078	
	100 μM BSA			300	0.9998	0.013– 0.20	0.005	0.015	
NBD-C6	10 μM BSA		Ex: 450 Em: 530	200	0.9999	0.08 – 2.7	0.029	0.087	
	100 μM BSA			300	0.9999	0.006– 0.20	0.004	0.013	
NBD-C8	10 μM BSA			200	0.9979	0.05 – 1.7	0.15	0.46	
	100 μM BSA			300	0.9995	0.006– 0.20	0.0086	0.026	

Methods

^a For the calibration curves, three independent samples were analysed for each concentration. ^b method detection limit (MDL) calculated as $3 \times S_{y/x}/b$ where $S_{y/x}$ is the standard error of the estimated curve and b is the slope of the calibration curve. ^c method quantitation limit (MQL) calculated as $10 \times S_{y/x}/b$

III.7 – Data analysis

III.7.1 – Calculation of mass balance

The conservation of the total amount of compound at the end of the permeability assay was evaluated prior to its transport analysis. The mass balance (recovery) was calculated according to Equation III.1:

$$\text{Recovery (\%)} = \frac{Q_f^D + \sum(Q_{S(t)}^A) + Q_f^A}{Q_0^D} \times 100 \quad \text{III.1}$$

where Q_f^D and Q_f^A are the amount of compound (mol) that remains at the donor and acceptor compartment at the end of the assay, $Q_{S(t)}^A$ is the amount of compound sampled from the acceptor compartment at each time interval (t), and Q_0^D is the amount of compound in the donor compartment at the beginning of the assay.

Recoveries much smaller than 100% at the end of an experiment can indicate that the compound (i) is metabolized; (ii) is adsorbed in significant amounts to the assay apparatus (plastic of the apical and basolateral containers and filter support), or (iii) is sequestered by the cells (inside or in cell membrane).

III.7.2 – Calculation of P_{app}

The apparent permeability coefficients (P_{app}) values were determined using Equation (III.2), also described in Chapter I as Equation (I.6) and reported in cm/s:

$$P_{app} = \frac{\Delta Q^A}{\Delta t} \frac{V^D}{AQ_0^D} \quad \text{III.2}$$

where ΔQ^A is the amount of compound (mol) that accumulates in the acceptor compartment during the time interval Δt (in seconds), A is the surface area of the filter (1.12 cm²), V^D is the volume of the donor compartment (cm³) and Q_0^D is the amount of compound in the donor compartment (mol) at the beginning of the time interval considered.

When several sampling times were performed, the Q_0^D was determined considering the donor compound amount after each sampling, which was recalculated from that in the beginning of the experiment by subtracting the compound that reached the acceptor compartment in the preceding sampling times. This equation is equivalent to that indicated in the reference protocol for the instantaneous permeability coefficient [128]. The only difference is that, instead of directly considering the initial concentration of the tested compound in the donor compartment, we explicitly indicate the amount of compound and the volume of the compartment. This avoids subjectivity when using different units for the distinct variables. In Equation (III.2), the amount of compound may be in the most convenient units, provided that the same units are used for the compound in both compartments (ΔQ^A and Q_0^D). Additionally, it becomes more intuitive that the surface and the volume must use the same length units, which will be that of the resulting P_{app} .

In the B→A permeability assays, ΔQ^A was calculated considering the sample replacement at each time sampling, by applying a factor of $f = 1 - V_s/V_A$, where V_s and V_A are the volumes of the sample taken, and the total volume of the acceptor compartments (cm³), respectively.

III.8 – Confocal laser scanning microscopy and image analysis

For morphological studies by confocal laser scanning microscopy, cell monolayers were stained directly on the Transwell™ inserts. Cell monolayers were first fixed with 4% (w/v) paraformaldehyde in phosphate-buffered saline solution (PBS) for 10 min. After washing three times with PBS (incubated for 5 min), cells were permeabilized for 10 min using 0.1% (w/v) Triton X-100 in PBS and then washed again. Nonspecific binding sites in the samples were subsequently blocked with 1% (w/v) BSA in PBS for 30 min. The tight junction protein ZO-1 was stained with ZO-1 rabbit polyclonal antibody at a dilution of 1:200 overnight at 4 °C. After incubation, cells were washed 3 times with PBS and

Methods

incubated with a secondary antibody, cyanine 3 conjugated goat anti-rabbit IgG, at a dilution of 1:100 for 30 min at room temperature, protected from light. Cell nucleus was stained with Hoechst 33342 dye, 1 µg/mL, for 10 min. All stains were prepared in PBS containing 1% (w/v) of BSA. At the end of this incubation, the cells were washed with PBS and the filter was cut from the insert and mounted cell side up on a glass slide using Dako fluorescence mounting medium.

Confocal images of the slides were captured on a Zeiss LSM 710 (Carl Zeiss MicroImaging, GmbH) inverted confocal microscope at 20x magnification.

A z-stack was performed with a z-interval of 1µm, with the cell layer being typically enclosed in 8 or 12 optical slices indicating the formation of a single cell layer [81]. Image acquisition and analysis of maximal intensity Z projection of these stacks was performed using Zen 2012 software (Black edition, version 1.1.2.0, Zeiss). For the labeled cell monolayers, the following two filters' settings were used to collect the confocal fluorescence images: ex: 405 nm or 561 nm with emission detection at 415–484 nm or 577–735 nm, respectively.

Images post-processing and analysis was performed using ImageJ software (version 1.8, National Institutes of Health, Bethesda, MD, USA). Orthogonal projections of the XZ-plane were created from all the z-slices.

For characterization of the cell monolayers used in permeability assays with 2-NBDG, first, the cell monolayers were fixed in the inserts (see above). After washing 3 times with PBS, the filter was cut, mounted on a glass slide, covered with Dako mounting medium and stored at 4 °C in the dark until analysis. For each condition, an average of 12 z-stacks were acquired with a slice distance of 1 µm. The samples were excited at 458 nm and the emission was collected at 459–551 nm. Orthogonal projections of the XZ-plane were created from all the z-slices to view in detail the localization of the fluorescence in the cell monolayers.

III.9 – Flow cytometry analysis of P-gp expression

To prepare the cell monolayers for flow cytometric analysis, the culture media was first removed from the inserts and the cells monolayers were washed three times with HBSS (500 µL, 5 min each). Three inserts *per* condition were used to obtain the number of cells necessary for the analysis. The cells were detached

with 250 μ L of 0.25% (v/v) trypsin-EDTA solution for 5 min at 37 °C. Then, PBS with 5 % (v/v) FBS (250 μ L) was added to inactivate the trypsin, the cell suspension was centrifuged (300 g/5 min) and resuspended in ice-cold PBS containing 5 % (v/v) FBS. The cells were passed through a 23 gauge syringe needle (BD Falcon) up to 3 times to dis-aggregate clumps and divided into two aliquots of 100 μ L. The first was kept on ice until analysis by flow cytometry (control cells sample). The second was incubated with 20 μ L of P-gp antibody FITC-conjugated for 30 min in the dark on ice. After this incubation period, both aliquots were centrifuged, resuspended in 200 μ L of ice-cold PBS containing 5 % (v/v) FBS and measured on a BD Accuri™ C6 flow cytometer (BD Biosciences, San Jose, CA, USA) using λ_{ex} =488 nm and a 530/30 nm band-pass filter for emission detection. The data collected for 3000 - 10,000 events was gated to include viable cells based on their forward (FSC) and side light scatters (SSC). Gating strategies were the same for all samples measured on the same day. Data was analyzed by FlowJo software version 7.6.1 (Ashland, OR, USA) to obtain the median fluorescence intensity, which was the parameter used for comparison between samples and control cells.

Chapter IV

Re-use of Caco-2 monolayers in permeability assays — Validation regarding cell monolayer integrity

This work was published at, Pires, C.L.; Praça, C.; Martins, P.A.T.; Batista de Carvalho, A.L.M.; Ferreira, L.; Marques, M.P.M.; Moreno, M.J. Re-Use of Caco-2 Monolayers in Permeability Assays—Validation Regarding Cell Monolayer Integrity. *Pharmaceutics* 2021, 13, 1563. <https://doi.org/10.3390/pharmaceutics13101563>

IV.1 – Abstract

Caco-2 monolayers are a common *in vitro* model used to evaluate human intestinal absorption. The reference protocol requires 21 days post-seeding to establish a stable and confluent cell monolayer, which is used in a single permeability assay during the period of monolayer stability (up to day 30). In this work, we characterize variations in the tightness of the cell monolayer over the stable time interval and evaluate the conditions required for their re-use in permeability assays. The monolayer integrity was assessed through TEER measurements and permeability of the paracellular marker Lucifer Yellow (LY), complemented with nuclei and ZO-1 staining for morphological studies and the presence of tight junctions. Over 150 permeability assays were performed, which showed that manipulation of the cell monolayer in the permeability assay may contribute significantly to the flux of LY, leading to P_{app} values that are dependent on the sampling duration. The assay also leads to a small decrease in the cell monolayer TEER, which is fully recovered when cell monolayers are incubated with culture media for two full days. When this procedure is followed, the cell monolayers may be used for permeability assays on days 22, 25, and 28, tripling the throughput of this important assay.

IV.2 – Introduction

In vitro cell-based assays are the screening tool of choice for permeability assessment by the pharmaceutical industry, due to the right balance between predictability and ethical issues [176,177]. The Caco-2 cell line, derived from human colonic adenocarcinoma cancer cells, is the most extensively characterized *in vitro* model for predicting *in vivo* human oral absorption of novel drugs [178-181]. There are several reported protocols for the use of Caco-2 cells in permeability assays. They vary in the cell source, passage number, days after seeding in the Transwell™ filter, size and characteristics of the filter, and transport media, among other experimental parameters. The variety of procedures is an intrinsic characteristic of scientific research, which is always in search of better and faster protocols. In an attempt to standardize the procedures for well-established assays, the journal Nature Protocols publishes detailed protocols that may be easily followed by the scientific community. This is the case

Re-use of Caco-2 monolayers – integrity validation

for the protocol defined by Hubatsch et al. in 2007 regarding the use of Caco-2 monolayers in permeability assays [182]. The major limitation of this reference protocol is its very low throughput due to the long culture period (at least 21 days), although this has been shown to be required to obtain a fully differentiated and confluent monolayer [183,184]. Additionally, in the standard protocol the assay is performed on 12 wells *per* plate, leading to very high implementation costs for the assay of only a small number of compounds [176,182]. In an effort to accomplish a higher throughput, several groups have developed new protocols, which include accelerated processes for cell differentiation, miniaturization procedures, or the use of several test compounds in each assay.

Filter coating and the use of supplemented culture media has been shown to accelerate cell differentiation, and the post-seeding time has been reduced to 3–7 days [185-188]. Despite the significant advantages of these shorter-period assay models, several issues have been raised regarding the presence of active transporters and the integrity of the cell monolayer [185,186]. Additional issues with patents and poor clarification of the supplement's effect on the cell properties have also been pointed out as reasons for the limited use of these accelerated models [188]. Miniaturization to 96- and 384-well plate formats have been employed, allowing for the testing of more compounds and the use of smaller amounts of cells and test drugs [189-191]. However, the small cell surface area and the high total surface *per* volume may lead to artifacts due to compound loss by adsorption to the container's material [192]. Several authors have explored the use of up to ten test compounds in a single permeability assay, based on the assumption that the multiple analytes can be quantified simultaneously with analytical techniques [193-195]. Although this approach has been shown to be valid for some groups of test molecules, it cannot be followed for poorly defined compounds due to possible interferences such as, for example, the coexistence of substrates and inhibitors of P-glycoprotein. An interesting compromise is the combination of a well-defined control marker and the test compound, as has been done previously [130,196].

Despite all efforts, only moderate success has been achieved with these higher throughput protocols, and Caco-2 cells grown for 21 days in 12-well plates is still the standard procedure. An analysis of the literature in the last 5 years shows that in 74% of the publications the permeability assay is performed at least 21 days after seeding (only 4% follows accelerated protocols, with ≤ 7 days after seeding), and 12-well plates are the most common setup.

In the present work, we propose an alternative strategy to increase the throughput of this permeability assay, while following the procedure proposed in the reference protocol [182]. Several studies have shown that the Caco-2 cells maintain their morphology and functional properties from day 21 until day 30 after seeding [183,184,197]. The maintenance of the cell monolayer properties for this extended period has been used to add flexibility in the choice of the day of the experiment while performing a single permeability assay. Although it has never been explored, this stability also points towards the possibility of performing several consecutive assays. The permeability assay requires manipulation of the cell monolayer and exposure to the tested compounds and transport media, which may lead to perturbations to the monolayer integrity. The use of non-toxic concentrations of the tested compounds is a general requirement in any permeability assay, and it can be easily pre-evaluated using standard assays, such as MTT (3-(4,5-Dimethylthiazol-2-yl)-2,5-Diphenyltetrazolium Bromide) [198]. The major concern regarding the re-use of a cell monolayer in consecutive permeability assays is therefore the possible loss of cell monolayer integrity due to continued manipulation of the filter. Development of methodologies for the re-use of the cell monolayers must first guarantee a full recovery of the cell monolayer properties between assays.

The aim of this study is three-fold: (i) to evaluate the effect of the permeability assay on the monolayer integrity; (ii) to evaluate whether cell incubation with culture media is sufficient for recovery of the monolayer integrity; (iii) to determine the optimal duration of the interval between consecutive permeability assays. Assessment of the monolayer integrity was based on its transepithelial electrical resistance (TEER), on the permeability of the well-known marker of the paracellular pathway Lucifer Yellow (LY), and on the distribution of the tight junction protein zonula occludens-1 (ZO-1). A preliminary evaluation showed that one day of incubation with culture media is not enough for a full recovery. An extensive characterization has therefore been performed for a two-day incubation period, with consecutive permeability assays being performed at days 22, 25, and 28 after seeding. Single sampling (at 60 min) and multiple time sampling (10, 20, 30, and 60 min) was evaluated to support the applicability of the cell monolayer re-use when following both procedures.

More than 150 permeability assays were performed, and over 50 cell monolayers were characterized by confocal microscopy. With this extensive

Re-use of Caco-2 monolayers – integrity validation

work, the statistical distribution of the permeability parameters could be described, allowing a quantitative comparison between the distinct procedures and conditions.

IV.3 – Methods

Incubation of the cell monolayer with HBSS and the manipulation required for the permeability assays may lead to perturbation of the monolayer integrity. In fact, we (and others [196,199]) have observed a small but systematic decrease in the TEER value after the permeability assay. Hence, for the re-use of the cell monolayer in additional permeability assays, it is necessary to first ensure that the monolayer integrity is fully recovered. One hypothesis of this work is that this may be achieved by incubation of the cell monolayer in the culture media. Preliminary experiments showed that one day of incubation was not enough to re-establish the cell monolayer integrity. In the work currently described, the cells were incubated for 2 full days in supplemented DMEM in a humidified atmosphere of 5% CO₂ at 37 °C. To maximize the use of the already established cell monolayers up to three times during the total period where the monolayers are stable (21–30 days) [183,184,197], the days selected for the permeability experiments were 22, 25, and 28 post-seeding.

All cell monolayers presented TEER values above 200 Ω cm² (n= 208), both before and after the permeability assays and were considered for analysis. From each set of 12 inserts, at least one insert of the set was fixed and stained for confocal microscopy analysis. The remaining ones were used to perform permeability assays with LY (20 μM) in the A →B direction. The high fluorescence quantum yield of LY allows its detection by HPLC, even for the very small amount expected to permeate during short permeation intervals (see Chapter III, section III.6 for details). In this work, the transport of LY was evaluated using either a single sampling at t₆₀ or multiple samplings at t₁₀, t₂₀, t₃₀ and t₆₀ min. At the defined time points, the inserts were moved to new wells containing 1.2 ml of HBSS. At the end of the assay, some selected monolayers were prepared for microscopy; and the remaining were incubated with culture media for re-use.

Experiments were carried out at least in triplicate (wells per plate) and were independently repeated at least two times in different cell batches and cell passages. The very large number of assays performed allowed for the

characterization of the parameter statistical distribution, which was shown to be a LogNormal for P_{app} . This is in fact the statistical distribution expected for rate constants [200]. The characteristic values and uncertainty associated with this parameter cannot therefore be obtained directly from the average and standard deviation of the P_{app} values measured. Instead, the most probable value was obtained from the average of $\text{Log}P_{app}$, and uncertainty is expressed as 95% confidence intervals (CI_{95}) [200,201]. The CI_{95} values were calculated from the average ($\mu_{\text{Log}P_{app}}$) and standard deviation ($\sigma_{\text{Log}P_{app}}$), and the critical t value for the number of replicates used in the calculations, Equation IV.1:

$$CI_{95}(\text{Log}P_{app}) = [\mu_{\text{Log}P_{app}} - t \sigma_{\text{Log}P_{app}}, \mu_{\text{Log}P_{app}} + t \sigma_{\text{Log}P_{app}}] \quad \text{IV.1}$$

This statistical analysis was performed using Microsoft Excel.

A multivariate analysis (MVA) was applied to assess the correlation between the parameters and all potentially relevant independent variables. The multivariate regression model used to fit the data is given below:

$$Y = \beta_0 + \beta_1 * X_1 + \beta_2 * X_2 + \dots + \beta_i * X_i \quad \text{II.7}$$

where the dependent variable (Y) is described as a linear function of the independent variables (X_i). β_0 is the Y -intercept, and each coefficient (β_i) reflects the effect of the corresponding independent variable (X_i) on Y . The values of β_i are estimate by minimizing the sum-of-squares of the differences between the values of Y predicted by the equation and the Y values in the data. The coefficients have the units of Y divided by the units of the corresponding X . The confidence interval CI_{95} and the p -value were calculated for each β_i ; $p < 0.05$ was considered as statistically different from zero. This statistical analysis was performed using GraphPad Prism (version 8.4.2, San Diego, CA, USA).

A total of 52 cell monolayers were characterized by confocal microscopy to evaluate for possible changes in cell monolayer integrity and morphology. This analysis included cell monolayers at different days post-seeding (22, 25 and 28), both before and after the permeability assays, with cell monolayers used in a single permeability assay or re-used. From the acquired images, it was determined the cell density and the fractional area occupied by nuclei and by the tight junction protein ZO-1. The image area ($428 \times 428 \mu\text{m}^2$) was analyzed on at least 2 independent cell monolayers *per* condition. Each image was manually

Re-use of Caco-2 monolayers – integrity validation

threshold to select nuclei and ZO-1 only fluorescence. Orthogonal projections of the XZ-plane were created from all the z-slices to view the localization of the fluorescence of ZO-1 protein.

IV.4 – Results and discussion

IV.4.1 – Effect of re-use on the cell monolayer integrity after single-time sampling permeability assays.

Caco-2 monolayers have previously been shown to be stable and adequate for performing transport studies from day 21 to day 30 after seeding in the Transwell™ filter [183,184,197]. In this work, we evaluate whether the same cell monolayer may be re-used in consecutive permeability assays during this interval. Preliminary results showed that one day between the assays was not enough for full recovery of cell monolayer integrity. Therefore, the systematic study presented in this work was performed with an interval of two full days between consecutive permeability assays. The selected days for the assays were 22, 25, and 28.

To distinguish between the effects of performing the permeability assay from eventual variations of the cell monolayer properties between days 22 and 28, single use monolayers were also evaluated on day 25 and day 28. The tightness of the cell monolayer was first assessed by measuring its TEER, both before and after the permeability assays. The very large number of assays performed in this work permit the characterization of the distribution probability of TEER values, and the results obtained before the execution of the permeability assay are shown in Figure IV. 1.A. Broad distributions are obtained at all days, with a small increase at day 28 (best fit Normal distribution with $\mu \pm \sigma = 1228 \pm 248 \Omega \text{ cm}^2$) when compared to day 22 and day 25, which show a similar value of TEER (1036 ± 491 and $986 \pm 432 \Omega \text{ cm}^2$, respectively), the overall distribution at all days being $1067 \pm 473 \Omega \text{ cm}^2$. The distribution of TEER values after the execution of a permeability assay are represented in Figure IV. 1.B. It is observed that there is a small decrease in the mean value of TEER ($766 \pm 383 \Omega \text{ cm}^2$, for the best fit distribution of the cumulative data at all days), which is mostly due to a decrease

in the TEER values obtained after the permeability assay for monolayers on day 22 (from 1036 to 719 $\Omega \text{ cm}^2$), but also for monolayers on day 28. Nevertheless, TEER values above the threshold of 200 $\Omega \text{ cm}^2$, which is commonly accepted for a confluent cell monolayer [202,203], are obtained in all cases; see Table IV. S1 in the supplementary material for further details.

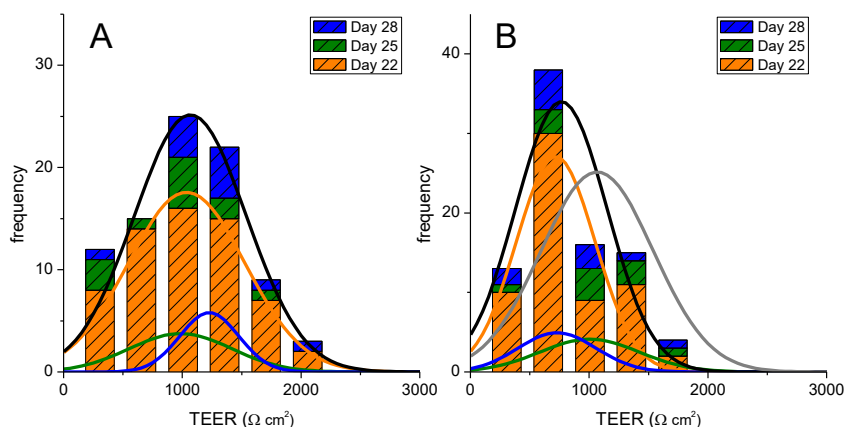


Figure IV. 1 Evaluation of the Caco-2 monolayer integrity when used for a single permeability assay at distinct days after seeding (22, 25, and 28). The TEER values obtained before are shown in Plot A, and after the permeability assay in Plot B. The lines are the best fit of a Normal distribution to the results obtained on each day (colored lines) or cumulatively at all days (black line). The grey line in Plot B is the overall distribution obtained before the permeability experiment.

After the execution of the permeability assay, the cell monolayers were incubated in culture media for two full days to evaluate if their barrier properties could be re-established. The results obtained for TEER are shown in Figure IV. 2. The statistical distributions achieved for the TEER values of cell monolayers not previously used on permeability assays are undistinguishable from those of the cell monolayers previously used and incubated in culture media for two full days. This indicates that the 2 days of incubation with the culture medium allows for the re-establishment of the cell monolayer integrity, overcoming the small perturbations induced by the permeability assay (including manipulation and incubation in HBSS).

Re-use of Caco-2 monolayers – integrity validation

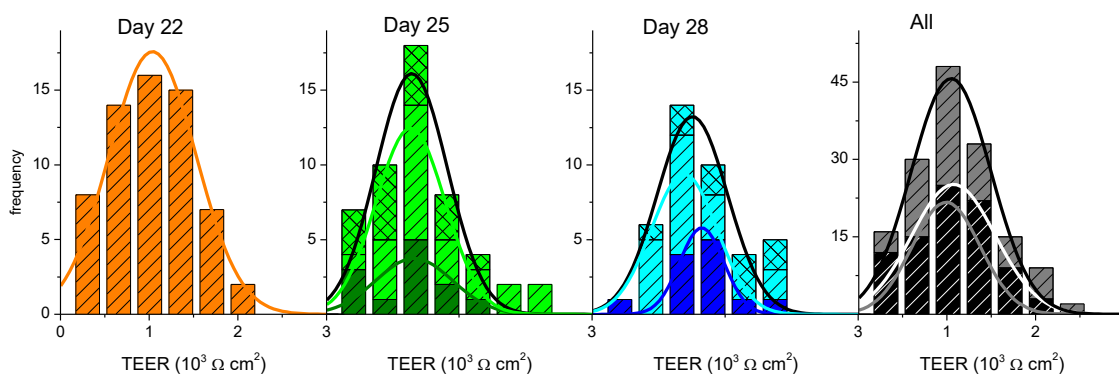


Figure IV. 2 Evaluation of the re-establishment of Caco-2 monolayer integrity when incubated in culture media for two full days after being used for a permeability assay. The TEER values for cell monolayers not used on permeability assays are shown in dark colors (orange, green, blue), and those previously used are shown in light colors (light green and light blue, TEER on day 25 previously used on day 22; light cyan and light blue, TEER on day 28 previously used on days 22 and 25, on single light green/light blue or multi-time light green/light blue sampling). The lines are the best fit of a Normal distribution to the results obtained on single use or re-used cell monolayers (colored lines) or cumulatively for each day (black line), with the parameters given in the supplementary material – Table IV. S2. The cumulative results at all days are shown on the right plot (dark grey, TEER before assay on days 22, 25, or 28; light grey, TEER before assay on days 25 or 28 after being used on day 22 or on days 22 and 25).

The analysis above is based on the average values obtained for each experimental condition. A closer look at the results for each individual cell monolayer is presented in the supplementary material—Figure IV. S1 and shows that: (i) a large decrease in the value of TEER after the permeability assay was only observed in 1/3 of the cell monolayers, while in the vast majority of the inserts, TEER varied by less than 20% (increase or decrease); (ii) from day 22 to 25 (before the permeability assay in both days), the TEER value increased for all inserts. Thus, the decrease observed after the assay on day 22 was fully recovered for all inserts. When analyzing the results between the 2nd and the 3rd use of the cell monolayer in the permeability assays, a full recovery of TEER was also observed in the majority of the inserts.

The results obtained with TEER suggest that the procedure developed in this work leads to full recovery of the cell monolayer integrity and that they can be re-used in permeability assays at days 25 and/or 28 after being used on day 22. However, due to the high variability in this parameter, it may be questioned if it accurately reflects the integrity of the cell monolayer [183,204-206]. We have

therefore also evaluated the effect of monolayer re-use through the results obtained for the permeability of a paracellular marker.

The results obtained for LY P_{app} , calculated from a single 60 min sampling interval, are shown in Figure IV. 3. At day 22, a large number of permeability assays were performed ($N = 34$), leading to a well-defined distribution frequency. A clear misfit is observed when the best fit of a Normal distribution is performed (grey dashed line), with the experimental data showing strong asymmetry towards high P_{app} values. The quality of the best fit is significantly improved when a LogNormal distribution is considered (black line), which is in fact the statistical distribution expected for rate constants [200]. Due to the asymmetry in the distribution, the uncertainty associated with this parameter should be expressed as a confidence interval [200]. This interval may be calculated from the parameters of the LogNormal distribution that best describes the results, or directly from the average and standard deviation of the observed values of $\text{Log}P_{app}$, leading, respectively, to $[1.1, 4.0] \times 10^{-7}$ cm/s and $[1.2, 3.9] \times 10^{-7}$ cm/s at 95% confidence (CI_{95}), and an average value of P_{app} equal to 2.1×10^{-7} cm/s for both analyses.

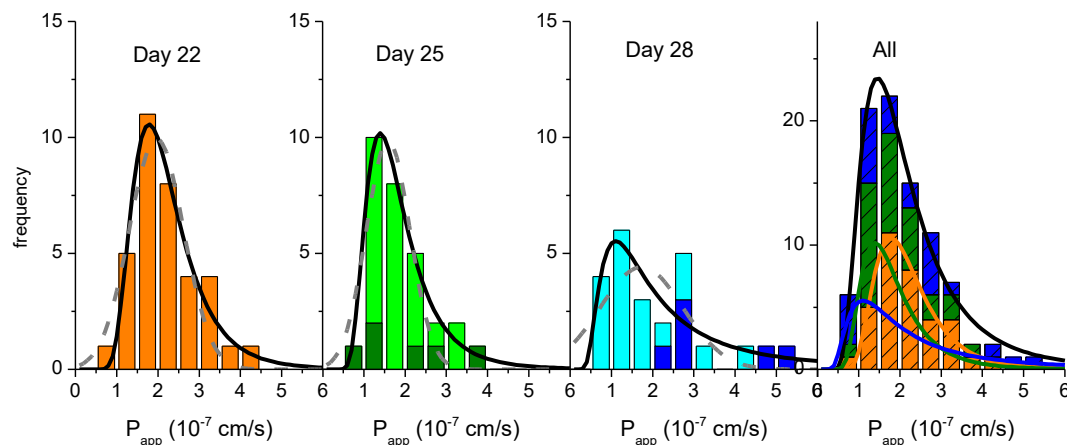


Figure IV. 3 Dependence of LY P_{app} (one sampling at 60 min) on the day post-seeding and on the re-use of the monolayer for additional permeability assays after incubation with culture media for two full days. The left plots show the distribution of P_{app} values obtained on the different days after cell seeding; dark colors represent results for single use and light colors for re-used cell monolayers; the lines are the best fit of a Normal distribution (grey dashed) or a LogNormal distribution (black continuous). The plot on the right shows the cumulative results at all days and conditions; the lines are the best fit of a LogNormal distribution for data from each day (colored) and collectively for all days (black), with the parameters given in the supplementary material – Table IV. S3.

Re-use of Caco-2 monolayers – integrity validation

The distribution frequency of LY P_{app} values obtained with cell monolayers on days 25 and 28 is also shown in Figure IV. 3. The number of assays performed with cell monolayers on day 25 that have been previously used on day 22 is large ($N = 23$) and leads to a well-defined distribution frequency (light green). However, the number of assays performed on day 25 for cell monolayers used on a single day (dark green, $N = 6$) is too small to allow the characterization of the frequency distribution. The characteristic value and confidence intervals must therefore be calculated from the average and standard deviation of the observed values of $\text{Log } P_{app}$, leading to $\mu = 1.8 \times 10^{-7}$ cm/s and CI_{95} equal to $[0.6, 5.3] \times 10^{-7}$ cm/s. The same average value is also obtained for P_{app} on re-used cell monolayers. In this case, the much larger number of assays leads to a smaller uncertainty, with the CI_{95} being $[1.1, 2.6] \times 10^{-7}$ cm/s. This shows that the two conditions do not lead to statistically different results and, thus, the cell monolayers that have been used on day 22 may be re-used on day 25 if following the proposed protocol. When this treatment is performed for cells on day 28 post-seeding, the parameters obtained are $\mu = 3.2 \times 10^{-7}$ cm/s and CI_{95} equal to $[1.7, 6.1] \times 10^{-7}$ cm/s for cell monolayers used a single time ($N = 6$) and $\mu = 1.6 \times 10^{-7}$ cm/s and CI_{95} equal to $[0.7, 3.6] \times 10^{-7}$ cm/s for cell monolayers previously used on day 22 and 25 ($N = 18$). As observed on day 25, the small number of assays performed with single use cell monolayers lead to a large uncertainty, and the two conditions are not statistically different. The collective result led to $\mu = 1.9 \times 10^{-7}$ cm/s and CI_{95} equal to $[0.8, 4.7] \times 10^{-7}$ cm/s. When the results obtained on all days are analyzed (right plot in Figure IV. 3), it is observed that they are very well described by a single LogNormal distribution. This shows that, although a small decrease is observed in the P_{app} values as cell monolayers are maintained on the inserts (specially at day 28), the distributions are not statistically independent. The parameters obtained from the collective values at all days and conditions are $\mu = 2.0 \times 10^{-7}$ cm/s and CI_{95} equal to $[1.0, 3.8] \times 10^{-7}$ cm/s. The small values obtained for LY permeability show that the cell monolayers are intact and tightly sealed at all conditions, $P_{app} < 5 \times 10^{-7}$ cm/s [182,202,207]. Thus, the results show that, when the cell monolayer is allowed to recover in culture media for 2 full days between assays, its integrity is not compromised, and they may be re-used on days 25 and 28.

IV.4.2 – Effect of multiple sampling time points on the paracellular permeability through Caco-2 monolayers

For the evaluation of new compounds' permeability, the use of several time points is usually required in order to allow the characterization of fast permeating compounds, while sink conditions are guaranteed. The sampling may be performed either with the replacement method (removing part of the solution in the acceptor compartment and replacing it with fresh transport media), or with the transfer method (where the insert is transferred to new wells containing fresh transport media). The latter is preferable for fast permeating solutes, as it takes only a few seconds to transfer several inserts and no test compound is present in the acceptor compartment at the beginning of each new time interval.

In this section we evaluate the impact of multiple sampling and different time intervals in the permeability of LY. The inserts were transferred to wells containing pre-warmed HBSS at time points 10, 20, 30, and 60 min. The results obtained for the instantaneous permeability during the first 10 min sampling interval are shown in Figure IV. 4 (upper plots), together with those previously obtained for the single-time point sampling at 60 min. As observed before (Figure IV. 3), the distribution frequency obtained for a 10 min sampling time interval is best described by a LogNormal distribution (a Normal distribution for the parameter represented in Figure IV. 4, $\text{Log}P_{\text{app}}$). Independent distributions, however, are observed for both sampling time intervals, with higher P_{app} values obtained for the shorter sampling time interval ($\mu = 15 \times 10^{-7}$ cm/s and CI_{95} equal to $[7.6, 29] \times 10^{-7}$ cm/s).

An alternative procedure to quantify permeability is directly through the amount of LY that reaches the acceptor compartment (Q_A) during the sample time interval (Figure IV. 4, lower plots). In this case, it is observed that a Normal distribution centered at around -0.6 is obtained for $\text{Log}Q_A$ during both sampling intervals (10 or 60 min), corresponding to Q_A around 0.2% (for details see the supplementary material – Table IV. S4). A very similar amount of LY was also observed to permeate through Caco-2 monolayers on day 23 post-seeding during a 90 min sampling interval, 0.27% [130]. This shows that, for cell monolayers on day 22 post-seeding, the manipulation during the permeability assay leads to a significant amount of LY transport and that very little permeation is observed during the sampling time interval, thus leading to P_{app} values that are strongly

Re-use of Caco-2 monolayers – integrity validation

dependent on the sampling time interval. When assessing the integrity of the cell monolayer using distinct incubation times, it is therefore preferable to refer to the observed permeability in terms of % of the control solute transported, which is usually indicated as below 0.5% for a tight Caco-2 monolayer [208].

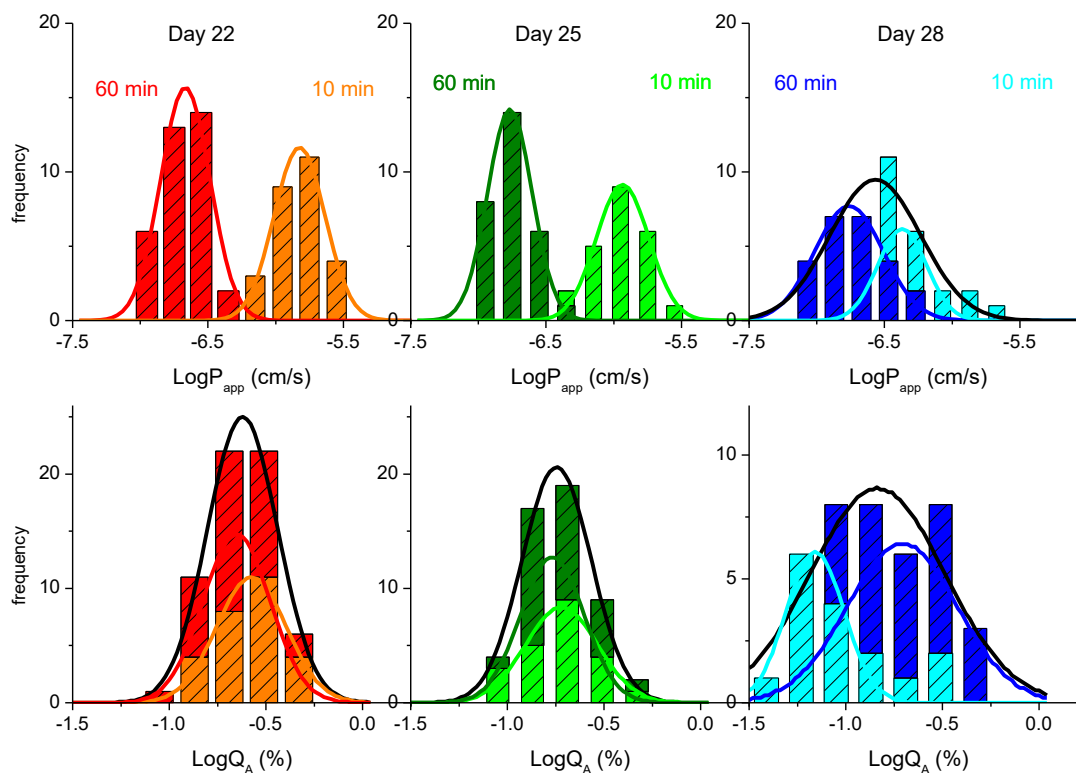


Figure IV. 4 Effect of the sampling time interval on the paracellular permeability of LY through Caco-2 monolayers at days 22, 25, or 28, post-seeding. The LY transport expressed as the Logarithm of the instantaneous permeability ($\text{Log}P_{\text{app}}$) is shown in the upper plots, while that expressed as the Logarithm of the amount of LY that permeates ($\text{Log}Q_A$) is shown in the lower plots, for a sampling interval of 10 min (light colors) or 60 min (dark colors). The lines are the best fit of a Normal distribution, with the parameters given in the supplementary material – Table IV. S4, the black line corresponding to the cumulative data from both sampling time intervals.

Very similar results are observed for cell monolayers on day 25 post-seeding (Figure IV. 4, middle plots). When considering cell monolayers on day 28 (right plots), the values obtained for LY P_{app} are still dependent on the sampling time interval, but a significant overlap is observed between the frequency distribution obtained for both conditions. Conversely, the frequency distributions of the amount of LY that permeates shows significant differences between the two sampling time intervals, being higher for the longer sampling interval.

A closer look on the effect of days post-seeding in the amount of LY that permeates through cell monolayers shows that the major variation is observed for the 10 min time sampling, with a decrease from $\mu = 0.25\%$ at day 22 to 0.19% at day 25, and 0.09% at day 28. This indicates that the contribution from the manipulation of the insert is very substantial on day 22 and becomes less significant for cell monolayers maintained in the insert for longer times, supporting an increase in the cell monolayer tightness, as previously suggested by the small increase in TEER (Figure IV. 1 and supplementary material – Table IV. S2). Therefore, when comparing the values of P_{app} for different analytes, it is important that the same conditions are used in the permeability assays, namely the day post-seeding and, most importantly, the sampling time intervals.

We have also analyzed the effect of multiple time sampling on the observed instantaneous amount of LY that permeates and the corresponding value of P_{app} ; the results obtained for the amount of LY that reaches the acceptor compartment are shown in Figure IV. 5. A small increase in Q_A is observed for consecutive sampling with the same time interval: $\mu = 0.25, 0.29$ and $\mu = 0.37\%$ on day 22; $\mu = 0.19, 0.25$ and $\mu = 0.25\%$ on day 25; and $\mu = 0.09, 0.10$, and $\mu = 0.13\%$ on day 28. An increase is also observed on the width of confidence intervals (see supplementary material – Table IV. S4). This shows that repeated manipulation of the cell monolayer leads to more significant perturbation and that the effect is not the same for all cell monolayers. When the cumulative amount of LY that reaches the acceptor compartment during the first 30 min (with sampling at each 10 min) is analyzed, an upward curvature is therefore observed (supplementary material – Figure IV. S2). However, when the final sampling at 60 min ($\Delta t = 30$ min) is included in the cumulative transport, the non-proportionality between Q_A and the sampling time interval dominates, and a downward curvature is observed for the whole 60 min sampling.

Re-use of Caco-2 monolayers – integrity validation

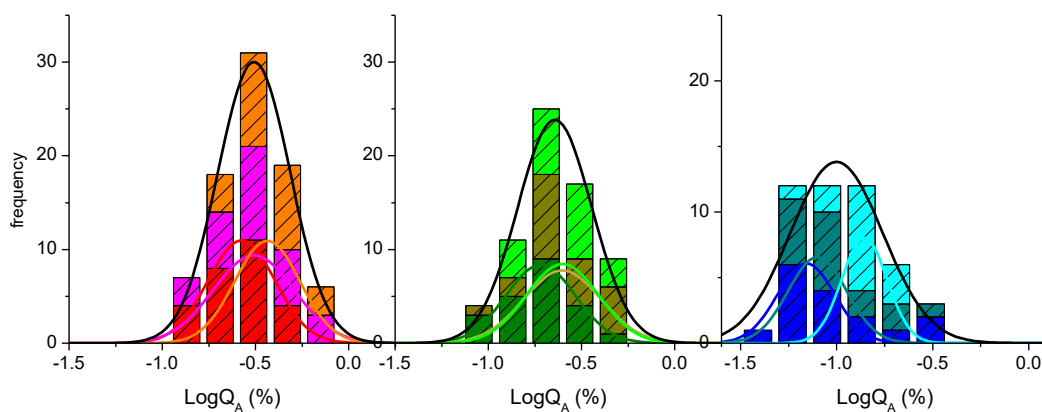


Figure IV. 5 Effect of multiple time sampling on the paracellular permeability of LY through Caco-2 monolayers at days 22, 25, or 28, post-seeding. The LY transport is expressed as the Logarithm of the amount of LY that reaches the acceptor compartment ($\text{Log}Q_A$) for 3 consecutive 10 min sampling intervals (at 10, 20, and 30 min): 1st 10 min sampling (■, ■, ■), 2nd 10 min sampling (■, ■, ■), and 3rd 10 min sampling (■, ■, ■). The lines are the best fit of a Normal distribution, with the parameters given in supplementary material –Table IV. S4, the black line corresponding to the sum of the results from the 3 sampling time points.

The results shown above have been obtained with transfer of the insert into wells containing fresh transport media at the end of each sampling interval. During transfer, the level of transport media across the cell monolayer is not balanced, with a hydrostatic pressure being applied on cell monolayer in the direction A \rightarrow B (top-to-bottom compartment). The results presented show that this force may lead to a significant amount of analyte transport, at least for analytes that permeate very slowly and paracellularly, as is the case of LY.

IV.4.3 – Morphological features and integrity of the cell monolayer

The effects of the day post-seeding and execution of permeability assays on the morphological features and integrity of the cell monolayer were also characterized by confocal laser scanning microscopy, both for cell monolayers used on a single assay or re-used. Representative images of the tight junctions at each condition are displayed in Figure IV. 6, and a larger area including the nuclei is shown in the supplementary material –Figure IV. S3. A quantitative analysis

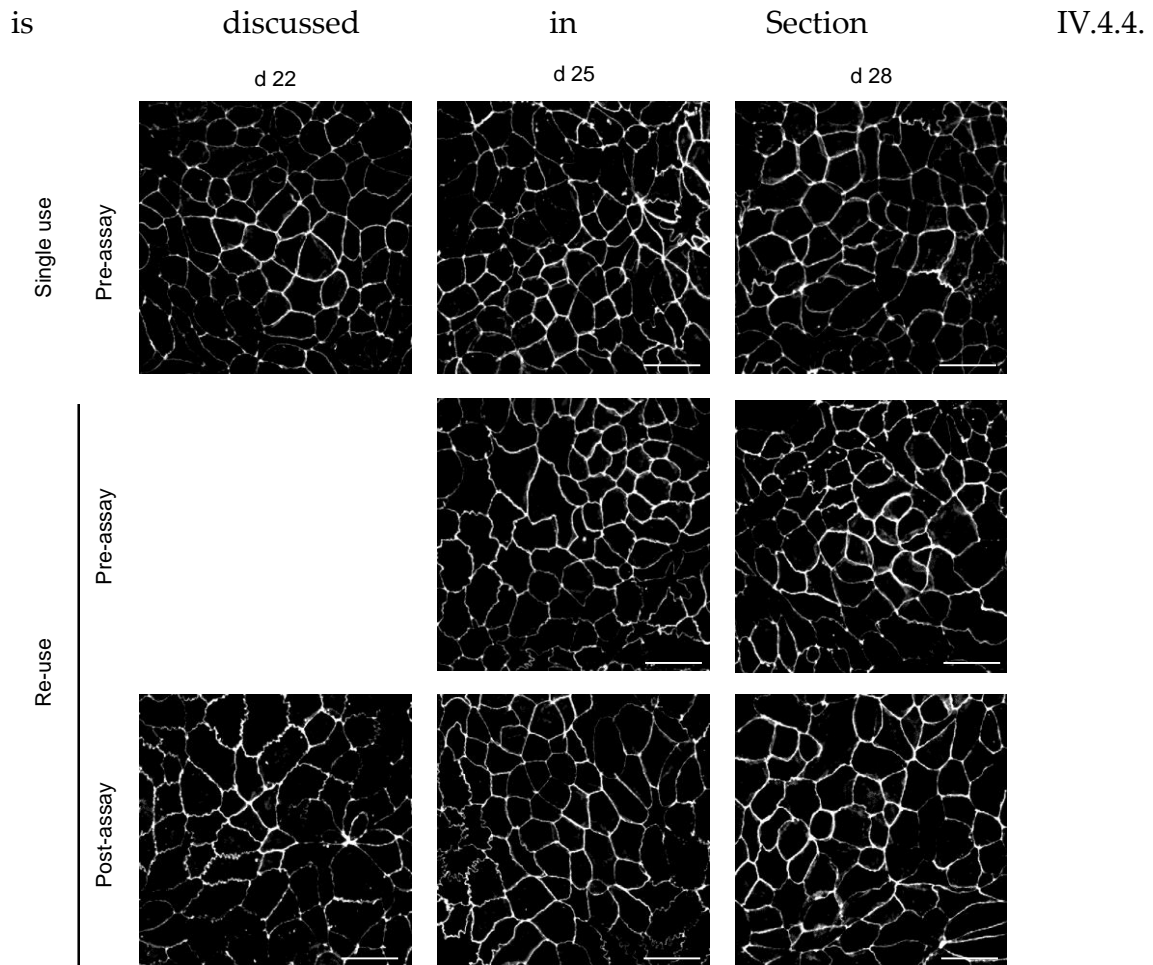


Figure IV. 6 Immunofluorescence ZO-1 staining of Caco-2 monolayers. Representative images for cell monolayers at days 22, 25, and 28 are shown in the left, middle, and right panels, respectively. In the upper plots, the monolayer was not used in permeability assays, while in the additional plots the monolayers were previously used. The lower plots correspond to monolayers immediately after the LY permeability assay, and in the middle plots the images correspond to cell monolayers that were maintained in culture media for 2 days after the permeability assay. Scale bar 50 μm .

All cell monolayers show an extensive network of tight junctions, as stained by ZO-1, and a similar cell density. This suggests that the execution of the permeability assays does not lead to significant perturbations of the cell monolayers, which is not in agreement with the results obtained with the permeability assays that show a small increase in the leakiness for multiple time point sampling. It should be noted, however, that the permeating solutes are several orders of magnitude smaller than the resolution of confocal microscopy (a few \AA as compared with several hundreds of nm). Although the tight junction's network remains apparently intact when observed at a microscopic

Re-use of Caco-2 monolayers – integrity validation

resolution, its integrity may be compromised, allowing the passage of small molecules. In this respect, it is important to consider the size of the pores in the tight junctions of confluent Caco-2 monolayers. Using a large set of paracellularly permeating solutes of different radii, Adson et al. obtained an effective pore radius of 12 Å for Caco-2 monolayers at days 21–23 after seeding [207]. Similar results have recently been obtained by other authors, with an effective pore radius varying between 6 and 16 Å [209,210]. A strong correlation has also been obtained between the tight junctions' pore radius and the LY permeability [209]. From this relationship, the P_{app} values obtained in the present work suggest a pore radius of approximately 6 Å. Given the several orders of magnitude difference between the resolution of the confocal images, and the tight junctions' pores through which LY permeates, it is not surprising that a continuous tight junction's network was observed despite the increased LY permeability.

To provide information regarding the transversal position of the tight junction protein ZO-1, the z-stack projection for the inserts with monolayers on day 28 post-seeding is shown in Figure IV. 7. It is observed that ZO-1 is located only at the apical side in all conditions. Therefore, the execution of the permeability assays does not lead to a redistribution of tight junctions, even when three permeability assays are performed with the same cell monolayer.

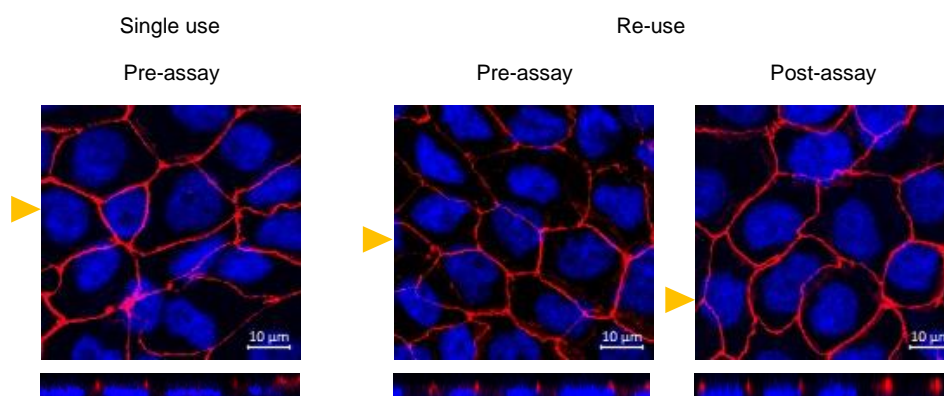


Figure IV. 7 Staining of ZO-1 (red) and nuclei (blue) for Caco-2 monolayers at day 28 post-seeding. In the left plots, the monolayer was not used in permeability assays, in the middle plots the monolayer was previously used on days 22 and 25 and maintained in fresh media until day 28, and the right plots correspond to cell monolayer immediately after a permeability assay on day 28 (after being previously used on days 22 and 25). The lower plots correspond to the z-stacks at the cross section, indicated by the respective yellow triangle.

IV.4.4. – Multivariate analysis

The very large set of experiments presented in this study ($N = 156$) was performed over several months, using a large set of cell monolayers (three batches at passages 95 to 105, see supplementary material – Table IV. S5 for all experimental results, and Figure IV. S4 for LY P_{app} obtained for cell monolayers at day 22 post-seeding). This introduces some uncertainty in the results, but significantly improves the robustness of the conclusions achieved. A multivariate analysis has been performed to evaluate the correlation between the permeability parameters and the independent variables. When TEER before the permeability assay is considered, the independent variables are the cell batch, cell passage number (between 95 and 105), day post-seeding, re-use of the cell monolayers, and sampling time points used on the previous permeability assays. For the TEER value after the permeability assay, the variable TEER before the assay was also included as an independent variable, and the TEER after the assay was also considered when the multivariate analysis was performed for LY transport (quantified by P_{app} and Q_A). The results obtained are presented in the supplementary material – Table IV. S6, a brief discussion of the major findings is given here.

The value of TEER before the permeability assay was found to be strongly correlated only with the cell batch, while the correlation of TEER after the assay with that before the assay is the only one that is statistically significant. However, the amount of LY transported showed no significant correlation between the value of TEER (both before and after the permeability assay), showing that the two variables are reporting on distinct properties of the cell monolayer. On the other hand, when LY transport is quantified by its P_{app} , a strong correlation is observed with the duration of the sampling interval, Δt , smaller sampling intervals leading to higher LY P_{app} . As discussed in Section IV.4.2, a small negative correlation (not statistically significant) is observed for Q_A . A significant correlation is also observed between P_{app} and the day post-seeding (cell monolayers becoming more impermeable to LY from day 22 to 28).

The nuclei and the tight junction protein ZO-1 of 52 cell monolayers were stained and analyzed by confocal microscopy. The variables considered were the cell density (number of nuclei in an area with $428 \times 428 \mu\text{m}^2$), the area occupied by nuclei, and that occupied by tight junctions containing ZO-1. The results obtained are shown in the supplementary material – Tables IV. S7 and S8. A high

Re-use of Caco-2 monolayers – integrity validation

variability is observed for the cell density: $3.1 (\pm 0.7) \times 10^5$ cells/cm² at day 22 before any permeability assay (N = 7) and $3.3 (\pm 0.8) \times 10^5$ cells/cm² for all cell monolayers (N = 52). The correlation is not, however, statistically significant with cell batch, passage number, day post-seeding, or cell monolayer use/re-use. As expected, a positive correlation is obtained between the cell density and the area occupied by the nuclei. This correlation is, however, sub-linear, which indicates that cells (and their nucleus) are more elongated when at higher density and is consistent with a continuous cell monolayer in all situations. A positive correlation was also observed between the cell density and TEER, suggesting that the thickness of the monolayer may influence the value of TEER obtained. This correlation was strong when only the cell monolayers at day 22 (N = 7) were considered (see supplementary material – Figure IV. S5) but become not statistically significant when cell monolayers at all conditions were considered (for details see the supplementary material – Section IV.6.7). No correlation, however, is observed between the area occupied by nuclei and by tight junctions, or with the amount of LY that has permeated during the assay. This shows that TEER is affected by parameters not related to the cell monolayer tightness, this being better evaluated by the permeability of paracellular markers such as LY. The area occupied by tight junctions does not show statistically significant correlations (or any weak correlation) with any of the variables considered.

Overall, the results obtained show that the cell monolayer integrity are not affected by their re-use at days 25 and 28 when maintained in culture media for two full days between the permeability assays.

IV.5 – Conclusions

The present study shows that, after using a Caco-2 monolayer in a permeability assay, two days of incubation in culture media are required and are sufficient for the re-establishment of the cell monolayer integrity. This enables the re-use of the cell monolayer in two additional permeability assays, triplicating the throughput of this *in vitro* model relative to the reference protocol.

The large set of permeability assays performed in this study allowed the characterization of the frequency distribution of the P_{app} parameter, which was shown to be skewed towards higher values following a LogNormal distribution. The characteristic value and associated uncertainty cannot therefore be obtained

from the average and standard deviation of the observed values of P_{app} . Instead, the more probable P_{app} should be calculated from the average of $\text{Log}P_{app}$ and the confidence intervals obtained from the standard deviation of $\text{Log}P_{app}$ and the number of assays [200,201].

It is also observed that manipulation of the cell monolayer during the permeability assay contributes significantly to the amount of analyte transported from the apical (top) to the basolateral (bottom) compartment, at least for solutes that permeate through the paracellular route. This leading to permeability coefficients strongly dependent on the incubation time. It is concluded that the integrity of the cell monolayer should be evaluated through the amount of paracellular marker that reaches the acceptor compartment during the sampling period, and not by the calculated instantaneous permeability coefficient.

Another important conclusion of this work is that the leakiness of the cell monolayers decreases from day 22 to 28 (both for cell monolayers used on a single permeability assay or re-used following the proposed protocol), and that the contribution of cell manipulation to the observed transport is less significant for cell monolayers on day 28 post-seeding. Therefore, cell monolayers on day 28 may be preferable when characterizing the permeability of a set of analytes requiring different sampling time intervals.

The full validation of the methodology proposed for the re-use of the Caco-2 monolayer in consecutive permeability assays requires the characterization of the transport of analytes permeating through distinct routes, including passive and transporter mediated influx as well as efflux. The validation regarding cell monolayer integrity performed in this work represents the first step towards this goal.

IV.6 – Supplementary material

IV.6.1 – Effect of a single-time point permeability assay (60 min) on the cell monolayer TEER values

The characteristic values of TEER before and after the LY permeability assay with a single sampling point at 60 min were evaluated for Caco-2 monolayers at different days after cell seeding. The very large number of assays performed allowed the characterization of the statistical distribution of TEER values, to obtain the characteristic average (μ) and standard deviation (σ) from which the confidence intervals at 95 % confidence (CI_{95}) were calculated. This was performed for μ and σ obtained directly from the TEER values, and from the parameters obtained for the best fit of a Normal distribution to the frequencies observed. Both statistical analysis led to an underestimation of the lower limit of CI_{95} in some of the conditions analysed (lower than the lowest values obtained experimentally, values in grey) indicating that the distribution of TEER is skewed towards higher values. Given the expected LogNormal probability distribution of rate constants [200], and the inverse relation between TEER (a resistance) and the corresponding rate of ion permeation, the statistical analysis obtained from the best fit of a Normal distribution to $\text{Log}(1/\text{TEER})$ was also performed. This leads to an overestimation of the CI_{95} upper limits (higher than the highest values obtained experimentally, values in grey) indicating that the distribution of $\text{Log}(1/\text{TEER})$ is skewed towards lower values. This indicates that random variables other than the energy barrier for ion permeation are influencing the values measured for TEER, and that those are likely well described by a Normal distribution. Given the inadequacy of both statistical distributions to accurately describe the TEER variable, the simpler approach was selected, which is the calculation of μ and σ directly from the TEER values obtained experimentally (columns shaded in green).

Table IV. S1 Characteristic TEER values and confidence intervals for the different cell monolayers before and after LY permeability assays with a 60 min sampling time point.

TEER values (k Ω cm ²)		Directly from TEER			Best Fit Normal distribution to TEER values			Best Fit Normal distribution to Log(1/TEER)	
Day		μ	σ	CI ₉₅ ^a	μ	σ	CI ₉₅ ^a	μ	CI ₉₅ ^a
22 N=34	Before	1.0	0.5	0.1, 1.8	1.2	0.5	0.3, 2.0	0.9	0.3, 2.2
	After	0.7	0.4	0.1, 1.3	0.7	0.2	0.4, 1.1	0.6	0.3, 1.4
25 N=29	Before	1.2	0.6	0.2, 2.1	1.0	0.4	0.3, 1.7	1.1	0.4, 2.6
	After	0.9	0.5	0.1, 1.6	0.9	0.5	0.1, 1.7	0.8	0.3, 2.0
28 N=24	Before	1.1	0.4	0.5, 1.8	1.0	0.3	0.5, 1.5	1.1	0.6, 1.9
	After	1.0	0.3	0.5, 1.6	1.1	0.2	0.7, 1.5	1.0	0.5, 2.0
All N=87	Before	1.1	0.5	0.2, 1.9	1.0	0.5	0.2, 1.7	1.1	0.4, 2.3
	After	0.8	0.4	0.2, 1.5	0.9	0.4	0.3, 1.6	0.8	0.3, 1.8

^a lower and upper limits of the CI₉₅ that are outside than the range of values obtained experimentally are shown in grey.

Some representative results obtained for individual cell monolayers are shown in Figure IV. S1. The TEER values before the permeability assay are shown in grey, and those after are shown in white. For a small number of cell monolayers it is observed a small increase in TEER after the execution of the permeability experiment, but for most cell monolayers a decrease in TEER is observed. This decrease is usually small (less than 20 % variation), although a large decrease is observed in 1/3 of the cell monolayers. Incubation in culture media for two full days leads to the complete recovery of the TEER values pre-assay which usually become even larger than the value observed before the permeability assay. This over-recovery is frequently observed between day 22 to 25, while between day 25 and 28 the behavior observed for the individual cell monolayers is very diverse (from small increases to a significant decrease). In all cell monolayers analyzed, the TEER value observed before and after the permeability assay is always equal to or higher than 200 Ω cm², which is the value usually considered for tight Caco-2 monolayers [202,203].

The values obtained for the permeability coefficient of LY (P_{app}) are also shown in Figure IV.S1. No systematic dependence is observed between P_{app} and TEER. This is the case for each day post-seeding when comparing distinct cell monolayers and for a given cell monolayer along the days post-seeding. This suggests that the high variability observed for the TEER values is not directly

Re-use of Caco-2 monolayers – integrity validation

related with cell monolayer integrity. Among the factors that may influence the value of TEER, the electrode position relative to the cell monolayer may be of high relevance. It should be noted that while the TEER measurement is performed in a single location, LY permeability assay reflects the properties of the whole cell monolayer.

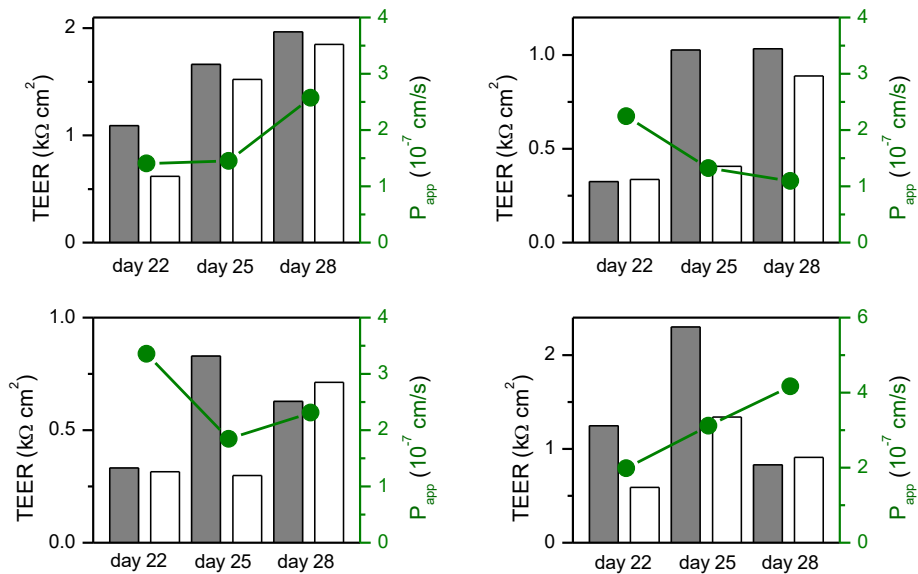


Figure IV. S1 Representative results obtained for individual cell monolayers in days 22, 25 and 28 post-seeding, for the variation of their TEER values (before and after the LY permeability assays) and the permeability coefficient obtained for LY with a single-time sampling at 60 min.

IV.6.2 – Effect of single and multiple sampling on the cell monolayer TEER values

Table IV. S2 Characteristic TEER values (in $k\Omega\text{ cm}^2$) and confidence intervals for the different cell monolayers before and after LY permeability assays with a single (60 min) or multi (10, 20, 30, 60 min) sampling time points. The statistical analysis was performed directly from the TEER values obtained.

Day	Conditions (number of experiments)		TEER values ($k\Omega\text{ cm}^2$)				
			min	max	μ	σ	CI ₉₅ ^a
all	all (153)	Before	0.2	2.3	1.1	0.5	0.3, 1.9
		After	0.2	1.8	0.9	0.4	0.3, 1.5
22	all (62)	Before	0.3	2.0	1.0	0.4	0.3, 1.7
		After	0.3	1.6	0.8	0.4	0.2, 1.4
	one-time (34)	Before	0.3	2.0	1.0	0.5	0.1, 1.8
		After	0.3	1.6	0.7	0.4	0.1, 1.3
	multi-time (28)	Before	0.4	1.7	1.1	0.3	0.5, 1.7
		After	0.4	1.5	0.9	0.3	0.4, 1.5
25	all (51)	Before	0.2	2.3	1.0	0.5	0.2, 1.9
		After	0.2	1.8	0.9	0.4	0.2, 1.6
	single use all (12)	Before	0.2	1.8	1.0	0.5	0.1, 1.9
		After	0.3	1.7	1.0	0.4	0.2, 1.8
	single use, one-time (6)	Before	0.2	1.5	0.8	0.6	-0.2, 1.9
		After	0.3	1.3	0.8	0.4	0, 1.6
	single use, multi-time (6)	Before	0.4	1.8	1.1	0.4	0.2, 1.9
		After	0.8	1.7	1.2	0.4	0.5, 1.9
	re-use all (39)	Before	0.2	2.3	1.1	0.5	0.2, 2.0
		After	0.2	1.8	0.9	0.4	0.2, 1.6
	re-use, one-time (23)	Before	0.4	2.3	1.2	0.5	0.3, 2.2
		After	0.2	1.8	0.9	0.5	0, 1.7
re-use, multi-time (16)	Before	0.2	1.6	0.8	0.4	0.1, 1.5	
	After	0.5	1.5	0.9	0.3	0.4, 1.4	
28	all (40)	Before	0.5	2.0	1.2	0.4	0.5, 1.9
		After	0.2	1.8	1.0	0.4	0.3, 1.6
	single use all (12)	Before	0.5	1.9	1.3	0.4	0.5, 2.0
		After	0.2	1.5	0.8	0.4	0.2, 1.5
	single use, one-time (6)	Before	0.5	1.5	1.2	0.4	0.5, 2.0
		After	0.2	1.3	0.8	0.4	0.1, 1.6
	single use, multi-time (6)	Before	0.9	1.9	1.3	0.4	0.4, 2.2
		After	0.5	1.5	0.8	0.4	0.1, 1.6
	re-use all (28)	Before	0.5	2.0	1.2	0.4	0.4, 2.0
		After	0.5	1.8	1.0	0.4	0.4, 1.6
	re-use, one-time (18)	Before	0.6	2.0	1.1	0.4	0.4, 1.7
		After	0.6	1.8	1.1	0.3	0.6, 1.6
re-use, multi-time (10)	Before	0.5	1.9	1.4	0.5	0.6, 2.3	
	After	0.5	1.7	0.9	0.5	0.1, 1.7	

^a lower and upper limits of the CI₉₅ that are outside than the range of values obtained experimentally are shown in grey.

Re-use of Caco-2 monolayers – integrity validation

IV.6.3 – Effect of cell monolayer re-use on LY P_{app} for a single time point sampling (60 min)

The characteristic values of the Apparent Permeability Coefficient of Lucifer Yellow (LY P_{app}) obtained for a single-time sampling at 60 min were evaluated through Caco-2 monolayers at different days after cell seeding. The very large number of assays performed allowed the characterization of the statistical distribution of P_{app} values, to obtain the characteristic average (μ) and standard deviation (σ) from which the confidence intervals at 95 % confidence (CI_{95}) were calculated. This was performed for μ and σ obtained directly from the P_{app} values, and from the parameters obtained for the best fit of a Normal distribution to the frequencies observed. Both statistical analysis led to an underestimation of the lower limit of CI_{95} in all conditions analysed (lower than the lowest values obtained experimentally, values in grey) indicating that the distribution of P_{app} is skewed towards higher values. Given the expected LogNormal probability distribution of rate constants [200], the statistical analysis obtained from $\text{Log}(P_{app})$ was also performed, leading to an adequate statistical description in all cases. For the experimental conditions where a large set of data was available ($N \geq 18$) the statistical parameters obtained from the best fit of a Normal distribution to $\text{Log}(P_{app})$ are also shown. The results obtained were very similar to those obtained directly from $\text{Log}(P_{app})$. The simpler approach was therefore selected, with the calculation of μ and σ directly from the Log of the values of P_{app} obtained experimentally (columns shaded in green).

Table IV. S3 Characteristic LY P_{app} values and confidence intervals at 95 % confidence (CI_{95}) obtained directly from the results and from the best fit of a Normal distribution to the frequency distribution of the P_{app} or $\text{Log}(P_{app})$ values. The numbers in grey correspond to limits of the confidence intervals that are outside the range of experimentally obtained values.

Day	Conditions (number of experiments)	LY P_{app} (10^{-7} cm/s)									
		Directly from P_{app}			Best Fit to P_{app}			Directly from Log(P_{app})		Best Fit to Log(P_{app})	
		μ	σ	CI_{95}^a	μ	σ	CI_{95}^a	μ	CI_{95}^a	μ	CI_{95}^a
22	all (35)	2.3	0.8	0.9, 3.6	2.0	0.7	0.9, 3.2	2.1	1.2, 3.9	2.1	1.1, 4.0
	All (29)	1.9	0.7	0.8, 3.1	1.7	0.5	0.9, 2.5	1.8	1.0, 3.2	1.7	1.0, 2.9
25	Single use (6)	2.1	1.1	-0.1, 4.2				1.8	0.6, 5.3		
	Re-use (23)	1.9	0.5	0.9, 2.8	1.7	0.4	1.1, 2.4	1.8	1.1, 2.6	1.7	1.1, 2.6
28	All (24)	2.2	1.2	0.1, 4.2	1.8	1.0	0.2, 3.4	1.9	0.8, 4.7	1.8	0.8, 4.2
	Single use (6)	3.3	1.2	1.0, 5.6				3.2	1.7, 6.1		
	Re-use (18)	1.8	0.9	0.2, 3.4	1.4	0.6	0.4, 2.4	1.6	0.7, 3.6	1.5	0.6, 3.5
All days	All (88)	2.1	0.9	0.6, 3.6	1.9	0.7	0.7, 3.0	2.0	1.0, 3.8	1.9	1.0, 3.9
	Single use (47)	2.4	0.9	0.8, 4.0	2.1	0.8	0.8, 3.5	2.1	1.2, 3.9	2.1	1.1, 4.0
	Re-use (41)	1.8	0.7	0.6, 3.1	1.6	0.5	0.8, 2.4	1.7	0.9, 3.2	1.7	0.9, 3.0

^a lower and upper limits of the CI_{95} that are outside than the range of values obtained experimentally are shown in grey.

IV.6.4 – Effect of cell monolayer re-use and multiple time sampling on LY transport

Table IV. S4 Statistical analysis of LY Permeability (P_{app}) and amount of LY transported into the acceptor compartment (Q_A (%)) for all the conditions tested. The average and standard deviation, and the corresponding confidence intervals at 95 % confidence (CI_{95}), were obtained directly from the analysis of $\text{Log}(P_{app})$ or $\text{Log}(Q_A)$. The numbers in grey correspond to limits of the confidence intervals that are outside the range of experimentally obtained values.

Day	Assay Conditions		LY P_{app} (10^{-7} cm/s)		LY Q_A (%)	
	Sampling (N)	Monolayer use	μ	CI_{95}	μ	CI_{95}
all	all (346)	Single use & re-use	7.0	1.4, 34.1	0.23	0.09, 0.61
	all 1 st (153)		4.0	0.8, 19.8	0.19	0.08, 0.44
	1 st 60 min (88)		2.0	1.0, 3.8	0.20	0.10, 0.39
	1 st 10 min (65)		10.5	3.8, 29.1	0.18	0.06, 0.49
	2 nd 10 min (66)		12.8	4.4, 36.7	0.21	0.07, 0.62

Re-use of Caco-2 monolayers – integrity validation

	3 rd 10 min (62)		14.9	5.9, 38.1	0.25	0.10, 0.64	
	4 th 30 min (62)		7.0	2.7, 18.1	0.35	0.14, 0.91	
	all (144)		9.4	1.8, 47.7	0.30	0.13, 0.71	
	all 1 st (62)		5.0	0.9, 28.2	0.23	0.12, 0.43	
22	1 st 60 min (35)	Single use	2.1	1.2, 3.9	0.21	0.12, 0.39	
	1 st 10 min (27)		14.9	7.6, 29.2	0.25	0.13, 0.49	
	2 nd 10 min (28)		17.6	8.0, 38.5	0.29	0.13, 0.65	
	3 rd 10 min (26)		22.0	11.1, 43.6	0.37	0.19, 0.72	
	4 th 30 min (28)		9.5	3.9, 23.0	0.48	0.20, 1.16	
	all (117)		7.3	1.6, 33.9	0.23	0.11, 0.50	
	all 1 st (51)	Single use & re-use	4.0	0.8, 20.7	0.18	0.10, 0.34	
	1 st 60 min (29)		1.8	1.0, 3.2	0.18	0.10, 0.32	
	1 st 10 min (22)		11.2	5.5, 22.9	0.19	0.09, 0.38	
	2 nd 10 min (22)		14.9	7.0, 32.0	0.25	0.12, 0.54	
	3 rd 10 min (22)		14.8	7.3, 30.0	0.25	0.12, 0.50	
	4 th 30 min (22)		7.1	3.9, 13.0	0.36	0.20, 0.66	
25	all 1 st (12)	Single use	3.6	0.8, 16.3	0.15	0.06, 0.35	
	1 st 60 min (6)		1.8	0.6, 5.4	0.18	0.06, 0.54	
	1 st 10 min (6)		7.3	4.3, 12.4	0.12	0.07, 0.21	
	2 nd 10 min (6)		11.3	5.9, 21.8	0.19	0.10, 0.37	
	3 rd 10 min (6)		11.7	5.0, 27.6	0.20	0.08, 0.46	
		4 th 30 min (6)		6.1	3.6, 10.3	0.31	0.18, 0.52
		all 1 st (39)	re-use	4.1	0.7, 23.3	0.20	0.12, 0.33
		1 st 60 min (23)		1.8	1.1, 2.9	0.18	0.11, 0.29
		1 st 10 min (16)		13.2	7.6, 35.8	0.22	0.13, 0.39
		2 nd 10 min (16)		16.5	7.6, 35.8	0.28	0.13, 0.60
	3 rd 10 min (16)	16.2		8.5, 31.0	0.27	0.14, 0.52	
	4 th 30 min (16)		7.5	3.9, 14.4	0.38	0.20, 0.73	
28	all (86)	Single use & re-use	4.1	1.3, 13.5	0.14	0.05, 0.37	
	all 1 st (40)		2.9	0.8, 10.4	0.14	0.05, 0.44	
	1 st 60 min (24)		1.9	0.8, 4.7	0.19	0.08, 0.47	
	1 st 10 min (16)		5.4	1.9, 15.7	0.09	0.03, 0.26	
	2 nd 10 min (16)		5.9	2.6, 13.6	0.10	0.04, 0.23	
	3 rd 10 min (14)		7.6	4.4, 13.1	0.13	0.07, 0.22	

4 th 30 min (16)	Single use	4.1	1.7, 9.6	0.20	0.09, 0.48	
all 1 st (12)		5.2	1.5, 18.8	0.22	0.07, 0.68	
1 st 60 min (6)		3.2	1.7, 6.1	0.32	0.17, 0.62	
1 st 10 min (6)		8.7	2.5, 30.2	0.15	0.04, 0.51	
2 nd 10 min (6)		8.2	3.0, 22.2	0.14	0.05, 0.37	
3 rd 10 min (6)		8.7	4.8, 15.6	0.15	0.08, 0.26	
4 th 30 min (6)		4.7	2.4, 9.3	0.24	0.12, 0.47	
all 1 st (28)		2.2	0.8, 6.6	0.12	0.04, 0.33	
1 st 60 min (18)		1.6	0.7, 3.6	0.16	0.07, 0.36	
1 st 10 min (10)		re-use	4.1	2.0, 8.4	0.07	0.03, 0.14
2 nd 10 min (10)			4.9	2.6, 9.1	0.08	0.04, 0.15
3 rd 10 min (8)			6.8	4.0, 11.7	0.11	0.07, 0.20
4 th 30 min (10)	3.7		1.3, 10.2	0.19	0.07, 0.51	

The average and standard deviation of the cumulative amount of LY that reaches the acceptor compartment is represented in Figure IV. S2, for cell monolayers used on days 22, 25 and 28.

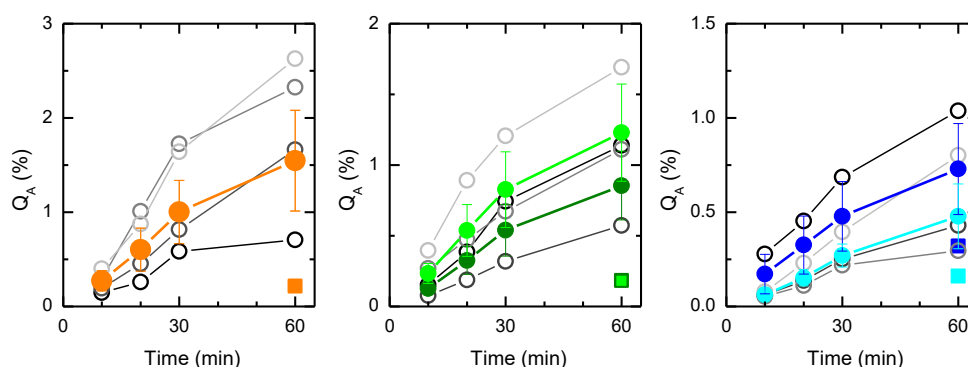
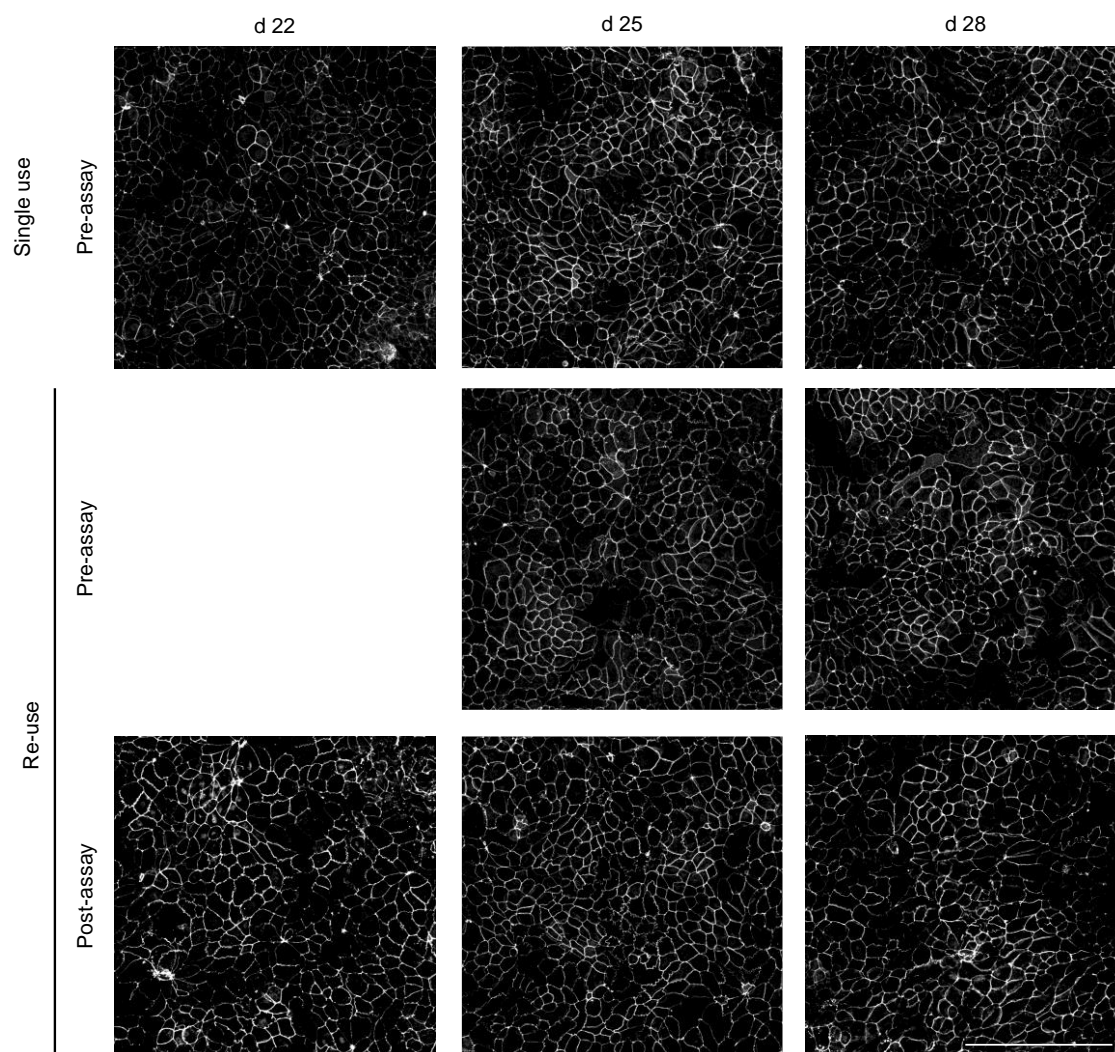


Figure IV. S2 Cumulative amount of LY that reaches the acceptor compartment for permeability experiments performed with multiple time sampling (circles) or with a single time sampling (squares) on cell monolayers at day 22 (left), 25 (middle) and 28 (right) post-seeding. On days 25 and 28, the results obtained for cell monolayers used in a single permeability experiment are shown in dark colours, and those obtained for re-used cell monolayers are in light colours. The average and standard deviation obtained for all assays in a given condition are shown as filled symbols and thick lines, and some representative results obtained for individual cell monolayers are shown by open symbols and thin lines.

Re-use of Caco-2 monolayers – integrity validation

IV.6.5 – Effect of the day post-seeding and re-use on morphological features and integrity of the cell monolayer



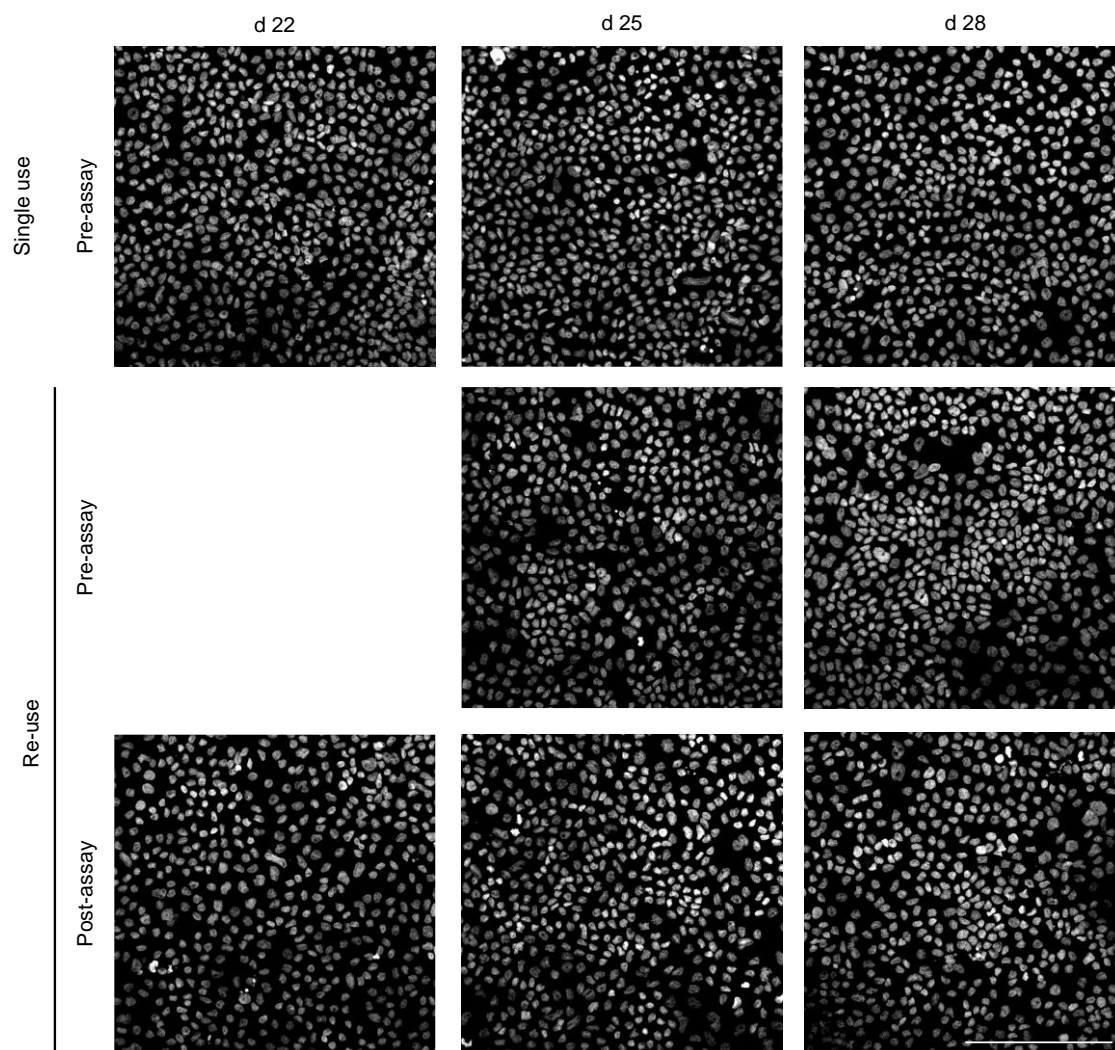


Figure IV. S3 Confocal microscopy images of Caco-2 monolayers stained for ZO-1 (top picture) and nuclei (bottom picture). Representative images for cell monolayers at day 22, 25 and 28 are shown in the left, middle and right panels, respectively. In the upper plots the monolayer was not used in permeability assays, while in the additional plots the monolayers were previously used. The lower plots correspond to monolayers immediately after the LY permeability assay, and in the middle plots the images correspond to cell monolayers that were maintained in culture media for two days after the permeability assay. Images are a maximum intensity projection of 8-9 z-stacks, scale bar 200 μm .

Re-use of Caco-2 monolayers – integrity validation

IV.6.6 – Effect of cell batch, passage number and day post-seeding on TEER and LY transport

Table IV. S5 Inter-variability between cell batches and passages regarding TEER values before the permeability assay and amount of LY transported during the first sampling interval (60 or 10 min for single or multi-time sampling, respectively).

Day	Cell conditions		Monolayer use	Sampling	Q _A (%) ^a		TEER (kΩ cm ²)	
	Batch	Passage Number			μ	CI ₉₅	μ	CI ₉₅ ^b
22	1	95	Single	One-time	0.18	0.12, 0.28	1.35	0.59, 2.11
	1	98			0.19	0.11, 0.31	1.10	-0.08, 2.29
	1	100		Multi-time	0.36	0.23, 0.56	1.06	0.63, 1.49
	1	104			0.16	0.07, 0.34	0.82	0.22, 1.42
	1	105		One-time	0.22	0.13, 0.36	1.27	0.80, 1.74
	2	95			0.27	0.19, 0.38	0.53	0.15, 0.90
	2	98		One-time	0.30	0.13, 0.72	0.67	-0.69, 2.02
	3	95			0.19	0.08, 0.43	0.87	0.18, 1.56
	1	95			0.13	0.04, 0.42	1.19	-0.15, 2.52
	25	1		95	Single	One-time	0.21	0.10, 0.44
1		98	Single	0.10	0.05, 0.21		1.31	0.33, 2.30
1		100	Re-use	Multi-time	0.25	0.15, 0.43	0.80	-0.18, 1.77
1		104	Single		0.14	0.08, 0.25	0.87	-0.05, 1.79
1		105	Re-use	One-time	0.20	0.11, 0.38	0.84	0.30, 1.38
2		95	Re-use		0.16	0.11, 0.22	0.96	0.67, 1.25
2		98	Single	One-time	0.25	0.07, 0.87	0.51	-0.27, 1.28
3		95	Re-use		0.19	0.14, 0.26	0.95	0.34, 1.57
1		95	Single		0.39	0.17, 0.90	1.35	1.03, 1.67
28		1	95	Re-use	One-time	0.33	0.19, 0.59	1.59
	1	98	Single	0.09		0.03, 0.26	1.27	0.19, 2.36
	1	100	Re-use	Multi-time	0.09	0.02, 0.38	1.42	0.44, 2.39
	1	104	Single		0.23	0.08, 0.69	1.29	0.02, 2.56
	1	105	Re-use	One-time	0.06	0.04, 0.09	1.44	0.43, 2.45
	2	95	Re-use		0.11	0.06, 0.22	0.98	0.62, 1.35
	2	98	Single	One-time	0.26	0.18, 0.37	1.11	-0.23, 2.45
	3	95	Re-use		0.17	0.10, 0.27	0.96	0.52, 1.41

^a μ and CI₉₅ calculated from the statistical parameters obtained for LogQ_A.

^b lower and upper limits of the CI₉₅ that are outside than the range of values obtained experimentally are shown in grey.

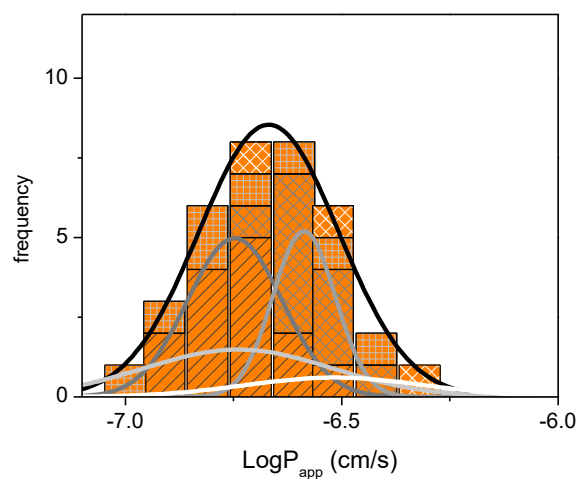
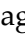
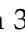
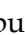



Figure IV. S4 Distribution of $\text{Log}P_{\text{app}}$ obtained on permeability assays with a 60 min sampling for cell monolayers from different batches and distinct passage numbers, at day 22 post-seeding: passage 95 with cell batch 1, ; passage 95 with cell batch 2, ; passage 95 with cell batch 3, ; and passage 98 with cell batch 2, . The lines are the best fit of a Normal distribution with the colours dark grey, grey, light grey and white, respectively. The black line is the best fit to the cumulative results at all cell passage numbers and batches.

Re-use of Caco-2 monolayers – integrity validation

IV.6.6.1 – Multivariate analysis

Table IV. S6 Multivariate analysis (MVA) to evaluate the correlation between the variables TEER (before and after the permeability assay) or the amount of LY transported into the acceptor compartment (QA) with the distinct experimental variables. The results obtained when this statistical analysis was performed for Papp were equivalent to those obtained for QA.

Independent Variables considered	TEER ($\Omega \text{ cm}^2$)						Q _A (%)			P _{app} (cm/s)		
	before assay			after assay			Coefficient	CI ₉₅	P-value	Coefficient	CI ₉₅	P-value
	Coefficient	CI ₉₅	P-value	Coefficient	CI ₉₅	P-value						
Cell batch	-317	-437, -196	<0.0001	-101	-205, 3	0.06	-2×10^{-2}	$(-5, 1) \times 10^{-2}$	0.29	-4×10^{-9}	$(-1, 1) \times 10^{-7}$	0.95
Cell passage	-12	-48, 23	0.49	-21	-49, 7	0.14	-3×10^{-3}	$(-1, 0.5) \times 10^{-2}$	0.49	-3×10^{-8}	$(-6, 0.4) \times 10^{-8}$	0.08
Day post-seeding	29	-6, 65	0.11	12	-17, 41	0.40	-7×10^{-3}	$(-2, 0.06) \times 10^{-2}$	0.07	-7×10^{-8}	$(-1, -0.3) \times 10^{-7}$	0.0002
Re-use	67	-110, 245	0.46	83	-59, 226	0.25	-3×10^{-2}	$(-7, 1) \times 10^{-2}$	0.16	2×10^{-8}	$(-1, 2) \times 10^{-7}$	0.78
Sampling time points	-162	-468, 144	0.29	141	-103, 386	0.26	-5×10^{-3}	$(-7, 6) \times 10^{-2}$	0.89	1×10^{-6}	$(0.9, 1) \times 10^{-6}$	<0.0001
TEER before assay				0.28	0.15, 0.42	<0.0001	-2×10^{-5}	$(-6, 2) \times 10^{-5}$	0.28	-8×10^{-11}	$(-2, 0.9) \times 10^{-10}$	0.36
TEER after assay							-7×10^{-5}	$(-5, 4) \times 10^{-5}$	0.77	5×10^{-11}	$(-2, 2) \times 10^{-10}$	0.65

Data analysed corresponds to 152 permeability assays. CI₉₅ is the confidence interval at 95 % confidence, *p*-values <0.05 are in bold.

Re-use of Caco-2 monolayers – integrity validation

IV.6.7 – Quantitative analysis of the monolayer images obtained by confocal microscopy

A very large number of cell monolayers (N=52) have been characterized by confocal fluorescence microscopy to evaluate the effect of the distinct conditions on the morphology of Caco-2 monolayers. The nuclei were stained with Hoechst 33342, and the tight junction protein ZO-1 was stained with rabbit polyclonal primary antibody and Cy3 goat anti-rabbit IgG. A quantitative analysis of the confocal images has been performed using ImageJ software, and the corresponding average and standard deviation for the cell density and area occupied by nuclei and ZO-1 is shown in Table IV. S7. A multivariate analysis was also performed for this set of data (including the cell batch and passage number, day post-seeding, cell monolayer use and sampling conditions, as well as the corresponding TEER values and amount of LY transported) and is shown in Table IV. S8.

Effect of days post-seeding

At day 22 post-seeding, a total of 7 independent cell monolayers were characterized by confocal microscopy before the execution of any permeability assay. It is observed that the number of nuclei in the area analysed ($1.8 \times 10^5 \mu\text{m}^2$, typically in the central area of the filter, selected to be representative of the cell monolayer after visualization of the total area of the filter) varies significantly, being 570 ± 136 , leading to a cell density of $3.1 (\pm 0.7) \times 10^5 \text{ cm}^{-2}$. The area occupied by the nuclei increases with the number of nuclei but not proportionally (the same behaviour is observed for the dependence of the fluorescence intensity from the stained nuclei due to the application of a threshold in the quantitative analysis of the image, to overcome differences in the staining efficiency). The non-proportionality between the area occupied and the number of nuclei indicates that the shape of the cell adjusts to the cell density in the monolayer, becoming wider or thicker in cell monolayers with lower or higher cell density respectively. A positive correlation is observed between the TEER value and the cell density ($R^2 = 0.82$, Figure IV. S5), most likely due to an increase in the cell monolayer thickness. A very small correlation was however observed between the number of z-stacks required to account for the thickness of the cell monolayer (8 ± 2) and the cell density ($R^2 = 0.1$).

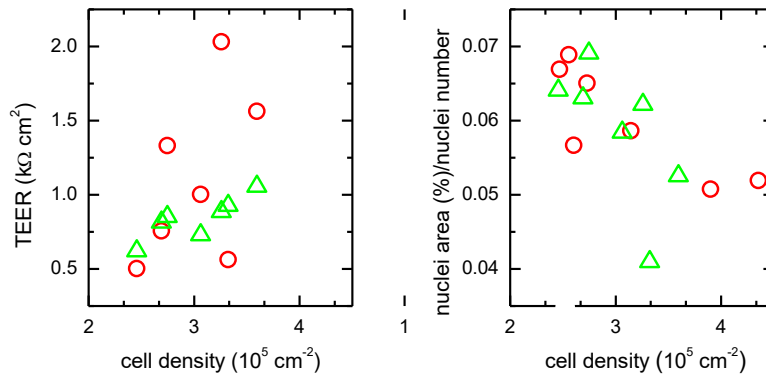


Figure IV. S5 Correlation between the TEER value (left plot) and normalized nuclei area (right plot), with the cell density for monolayers on day 22 post-seeding, before (○) and after (△) the execution of a LY permeability assay.

The 3 cell monolayers characterized at day 25 post-seeding (that were not previously used in permeability assays, table row single use/before) show a very small increase in the cell density ($\Delta\mu=4\%$), essentially no variation in the area occupied by the nuclei ($\Delta\mu=-1\%$), but a very significant increase in the area occupied by tight junctions (from stained ZO-1, ($\Delta\mu=80\%$). At day 28, the cell density and the area occupied by the nuclei in the 4 cell monolayers characterized is essentially the same observed on day 22 and 25. The area occupied by tight junctions is higher than that observed at day 22, but smaller than at day 25.

The variations observed along the days post-seeding suggest that the expression of ZO-1 increases over time, which is consistent with the small decrease observed in LY permeation and the increase in TEER. However, the variations observed are relatively small when compared to the variability at a given condition, leading to differences that are not statistically significant (see Table IV. S8).

Effect of the execution of a single permeability assay

The cell monolayers analysed after the execution of a LY permeability assay on day 22 post-seeding (3 for single time and 4 for multiple time sampling) show morphological characteristics very similar to those observed for unused cell monolayers. For single time sampling the cell density shows a small decrease which is not statistically significant and essentially no variation is observed in the cell monolayers subject to multiple time sampling. This indicates that the execution of the

Re-use of Caco-2 monolayers – integrity validation

permeability assay does not lead to significant detachment of cells from the filter. As observed for unused cell monolayers, there is a strong correlation between the value of TEER measured after the permeability assay and the cell density ($R^2 = 0.9$). The area occupied by tight junctions is 9 % smaller in the cell monolayers used on single time permeability assays, in agreement with the lower cell density. This variation is however smaller than the standard deviation observed in each condition and is therefore not statistically significant. When the cell monolayers from the same batch and passage number are compared, it is usually observed a small decrease in the cell density after the execution of the permeability assay (5 out of 7 independent sets), although a small increase is observed in two sets. A very high variability is observed in the area occupied by the tight junctions when pairs of monolayers are compared (increase or decrease) with the average values showing a small effect of the execution of the permeability assay. This highlights the difficulty in the quantification of the stained ZO-1, where a continuous network may be visible in the confocal images but which displays very large variations in the fluorescence intensity. This difficulty may be related with inhomogeneities in the cell monolayer staining, due to the slow dynamics of the strong interactions established (between the antibody and ZO-1, and between these and the fluorescent antibody).

When compared with cell monolayers on day 25 before the permeability assay, the confocal images of cell monolayers after execution of a single permeability assay with single time sampling show a decrease in the number of nuclei ($\Delta\Delta\mu = -33\%$), in the area occupied by the nuclei ($\Delta\Delta\mu = -15\%$) and by tight junctions ($\Delta\Delta\mu = -55\%$). It should however be noted that although the execution of the permeability assay leads to a decrease in the area occupied by tight junctions, this parameter is still higher than that observed on day 22 post-seeding ($\Delta\mu = 5\%$). Equivalent results are observed for multiple time sampling, and a very similar behaviour is observed for cell monolayers on day 28 post-seeding.

Globally, the results show that the execution of a permeability assay tends to decrease the number of cells in the monolayer and the area occupied by tight junctions, but that those effects are smaller than the variability within each condition, and thus not statistically significant.

Effect of cell monolayer re-use

The very high variability observed in the cell density and the relatively small number of cell monolayers characterized, does not allow the establishment of correlations between this morphological property and the re-use of the cell monolayer. Some tendencies are however observed which are discussed below. The cell density of the cell monolayers after two full days in culture media is usually similar to (or higher than) the density observed for cell monolayers at the same day post-seeding that were not previously used in permeability assays. This shows that the cell monolayer recovers from the small decrease observed after the execution of the permeability assay. The variations observed in the area occupied by tight junctions are also very small and always within the variability observed within each set of conditions. An interesting observation is that the variations induced by the execution of the permeability assay seems to be smaller for re-used cell monolayers than for cells used on a single permeability experiment.

Effect of the sampling time points

Given the small decrease (although not statistically significant) observed in the cell density and area occupied by nuclei and tight junctions after the execution of the permeability assay, one could expect a higher effect for a larger number of sampling time points. This is not however observed in the cell monolayers characterized in this work. In fact, the effects observed when using multiple time sampling are smaller than when using only single time sampling. The differences are however within the uncertainty of the variables and are not statistically significant.

Multivariate Analysis

The multivariate analysis performed on the set of cell monolayers characterized by confocal microscopy is shown in Table IV. S8. All conditions have been included in the statistical analysis. No strong correlations were observed between the different parameters, with p -values being always larger than 0.05. Correlations with p -value < 0.2 are nevertheless identified and discussed below.

The number of nuclei in the area analyzed shows a positive correlation with the total area occupied by nuclei, and for cell monolayers used in permeability assays it

Re-use of Caco-2 monolayers – integrity validation

also shows a positive correlation with the TEER value of the monolayer. Those correlations were already discussed above, when analyzing the results obtained for day 22. The MVA shows that a weak correlation is also observed for cell monolayers at all days post-seeding and all conditions of the permeability assay. No correlation was observed between the cell density and the TEER value before the permeability assay (including the cell monolayers characterized before the permeability assay). In fact, no correlation was also observed between TEER before and after the permeability assay, although a strong correlation is observed when the complete set of permeability experiments is considered (Table IV. S6, $p < 0.001$). This reflects the extremely large variability in the TEER value measured for the cell monolayers, that is statistically not well described by the relatively small set of cell monolayers characterized by confocal microscopy.

The area occupied by the nuclei shows the expected positive correlation with the cell density and a weak negative correlation with the cell passage number.

The area occupied by tight junctions (as seen by ZO-1 staining) shows a positive correlation with the sampling used in the permeability assay, being higher for cell monolayers used in multiple time sampling.

Re-use of Caco-2 monolayers – integrity validation

Table IV. S7 Cell density and fractional area occupied by nuclei (stained with Hoechst 33342), and by tight junctions (from ZO-1 staining with a rabbit polyclonal antibody and Cy3 goat anti-rabbit IgG), for images obtained by confocal microscopy (428×428 μm²) of cell monolayers in different conditions: not used on permeability assays, before re-use in permeability assays after incubation in culture media for two full days, and immediately after a permeability assay with one-time sampling (60 min) or multi-time sampling (10, 20, 30, and 60 min). The images were analyzed using the software Image J. Each image was manually threshold to select nuclei or ZO-1 only fluorescence.

Day	Monolayer use	Permeability assay conditions (N) ^a	Nuclei						ZO-1		
			Cell density (x 10 ⁵ cm ⁻²)			Area (%)			Area (%)		
			μ ± σ	Δμ (%) ^b	ΔΔμ (%) ^c	μ ± σ	Δμ (%) ^b	ΔΔμ (%) ^c	μ ± σ	Δμ (%) ^b	ΔΔμ (%) ^c
22	Single	Before (7)	3.1 ± 0.7			33 ± 5			6 ± 2		
		One-time (3)	2.8 ± 0.4	-9	-9	34 ± 4	1	1	6 ± 2	-9	-9
		Multi-time (4)	3.2 ± 0.4	2	2	31 ± 4	-8	-8	7 ± 3	4	4
25	Single	Before (3)	3.2 ± 0.8	4	4	33 ± 7	-1	-1	12 ± 5	80	80
		One-time (2)	2.2 ± 0.1	-30	-33	28 ± 2	-15	-15	5 ± 2	-20	-55
		Multi-time (2)	2.7 ± 0.3	-13	-16	30 ± 5	-9	-9	7 ± 1	5	-42
25	Re-use	Before One-time (3)	4.6 ± 2	48	63	38 ± 5	15	14	8 ± 2	31	44
		Before Multi-time (3)	3.0 ± 0.4	-4	-6	33 ± 3	-1	7	8 ± 1	28	23
		One-time (3)	4.5 ± 1	44	-3	39 ± 6	18	3	9 ± 3	43	9
		Multi-time (3)	3.0 ± 0.1	-4	1	32 ± 5	-3	-2	9 ± 2	33	4
28	Single	Before (4)	3.0 ± 0.1	-3	-7	32 ± 7	-4	-4	8 ± 2	25	-31
		One-time (2)	2.8 ± 0.1	-11	-8	34 ± 3	1	5	6 ± 2	1	-19
		Multi-time (2)	2.7 ± 0.3	-12	-10	29 ± 4	-14	-10	7 ± 1	7	-14
28	Re-use	Before One-time (3)	3.3 ± 0.7	7	-26	39 ± 4	16	-2	6 ± 1	-11	-37
		Before Multi-time (3)	3.4 ± 0.6	8	12	35 ± 9	6	9	8 ± 2	30	-2
		One-time (2)	3.1 ± 0.6	1	-5	39 ± 10	18	2	5 ± 2	-28	-19
		Multi-time (3)	3.0 ± 0.1	-2	-9	33 ± 2	0	-6	8 ± 1	20	-8

^a number of cell monolayers characterized. ^b Percent variation relative to the first condition analysed (day 22 post-seeding, before any permeability assay). ^c Percent variation relative to the condition immediately before (e.g. single use before day 25 *vs* single use before 22, one-time/multi-time *vs* before in the same condition, re-use one-time/multi-time at day 25 before *vs* after one-time/multi-time at day 22).

Chapter III

Table IV. S8 Multivariate analysis (MVA) of the cell monolayers whose morphological characteristics have been characterized by confocal microscopy. The total number of cell monolayers in this analysis is 52, including cells from batches 1 and 2, in passage numbers 95 to 105, days post-seeding 22, 25 and 28 (single use and re-use), and one-time or multiple sampling (see Table IV. S7 for the number of cell monolayers in each condition).

	TEER ($\Omega \text{ cm}^2$)						QA (%)			Cell density (cm^{-2})			Nuclei Area (%)			ZO-1 Area (%)		
	Before assay			After assay			Coefficient	CI ₉₅	P-value	Coefficient	CI ₉₅	P-value	Coefficient	CI ₉₅	P-value	Coefficient	CI ₉₅	P-value
	Coefficient	CI ₉₅	P-value	Coefficient	CI ₉₅	P-value												
Cell batch	-3×10^2	$(-9, 1) \times 10^3$	0.19	-1×10^2	$(-6, 4) \times 10^2$	0.64	-6×10^{-2}	$(-2, 1) \times 10^{-1}$	0.50	-5×10^4	$(-1, 0.3) \times 10^5$	0.23	-3	-9, 4	0.39	2	-2, 6	0.24
Cell passage	3×10^1	$(-3, 8) \times 10^2$	0.37	-1×10^1	$(-8, 5) \times 10^1$	0.75	1×10^{-2}	$(-1, 4) \times 10^{-2}$	0.31	7×10^3	$(-0.4, 2) \times 10^3$	0.20	-0.6	-1, 0.2	0.12	-0.2	-0.8, 0.3	0.45
Day post-seeding	5×10^1	$(-0.05, 1) \times 10^2$	0.07	-1×10^1	$(-7, 5) \times 10^1$	0.69	-1×10^{-3}	$(-2, 2) \times 10^{-2}$	0.93	-6×10^3	$(-2, 0.4) \times 10^4$	0.21	-1×10^{-2}	-0.8, 0.7	0.97	-0.09	-0.6, 0.4	0.72
Re-use	-3×10^1	$(-3, 3) \times 10^3$	0.85	8×10^2	$(-3, 5) \times 10^2$	0.63	-1×10^{-1}	$(-2, 0.3) \times 10^{-1}$	0.13	4×10^4	$(-3, 9) \times 10^4$	0.17	2	-2, 7	0.31	1	-2, 4	0.42
Sampling time points	-4×10^2	$(-1, 0.1) \times 10^3$	0.12	-1×10^2	$(-7, 4) \times 10^2$	0.59	-2×10^{-1}	$(-4, 0.5) \times 10^{-1}$	0.12	-6×10^4	$(-2, 0.5) \times 10^5$	0.27	-1	-9, 6	0.79	3	-2, 8	0.18
Cell density	3×10^{-3}	$(-0.05, 5) \times 10^{-3}$	0.05	2×10^{-3}	$(-7, 5) \times 10^{-3}$	0.13	-1×10^{-7}	$(-1, 1) \times 10^{-6}$	0.83				3×10^{-5}	$(-0.9, 7) \times 10^{-5}$	0.12	9×10^{-6}	$(-2, 4) \times 10^{-5}$	0.49
Nuclei Area	1×10^1	$(-2, 5) \times 10^1$	0.39	-2×10^1	$(-5, 2) \times 10^1$	0.40	1×10^{-2}	$(-0, 3) \times 10^{-2}$	0.05	5×10^3	$(-0.2, 1) \times 10^4$	0.12				0.01	-0.3, 0.3	0.93
ZO-1 Area	4	$(-5, 6) \times 10^1$	0.89	-2×10^1	$(-8, 4) \times 10^1$	0.42	9×10^{-3}	$(-1, 3) \times 10^{-2}$	0.41	4×10^3	$(-0.7, 1) \times 10^4$	0.49	0.03	-0.8, 0.9	0.93			
TEER before assay				2×10^{-2}	$(-3, 3) \times 10^{-1}$	0.75	-8×10^{-5}	$(-2, 0.2) \times 10^{-4}$	0.11	2×10^1	$(-4, 8) \times 10^1$	0.34	2×10^{-3}	$(-2, 6) \times 10^{-3}$	0.41	3×10^4	$(-2, 3) \times 10^{-3}$	0.77
TEER after assay							4×10^{-5}	$(-2, 2) \times 10^{-4}$	0.66	7×10^1	$(-0.2, 2) \times 10^2$	0.14	-3×10^{-3}	$(-1, 0.4) \times 10^{-3}$	0.40	-2×10^{-3}	$(-6, 3) \times 10^{-3}$	0.42

Re-use of Caco-2 monolayers – integrity validation

Chapter V

Re-use of Caco-2 monolayers for a higher throughput assessment of compounds permeability — initial validation regarding cell properties

V.1 – Abstract

Evaluation of drug permeability using cell monolayers is an important *in vitro* assay in the process of drug development, with the identification of compounds with favorable pharmacokinetics that may proceed to *in vivo* studies. When allowed to grow and differentiate on permeable filters for at least 21 days, monolayers of Caco-2 cells develop morphological and functional properties similar to those of the intestinal epithelium, which are maintained up to day 30. Permeability through Caco-2 monolayers is thus particularly relevant in the assessment of drug absorption after oral administration. The major drawback of this assay is its very low throughput, with the cell monolayers being used in a single permeability assay. We have previously proposed a protocol to allow the re-use of the cell monolayer on additional permeability assays during the stable period, and shown that the cell monolayer integrity is maintained when assessed by Lucifer Yellow permeability and TEER.

In this work we evaluate the effect of re-use on the permeability of several reference compounds that permeate through passive (paracellular and transcellular) and carrier-mediated routes. The cell monolayers were used in permeability assays on day 22 post-seeding, and re-use on days 25 and 28 after incubation with culture media for two full days between permeability assays. With more than 300 monolayers being analyzed, the results show that the cell monolayers can be re-used for evaluation of the permeability of passive permeating compounds when following the proposed regeneration protocol. Preliminary data was obtained regarding the maintenance of functional properties of transporters in cell monolayers during the re-use period. Once complete validated for all the transport routes, the re-use methodology can be potentially used to triplicate the throughput of drug permeability assessments.

V.2 – Introduction

The prediction of pharmacokinetics is a major step in drug development as it determines drug availability at the target site. In the assessment of this property, the well-established Caco-2 model is one of the most extensively used *in vitro* cell based assay, before proceeding to studies using animal models [61,63,107]. A major limitation of this model is its low throughput. When following

the standard procedure [128], Caco-2 cells must be maintained in a permeable filter for at least 21 days to attain a confluent and fully differentiated cell monolayer, and are used in a single permeability assay during their stable period (days 21 to 30 after cell seeding) [112,113]. Moreover, this assay has a reduced screening capacity (12 wells per plate) and high implementation costs (media renewals, Transwell™ inserts, and human resources) that also contributes to its low throughput [60,91].

An approach to increase the throughput of the standard assay is to re-use the Caco-2 monolayer in additional permeability assays during its stable period. This has been explored by us and it was shown that incubation of the cell monolayer in culture medium for two full days after the permeability assay is required and sufficient for the re-establishment of cell monolayer integrity (see Chapter IV and ref [211]). This would allow the use of the cell monolayers for three permeability assays during the period where their morphological and functional characteristics are maintained (between day 21 to day 30 [112,113]). An important advantage of this approach is that the standard protocol is followed for the preparation of the cell monolayer [128], thus allowing a quantitative comparison of the permeability coefficients obtained with the extensive data available in literature. More than just a need to increase throughput, the re-use of Caco-2 monolayers is also an obligation to reduce resources, fully aligned with the 3 R's principles. However, before this procedure may become an established methodology, it is first necessary to guarantee that the preservation of the cell monolayer integrity is accompanied by the maintenance of other functional properties of the Caco-2 monolayers.

In this work, a more extensive evaluation of the effect of the re-use protocol on distinct cell properties is performed, using compounds that are transported passively through paracellular and transcellular pathways, as well as through carrier-mediated influx and efflux pathways.

The permeability of a test set of compounds was characterized on days 22, 25 and 28 post-seeding, both for cell monolayers used in a single permeability assay or re-used following the regeneration protocol proposed by us. The following reference compounds were selected to evaluate the effects on passive permeation pathways: (1) sodium fluorescein and atenolol, to complement the results previously obtained with the paracellular marker Lucifer Yellow; and (2) the positively and negatively charged drugs propranolol and salicylic acid, to assess the effects on transcellular permeation.

Re-use of Caco-2 monolayers – cell properties validation

Carrier-mediated transport pathways were also evaluated, noting the presence of several transporters in the apical and basolateral membranes of Caco-2 monolayers that may contribute to the influx or efflux of solutes [76,212]. Among the influx carriers, we selected the hexoses transporters due to the existence of glucose analogues with a fluorescence label that may allow the evaluation of the glucose permeation in a high throughput manner. The analogue of D-glucose 2-[N-(7-nitrobenz-2-oxa-1,3-diazol-4-yl) amino]-2-deoxy-D-glucose (2-NBDG) has been increasingly used in several cell lines to study glucose absorption and to evaluate the effect of bioactive compounds from plant extracts on glucose absorption [84,213]. After incubating the cells with 2-NBDG, its uptake is usually determined by measuring the fluorescence of 2-NBDG using a microplate reader, flow cytometer and microscopy imaging [214]. It has been suggested that the transport of 2-NBDG across the apical membrane of Caco-2 monolayers occurs mainly through the sodium dependent glucose transporter (SGLT1) and glucose transporters (GLUTs), similarly to D-glucose transport [213,215,216]. The specificity of these transporters to 2-NBDG was in fact demonstrated by inhibition of its uptake by D-glucose [217] and phlorizin, an inhibitor of SGLTs [213,215,216,218]. Nevertheless, the quantitative characterization of 2-NBDG permeability across cell monolayers has not been reported.

Caco-2 permeability assays are often used to identify the involvement of carrier-mediated efflux, in particular by P-glycoprotein (P-gp) which is a member of the ATP binding cassette transporter family [219]. The P-gp mediated efflux of Rhodamine 123 (Rho) was selected due to its high fluorescence quantum yield, providing high sensitivity in the detection of P-gp transport activity in Caco-2 cells [220].

The analysis of the functional properties of glucose carriers and P-gp in Caco-2 monolayers during the re-use period was performed by measuring the transport of 2-NBDG and Rho in the apical-to-basolateral (A→B) and basolateral-to-apical (B→A) directions. To further examine the effect of re-use on P-gp-mediated efflux activity, the bi-directional transport of Rho was also assessed after pre-incubating the cell monolayers with the well-known P-gp inhibitor, Verapamil. Additionally, the expression of P-gp in the plasma membrane was characterized through binding of a FITC-conjugated anti-P-gp antibody and detection by flow cytometry.

The structure and some molecular descriptors of the test compounds used in this study are shown in Table III. 1 (Chapter III). More than 300 permeability

assays were performed across Caco-2 monolayers to quantitatively characterize the distinct cell properties when applying the re-use protocol. This is an initial study to validate the re-use, as it does not cover all the transporters and permeation routes (namely transcytosis) present in Caco-2 cells.

V.3 – Methods

The first permeability assay was performed for cell monolayer on day 22 post-seeding, and two additional assays were conducted using the same cell monolayer on days 25 and 28. At first sight, the handling of cells during and after the transport experiments under aseptic conditions may be seen as a disadvantage of re-use methodologies relative to the standard procedure. However, it is also a fact that every cell culture laboratory has already implemented these technical norms. The high throughput that will be given by this methodology largely compensates the time, effort, and availability at the flow laminar hood to perform the protocol under aseptic conditions. Several parameters were used as quality control of the monolayer's integrity to rule out possible toxicity after incubation with compounds and contaminations before perform the 2nd and 3rd assays: i) the TEER values of the cell monolayers measured at the beginning of the next permeability were similar or higher to those obtained before the first assay, and always higher than $200 \Omega \text{ cm}^2$; ii) the TEER value of a cell-free filter (subject to the same treatment of those with cells) was maintained; and iii) the paracellular marker (such as LY) was included in some of the tested solutions to evaluate simultaneously the cell monolayer integrity and the permeability of the compounds of interest.

All cultured cell monolayers achieved TEER values exceeding $200 \Omega \text{ cm}^2$ ($n=334$) both before and after the permeability assays. The transport of LY ($20 \mu\text{M}$), Flu ($20 \mu\text{M}$), atenolol ($25 \mu\text{M}$), Prop ($25 \mu\text{M}$) and SA ($25 \mu\text{M}$) was evaluated unidirectionally, in A→B direction. In the assays, the inserts were moved to new wells containing 1.2 ml of HBSS. The permeability assays were performed with either a single sampling at t_{60} and/or multiple samplings at t_{10} , t_{20} , t_{30} and t_{60} min.

To assess the functionality of transporters in the cell monolayers, the transport of 2-NBDG ($250 \mu\text{M}$) and Rho ($5 \mu\text{M}$) was studied in both A→B and B→A directions. The permeability assays were performed using samplings at t_{10} , t_{20} , t_{30} and t_{60} min for 2-NBDG and t_{20} , t_{40} , t_{60} , t_{80} , t_{100} , and t_{120} for Rho. A longer

Re-use of Caco-2 monolayers – cell properties validation

sampling period was chosen for Rho to avoid the appearance of experimental lag times in the permeability data resulting from the need of Rho to translocate into the inner leaflet of the plasma membrane before interaction with P-gp [221,222]. For the A→B assays, the inserts were moved to new wells containing 1.5 ml of the HBSS. For the B→A assays, samples were drawn from the apical side at the same time points and replaced with equivalent volumes of fresh HBSS solution.

The bi-directional transport of Rho was also evaluated after the pre-incubation of the cell monolayers with the well-known P-gp inhibitor, Verapamil. At the time of the experiment, the cell monolayers were incubated with 100 μM of Verapamil in both the apical (400 μL) and basolateral compartments (1200 μL) during 30 min. Then, the verapamil solution was removed and Rho alone in HBSS was added to the donor compartments to start the permeability assays. The receiver compartments solution consisted of pre-warmed HBSS.

Experiments were carried out at least in duplicate (wells per plate for the same cell preparation) and were independently repeated at least two times with different cell preparations. The mass balance was estimated between 90–100% for less lipophilic compounds (LY, Flu, atenolol, SA, 2-NBDG and Rho), and 70–80% for more lipophilic compounds (Prop).

The P_{app} values were statistically analyzed in terms of $\text{Log}P_{app}$, since it was previously shown that this is the variable that follows a normal distribution [15], as was in fact expected [28]. The average values and the 95% confidence intervals (CI₉₅) for P_{app} were calculated from the corresponding parameters for $\text{Log}P_{app}$ (Equation IV.1 in chapter IV). This statistical analysis was performed using Microsoft Excel.

Generally, the existence of carrier-mediated influx or efflux transport is evaluated through the calculation of the ratio between the P_{app} obtained in both directions (A→B, and B→A) according to Equation V.1:

$$\begin{aligned} \text{Efflux Ratio} &= \frac{P_{app}^{B \rightarrow A}}{P_{app}^{A \rightarrow B}} \\ \text{Influx Ratio} &= \frac{P_{app}^{A \rightarrow B}}{P_{app}^{B \rightarrow A}} \end{aligned} \tag{V.1}$$

An alternative approach to evaluate the contribution of active transport in is to explicitly consider that the observed P_{app} is the result of both passive (P_{app}^{PP}) and

active (P_{app}^{AE}) processes. For the case of active efflux, the observed permeability in both directions is given by Equation V.2:

$$\begin{aligned} P_{app}^{A \rightarrow B} &= P_{app}^{PP} - P_{app}^{AE} \\ P_{app}^{B \rightarrow A} &= P_{app}^{PP} + P_{app}^{AE} \end{aligned} \quad V.2$$

Rearranging Equation V.2, and assuming that the values of P_{app}^{PP} and P_{app}^{AE} are the same in both directions, it is possible to calculate the contribution from passive and active processes, Equation V.3:

$$\begin{aligned} P_{app}^{PP} &= \frac{P_{app}^{B \rightarrow A} + P_{app}^{A \rightarrow B}}{2} \\ P_{app}^{AE} &= \frac{P_{app}^{B \rightarrow A} - P_{app}^{A \rightarrow B}}{2} \end{aligned} \quad V.3$$

This approach has the advantage that it allows evaluation of the effect of the tested condition on both the passive and active processes.

The cell monolayers used in the permeability assays with 2-NBDG were characterized by confocal microscopy to evaluate the localization of this glucose fluorescent analogue. This analysis included cell monolayers without being used for assays, and cell monolayers exposed to 250 μ M of 2-NBDG for 60 min during permeability assays in both the A \rightarrow B and B \rightarrow A directions. Orthogonal projections of the XZ-plane were created from all the z-slices to view in detail the localization of the fluorescence in the cell monolayers.

The level of P-gp expression at the apical membrane of cell monolayers was monitored by flow cytometry. Caco-2 monolayers at days 22, 25 and 28 post-seeding were prepared for analysis, using both cell monolayers not used in permeability assays and re-used. In the later, the permeability assay has been performed with 5 μ M Rho in the A \rightarrow B direction, and the cell monolayers were previously washed and maintained on culture media for 2 full days.

V.4 – Results and discussion

V.4.1 – Effect of re-use on the passive permeation of reference compounds after single-time and multi-time sampling permeability assays

Re-use of Caco-2 monolayers – cell properties validation

We have previously shown that cell monolayer integrity is maintained when Caco-2 monolayers are re-used in permeability assays on days 25 and 28 (after being used on day 22) and regenerated by incubation with culture medium between the assays. The maintenance of the monolayer integrity is the first requirement for the re-use of the cell monolayers. However, to validate the proposed protocol it is necessary to perform a systematic assessment regarding the effect of re-use on distinct properties of the Caco-2 monolayers. Towards this goal, in this study we evaluate the permeability of several reference compounds that are known to permeate passively or through carrier-mediated pathways (both influx and efflux). The solutes that permeate passively were divided in two sets, for low (mostly paracellular) and high (mostly transcellular) permeability coefficients. The permeability results of the test compounds through Caco-2 monolayers are shown in the next sections.

V.4.1.1 – Low passive permeability – Lucifer Yellow, Sodium fluorescein and atenolol

The results previously obtained with the effect of the sampling time and re-use of the Caco-2 monolayer on the permeability of the paracellular marker Lucifer Yellow (LY) in Chapter IV and [211] were complemented with new data obtained in this study and are shown in Figure V. 1. The results are presented in terms of $\text{Log } P_{\text{app}}$, because it has previously shown that this is the variable that follows a Normal distribution [211], as is in fact expected for kinetic parameters [200]. The large variability in P_{app} at each condition reflects the intrinsic variability of the Caco-2 model, the results corresponding to measurements in more than 10 independent cell preparations performed over 4 years by the same researcher and assay conditions.

As previously reported [211], no significant variation is observed in the LY P_{app} with the day post-seeding when a single sampling time at 60 min is performed, both for cell monolayers used in a single permeability assay or re-used. However, a small decrease is observed in P_{app} with the increase in the sampling time. This effect was independent on cell monolayers being used a single time in permeability assays or re-used (dark or light colours, respectively). The effect of the sampling time was however dependent on the day post-seeding, being less significant for cell monolayers on day 28 post-seeding (blue).

In spite of the small differences obtained for LY P_{app} from day 22 to 28 post-seeding and with the different sampling times, all conditions lead to permeability values compatible with a tight cell monolayer [128,211].

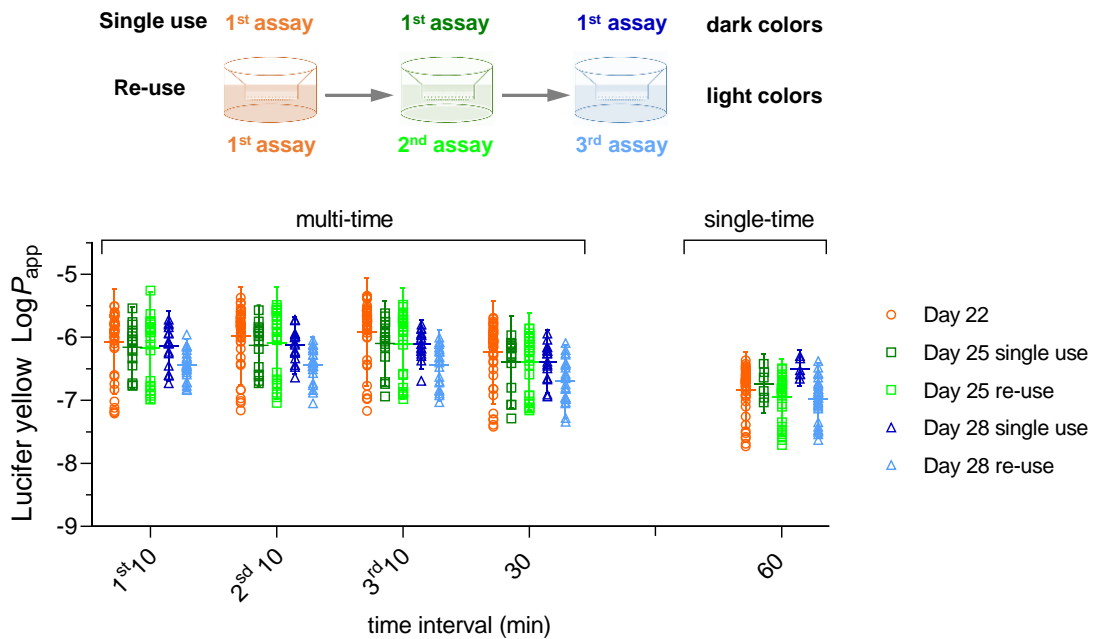


Figure V. 1 Dependence of LY P_{app} on the sampling interval, day post-seeding and re-use of the cell monolayers in multi-time and single-time sampling permeability assays. For a given data set, each data point corresponds to an independent cell monolayer. The mean and the corresponding CI_{95} of the P_{app} values for each data set ($n \geq 6$) are also shown.

The results obtained with LY were complemented with sodium fluorescein (Flu), which is also commonly used to evaluate the cell monolayer integrity [223]. The properties of Flu are similar to those of LY, both being very polar and negatively charged at pH 7.4 [224] (Table III.1). The results obtained for a single sampling at 60 min or with multiple time samplings within 60 min are shown in Figure V. 2. The values measured for Flu P_{app} at days 22 and 25 after seeding were very similar to those obtained for LY. Significant differences were however obtained on day 28, with P_{app} for Flu being statistically equivalent to that obtained at day 22 and 25, while it was lower for LY. The variation of P_{app} in consecutive samplings and with the increase in the sampling interval is lower for Flu than previously observed for LY.

Although Flu is commonly used as a paracellular marker, the results obtained suggests a significant contribution of permeation through a transcellular pathway, which is consistent with its lower polarity when

Re-use of Caco-2 monolayers – cell properties validation

compared with LY (Table III.1). This shows that LY is a better reporter of cell monolayer integrity.

The drug Atenolol was used as another polar compound that is considered to permeate mostly through the paracellular pathway. The results obtained are shown in Figure V. 2 and are very similar to those obtained for Flu, except for a smaller effect of the sampling time interval. The detailed statistical analysis of Flu and Atenolol P_{app} values are provided in supplementary material – Table V. S1.

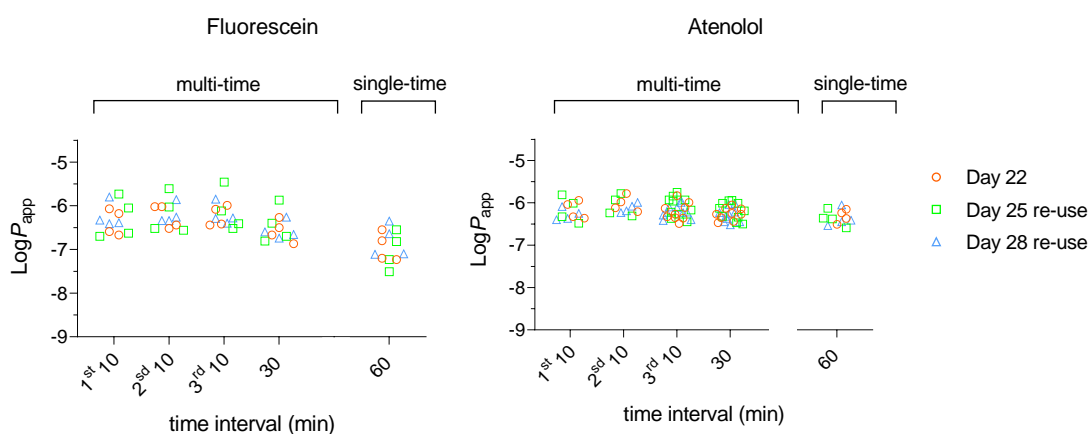


Figure V. 2 Effect of re-use and day post-seeding on Fluorescein and Atenolol passive permeability through Caco-2 monolayers after multi-time and single-time sampling assays.

V.4.1.2 – High passive permeability – Propranolol and salicylic acid

To further validate the re-use protocol, two reference compounds commonly used to characterize fast transcellular permeation were characterized [81]. Propranolol (Prop), which is positively charged at pH=7.4 (the most lipophilic member of the class of β -blockers which also includes Atenolol); and salicylic acid (SA), which is negatively charged at pH=7.4 (Table III. 1). The results obtained are shown in Figure V. 3 and the detailed statistical analysis is provided in supplementary material – Table V. S2. The first observation is that the results obtained for the re-used cell monolayers (light colours) are undistinguishable from those of cell monolayers used in a single permeability assay (dark colours). It is also observed that, as expected, the values obtained for P_{app} are significantly larger than those obtained for the solutes that permeate mostly through paracellular routes (Figure V. 1 and V. 2). The effect on P_{app} of the sampling time

interval and day post-seeding is similar to that observed for Flu and Atenolol, and smaller than observed for LY. This reinforces the conclusion that the day post-seeding and manipulation of the cell monolayer has a higher impact on paracellular permeability.

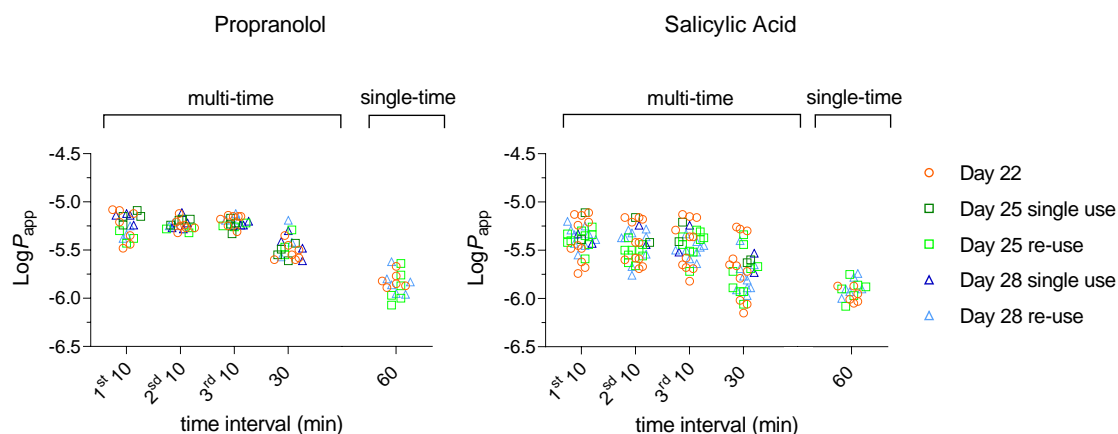


Figure V. 3 Effect of re-use and day post-seeding on Prop and SA passive permeability through Caco-2 monolayers after multi-time and single-time sampling assays.

V.4.2 – Effect of re-use on the permeability of a fluorescent glucose derivative (2-NBDG)

Glucose is a crucial cell nutrient, and Caco-2 cells have glucose transporters in their apical and basolateral membranes oriented to generate an absorptive flux of glucose. Glucose derivatives are commonly used to characterize glucose transport, to provide sensitivity in the detection method and allows an independent control of the glucose levels. The most commonly used glucose derivatives are radio- or fluorophore-labelled glucose [225], 2-NBDG being the most used fluorescent analogue [217,226]. However, despite the use of 2-NBDG to visualize and estimate the glucose accumulation in Caco-2 cells [19,20], the quantitative characterization of its transport across Caco-2 monolayers has not been reported.

In the present study, we determined the bi-directional transport of 2-NBDG through Caco-2 monolayers that were used for a single permeability assay or re-used for additional assays, to evaluate if the functionality of glucose transporters remained unaltered after the re-use of the Caco-2 monolayers. The permeability assays were carried out in HBSS containing glucose at a concentration of 5.6 mM, which competes with 2-NBDG. In fact, based on the work of Yamada et al in

Re-use of Caco-2 monolayers – cell properties validation

mammalian cells, the uptake of 2-NBDG at a concentration of 600 μM was inhibited in almost 38 % when in the presence of 5.6 mM of D-glucose [217]. Thus, to allow competition with glucose for transport, a relatively high concentration of 2-NBDG (250 μM) was used. The paracellular marker LY was added to the 2-NBDG solution to simultaneously quantify the paracellular permeability. The permeability of 2-NBDG +LY was measured in the A \rightarrow B and B \rightarrow A directions, using multi-time sampling (10, 20, 30 and 60 min). The results of the cumulative amount of 2-NBDG that reaches the acceptor compartment in both directions are shown in Figure V. 4.

In contrast with the expectations, the amount of 2-NBDG that permeates in the A \rightarrow B direction (absorptive pathways) is not higher than in the B \rightarrow A direction. Also, the amount of glucose analogue that reaches the acceptor compartment is very small, leading to an average value of $P_{\text{app}} \cong 0.5 \times 10^{-6}$ cm/s in both directions (see statistical analysis in the supplementary material – Table V. S3). This low permeability shows that 2-NBDG is not efficiently transported by the glucose carriers. Given the very high polarity of 2-NBDG (Table III. 1), it is anticipated that paracellular permeation is the most significant passive route. In fact, the P_{app} value of 2-NBDG was essentially the same as that of the paracellular marker LY.

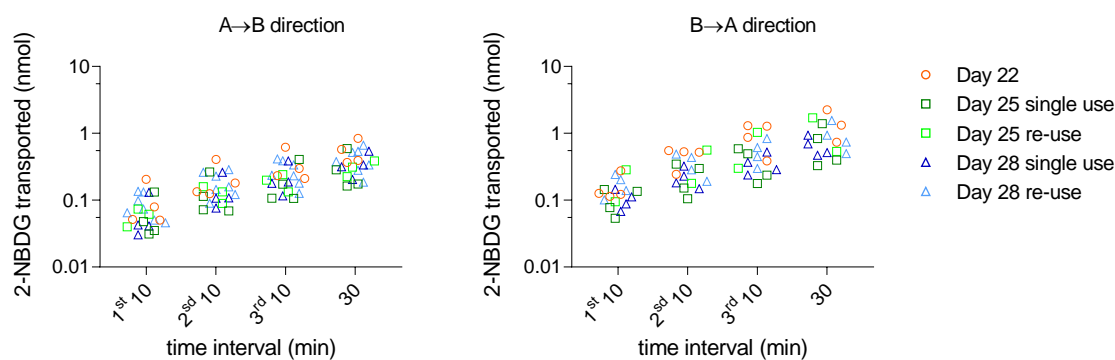


Figure V. 4 Effect of re-use and day post-seeding on the cumulative amount of 2-NBDG that reaches the acceptor compartment during multi-time sampling permeability assays.

In an attempt to understand the interaction of 2-NBDG with the Caco-2 monolayers, the cell monolayers were visualized by confocal fluorescence microscopy. Representative images obtained for the control (cell monolayers not used in permeability assays) and after the 60 min permeability assays with 2-NBDG in the A \rightarrow B and B \rightarrow A directions are displayed in Figure V. 5. Some autofluorescence diffused throughout the cells surface is observed in the control

(panel A). Incubation with 2-NBDG leads to an increase in fluorescence, both for 2-NBDG added to the apical (panel B) and basolateral (panel C) compartments, the increase in fluorescence being mainly localized along the cell plasma membranes. These results show that 2-NBDG associated efficiently with the cell membranes (supposedly due to binding to the glucose transporters), but that it was not internalized. The recoveries obtained with those assays were always higher than 95% when considering only the donor and acceptor aqueous compartments, showing that only a small fraction of 2-NBDG is associated with the cell membrane.

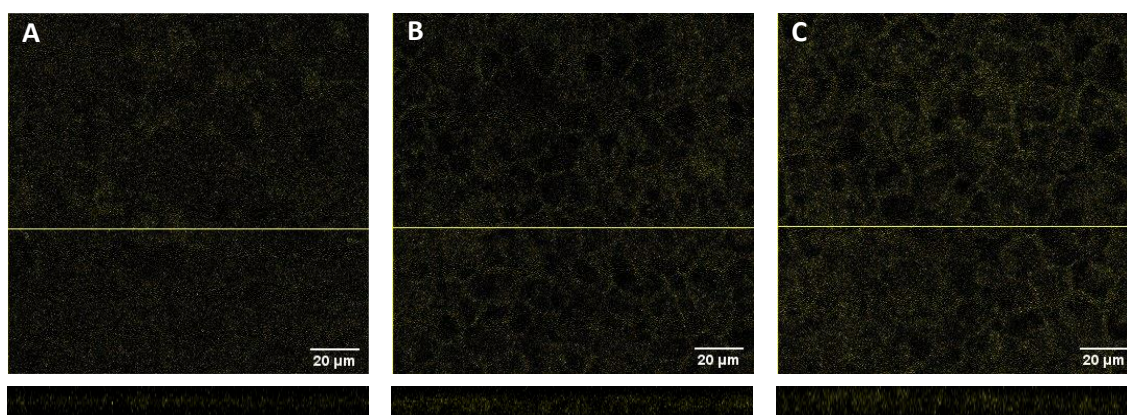


Figure V. 5 Confocal microscopy images of Caco-2 monolayers obtained with $\lambda_{ex}= 458$ nm and $\lambda_{em}= 459\text{--}551$ nm. Representative optical section images along the z-axis ($1\ \mu\text{m}$) are shown for (A) cell monolayers not used in permeability assays and for cell monolayers exposed to $250\ \mu\text{M}$ of 2-NBDG for 60 min during permeability assays in the A→B (B) and in the B→A (C) directions. The lower insets show the localization of the fluorescence in the cross section of a z-x plane corresponding to the yellow line. The mean fluorescence intensity in the $160\times 160\ \mu\text{m}^2$ images shown is 8.8 for (A) 11 (B) and 15 for (C), being respectively 16, 22 and 24 in the full image acquired (supplementary material – Figure V. S1).

At the conditions studied, the overall results shows that 2-NBDG is not a substrate of glucose transporters. Although surprising at first given the extensive use of this glucose analogue to visualize and estimate the glucose accumulation in cells [84,225], our findings agree with recently published studies. Some internalization of 2-NBDG in mammalian cells was observed, but with a kinetics distinct from that of radio-labelled glucose, and not affected by high-affinity GLUT inhibitors [227-229]. The confocal results obtained in this work (Figure V. 5) suggest that although not transported, 2-NBDG binds efficiently to the glucose transporters. This may explain previous results reported in literature where

Re-use of Caco-2 monolayers – cell properties validation

accumulation of 2-NBDG in the cells were observed, with the extent of accumulation being inhibited by the presence of glucose. This fluorescent glucose analogue may therefore be of interest to identify the presence of glucose transporters but cannot be used to monitor glucose transport. Similar results are anticipated for other fluorescent glucose derivatives due to the effect of the fluorescent moiety on glucose properties and transporter activity, invalidating their use in permeability assays.

Further, the proper validation of the function of glucose transporters upon re-use of cell monolayers may be carried out with radio-labelled glucose analogs for which glucose transport has been quantitatively characterized in Caco-2 monolayers. Nevertheless, independently of the pathway for internalization and transport of 2-NBDG, no significant differences were observed between the results obtained with Caco-2 monolayers used in a single permeability assay or re-used when following the proposed protocol.

V.4.3 – Effect of re-use on the permeability of rhodamine 123 and P-glycoprotein expression

The effective transport of drug-like molecules through cell monolayers may be influenced by the presence of efflux transporters that actively counteract their accumulation in the cell membrane [59,230]. P-glycoprotein is the most studied efflux transporter [23,231,232], and a significant expression has been observed in the apical membrane of Caco-2 cells [212,233]. The expression level is dependent on the cell passage number, day after seeding on permeable inserts, and on pre-incubation with P-gp substrates [115,116,234]. It is therefore important to evaluate whether the re-use of Caco-2 monolayers influences P-gp expression and/or activity. This was evaluated through the characterization of P_{app} for the well-known P-gp substrate, Rhodamine 123 (Rho) [220,235].

At the beginning of the assays with Rho, no lag phase appears in the variation of instantaneous permeability with incubation time, both in the A→B and in the B→A direction (see supplementary material – Figure V. S2). The overall P_{app} was calculated from the average value of the instantaneous permeability at each time interval and is presented in Figure V. 6A.

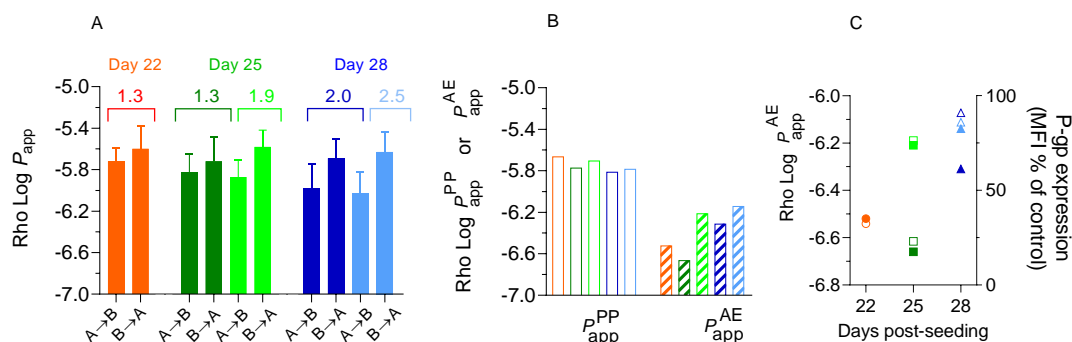


Figure V. 6 Effect of re-use and day post-seeding on Rho permeability and P-gp expression across Caco-2 monolayers. Plot A: Log P_{app} values measured in the A→B and B→A directions (mean and CI₉₅, n ≥ 2), the efflux ratios are presented above the bars. Plot B: contribution of passive permeation (P_{app}^{PP}) and active efflux (P_{app}^{AE}) to the measured Rho P_{app} values, calculated using Equation (V.3). Comparison of efflux activity P_{app}^{AE} (filled symbols, left axis) and P-gp expression (hollow symbols, right axis). The results obtained for cell monolayers used in a single permeability assay are shown in dark colours, and those obtained for re-used cell monolayers are in light colours.

The first observation is that the results are not significantly influenced by the re-use of the Caco-2 monolayers. Some interesting observations for the effect of the day post-seeding are discussed below.

The efflux ratio is very close to 1 for cell monolayers on day 22 post-seeding, and increases to somewhat above 2 for cells on day 28, suggesting an increase in Rho efflux by P-gp. In agreement, a decrease is observed for P_{app} in the A→B direction. However, this decrease is not accompanied by the expected increase of P_{app} in the B→A direction. Those apparently conflicting results may be reconciliated if one considers that the observed P_{app} is the result of both passive (P_{app}^{PP}) and active (P_{app}^{AE}) processes, Equation V.2. For permeation in the A→B direction, the active efflux leads to a decrease in the observed P_{app} , while in the B→A direction both processes sum up. The contribution from passive and active processes may be calculated from Equation V.3 and the results obtained are shown in Figure V. 6B. A small decrease is observed with the day post-seeding for P_{app}^{PP} (from 2×10^{-6} cm/s on day 22 to 1.6×10^{-6} cm/s on day 28). In contrast, it is observed a significant increase on P_{app}^{AE} with the day post-seeding, from 1.5×10^{-7} cm/s on day 22, to 6×10^{-7} cm/s on day 28 (see detailed statistical analysis in supplementary material — Table V. S4). The values obtained for the permeability coefficient through both permeation routes (P_{app}^{PP} and P_{app}^{AE}) are similar and in the

Re-use of Caco-2 monolayers – cell properties validation

B→A direction the opposite variation cancel out, leading to no variation in the overall permeability. The deconvolution of the observed P_{app} in the contributions from passive process and efflux, thus lead to a better understanding of the observed permeability. This treatment has the additional advantage of increasing the sensitivity on the evaluation of active efflux, when compared to the common analysis based on the efflux ratio, Equation V.1.

The values of P_{app}^{PP} obtained for Rho are somewhat higher than those of the paracellular marker LY measured in the same assays ($\cong 0.5 \times 10^{-6}$ cm/s), showing that the transcellular route is significant in the case of Rho permeation through the Caco-2 monolayers. This agrees with the lower global charge and higher hydrophobicity of Rho when compared with LY (Table S1, and [236]).

To further elucidate on the variations of the rate of Rho efflux, we have quantified the effect of the day post-seeding (and monolayer re-use) on the amount of P-gp on the plasma membrane of Caco-2 cells. The expression level was accessed by flow cytometry after immunostaining P-gp with a FITC-conjugated antibody. The median fluorescence intensity (MFI) is show in Figure V. 6C (raw data in supplementary material – Figure V. S4). A low level of P-gp expression was observed at all conditions tested, in spite of a small increase with the day post-seeding. The low expression level of the efflux transporter P-gp observed in this work agree with the results previously observed by other authors for Caco-2 cell monolayers grown at the same conditions [115,116,212]. Those results support the above interpretation for the dependence of $P_{app}^{A \rightarrow B}$ and $P_{app}^{B \rightarrow A}$ on the day post-seeding, with a relatively small contribution of active efflux to the overall P_{app} at all days

Importantly, in what concerns the objectives of this work, regardless of the details on Rho permeation mechanism and P-gp expression, a similar behavior was observed for cell monolayers used in a single permeability assay or re-used.

As a final evaluation regarding the effect of re-use on P-gp efflux activity, the cell monolayers were incubated for 30 minutes with a high concentration (100 μ M) of Verapamil on both compartments. After the removal of the Verapamil solution, the transport of Rho across the cell monolayers was evaluated. The variation of instantaneous P_{app} with incubation time is characterized by a lag phase in the B→A direction. A steady-state is never attained, with P_{app} B→A

direction slightly increasing during the duration of the assay (see supplementary material — Figure V. S3). The average values obtained for Rho P_{app} in both directions and the contributions of P_{app}^{PP} and P_{app}^{AE} considering the time interval up to 120 min are displayed in Figure V. 7 for Caco-2 monolayers used at day 22 and re-used at days 25 and 28.

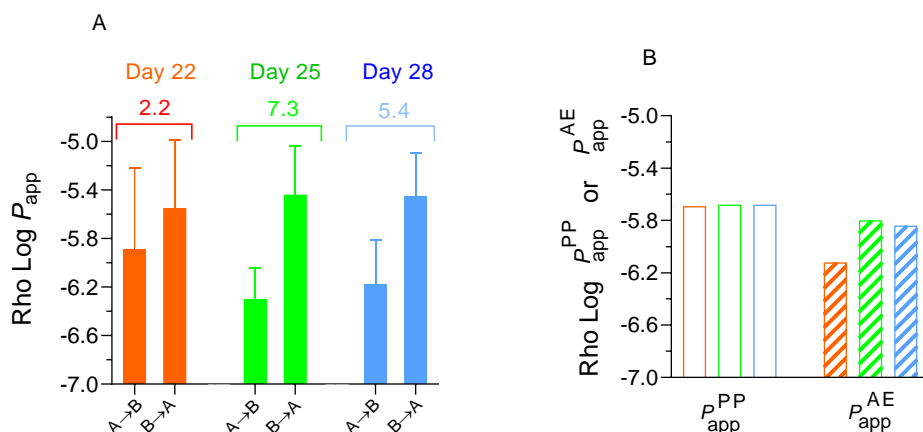


Figure V. 7 Effect of re-use and day post-seeding on Rho permeability across Caco-2 monolayers after the pre-incubation with Verapamil at 100 μ M. Plot A: $\text{Log}P_{app}$ values measured in the A→B and B→A directions (mean and CI₉₅, n = 4), the efflux ratios are presented above the bars. Plot B: contribution of P_{app}^{PP} and P_{app}^{AE} components to the measured Rho P_{app} values, calculated using Equation V.3. The results are shown for cell monolayers used in a single permeability assay at day 22 and re-used at day 25 and 28.

The pre-incubation with Verapamil leads to a small decrease in the Rho P_{app} for the transport in the A→B direction (from 1.9×10^{-6} cm/s for monolayers with no pre-incubation with Verapamil to 1.3×10^{-6} cm/s on day 22), while a small increase is observed in Rho transport in the B→A direction (from 2.5×10^{-6} cm/s for monolayers with no pre-incubation with Verapamil to 2.8×10^{-6} cm/s on day 22). This result does not support inhibition of P-gp by Verapamil. In fact, it suggests a higher efflux activity for the cells pre-incubated with Verapamil, as shown by the high efflux ratios obtained at all days after cell seeding (from 1.3 to 2.2 at day 22, from 1.9 to 7.3 at day 25, and from 2.5 to 5.4 at day 28, see supplementary material — Figure V. S3 for details). The contributions from passive (P_{app}^{PP}) and active efflux (P_{app}^{AE}) are presented in Figure V.7B, and show that P_{app}^{PP} is not affected by the pre-incubation with Verapamil while P_{app}^{AE} increases. Altogether, the results suggest that pre-incubation with Verapamil leads to an increase in the amount of P-gp in the cells plasma membrane. The stimulating

Re-use of Caco-2 monolayers – cell properties validation

effect of Verapamil may be caused by induction of P-gp trafficking from the intracellular membranes to the apical membrane [237] or by induction of P-gp expression levels. A report published by Anderle et al showed that the culture of Caco-2 cells in medium containing Verapamil (100 μ M) induced the expression levels of P-gp [234]. But more recently, Miao et al. reported that Verapamil decreased the P-gp levels in Caco-2 cells after incubation for 72h [238]. Thus, the effect of Verapamil on P-gp expression and activity in Caco-2 monolayers is still unclear and a matter of debate. The results obtained in this study support an increase in P-gp expression levels due to incubation with Verapamil.

Regarding the objectives of this work, the results obtained with Verapamil at days 25 and 28 with the re-used Caco-2 monolayers were similar to those obtained at day 22 for monolayers used a single time. These findings indicate that the incubation with culture medium for two days between each assay was sufficient and necessary for the cells lose the memory of the Verapamil treatment they received the day before.

V.4.4 –Additional validation studies and advantages of the re-use methodology

For a more robust validation of the re-use of Caco-2 monolayers regarding the transporter's functions, compounds targeting other transporters with significant levels of expression in these monolayers should be also evaluated. This includes the peptide influx transporter (PepT1) which active transport and expression has been well-characterized in Caco-2 monolayers [160,233]. Its substrates, namely the β -lactams antibiotics (e.g., cephalosporins) are suitable compounds to perform the re-use validation studies since they are effectively transported and the kinetics of transport have already been studied in this cells [160]. The transcytosis pathways, followed by large macromolecules to permeate across Caco-2 monolayers should also be characterized after the re-use of the cell monolayers. Among those pathways, the receptor-mediated endocytosis of low and high density lipoproteins can be evaluated in Caco-2 cells by previous equilibration of the lipoproteins with the fluorescent sterol dehydroergosterol (DHE) [239]. Iron transport through Ferritin receptor-mediated endocytosis could also be evaluated using iron-sensitive fluorescent probes [240].

The complete validation of the re-use methodology will require an extensive and systematic work. It will only be possible to generate such a quantity of permeability data for distinct molecules with multiple contributions from the scientific community over the coming years. When the Caco-2 model started to demonstrate its potential to predict intestinal permeability, a very low quantity of permeability data was available in the literature. In the present days, the use of this model by the scientific community generated a large amount of permeability data for a large set of molecules, continuously contributing to the validation of this permeability assay as an important tool in drug discovery and development. A similar path is required for the full validation (or its refusal) of re-use methodologies such as that proposed by us. The advantages of re-using the cell monolayers in permeability assays fully justify the investment by the scientific community in the validation of the re-use protocols. The first obvious advantage is the increase in the throughput of the assay, which triplicates when following the proposed protocol. This allows obtaining information on the permeability of a larger number of compounds, increasing the efficiency and expanding the drug chemical space evaluated. Another important advantage is the downscaling of the culture materials (number of Transwell™, media quantity) and human resources needed *per* assay. Finally, the variability in the properties of the cell monolayers during their stable period (21 to 28 days, both when used in a single assay or re-used) is much lower than between different cell batches. Thus, re-using the cell monolayers will lead to a decrease in the dispersion associated with compound permeability. Overall, these advantages will significantly contribute to the collection of accurate P_{app} values for larger compound datasets, allowing the application of AI tools for the establishment of QSPRs to predict drug permeability from their structural properties.

V.5 – Conclusions

The present study shows that the re-use of Caco-2 monolayers after applying the proposed regeneration protocol can be implemented for compounds that follow the passive permeation route. This allows to triplicate the throughput of the standard Caco-2 permeability assay. The results obtained regarding the glucose transporters cannot be used to accurately validate the effect of re-use on these transporters due to the inefficient transport of the fluorescent

Re-use of Caco-2 monolayers – cell properties validation

glucose derivative 2-NBDG. Given the small size of glucose, we anticipate that the introduction of any fluorescent moiety will significantly influence the overall properties of the molecule and compromise the activity of the transporter. The effects on this permeation pathway must therefore be performed with better glucose mimetic compounds, such as with the use of radioactive or deuterated derivatives [216,229,241]. Additional studies are also required for the accurate characterization of the effect of re-use on the activity of efflux transporters. This includes the use of additional substrates specific for distinct transporters. A re-design is also required regarding the standard procedure followed for evaluation of transport after the inhibition of the carrier, pre-incubation with Verapamil in the case of P-gp. Verapamil is a P-gp substrate, not an inhibitor, and the effect of Verapamil on P-gp efflux activity on other compounds is due to competition for the transporter. The effective concentration of Verapamil inside the cells is therefore a major determinant of the result obtained and depends on the efflux activity by the cells. The uncertainty in the intracellular concentration of Verapamil is further increased due to the removal of Verapamil from the transport medium before the permeability assay. The exposure of the cells to high levels of the efflux transporter' substrate can also lead to an increase in its levels at the cell plasma membrane, introducing additional variability in the outcome of the assay. The limitations of this approach go beyond its applicability in the evaluation of cell monolayer re-use, but are of particular relevance in this case. Despite the limitations of the study here presented, the results clearly indicate that re-using Caco-2 monolayers in consecutive permeability assays shows great promise. We hope these findings will inspire further validation of this approach within the scientific community.

The detailed work performed in this study also provided important insights regarding the experimental methodology and data analysis in permeability assays. The results obtained in this work show that the manipulation of the monolayer required for sampling has some impact on monolayer integrity, and that those effects decrease as the days post-seeding increase from day 22 to 28, both for cell monolayers used in a single permeability assay or re-used following the proposed protocol. The impact is most significant for compounds that permeate paracellularly, and negligible for transcellular permeation. It is also shown that the intrinsic variability of the results obtained with the Caco-2 permeability assay (regarding cell passage number and cell batch, in addition to the day post-seeding) is higher for compounds that permeate paracellularly. This

suggests that when the conditions of the assays are maintained, the major source of variability is the cell monolayer integrity.

It is also shown that the contribution from active and passive processes should be calculated when evaluating active transport from the overall P_{app} observed. This analysis allows the quantitative assessment of the effective permeation through the distinct routes, accounts for variations in the cell monolayer tightness, and leads to a higher sensitivity in permeation through the active pathway.

To capture the intrinsic variability of distinct cell batches, it is recommended that replicates for a given compound are performed with distinct cell preparations, not from distinct inserts with the same cell preparation. In following with this recommendation, the re-use assays should not be used as replicates for a given compound. The increase in the throughput provided by the re-use of the cell monolayers is however of very high value to evaluate the permeability of distinct compounds.

V.6 – Supplementary material

Chapter V

25	all 1 st	22		4.8	0.9; 25.9	0.13	0.03; 0.51								
	1 st 60 min	6		1.8	0.6; 5.4	0.18	0.06; 0.54								
	1 st 10 min	16		6.9	1.6; 30.5	0.12	0.03; 0.51								
	2 nd 10 min	16		7.4	1.7; 32.6	0.15	0.05; 0.45								
	3 rd 10 min	16		7.9	1.7; 38.1	0.18	0.08; 0.40								
	4 th 30 min	16		4.1	0.8; 21.7	0.28	0.13; 0.62								
	all	133 & 20 & 32		4.2	0.5; 37.9	0.14	0.02; 0.90							3.9	0.5, 30.7
25	all 1 st	58 & 8 & 8	Re-use	2.4	0.3; 22.7	0.11	0.02; 0.57	2.2	0.2, 26.3	0.09	0.02, 0.54	5.5	1.8, 16.5	0.23	0.04, 1.2
	1 st 60 min	33 & 4 & 4		1.1	0.3; 4.5	0.11	0.03; 0.45	0.9	0.1, 7.6	0.09	0.01, 0.76	4.3	1.7, 10.8	0.44	0.17, 1.1
	1 st 10 min	25 & 4 & 4		6.8	0.9; 51.5	0.11	0.02; 0.82	5.3	0.5, 52.5	0.09	0.01, 0.88	7.0	1.6, 30.6	0.12	0.03, 0.51
	2 nd 10 min	25 & 4 & 4		8.0	1.0; 61.5	0.15	0.02; 1.2	6.6	0.7, 61.1	0.11	0.01, 1.0	8.6	2.5, 29.8	0.14	0.04, 0.50
	3 rd 10 min	25 & 4 & 10		7.8	1.0; 60.2	0.15	0.02; 1.2	7.5	0.7, 76.5	0.13	0.01, 1.3	8.2	3.0, 22.0	0.21	0.07, 0.65
	4 th 30 min	25 & 4 & 10		4.1	0.7; 24.2	0.23	0.03; 1.5	3.6	0.5, 28.6	0.18	0.02, 1.4	6.5	2.7, 15.8	0.33	0.14, 0.79
	28	all		70	Single use	6.0	2.0; 18.7	0.18	0.07; 0.47						
all 1 st		22	5.9	1.6; 20.6		0.16	0.04; 0.60								
1 st 60 min		6	3.2	1.7; 6.1		0.32	0.17; 0.62								
1 st 10 min		16	7.2	2.0; 25.9		0.12	0.03; 0.43								
2 nd 10 min		16	7.4	2.6; 20.9		0.14	0.07; 0.32								
3 rd 10 min		16	7.7	3.1; 19.3		0.17	0.09; 0.30								
4 th 30 min		16	4.1	1.3; 13.2		0.28	0.15; 0.53								
28	all	118 & 20 & 32	Re-use	2.4	0.6; 10.1	0.09	0.02; 0.35	4.0	1.0, 15.9	0.12	0.04, 0.33	5.7	2.9, 11.0	0.19	0.07, 0.53
	all 1 st	51 & 8 & 8		1.8	0.4; 8.7	0.08	0.03; 0.28	3.1	0.5, 19.5	0.13	0.03, 0.51	4.9	2.3, 10.2	0.20	0.03, 1.1
	1 st 60 min	23 & 4 & 4		1.0	0.3; 3.9	0.11	0.03; 0.38	1.6	0.3, 9.8	0.16	0.03, 0.99	4.4	1.5, 12.6	0.44	0.15, 1.3
	1 st 10 min	23 & 4 & 4		3.6	1.4; 9.3	0.06	0.02; 0.16	5.9	1.4, 24.2	0.10	0.02, 0.41	5.3	2.6, 10.7	0.09	0.04, 0.18
	2 nd 10 min	23 & 4 & 4		3.6	1.3; 10.3	0.07	0.02; 0.25	6.3	2.0, 19.6	0.11	0.03, 0.33	7.5	4.5, 12.7	0.13	0.08, 0.21
	3 rd 10 min	23 & 4 & 10		3.5	1.0; 12.8	0.09	0.02; 0.44	6.2	1.9, 20.5	0.10	0.03, 0.34	6.4	3.3, 12.5	0.16	0.07, 0.36
	4 th 30 min	23 & 4 & 10		2.0	0.5; 7.7	0.15	0.03; 0.64	2.7	1.0, 7.7	0.14	0.05, 0.39	5.2	2.6, 10.4	0.26	0.13, 0.52

No statistically significant differences are observed between the distinct experimental days and monolayers use. ^a Number of time points sampled for Lucifer yellow & Flu & Atenolol permeability assays.

Re-use of Caco-2 monolayers – cell properties validation

V.6.1.2 – High permeation reference compounds – Propranolol and salicylic acid

Table V. S2 Statistical analysis of P_{app} values of Propranolol and Salicylic Acid after single time and multi-time sampling permeability assays through single use and re-used Caco-2 monolayers from day 22 to 28. The average and the corresponding confidence intervals at 95 % confidence (CI_{95}) were obtained directly from the analysis of $\text{Log}(P_{app})$.

Day	Assay Conditions Sampling (N) ^a	Monolayer use	P_{app} (10^{-6} cm/s)				
			Propranolol		Salicylic Acid		
			μ	CI_{95}	μ	CI_{95}	
All	all (102 & 150)	Single use & re-use	4.1	1.6, 10.8	2.9	1.1, 7.6	
	all 1 st (39 & 51)		3.0	0.8, 10.8	2.7	0.9, 8.6	
	1 st 60 min (18 & 18)		1.4	0.9, 2.3	1.2	0.8, 1.8	
	1 st 10 min (21 & 33)		5.7	3.4, 9.5	4.2	2.3, 7.9	
	2 nd 10 min (21 & 33)		5.8	4.7, 7.3	3.6	1.9, 7.0	
	3 rd 10 min (21 & 33)		6.2	4.9, 7.7	3.6	1.9, 7.1	
	4 th 30 min (21 & 33)		3.3	2.1, 5.3	1.9	0.8, 4.9	
22	all (34 & 50)	Single use	4.1	1.5, 10.8	2.9	0.9, 9.2	
	all 1 st (13 & 17)		3.1	0.8, 11.4	2.6	0.7, 10.0	
	1 st 60 min (6 & 10)		1.5	1.1, 2.2	1.1	0.8, 1.6	
	1 st 10 min (7 & 11)		5.6	2.7, 11.7	4.1	1.6, 10.7	
	2 nd 10 min (7 & 11)		5.8	4.4, 7.6	3.8	1.6, 9.1	
	3 rd 10 min (7 & 11)		6.4	4.9, 8.5	3.6	1.3, 10.1	
	4 th 30 min (7 & 11)		3.0	2.0, 4.5	2.1	0.6, 7.7	
25	all (34 & 50)	Single use & re-use	3.9	1.4, 11.1	2.9	1.1, 7.2	
	all 1 st (13 & 17)		2.9	0.7, 12.4	2.8	0.9, 9.1	
	1 st 60 min (6 & 6)		1.3	0.6, 2.7	1.2	0.8, 2.0	
	1 st 10 min (7 & 11)		5.7	3.2, 9.9	4.4	2.7, 7.2	
	2 nd 10 min (7 & 11)		5.8	4.6, 7.3	3.3	1.9, 5.8	
	3 rd 10 min (7 & 11)		5.8	4.7, 7.2	3.9	2.2, 6.8	
	4 th 30 min (7 & 11)		3.3	2.1, 5.2	1.9	0.8, 4.7	
	1 st 10 min (4 & 2)	Single use	7.0	5.1, 9.5	5.7	1.5, 21.1	
	2 nd 10 min (4 & 2)		6.3	5.5, 7.3	5.2	1.5, 17.6	
	3 rd 10 min (4 & 2)		5.8	4.2, 8.1	4.9	1.9, 12.7	
	4 th 30 min (4 & 2)		3.0	2.0, 4.5	2.4	2.1, 2.8	
	1 st 60 min (6 & 6)		Re-use	1.3	0.6, 2.7	1.2	0.8, 2.0
	1 st 10 min (3 & 9)			4.3	3.1, 6.0	4.2	2.8, 6.3
	2 nd 10 min (3 & 9)			5.1	4.5, 5.9	3.0	2.1, 4.4
3 rd 10 min (3 & 9)	5.7	5.1, 6.4		3.7	2.1, 6.5		
4 th 30 min (3 & 9)	3.7	1.8, 7.6	1.8	0.7, 5.0			
28	all (34 & 50)	Single use & re-use	4.3	1.6, 11.4	2.9	1.2, 6.9	
	all 1 st (13 & 17)		3.1	0.8, 12.0	2.9	1.0, 8.4	
	1 st 60 min (6 & 6)		1.5	0.8, 2.5	1.3	0.9, 2.0	
	1 st 10 min (7 & 11)		5.9	3.8, 9.2	4.3	2.9, 6.5	
	2 nd 10 min (7 & 11)		5.9	4.6, 7.6	3.8	1.9, 7.5	
	3 rd 10 min (7 & 11)		6.3	5.1, 7.7	3.4	2.1, 5.4	
	4 th 30 min (7 & 11)		3.7	2.0, 7.1	1.8	0.9, 3.7	

Re-use of Caco-2 monolayers – cell properties validation

1 st 10 min (4 & 2)	Single use	6.9	5.4, 8.9	4.2	2.6, 6.7
2 nd 10 min (4 & 2)		6.0	4.1, 8.8	4.6	1.8, 11.4
3 rd 10 min (4 & 2)		5.9	5.2, 6.6	4.2	1.1, 15.7
4 th 30 min (4 & 2)		3.5	1.9, 6.7	2.3	0.9, 6.2
1 st 60 min (6 & 6)	Re-use	1.5	0.8, 2.5	1.3	0.9, 2.0
1 st 10 min (3 & 9)		4.8	3.4, 6.8	4.4	2.8, 6.9
2 nd 10 min (3 & 9)		5.8	5.4, 6.2	3.7	1.8, 7.6
3 rd 10 min (3 & 9)		6.9	5.5, 8.6	3.3	2.2, 4.8
4 th 30 min (3 & 9)		4.0	1.4, 11.3	1.7	0.8, 3.5

No statistically significant differences are observed between the distinct experimental days and monolayers use.

^a Number of time points sampled for Prop & SA permeability assays.

V.6.2 – Effect of Caco-2 monolayer re-use on transport of 2-NBDG

Table V. S3 Statistical analysis of P_{app} values of 2-NBDG in the absorptive (A→B) and secretory (B→A) directions and the resulting influx ratio. The paracellular marker LY was applied together with 2-NBDG and the resulting P_{app} is also show, as well as the ratio between the P_{app} values of 2-NBDG and LY.

Day	Monolayer use (number of cell monolayers in A→B & B→A))	2-NBDG P_{app} (10^{-7} cm/s)					LY P_{app} (10^{-7} cm/s)					P_{app} 2-NBDG/ P_{app} LY	
		A→B		B→A		Influx Ratio	A→B		B→A		A→B	B→A	
		μ	CI ₉₅	μ	CI ₉₅		μ	CI ₉₅	μ	CI ₉₅			
All	Single use (12 & 12)	3.5	1.3, 9.1	7.7	2.4, 24.4	0.5	0.1, 2.0	2.8	0.8, 10.2	8.2	2.8, 24.6	1.2	0.9
	Re-use (11 & 10)	3.5	1.6, 7.9	9.0	3.2, 25.2	0.4	0.2, 1.4	3.4	0.7, 17.5	9.0	3.8, 20.9	1.0	0.9
	Single use & re- use (23 & 22)	3.5	1.4, 8.5	8.1	2.7, 24.4	0.4	0.1, 1.8	3.0	0.7, 12.9	8.5	3.1, 23.1	1.2	0.9
22	Single use (4 & 4)	5.0	2.1, 11.6	14	3.9, 48.4	0.4	0.09, 1.7	4.4	0.9, 21.0	14	4.2, 45.5	1.1	1.0
25	Single use (4 & 4)	2.6	0.9, 7.6	5.6	2.0, 15.7	0.5	0.1, 1.9	1.7	0.6, 4.7	6.2	2.4, 15.9	1.5	0.9
	Re-use (3 & 2)	3.0	1.6, 5.3	11	2.4, 48.1	0.3	0.06, 1.3	4.5	0.4, 56.3	9.3	2.7, 32.1	0.7	1.0
	Single use & re- use (7 & 6)	2.8	1.2, 6.5	7.1	2.0, 24.8	0.4	0.09, 1.7	2.6	0.4, 17.2	7.1	2.5, 19.9	1.1	0.9
28	Single use (4 & 4)	3.2	1.5, 7.1	5.8	3.6, 9.5	0.5	0.2, 1.4	2.8	1.1, 7.1	6.5	3.4, 12.6	1.0	0.7
	Re-use (7 & 4)	3.8	1.6, 9.1	8.2	3.8, 17.7	0.5	0.2, 1.5	3.0	0.9, 10.0	8.8	4.3, 18.0	1.3	0.9
	Single use & re- use (11 & 8)	3.6	1.6, 8.2	6.9	3.5, 13.7	0.5	0.2, 1.5	2.9	1.0, 8.6	7.6	3.8, 15.4	1.2	0.8

No statistically significant differences are observed between the distinct experimental days and monolayers use.

Re-use of Caco-2 monolayers – cell properties validation

To better understand the interaction of 2-NBDG with the Caco-2 cells, the monolayers were analyzed by confocal microscopy at wavelengths where the NBD group emits fluorescence. Representative images of the projections of maximum intensity of all z-stacks are shown in Figure S2. Images were taken of Caco-2 monolayers not used in permeability assays (panel A) and after the permeability assay with 2-NBDG in the A→B (panel B) and B→A (panel C) directions. A quantitative analysis of the fluorescence intensity was performed considering the total image area ($428 \times 428 \mu\text{m}^2$), leading to mean fluorescence intensity of 16 for (A) 22 for (B) and 24 for (C).

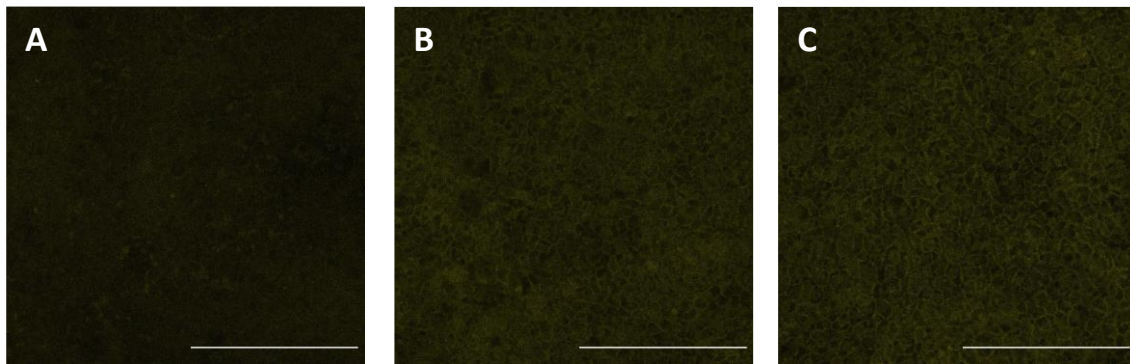


Figure V. S1 Confocal microscopy images of Caco-2 monolayers obtained with excitation light at 458 nm and emission detection from 459–551 nm. Maximum intensity projections of z-stacks are shown for (A) cell monolayers not used for any permeability assay and for cell monolayers exposed to 250 μM of 2-NBDG in the A→B direction (B) and in the B→A direction (C) during the permeability assays at day 28 post-seeding. Scale bar 200 μm .

V.6.3 – Effect of Caco-2 monolayer re-use on transport of Rho

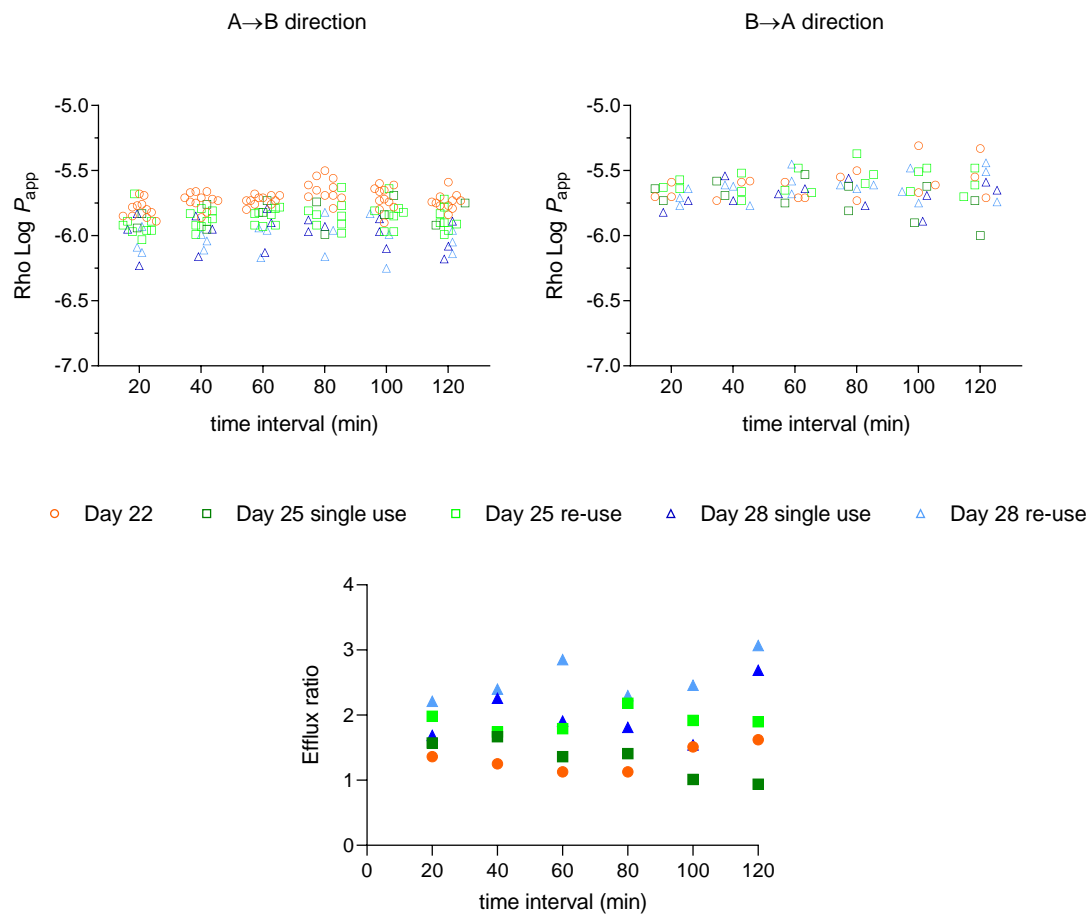


Figure V. S2 Effect of re-use and day post-seeding on Rho permeability. The upper plots represent the instantaneous $\text{Log}P_{\text{app}}$ values as a function of the incubation time in the A→B and B→A direction, and lower plot is the instantaneous efflux ratio calculated from the $P_{\text{app}}^{\text{B} \rightarrow \text{A}} / P_{\text{app}}^{\text{A} \rightarrow \text{B}}$.

Re-use of Caco-2 monolayers – cell properties validation

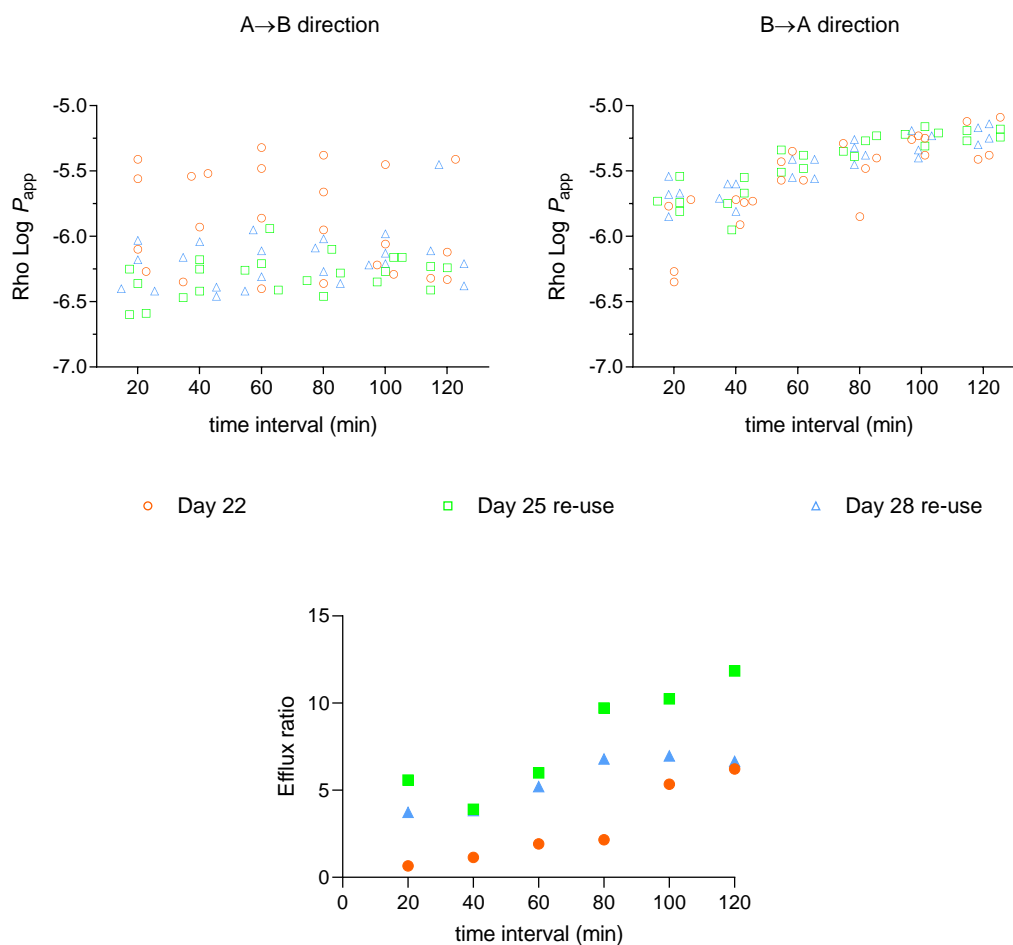


Figure V. S3 Effect of re-use and day post-seeding on Rho permeability after pre-inhibition of P-gp efflux with 100 μ M of Verapamil. The upper plots represent the instantaneous $\text{Log}P_{app}$ values as a function of the incubation time in the A→B and B→A direction, and lower plot is the instantaneous efflux ratio calculated from the $P_{app}^{B \rightarrow A} / P_{app}^{A \rightarrow B}$.

Table V. S4 Statistical analysis of the P_{app} values of Rho in the absorptive (A→B) and secretory (B→A) directions. The resulting efflux ratio and the contribution of passive permeation (P_{app}^{PP}) and active efflux (P_{app}^{AE}) to the measured Rho P_{app} values were determined using Equations V.2 and V.3 in the main text. The paracellular marker was applied together with Rho, and the permeability obtained is also shown. The permeability of Rho was measured after pre-incubation of the cell monolayers with 100 μ M Verapamil for a period of 30 min, and the statistical analysis of the obtained P_{app} values was also shown.

Day	Monolayer use (number of cell monolayers in A→B & B→A)	Rho P_{app} (10^{-6} cm/s)				Rho P_{app} (10^{-6} cm/s)				LY P_{app} (10^{-7} cm/s)			
		A→B		B→A		Efflux Ratio		P_{app}^{PP}	P_{app}^{AE}	A→B		B→A	
		μ	CI ₉₅	μ	CI ₉₅	μ	CI ₉₅	μ	μ	μ	CI ₉₅	μ	CI ₉₅
All	Single use (16 & 7)	1.6	1.0, 2.8	2.2	1.3, 3.6	1.3	0.6, 2.7	1.9	0.27	6.7	2.7, 16.8	5.9	1.8, 19.4
	Re-use (11 & 6)	1.2	0.8, 2.0	2.5	1.7, 3.7	2.0	1.1, 3.7	1.9	0.63	4.8	2.3, 9.8	7.3	2.6, 20.4
	Single use & re- use (27 & 13)	1.5	0.8, 2.5	2.3	1.5, 3.7	1.6	0.8, 3.3	1.9	0.43	5.8	2.4, 13.6	6.6	2.2, 19.5
22	Single use (11 & 3)	1.9	1.4, 2.6	2.5	1.5, 4.1	1.3	0.7, 2.3	2.2	0.30	9.3	4.9, 17.5	8.6	3.9, 18.9
25	Single use (2 & 2)	1.5	1.0, 2.2	1.9	1.1, 3.3	1.3	0.9, 3.1	1.7	0.22	4.7	2.4, 9.5	7.1	2.1, 23.2
	Re-use (8 & 3)	1.4	1.0, 1.9	2.6	1.8, 3.8	1.9	0.7, 2.5	2.0	0.62	5.6	3.1, 9.9	11	4.2, 28.2
	Single use & re- use (10 & 5)	1.4	1.0, 2.0	2.3	1.4, 3.8	1.7	1.2, 3.2	1.8	0.46	5.3	3.0, 9.4	9.4	3.4, 25.8
28	Single use (3 & 2)	1.0	0.6, 1.8	2.0	1.3, 3.1	2.0	1.2, 4.3	1.5	0.49	5.7	1.9, 17.2	2.4	1.6, 3.6
	Re-use (3 & 3)	0.9	0.6, 1.5	2.4	1.6, 3.6	2.5	1.0, 3.8	1.7	0.72	4.1	1.8, 9.3	4.8	2.8, 8.2
	Single use & re- use (6 & 5)	1.0	0.6, 1.6	2.2	1.5, 3.4	2.3	1.4, 3.7	1.6	0.62	4.9	1.9, 12.6	3.8	1.8, 8.0
After pre-incubation with 100 μM Verapamil													
All	Single use & re- use (12 & 12)	0.8	0.2, 2.6	3.3	1.2, 9.0	4.4	0.9, 21	2.0	1.3				
22	Single use (4 & 4)	1.3	0.3, 6.0	2.8	0.8, 10	2.2	0.3, 15	2.1	0.75				
25	Re-use (4 & 4)	0.5	0.3, 0.9	3.7	1.5, 9.2	7.3	2.5, 22	2.1	1.6				
28	Re-use (4 & 4)	0.7	0.3, 1.6	3.5	1.6, 8.0	5.4	1.7, 17	2.1	1.4				

Re-use of Caco-2 monolayers – cell properties validation

V.6.4 – Effect of Caco-2 monolayer re-use on P-gp expression

The effect of re-use and day post-seeding on P-gp expression of Caco-2 monolayers was accessed by flow cytometry after incubation of the cells with a FITC-conjugated antibody to human P-gp. Caco-2 cells from monolayers maintained in culture and that were not used in any permeability assays were labeled to evaluate the P-gp expression at days 22, 25 and 28. Caco-2 cells from monolayers before their re-use for permeability assays with Rho at day 25 (previously used at day 22 in Rho permeability assay) and day 28 (previously used at days 22 and 25 in Rho permeability assays) were also labeled. The green fluorescence due to FITC was recorded using a 530/30 nm band-pass filter (FL1) and plotted as a histogram of FL1 staining. Non-labeled Caco-2 cells were also analyzed for each condition to evaluate the possible contribution from cells autofluorescence to the FL1 signal (negative control sample). The histogram overlays are presented in Figure S4. The median fluorescence intensity (MFI) was the parameter used for comparison. The P-gp expression values were calculated through the shift in the MFI of the cells in the presence of the antibody in relation to the non-labeled cells.

A small population of Caco-2 cells displayed a relatively high fluorescence intensity for the re-used cell monolayers. Since those cell monolayers were previously used in permeability assays with Rho, we pose the question if all the Rho has been removed from the cells. To answer that we have incubated Caco-2 cells in a 12 well-plate with Rho for 2h. After incubation, one batch of cells was washed with HBSS and prepared for flow cytometry. The other batch was maintained in culture and incubated with DMEM following the cell monolayer regeneration procedure proposed.

It was observed that Rho is efficiently removed from cells after washing with HBSS, the fluorescence intensity becoming essentially equal to that of control cells. No further variation was observed for cells incubated with DMEM. This suggests that the presence of the cell population with higher fluorescence observed for the re-used cell monolayers is not due to an inefficient removal of Rho. The relative abundance of this population was higher when the number of counts was smaller, suggesting that it may be due to an artifact independent on the presence of the cells.

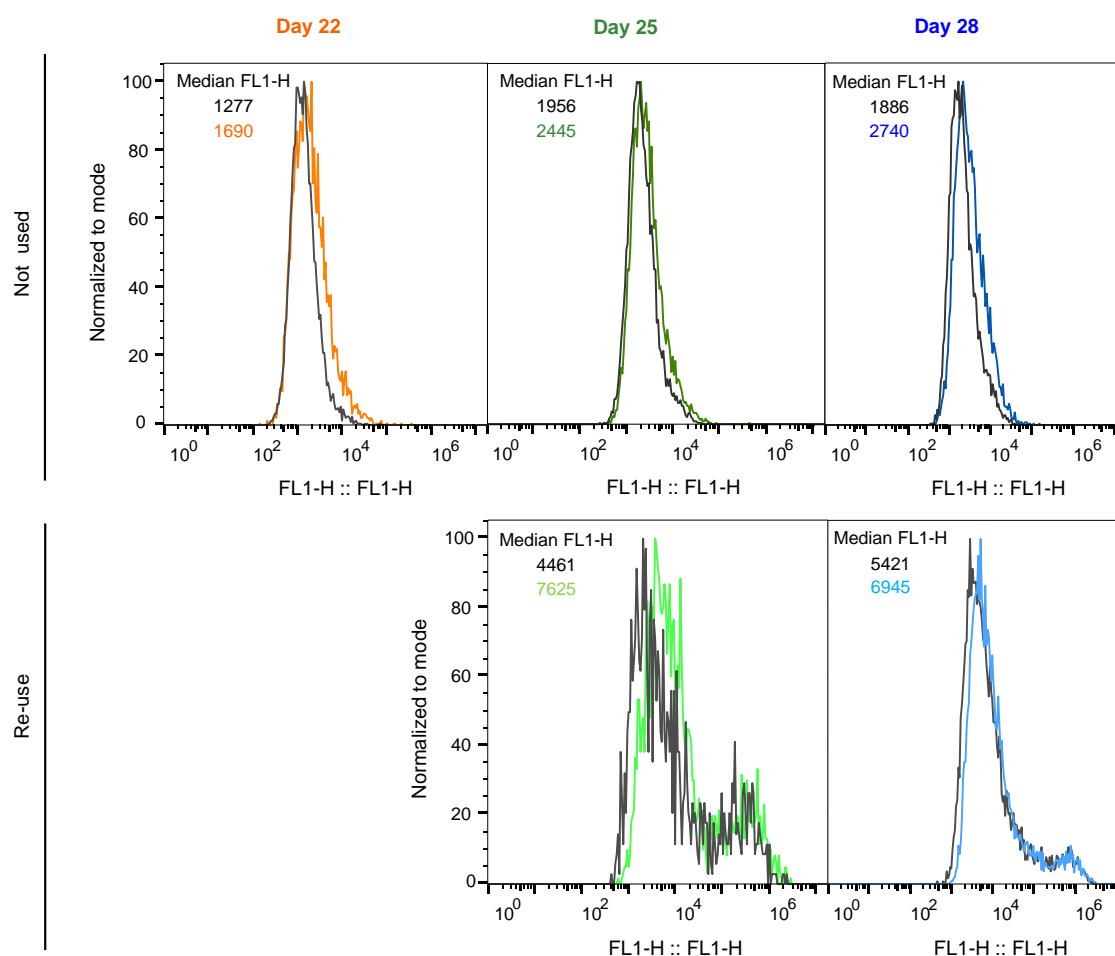


Figure V. S4 Representative histograms overlay of flow cytometric analysis to determine expression of P-gp in Caco-2 cells. The non-labeled Caco-2 cells (negative control) are displayed in black, and the cells incubated with P-gp antibody are displayed in colors. The expression of P-gp acquired in cells from monolayers at day 22, 25 and 28 are shown in the left, middle and right panels, respectively. The upper plots correspond to cells from monolayers that were not used in permeability assays, while the lower plots correspond to cells from monolayers before their re-use for Rho permeability assays at day 25 and 28. The number of events were normalized by mode. The median fluorescence intensity (MFI) was determined for each histogram. The experiments were performed for two independent cell monolayers and the average MFI is shown in Figure V. 6.

Chapter VI

Quantitative comparison of the distinct permeation pathways using MDCK-II, MDCK-MDR1 and Caco-2 monolayers

VI.1 – Abstract

Cell monolayers derived from the epithelial MDCK cell line have been used as an alternative to the traditional Caco-2 model for evaluating drug permeability across intestinal epithelium. The main advantage of using MDCK over Caco-2 cells is its faster grow and differentiation on permeable filters for only 3 to 7 days, meaning that less time is required for the monolayers to be ready for permeability assays. MDCK monolayers represents a possibility for increasing the throughput of compound's permeability assessments. The rationalization of drug permeability in terms of its structural properties using data from distinct cell models, first requires a quantitative comparison for reference compounds covering the distinct permeation routes between the models.

In this study we have performed a quantitative characterization of the morphology, tightness and distinct permeation pathways across the parental cell line MDCK-II, the corresponding cell line overexpressing P-gp (MDCK-MDR1) and Caco-2 monolayers. A systematic evaluation was performed under the same conditions and by the same researcher. The morphology was characterized in detail, regarding cell density and staining of ZO-1 protein measured by confocal microscopy. Also, the monolayers tightness was assessed using TEER measurements and the permeability of three paracellular markers with distinct properties. The monolayers were also evaluated for differences in the permeation across their membranes by analyzing the permeability of reference compounds that use the passive transcellular route and the contribution of efflux activity to the transport. The results showed the existence of small differences in cell and ZO-1 density among the two MDCK and Caco-2 monolayers. Although the main difference was found in relation to efflux activity. In the case of passive transcellular permeation, similar results were obtained for all cell monolayers tested and the data may be pooled in the same dataset for use in *in silico* approaches to predict permeability from the structure of the molecule.

VI.2 – Introduction

The Caco-2 cell line has been thoroughly used in academic and industrial contexts to evaluate the permeability of compounds due to its ability to model *in vivo* human absorption characteristics. Although it is a well-characterized system,

Comparison MDCK-II, MDCK-MDR1 and Caco-2

the application of Caco-2 permeability assays in the screening of large sets of compounds has been hampered by the 21-day period required for monolayers differentiation [91,128]. Our proposed approach of re-using the Caco-2 monolayers for additional permeability assays has shown to have the potential to triplicate its throughput [211]. However, before re-using the monolayers it is still necessary to wait for 21-days for them to be ready to conduct the permeability assays. It is of special interest if one intends to obtain a higher throughput assessment of compound's permeability to reduce the culture time of the monolayers. Since this has been shown not to be possible with Caco-2 monolayers without altering their properties [242-244], the only feasible approach is to replace the Caco-2 cells with a faster growing cell line with similar properties.

The Madin–Darby canine kidney (MDCK) cells, derived from dog kidney epithelia have also been used as a model to evaluate the ability of compounds to permeate across the intestinal epithelium [56,166]. Although non-intestinal, the epithelial origin of these cells give them the capacity to differentiate into polarized monolayers with tight intercellular junctions and apical brush microvilli, similar to the properties found in the Caco-2 system. The major advantages of MDCK over Caco-2 cells is that this differentiation can be accomplished in a much shorter time period, only 3 – 7 days [167,170,245].

The MDCK-II strain, derived from high passage MDCK cells, is the most commonly used for permeability assays due to its electrical resistance properties similar to those observed in the small intestine (TEER values about 100 Ω cm²) [168,170,246]. Studies have pointed out that P_{app} values measured with MDCK-II monolayers for passively permeating drugs correlate well with those from Caco-2 monolayers, which in turn correlate to *in vivo* human intestinal absorption [99,167]. Furthermore, prediction of MDCK P_{app} data using an *in silico* model that was constructed based on Caco-2 P_{app} data, indicated that passive permeability for the different cell lines can be predicted with similar molecular properties and descriptors [88]. Although these studies might indicate the utility of MDCK cells as a promising alternative model to Caco-2 monolayers for passive transport, it is important to account that MDCK cells are not of human origin. For this reason, inter-species differences in the expression levels of some transporters [247] and in carrier-mediated transport, namely in kinetic parameters and substrate specificity, should also be considered when performing studies using these two cell lines [248-250].

Another advantage of MDCK-II cells is the possibility of them being stably transfected with the human multi-drug resistance (*MDR1-1*) gene encoding for P-gp, generating a cell line with enhanced expression levels of human P-gp (MDCK-MDR1) [251]. Because no other efflux transporters are highly expressed, the observed efflux in the assays performed with monolayers of MDCK-MDR1 can usually be attributed directly to P-gp. This has made the use of this cell line as a very useful model to rapidly identify compounds that are subject to P-gp mediated efflux [252].

The existence of several differences, mainly in functionality, between the monolayers obtained from the Caco-2 and MDCK cell lines raises the question of how the permeability data generated with them are compared to each other. A quantitative comparison between the distinct cell models is important to gain valuable knowledge about the possible application of MDCK monolayers as an alternative to Caco-2 for high throughput assessment of compound's permeability. Carrying out their comparison require that the assays must be performed under the same experimental conditions and preferably by the same researcher. Such types of systematic studies are scarce in the literature. Some of the works compared the transport of analogous series of compounds in both models, [172,253,254] or investigated only one permeation pathway [249]. The comparison between cell lines regarding the morphology, gene expression and drug transport through passive and active pathways can only be found in two literature works [81,82]. Although this evaluation was performed with systematic and detail procedures, these works do not cover a full evaluation of all permeation pathways.

The aim of the present study was to provide additional information regarding the quantitative comparison of the monolayers obtained by the three cell lines. This includes the systematic evaluation of morphology, tightness and transport characteristics of compounds permeating through several pathways in the distinct cell models.

Monolayers grown from MDCK-II and MDCK-MDR1 cells were first compared to each other. Confocal microscopy images of nuclei and ZO-1 protein staining were evaluated to assess their morphological features and the presence and location of tight junctions. Assessment of the paracellular and transcellular pathways in each model was performed by determining the permeability across these cell monolayers for reference compounds that follow these routes. P-gp-mediated efflux was also evaluated in both cell models using Rhodamine 123

Comparison MDCK-II, MDCK-MDR1 and Caco-2

(Rho), which was chosen due to its high affinity for P-gp and high sensitivity in its quantification by fluorescence [255]. The bi-directional transport of Rho across the cell monolayers was analyzed regarding the contributions of passive and active efflux processes to the observed overall permeability. Further, the contributions of both processes were validated by repeating the Rho assays after inhibition of P-gp efflux with Verapamil.

Finally, the data obtained for the two variants of MDCK monolayers was compared with that obtained with Caco-2 monolayers, thus providing a systematic comparison of the distinct cell models.

VI.3 – Methods

The permeability assays performed on monolayers of MDCK-II and MDCK-MDR1 were conducted on day 7 post-seeding. The experiments were carried out using the conditions that were previously established for Caco-2 permeability assays and by the same researcher.

TEER values were measured both before and after the permeability assays and all the cell monolayers were considered for analysis (n= 52). The transport of LY, Flu, Atenolol, Prop and SA was evaluated in the A→B direction in multiple samplings at t_{10} , t_{20} , t_{30} and t_{60} min. The permeability assays with LY and Flu were also performed with a single sampling at t_{60} . Rho transport was evaluated in the A→B and B→A directions, with samplings at t_{20} , t_{40} , t_{60} , t_{80} , t_{100} , and t_{120} . As discussed in Chapter V, these sampling points were used to follow the eventual appearance of a lag phase at the beginning of the experiments. The sampling method followed for transport in the A→B direction was the transfer of the inserts to new wells previously loaded with HBSS (transfer method). This was selected because it is faster and more reliable when compared with the withdraw of an aliquot of transport medium from the acceptor compartment and replacement with fresh HBSS (replacement method). The replacement sampling had however to be followed for the evaluation of transport in the B→A direction to avoid turning the insert over. In this case the acceptor compartment has a much better accessibility, thus reducing the time required for sampling and improving its reproducibility (see Chapter VII, section VII.4.2). The bi-directional transport of Rho was also assessed in MDCK monolayers after its pre-incubation with Verapamil for 30 min (in the apical and basolateral sides). The Rho

permeability assay was initiated immediately after the removal of Verapamil solution.

Experiments were carried out in duplicate for the same cell preparation. The mass balance was estimated between 90–110% for all the test compounds, with the exception of Prop that had recoveries of 70–80%.

The statistical analysis of P_{app} values was performed for $\text{Log}P_{app}$, since it was previously shown that this is the variable that follows a normal distribution (see Chapter IV for details). From $\text{Log}P_{app}$, the average values and the 95% confidence intervals (CI_{95}) of P_{app} were calculated using the Equation IV.1 in Chapter IV. This statistical analysis was performed using Microsoft Excel.

After determining Rho P_{app} values in both directions of the assays, the analysis of P-gp efflux activity in the cell monolayers was performed using 3 different steps: i) through the calculation of the efflux ratio for each cell monolayer. This is the most common approach and corresponds to the ratio between the P_{app} values obtained in B→A and A→B, Equation V.1, Chapter V; ii) and an alternative approach proposed by us based on the calculation of the contributions from passive (P_{app}^{PP}) and active efflux (P_{app}^{AE}) processes to the observed P_{app} value. In this approach it is assumed that the absolute values of P_{app}^{PP} and P_{app}^{AE} are the same in the assays performed in both directions (A→B and B→A), Equation V.3, Chapter V; iii) and through the calculation of the net flux ratio by dividing the efflux ratio obtained in MDCK-MDR1 transfected cells by those obtained in the MDCK-II parental cell line, using Equation VI.1:

$$\text{Net Flux Ratio} = \frac{\text{Efflux ratio}_{\text{MDCK-MDR1}}}{\text{Efflux ratio}_{\text{MDCK-II}}} \quad \text{VI.1}$$

The later approach is generally applied when both cell lines are used simultaneously in experiments. It allows the correction of the efflux ratio observed in MDCK-MDR1 for efflux activity already present in MDCK cells.

The test compounds used in the permeability assays with MDCK cell lines were also measured across Caco-2 monolayers at days 22, 25 and 28 post-seeding. The Caco-2 P_{app} values obtained for these compounds were reported in Chapter IV and V and are included in the current chapter for comparison.

For characterization by confocal microscopy, MDCK-II and MDCK-MDR1 monolayers were stained after being used in permeability assays with LY. The

Comparison MDCK-II, MDCK-MDR1 and Caco-2

cell nucleus was stained with Hoechst 33342 and ZO-1 protein was stained with antibodies. Two cell monolayers were analyzed for each cell model. From the acquired images, orthogonal projections of the XZ-plane were created from all the z-slices to view in detail the localization of the fluorescence of ZO-1. For each image, it was also determined the cell density by counting the number of nuclei and the fractional area occupied by ZO-1 by applying a manual threshold to select only ZO-1 fluorescence. The values obtained for these parameters were compared with those previously determined in confocal images of Caco-2 monolayers.

VI.4 – Results and discussion

VI.4.1 – Quantitative comparison of permeation pathways in MDCK monolayers

The two variants of the MDCK cell line, MDCK-II and MDCK-MDR1, were grown as monolayers and used to perform permeability assays. To quantitatively characterize the distinct permeation pathways in both cell monolayers, the permeability assays were performed in a systematic manner and using the same experimental conditions. The passive permeability via paracellular and transcellular routes and active efflux transport were determined in both cell monolayers using reference compounds that are commonly applied for this purpose. The permeability of the test compounds and the morphological analysis obtained by confocal microscopy are shown and discussed in the next sections.

VI.4.1.1 – Characterization of paracellular permeability

VI.4.1.1.1 – TEER values

On day 7 post-seeding in the Transwell™ inserts, the TEER values of MDCK-II and MDCK-MDR1 monolayers were measured before and after the permeability assays. The TEER values obtained for cell monolayers before the assays were statistically equivalent, being 60 ± 5 and $69 \pm 8 \Omega\text{cm}^2$ for MDCK-II and MDCK-MDR1, respectively. TEER values of this magnitude for MDCK monolayers are systematically observed by other authors under the same experimental conditions [82,169]. This low TEER value is due to the many ion

transporters present in the MDCK cell line. These transporters are linked to the cell's natural function in reabsorbing ions, as it originates from kidney epithelial tissue. It is often overlooked that the electrical parameter of TEER represents the resistance to the flow of ions through the paracellular and also through the transcellular pathway via ion channels and pores [256]. The genes that encode for various types of claudin proteins with pores forming functions were found to be highly expressed in MDCK cells compared to other cell lines. This high level of ion pores facilitates the cation movement across MDCK monolayers and thereby it has been suggested to be responsible for decreasing their TEER [81,246,257]. As a consequence, the low TEER values obtained for MDCK monolayers cannot be directly attributed to a decreased tightness of the cell monolayer. TEER measurements alone cannot reflect the transport across the paracellular route, nor the tightness of the cell monolayer. A more informative indication regarding the monolayer confluence and tightness may be obtained from a morphological analysis by confocal fluorescence microscopy. In addition, the use of paracellular markers will provide a more quantitative evaluation of permeation through the paracellular route.

VI.4.1.1.2 – Morphological features and staining of tight junction protein ZO-1

MDCK-II and MDCK-MDR1 monolayers were analyzed by confocal microscopy after staining for nuclei and ZO-1 protein of tight junctions. Representative images of the cell monolayers obtained at the end of multi-time sampling permeability assays are displayed in Figure VI. 1, and the corresponding larger area images are provided in supplementary material – Figure VI. S1. A confluent monolayer of cells is visible in the confocal microscopic images of both cell models. A striking difference is observed in the cell density, with the cross-section of cells and nuclei being much smaller for MDCK-MDR1. The distinct morphology of the cells when grown as confluent monolayers has been reported before [81]. The average nuclei size of MDCK-MDR1 is ~5-10 μm while in MDCK-II monolayers is ~10-20 μm . It is important to note that the same initial cell density was used to seed the cells on inserts. Due to differences in the properties, the number of nuclei *per* area varied, with MDCK-MDR1 monolayers exhibiting a high cell density of $1.2 (\pm 0.1) \times 10^6$ cells/cm² compared to $6.5 (\pm 0.2) \times 10^5$ of MDCK-II monolayers.

Comparison MDCK-II, MDCK-MDR1 and Caco-2

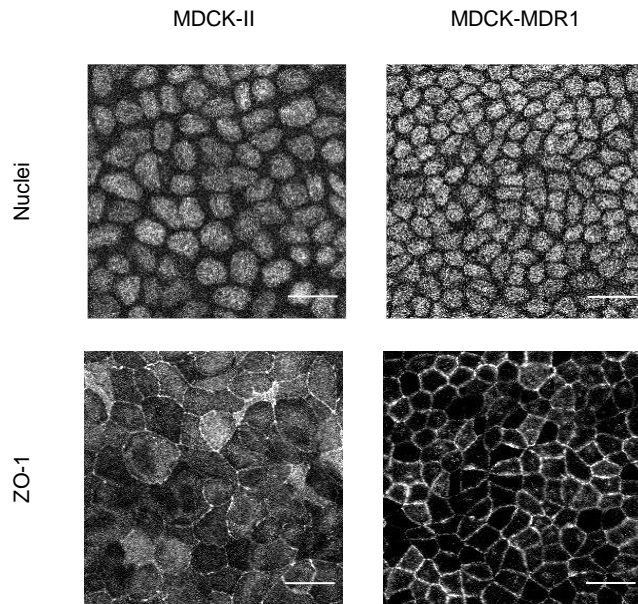


Figure VI. 1 Representative images of MDCK-II and MDCK-MDR1 monolayers observed at the confocal microscope. The nuclei were stained by Hoechst and tight junctions were stained by antibodies against the protein ZO-1. The images are the maximum intensity projection of z-stacks. Scale bar 20 μm .

ZO-1 staining is found in the regions of contact between the cells, both in MDCK-II and MDCK-MDR1 monolayers, indicating the formation of a continuous network of tight junctions. To provide information regarding the transversal position of ZO-1 in the cell monolayers, the cross-section view of the z-stack projections of confocal images is shown in Figure VI. 2. It is observed that ZO-1 protein is located in the apical side on both cell monolayers, as expected. A quantitative evaluation of ZO-1 fluorescence shows 56% higher intensity in the MDCK-MDR1 monolayers. This result is in agreement with the different sizes observed for the two variants of the MDCK cell line, with a higher cell-cell interface in the case of cells with a lower cross-section. The much higher density of cell-cell interface in the case of monolayers from MDCK-MDR1 leads to a higher relative surface of the paracellular pathway when compared to transcellular pathways. This is expected to have important consequences in the permeability coefficients observed for the distinct pathways in the two cell monolayers.

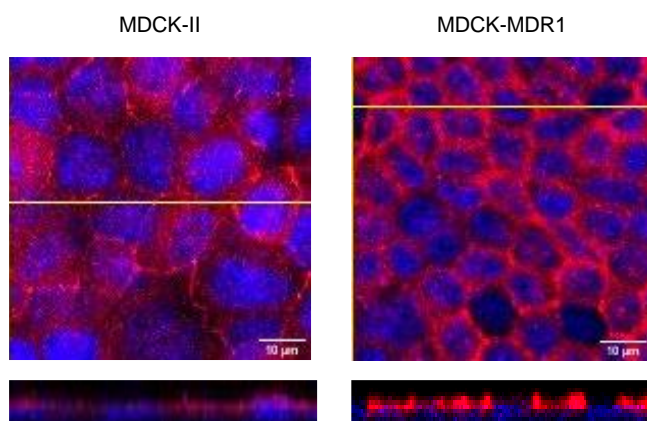


Figure VI. 2 Staining of ZO-1 protein (red) and nuclei (blue) for MDCK-II and MDCK-MDR1 monolayers. The localization of ZO-1 is shown in the lower plots that correspond to the z-stacks at the cross section indicated by the respective yellow line.

VI.4.1.1.3 – Paracellular markers: Lucifer yellow, fluorescein and atenolol

The permeation of small hydrophilic molecules is commonly used to assess the tightness of the paracellular route in cell monolayers. Those paracellular markers cannot show significant transport through the transcellular pathways, both through passive or active routes. LY is a model compound that fulfills these requirements and may be detected with high sensitivity due to its high fluorescence quantum yield. The permeability of LY across MDCK-II and MDCK-MDR1 monolayers was evaluated in assays using a single 60 min sampling or following multiple samplings within 60 min. The results are shown in Figure VI. 3 and the detailed statistical analysis is provided in supplementary material – Table VI. S1. When a single sampling was performed at 60 min, a small value for LY permeability of $0.7 [0.5;0.8] \times 10^{-7}$ cm/s was obtained in MDCK-II monolayers, indicating the presence of a tight cell monolayer. In MDCK-MDR1 monolayers, the obtained LY P_{app} value is high, increasing almost 13-fold in relation to MDCK-II to a value of $8.8 [3.9;19.9] \times 10^{-7}$ cm/s. This LY P_{app} value is slightly above the expected value for a tight monolayer, $P_{app} < 5 \times 10^{-7}$ cm/s [182,202,207]. The relative P_{app} observed for the two cell monolayers can be explained based on the results of the morphological analysis. The surface area available for the paracellular permeation of LY is higher in MDCK-MDR1 monolayers due to the smaller cross-sectional area of the cells. Therefore, the higher P_{app} obtained for LY with the MDCK-MDR1 monolayers may simply reflect the higher surface available for the

Comparison MDCK-II, MDCK-MDR1 and Caco-2

paracellular pathway, and cannot be taken as an indication of a lower tightness of the tight junctions in this cell monolayer.

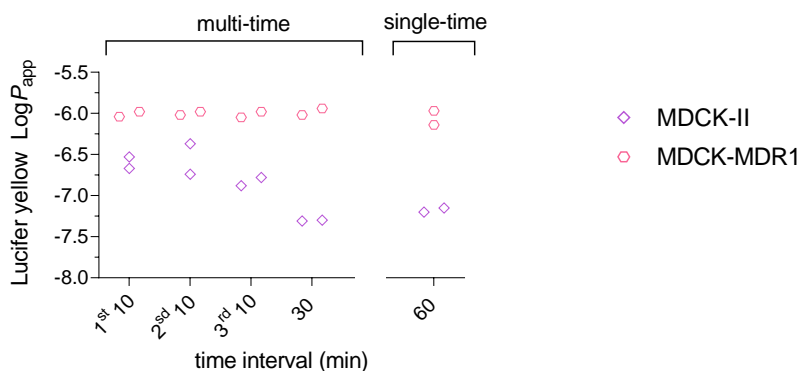


Figure VI. 3 Dependence of LY P_{app} values on the sampling interval in either MDCK-II and MDCK-MDR1 monolayers after multi-time and single-time sampling permeability assays.

The analysis of the LY P_{app} values on consecutive and distinct sampling times provides information regarding possible perturbations induced by the sampling and/or LY carry-over in consecutive sampling. Perturbation of the monolayer tightness is expected to lead to an increase in P_{app} for consecutive sampling, both using the same or different time intervals. On the other hand, carry-over of analyte in the acceptor compartment is expected to lead to a decrease in P_{app} as the time interval is increased. Both effects were observed in the case of Caco-2 monolayers (see Figure IV. 4 and IV. 5). A significant effect of the sampling time is also observed in the case of monolayers of MDCK-II. In these monolayers, LY P_{app} values are essentially maintained for consecutive sampling with a 10 min time interval, and decrease with the increase of the sampling time interval from 10 to 30 and to 60 min. In contrast, for MDCK-MDR1 monolayers, LY P_{app} values are essentially unchanged. These results may be interpreted in light of the much higher amount of LY that permeates during the sampling interval, thus less sensitive to small contributions from carry-over in consecutive sampling. It is also compatible with a lower sensitivity to manipulation for this thicker (and tight) cell monolayer.

Permeability assays were repeated with Flu and Atenolol, two other model compounds commonly used to access the paracellular transport. The results obtained are shown in Figure VI. 4 and the detailed statistical analysis is provided

in supplementary material – Table VI. S1. Regarding Flu permeability, the P_{app} values are similar for both cell monolayers, except in the single-time assays (60 min), with a 2-fold increase between MDCK-II and MDCK-MDR1 monolayers. A small decrease in P_{app} with the increase in the sampling time is observed MDCK-II monolayers, although the difference is not statistically significant. The sensitivity of Flu P_{app} regarding the sampling times and cell monolayer is much lower than observed for LY (Figure VI. 3). These results suggest a significant contribution of the transcellular pathway for the transport of Flu across the cell monolayers, as observed before for the Caco-2 cell line (Figure V. 2), and further support the superiority of LY as a paracellular marker.

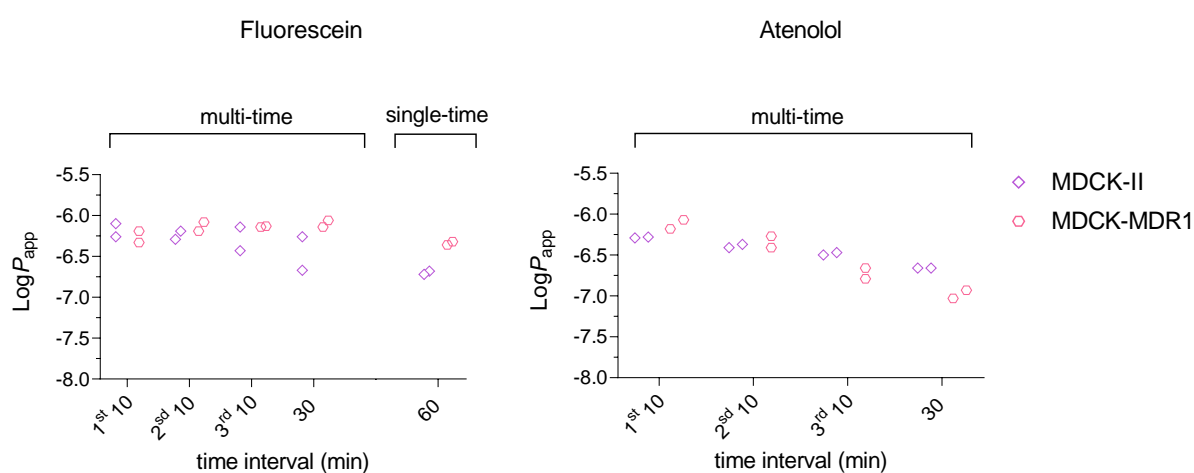


Figure VI. 4 Dependence of Fluorescein and Atenolol P_{app} values on the sampling interval for permeability assays performed across MDCK-II and MDCK-MDR1 monolayers.

The permeability behavior of Atenolol was equivalent to that of Flu for the assays performed across MDCK-II monolayers. However, a distinct behavior was observed for MDCK-MDR1 monolayers. In contrast with what was observed for the transport of LY and Flu across this cell line, Atenolol shows a marked decrease in P_{app} values in consecutive sampling and with the increase of the sampling time intervals. This decrease was even more accentuated than that observed for MDCK-II, with the values of P_{app} for 30 min sampling being lower for this cell type than for the parental MDCK-II. The results can be explained if there is transport of Atenolol against its concentration gradient showing a lag phase, thus being larger at longer times of incubation. One possibility is efflux by P-gp, which requires the previous permeation into the cell to reach the transporter binding site. In agreement with this interpretation, a lag phase is observed for the efflux

Comparison MDCK-II, MDCK-MDR1 and Caco-2

of Rhodamine by P-gp (Figure VI. 6 plot A). Also, it has in fact been previously suggested that Atenolol is a substrate of P-gp [81,258,259]. Atenolol should not therefore be used to evaluate permeability through the paracellular pathway since the observed P_{app} includes contributions from transcellular transport, both passive influx and active efflux.

VI.4.1.2 – Characterization of the transcellular permeability

Propranolol and salicylic acid were used as model compounds to evaluate passive transcellular permeation in MDCK-II and MDCK-MDR1 monolayers. The results obtained for P_{app} of PROP and SA are presented in Figure VI. 5, and the detailed statistical analysis is provided in supplementary material – Table VI. S2. The results obtained for the two cell monolayers were very similar. A tendency for smaller values of P_{app} were observed for MDCK-MDR1 monolayers, but the difference is not statistically significant. It is observed a small increase in P_{app} for consecutive samplings of 10 min, and a small decrease with the increase in the sampling interval for 30 min. This behavior has been observed previously and may reflect perturbation of the cell monolayer integrity, and/or carry-out of compound in the acceptor compartment when the inserts are transferred to new wells at the consecutive sampling time points (see Figure IV.4 and IV5, section IV.4.2, Figure V.3 and VII.4.2).

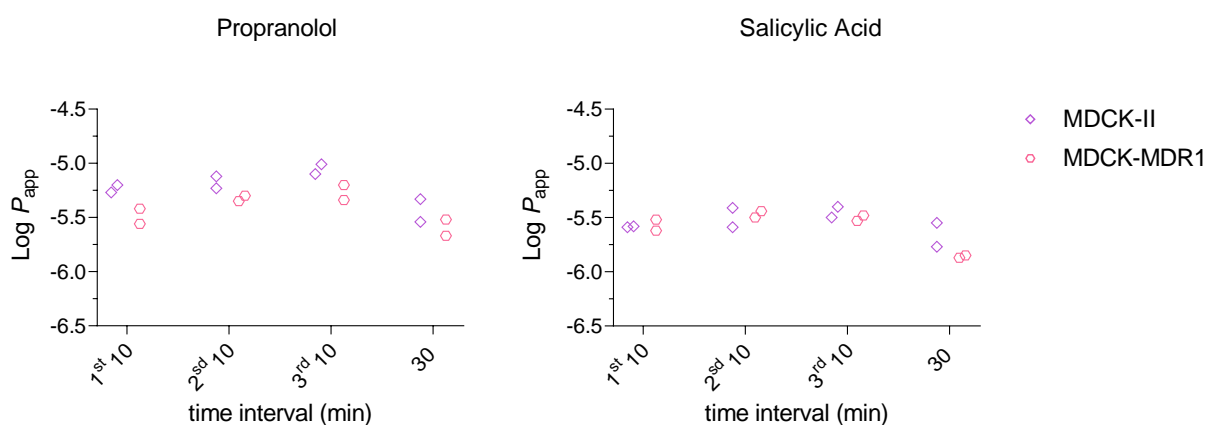


Figure VI. 5 Propranolol and Salicylic acid P_{app} values after a multi-time sampling permeability assay across MDCK-II and MDCK-MDR1 monolayers.

VI.4.1.3 – Characterization of the active efflux by P-gp

The evaluation of efflux transport was done by measuring P_{app} in both directions (A→B and B→A). This is a standard procedure used to identify compounds that are substrates of efflux transporters such as P-gp. In this study, we compared the efflux activity in MDCK-II and in the P-gp transfected MDCK-MDR1 cell line, using the well-known P-gp substrate Rhodamine 123 (Rho) [255].

The results obtained for P_{app} of Rho across MDCK-II and MDCK-MDR1 monolayers are presented in Figure VI. 6. The variation of the instantaneous permeability with the incubation time is presented in plot A, both in the A→B and B→A directions. It is observed a lag phase for transport in the B→A direction, which lasted up to 60 min and increased the Rho P_{app} values during this time interval. A steady-state is attained after 60 min, with the instantaneous permeability being maintained until the end of the assay, although small variations are still observed for the MDCK-II monolayers with a tendency for an increase in P_{app} in the B→A direction.

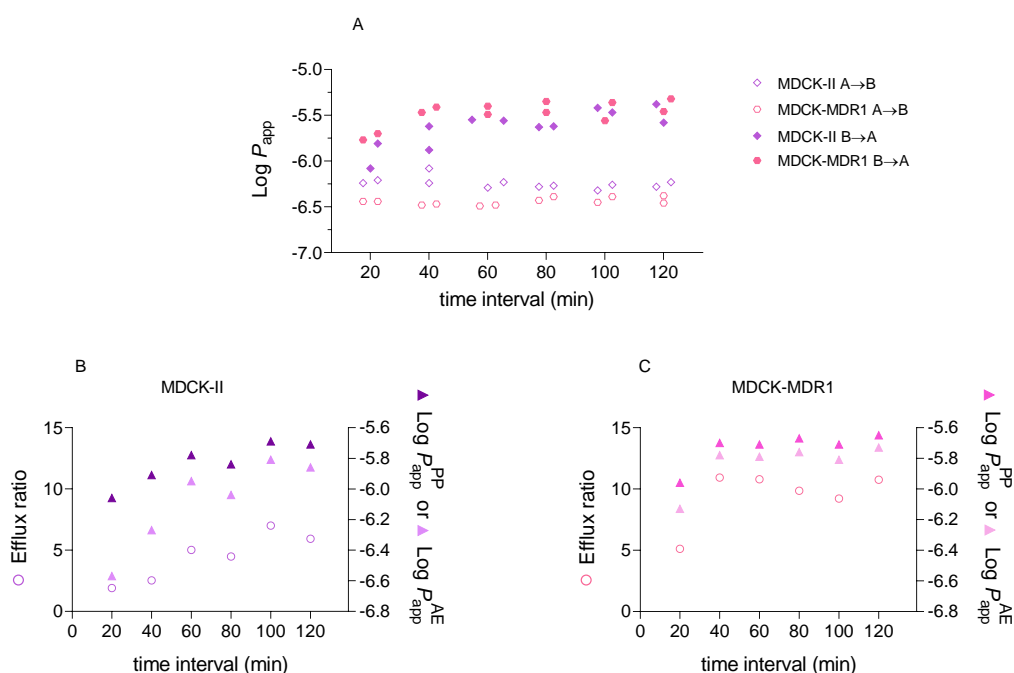


Figure VI. 6 Rho permeability across MDCK-II and MDCK-MDR1 monolayers. Plot A: Instantaneous $\text{Log } P_{app}$ values as a function of the incubation time in the A→B and B→A directions. Plot B and C: instantaneous efflux ratio (left y-axis) and contributions of passive (P_{app}^{PP}) and active efflux (P_{app}^{AE}) to the measured P_{app} values (right y-axis). The efflux ratio is calculated from the instantaneous $P_{app}^{B \rightarrow A} / P_{app}^{A \rightarrow B}$ and the parameters P_{app}^{PP} and P_{app}^{AE} are calculated using Equation (V. 3).

Comparison MDCK-II, MDCK-MDR1 and Caco-2

The first observation is that in both cell types, Rho showed a polarized transport, with P_{app} values being higher in the B→A than in the A→B direction. This leads to a significant efflux ratio of Rho (Figure VI. 6 plot B and C). For incubation times between 60 and 120 min, the average efflux ratio was 6 ± 1 in MDCK-II and increased to 10 ± 1 in MDCK-MDR1 cell monolayers. As expected, this indicates an increase in Rho efflux by P-gp in the transfected cell monolayers. It is well-known that the induction of Multidrug resistance (MDR) is not only the result of an increased expression of efflux transporters, but also includes changes in the fluidity of the lipid membrane that contribute to the decrease in permeability [260,261]. The contribution from changes in the properties of the lipid membrane is particularly important when MDR is induced by cell growth in the presence of high concentrations of drugs [262,263]. However, the overexpression of efflux transporters may by itself be associated with changes in the lipid composition of the cell membranes [264-266]. An increase in the efflux ratio could be originated from an increase in the efflux activity or by a decrease in the rate of passive permeation due to changes in the cell membrane properties. To evaluate for the contribution from the two effects, the overall permeability observed was deconvoluted into the contribution from passive P_{app}^{PP} and active P_{app}^{AE} processes (Equation V.3, Chapter V). This analysis procedure has the additional advantage of providing a quantitative evaluation of the rate of active efflux (Figure VI. 6 plot B and C). The results show that the P_{app}^{PP} values were similar for the two cell monolayers, although slightly higher (1.2-fold) for MDCK-MDR1. A more significant difference was observed for the active efflux component, which was higher (1.4-fold) for MDCK-MDR1 monolayers. This analysis shows that the increase in the efflux activity of MDCK-MDR1 is the major difference when compared with parental cells.

The deconvolution between the contribution of passive permeation and active efflux shows that the variation observed in the efflux ratio with the time of the permeability assay is the result of changes in both transport pathways. Surprisingly, a strong increase is observed in P_{app}^{AE} for the parental cell line (from a $\text{Log}P_{app}^{AE} = -6.6$ at 20 min to -5.8 at 100 min), leading to a 6-fold variation. This is however accompanied by a 2-fold increase in P_{app}^{PP} that partially counterbalances the increase in P_{app}^{AE} and leads to only a 3-fold variation in the efflux ratio. In contrast, the time dependence of both P_{app}^{PP} and P_{app}^{AE} is similar in MDCK-MDR1 monolayers, with only a 2-fold increase from 20 to 120 min. The reasons for the

increase in permeability with the assay time are not totally clear to us, and comparison with literature is not possible because the time dependence of P_{app} is usually not reported. An analysis to Equations V. 3 shows that the sensitivity of P_{app}^{PP} and P_{app}^{AE} is much larger when the efflux ratio is lower, which may explain the smaller variation with the assay time obtained for MDCK-MDR1. A possible explanation for the relatively low P_{app}^{PP} and P_{app}^{AE} values measured at short times in the permeability assay may be related with a slow flip-flop of Rho between the membrane leaflets. Eytan et. al. reported a characteristic time of 3 min for the flip-flop of Rho through model membranes composed of Egg Phosphatidylcholine with 2 15% cardiolipin [267]. The much lower fluidity of the cells plasma membrane [266,268] would significantly slow-down the rate of flip-flop [269] and could at least partially justify the lag-time observed.

The efflux ratio observed in MDCK-II indicates that these cells already express efflux transporters that are active for Rho, which may or may not include P-gp. An advantage of performing assays with the parental and overexpressing P-gp cells is the possibility of evaluating specifically the efflux activity of P-gp [252]. This comparison leads to a net flux ratio of 1.7 (Equation VI.1). The obtained value is lower than usually reported in the literature (e.g., Hellinger et al. [81] obtained a net flux ratio of 3.3, while Shang et al. [270] obtained a net flux ratio of 7.2). Variations in the expression of P-gp could result from changes in the transfection efficiency or in the relative populations of distinct cell phenotypes with increased cell passages. Changes at high passage numbers have been observed in the expression of GFP reporter gene in transfected Caco-2 and MCF7 cell lines [271]. The passage number and the composition of the culture medium have also been shown to influence the expression level of GFP in transfected CHO-K1 cells [272].

As a final quantitative characterization of the efflux pathway on these cell monolayers, the effect of Verapamil (100 μ M) on Rho efflux by P-gp was evaluated. The results obtained are presented in Figure VI. 7.

Comparison MDCK-II, MDCK-MDR1 and Caco-2

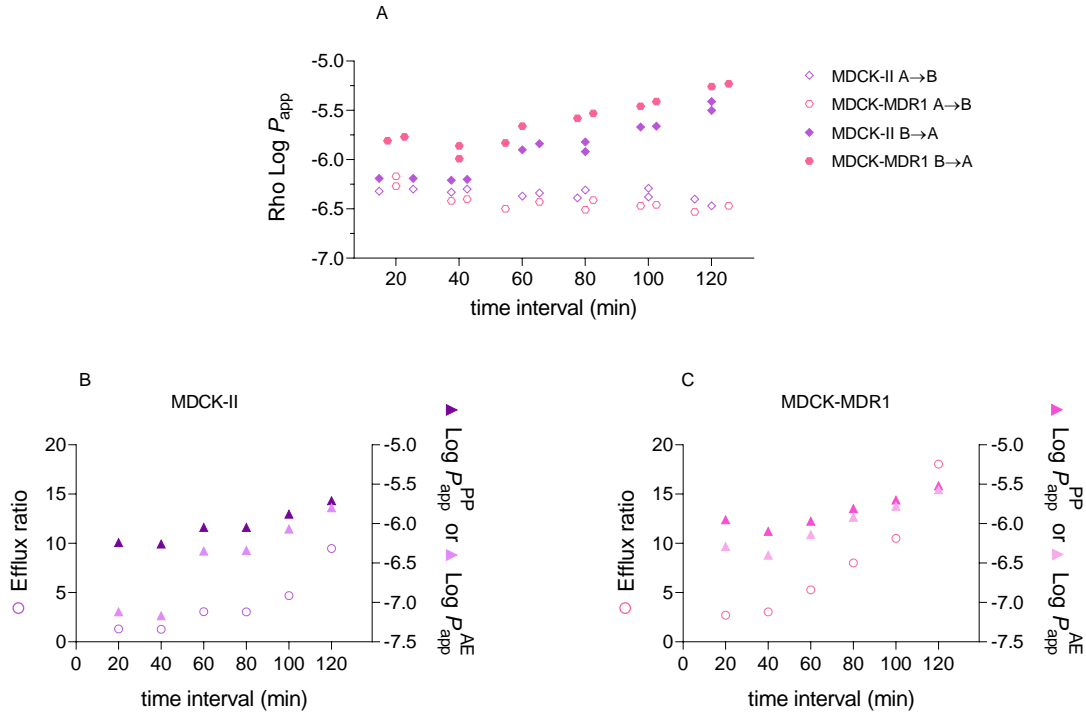


Figure VI. 7 Rho permeability across MDCK-II and MDCK-MDR1 monolayers after pre-incubation with 100 μM Verapamil for P-gp efflux inhibition. Plot A: Instantaneous $\text{Log } P_{\text{app}}$ values as a function of the incubation time in the A→B and B→A direction. Plot B and C: instantaneous efflux ratio (left y-axis) and contributions of passive ($P_{\text{app}}^{\text{PP}}$) and active efflux ($P_{\text{app}}^{\text{AE}}$) to the measured P_{app} values (right y-axis). The efflux ratio is calculated from the instantaneous $P_{\text{app}}^{\text{B}\rightarrow\text{A}}/P_{\text{app}}^{\text{A}\rightarrow\text{B}}$ and the parameters $P_{\text{app}}^{\text{PP}}$ and $P_{\text{app}}^{\text{AE}}$ are calculated using Equation (V. 3).

At the beginning of the assay, the expected behaviour was obtained. That is, a markedly low efflux ratio in both MDCK-II and MDCK-MDR1 (1.3 and 3, respectively) due to inhibition of the efflux transporters. However, for incubations longer than 40 min, there is a large increase in the efflux ratio reaching the value obtained in the absence of Verapamil at 100 min. In an attempt to interpret this behavior, the observed transport was deconvoluted in the contributions from passive and active transport (Figure VI. 7 plot B and C). As observed in the absence of Verapamil, there is a significant increase in both $P_{\text{app}}^{\text{PP}}$ and $P_{\text{app}}^{\text{AE}}$ over the time of the permeability assay. However, a steady state is not achieved during the 120 min of the permeability assay. Also, while a similar variation is observed for $P_{\text{app}}^{\text{PP}}$, a much higher increase is observed in $P_{\text{app}}^{\text{AE}}$, suggesting that inhibition of efflux transporters by Verapamil is becoming less efficient in both MDCK cells. Surprising at first, this result is actually a direct consequence of the methodology followed, where cells are pre-incubated with

Verapamil, but washed out before the permeability assay. In the initial time intervals, there are still large amounts of Verapamil associated with P-gp leading to a significant P-gp inhibition. However, at longer time intervals, the local concentration of Verapamil decreases due to equilibration with the transport media. The increase in P_{app}^{AE} is larger for MDCK-II than for MDCK-MDR1. This may reflect a lower concentration of Verapamil at the beginning of the assay in MDCK-MDR1 cells due to the higher active Verapamil efflux in these cells. During the incubation of the monolayers with Verapamil, passive permeation allows its entrance into the cells, which is counterbalanced by its active efflux by P-gp. Therefore, the concentration of Verapamil inside the cells is lower for the MDCK-MDR1 cells due to the over-expression of P-gp. After removal of Verapamil from the medium, the decrease in its intracellular concentration is also faster for the case of the MDCK-MDR1 cells. This leads to the disappearance of the inhibition of Rho efflux in MDCK-MDR1 monolayers, while it is still maintained in the MDCK-II monolayers.

The presence of high concentrations of Verapamil in the MDCK-II monolayers until 40 min may also explain the small decrease observed in Rho P_{app}^{PP} values in this time interval. Due to the moderate lipophilicity of Verapamil ($K_p \sim 10^3$ at pH=7.4 [273]), high local concentrations in the cell membranes are expected. Both Verapamil and Rho are positively charged at the assay pH, and the presence of Verapamil changes the surface potential at the cell membrane [274,275]. Depending on the local concentration of Verapamil, the surface potential will become less negative or even positive, leading to a decrease in the partition coefficient of Rho [274,275] and in the observed P_{app}^{PP} .

The time-dependent variations in the properties of the cell monolayers are due to the pre-incubation of the cell monolayers with a very high concentration of Verapamil and its removal from the transport media immediately before the permeability assay. In an alternative protocol used by some authors, the cell monolayers are pre-incubated with Verapamil at 50 μ M [270] and 100 μ M [276] and this condition is maintained through the permeability assays. A decrease in the efflux ratio was obtained in the presence of Verapamil, as it is expected for MDCK-MDR1 cells. Calculating the P_{app}^{AE} and P_{app}^{PP} values for these assays, it is observed a decrease in both the parameters when Verapamil is present. Although the instantaneous values of P_{app} were not reported in those studies, this methodology is expected to correct for the variation in Verapamil concentration throughout the

Comparison MDCK-II, MDCK-MDR1 and Caco-2

permeability assay. However, this approach does not correct for the effects on P_{app}^{PP} due to changes in the membrane electrostatic potential. At the high Verapamil concentrations needed to efficiently compete with P-gp, a significant decrease in the P_{app}^{PP} of cationic species is expected, artificially increasing the efflux ratio calculated from $P_{app}^{B \rightarrow A} / P_{app}^{A \rightarrow B}$. To avoid these artifacts, the use of non-competitive and more efficient inhibitors (e.g. Tariquidar [277,278]) may be recommended when evaluating the contribution of P-gp active efflux in permeability assays.

VI.4.2 – Quantitative comparison of permeation pathways between Caco-2 and MDCK monolayers

Caco-2 and MDCK cells are derived from epithelial tissues with different physiological functions, in addition from being of different species. The transport of compounds across monolayers obtained from these cell lines may be altered as a result of different transporters expression levels, lipid composition of their membrane bilayers and metabolic activity. The systematic characterization of the distinct permeation pathways in each of the cell monolayers is important to quantitatively compare the permeability data obtained from them. This study provides a systemic evaluation of the morphology, tightness and functionality of MDCK-II, the corresponding cell line overexpressing P-gp MDCK-MDR1 and Caco-2 monolayers. The comparison with Caco-2 monolayers included the use of these cell monolayers on days 22, 25 and 28 post seeding. The results are summarized and discussed in the next sections.

VI.4.2.1 – Morphological features and tight junctions staining

The confocal microscopy analysis was carried out for all cell monolayers after being used for a permeability assay. In the process of acquiring the images, the number of z-stacks needed to capture the entire cell monolayer is indicative of its thickness. For Caco-2 and MDCK monolayers, the number of z-stacks was found to be similar, ranging from 8 to 12 slices (8-12 μm). Enclosing the monolayers within this number of z-stacks allows them to be identified as a single layer of cell [81]. The most significant difference between the images of cell monolayers was observed for the average nuclei size. As a result, the number of

nuclei in the analyzed image area was different among the monolayers, and varied as follows: Caco-2 (day 22: 582 ± 71 ; day 25: 550 ± 12 ; day 28: 560 ± 26) < MDCK-II (1206 ± 40) < MDCK-MDR1 (2241 ± 236). This corresponds to significant differences in cell density, with MDCK-MDR1 monolayers exhibiting the highest cell density and Caco-2 the lowest.

ZO-1 protein staining was detected in all cell monolayers. The area occupied by tight junctions was found to be much lower in Caco-2 (8 % in all days) than in MDCK monolayers ($11 \pm 3\%$ in MDCK-II and $26 \pm 3\%$ in MDR1). These results reflect the different cell density in the distinct monolayers, with a higher contribution of cell-cell contacts in cells with a smaller size. The relative contribution of cell-cell interface taking into account the distinct cell size was estimated considering a squared cross-section for the cells and the average size obtained from confocal microscopy. This contribution was expected to increase 1.5-fold for MDCK-II and 2-fold for MDCK-MDR1 when compared to Caco-2 monolayers. This is in good agreement with the increase observed in ZO-1 staining for MDCK-II (1.4-fold). The very large increase in ZO-1 staining observed for MDCK-MDR1 (3.3-fold) suggests that the cell-cell contacts have a higher abundance of tight-junctions. This is in light with the up-regulation of ZO-1 expression at higher cell densities [279,280].

To our knowledge, the differences found in cell size and ZO-1 density between the distinct cell models although previously observed [81], have never been highlighted nor a relationship has been made between this property and the observed differences in permeability through the distinct routes. This is however an important parameter between the distinct cell models and justifies some of the differences observed.

VI.4.2.2 – Compounds with low passive permeability

TEER measurements have been used in many studies as the first parameter to assess the permeability through the paracellular pathway on cell monolayers. Generally, a cut-off value for TEER is defined as a criterion to consider the cell monolayer as confluent and tight and therefore ready to perform the permeability assays. This value corresponds to $> 200 \Omega \text{ cm}^2$ in the case of Caco-2 monolayers. This cut-off value cannot be applied to monolayers obtained from MDCK cell lines, which show TEER values about twelve times lower than those

Comparison MDCK-II, MDCK-MDR1 and Caco-2

of Caco-2 monolayers at day 22. If Caco-2 monolayers at day 28 are considered, the difference between both cell models is even higher (Table VI. 1). However, although the TEER values of MDCK monolayers are below the threshold, they do not reflect a compromise in tightness, as evidenced by the high density of ZO-1 at the cell-cell contacts. In the case of MDCK-II, this is also supported by the low permeability of the paracellular marker LY, MDCK-II (0.7×10^{-7} cm/s), Caco-2 day 22, day 25 and day 28 (from 2.1 to 1.8 and 1.9×10^{-7} cm/s, respectively). A relatively higher value is however observed for MDCK-MDR1 monolayers (8.8×10^{-7} cm/s). As discussed in section VI.4.1.1.3, this reflects the higher surface available for this pathway due to the much smaller cell size. According to LY P_{app} results, all the cell monolayers can be employed if we intended to perform permeability assays using a tight cell monolayer, for instance, to predict permeation across the Blood-Brain Barrier.

In relation to Flu permeability, the MDCK-MDR1 model also present slightly higher P_{app} values in comparison with MDCK-II and Caco-2 models. Although, the differences found between the distinct cell monolayers are not statistically significant. The slightly higher Flu permeability in the MDCK models than in the Caco-2 model is also reported in the other studies in literature that compared the three cell models [81,82]. As discussed above for LY, this observation may reflect the higher surface available for the paracellular pathway. The relatively smaller effect observed for Flu being due to a significant permeability through transcellular pathways.

Table VI. 1 Paracellular tightness of the distinct cell monolayers assessed by TEER measurements and permeability of model compounds that use the paracellular route.

Cell line	Day post-seeding	TEER Before Ωcm^2	TEER After Ωcm^2	P_{app} (10^{-7} cm/s) A \rightarrow B						
				Lucifer yellow			Fluorescein			
		N ^b	$\mu \pm \sigma$	$\mu \pm \sigma$	N	μ	CI ₉₅	N	μ	CI ₉₅
MDCK-II	7	23	60 ± 5.1	60 ± 6.9	2	0.7	0.5; 0.8	2	2.0	1.7; 2.4
MDCK-MDR1	7	23	69 ± 8.2	69 ± 6.1	2	8.8	3.9; 19.9	2	4.6	3.8; 5.5

	22	62	1021 ± 436	807 ± 352	35	2.1	1.2; 3.9	4	1.1	0.2, 5.8
Caco-2 ^a	25	51	1045 ± 515	910 ± 411	29	1.8	1.0; 3.2	4	0.9	0.1, 7.6
	28	40	1219 ± 428	969 ± 360	24	1.9	0.8; 4.7	4	1.6	0.3, 9.8

^a TEER values and P_{app} values obtained in Caco-2 monolayers are reported in Chapter V and VI.

^b Number of cell monolayers used in assays. The P_{app} values were obtained from a single 60 min sampling permeability assays. Statistically significant differences from the P_{app} values obtained in Caco-2 monolayers are in marked bold.

VI.4.2.3 – Compounds with high passive permeability

The P_{app} values of the compounds Prop and SA, which permeate mainly through the transcellular route, did not show a significant variation when evaluated across the distinct cell models (Table VI. 2). This indicates that the permeability of these compounds was not influenced by eventual differences in the composition of cell membranes nor by the distinct cell morphology. Equivalent results for SA and other compounds with high passive permeability across the three cell models have also been reported in other comparative studies [81,82]. Thus, both the Caco-2 and MDCK derived monolayers can be employed to evaluate the mechanism of transcellular permeation of compounds.

Table VI. 2 Permeability of model compounds that use the transcellular route measured across the distinct cell monolayers.

Cell line	Day post-seeding	P_{app} (10^{-6} cm/s) A → B					
		Propranolol			Salicylic Acid		
		N ^b	μ	CI ₉₅	N	μ	CI ₉₅
MDCK-II	7	2	6.0	3.0; 11.9	2	2.8	1.7; 4.7
MDCK-MDR1	7	2	3.8	2.0; 7.3	2	2.5	1.2; 5.1
	22	7	5.0	2.6; 9.5	11	3.3	1.2; 9.4
Caco-2 ^a	25	7	5.0	2.9; 8.5	11	3.2	1.5; 7.1
	28	7	5.3	3.2; 8.9	11	3.2	1.4; 6.9

^a P_{app} values obtained in Caco-2 monolayers are reported in Chapter VI.

^b Number of cell monolayers used in assays. The value of P_{app} was calculated from the average of the instantaneous permeability at each time interval of multi-sampling assays within 60 min. No statistically significant differences was found between the P_{app} values obtained in the distinct cell monolayers.

Comparison MDCK-II, MDCK-MDR1 and Caco-2

VI.4.2.4 – P-gp mediated efflux

The P_{app} values of Rho obtained across MDCK-II, MDCK-MDR1 and Caco-2 monolayer were compared to quantitatively evaluate the efflux activity in each cell model (Table VI. 3).

Table VI. 3 Permeability of Rho across the distinct cell monolayers. The results are presented as the values of P_{app} obtained in both the transport directions and the values for the components of passive and active efflux processes. The analysis was also performed after the inhibition of P-gp efflux with Verapamil.

		Rho P_{app} (10^{-6} cm/s) ^c									
Cell line	Day post-seeding	N ^c	A→B ^d		B→A ^d		Efflux ratio		P_{app}^{PP}	P_{app}^{AE}	
			μ	CI ₉₅	μ	CI ₉₅	μ	CI ₉₅			
MDCK-II ^a	7	2	0.54	0.47; 0.61	3.0	2.0; 4.5	5.5	3.7; 8.2	1.8	1.2	
MDCK-MDR1 ^a	7	2	0.37	0.31; 0.45	3.7	2.6; 5.3	10.1	7.0; 14.6	2.1	1.7	
	22	3-11	1.9	1.4, 2.6	2.5	1.5, 4.1	1.3	0.7, 2.3	2.2	0.30	
Caco-2 ^b	25	5-10	1.4	1.0, 2.0	2.3	1.4, 3.8	1.7	1.2, 3.2	1.8	0.46	
	28	5	1.0	0.6, 1.6	2.2	1.5, 3.4	2.3	1.4, 3.7	1.6	0.62	

		Rho P_{app} (10^{-6} cm/s)									
After pre-incubation with 100 μ M Verapamil											
Cell line	Day post-seeding	N ^b	A→B		B→A		Efflux ratio		P_{app}^{PP}	P_{app}^{AE}	
			μ	CI ₉₅	μ	CI ₉₅	μ	CI ₉₅			
MDCK-II ^e	7	2	0.49	0.46; 0.52	0.63	0.60; 0.67	1.3	1.2; 1.4	0.56	0.07	
MDCK-MDR1 ^e	7	2	0.49	0.27; 0.87	1.4	0.86; 2.2	2.9	1.3; 6.0	0.94	0.45	
	22	4	1.5	0.3; 7.2	1.3	0.41; 3.9	0.89	0.14; 5.3	1.4	0.10	
Caco-2 ^e	25	4	0.41	0.21; 0.81	1.9	1.1; 3.4	4.7	2.0; 10.8	1.2	0.75	
	28	4	0.55	0.26; 1.2	2.1	1.3; 3.3	3.8	1.7; 8.7	1.3	0.76	

^a values were calculated for time interval from 60 to 120 min

^b values were calculated for time interval from 0 to 120 min and are reported in Chapter VI

^c Number of cell monolayers used in assays. ^d The P_{app} values were calculated from the average of the instantaneous permeability in the time intervals considered for each cell model. ^e values were calculated for time interval from 0 to 40 min. Statistically significant differences from the P_{app} values obtained in Caco-2 monolayers are in marked bold.

Statistically significant differences are observed for Rho permeation in the A→B direction, with monolayers derived from MDCK cells presenting lower Rho P_{app} values than Caco-2 monolayers. In the opposite direction of transport, the values obtained for Rho permeation were slightly higher in MDCK-MDR1 monolayers relative to the other cell models. From these results, Rho efflux ratio is highest for both MDCK monolayers, anticipating an increase in efflux activity in these cells. To quantitatively characterize the efflux activity in each cell model it was performed an analysis of the contributions of P_{app}^{PP} and P_{app}^{AE} processes to the overall Rho P_{app} values. The results showed that Rho exhibits a similar passive permeability component in all the cell models. Contrarily, a significant difference is found for the efflux activity P_{app}^{AE} component, with MDCK-II and MDCK-MDR1 monolayers exhibit higher values than Caco-2 monolayers. The P_{app}^{AE} values obtained in Caco-2 monolayers are in agreement with the low expression levels of P-gp in these cells (Figure V. 6, Chapter V). However, the MDCK-MDR1 cells, which overexpress P-gp showed only a modest increase in P_{app}^{AE} values compared to MDCK-II monolayers which have a low P-gp expression [252]. This difference is not as high as expected and may reflect changes in the level of P-gp expression of MDCK-MDR1 cells.

The pre-incubation with Verapamil before the Rho permeability assays lead to complex results in MDCK-II and MDCK-MDR1 monolayers (section VI.4.1.3). The uncertainty in the intracellular concentration of Verapamil inside the cells was a major determinant of the result obtained. The effective concentration of Verapamil depends on the efflux activity by the cells, hindering the comparison between the P_{app}^{AE} values for the distinct cell monolayers. In addition to the difficulties and possible artifacts discussed in section VI.4.1.3, pre-incubation of the cells with high concentrations of the P-gp substrate Verapamil, could also lead to variations in the amount of P-gp in the plasma membrane [281]. This could justify the small increase in P_{app}^{AE} observed in Caco-2 monolayers previously incubated with 100 μ M Verapamil. Altogether, this detailed analysis indicates that although commonly followed, pre-incubation and subsequent removal of Verapamil is not a convenient procedure to quantitatively evaluate the transport of solutes through active efflux by P-gp.

Comparison MDCK-II, MDCK-MDR1 and Caco-2

Regarding the quantitative comparison performed of this study, it is possible to identify some significant disadvantage of Caco-2 and MDCK-II relative to MDCK-MDR1 monolayers. For Caco-2, is the fact that the activity of P-gp is low and variable among days in culture. In the case MDCK-II monolayers, its disadvantage comes from the fact that P-gp is from another specie. Our results agrees with that of the comparative study [81,82], where the MDCK-MDR1 cells among the other evaluated models are the one that is able to identify more molecules as P-gp substrates. The suitability of the MDCK-MDR1 model for evaluating P-gp activity is in fact expected, given its high expression of P-gp. However, variations in expression levels due to possible loss of transfected cells can be presented as a disadvantage.

VI.5 – Conclusions

The present study shows a detailed and quantitative evaluation of the properties of monolayers derived from MDCK and Caco-2 cells, adding information to previous studies which have compared the two models.

The parental MDCK-II and the human P-gp-transfected MDCK-MDR1 monolayers were first compared with each other. Significant differences were found regarding cell size, ZO-1 density, paracellular permeability and efflux activity.

MDCK-MDR1 cells were small in size, resulting in a higher cell density within their monolayers compared to those derived of MDCK-II cells. Moreover, a larger area covered by ZO-1 staining was also observed in MDCK-MDR1 monolayers. These findings were attributed to the higher contribution of the cell-cell contacts in these monolayers due to their small size. MDCK-MDR1 monolayers present higher permeability values to paracellular markers compared to MDCK-II. However, these values, which apparently could be attributed to a less tight cell monolayer, may reflect the higher surface available for this pathway due to the much smaller cell size. These relationship between the paracellular permeability and the density of tight junctions in the cell monolayers have never been highlighted in other works.

In respect to efflux activity, as expected, MDCK-MDR1 monolayers showed a higher P_{app}^{AE} values for Rho compared to MDCK-II. However, the P_{app}^{AE} increase was lower than expected considering the overexpression of P-gp in these cells.

This result points out to the intrinsic variability within this cell line regarding the P-gp expression levels.

Verapamil is a P-gp substrate, not an inhibitor, and the effect of Verapamil on P-gp efflux activity on other compounds is due to competition for the transporter. The effective concentration of Verapamil inside the cells is therefore a major determinant of the results obtained and depends on the efflux activity by the cells. The uncertainty in the intracellular concentration of Verapamil is further increased due to the removal of Verapamil from the transport medium before the permeability assay. A re-design of the procedures to quantitatively evaluate transport by P-gp is necessary, possibly with the use of high affinity inhibitors that allow the use of lower concentrations. Except if irreversible inhibitors are used, maintenance of the inhibitor in the transport medium during the permeability assay may also be necessary.

The traditional model of Caco-2 monolayers on days 22, 25 and 28 post-seeding were compared with those monolayers from the MDCK cell line. Caco-2 model displayed the largest cell size, along with the lowest cell density which leads to the lower ZO-1 density among the three models. In spite of the lower density of tight-junctions, paracellular permeability is similar for Caco-2 and MDCK-II monolayers. This shows that the lower density of tight-junctions results from the lower contribution of cell-cell contacts due to the larger size of Caco-2 cells, and not due to a less tight cell monolayer.

The three models lead to comparable results for permeability through the transcellular route. This further supports the potential use of MDCK monolayers as an alternative to enhance assay throughput for transcellularly permeating compounds.

The efflux activity P_{app}^{AE} of Rho was lower in Caco-2 monolayers than in both MDCK models, in agreement with the lowest P-gp expression. The P_{app}^{PP} component was also lower for Caco-2 monolayers, in agreement with a significant contribution of Rho permeation by paracellular routes and the lower density of this pathway in Caco-2 monolayers due to their larger cell size.

Comparison MDCK-II, MDCK-MDR1 and Caco-2

VI.6 – Supplementary material

VI.6.1 – Characterization of paracellular tightness

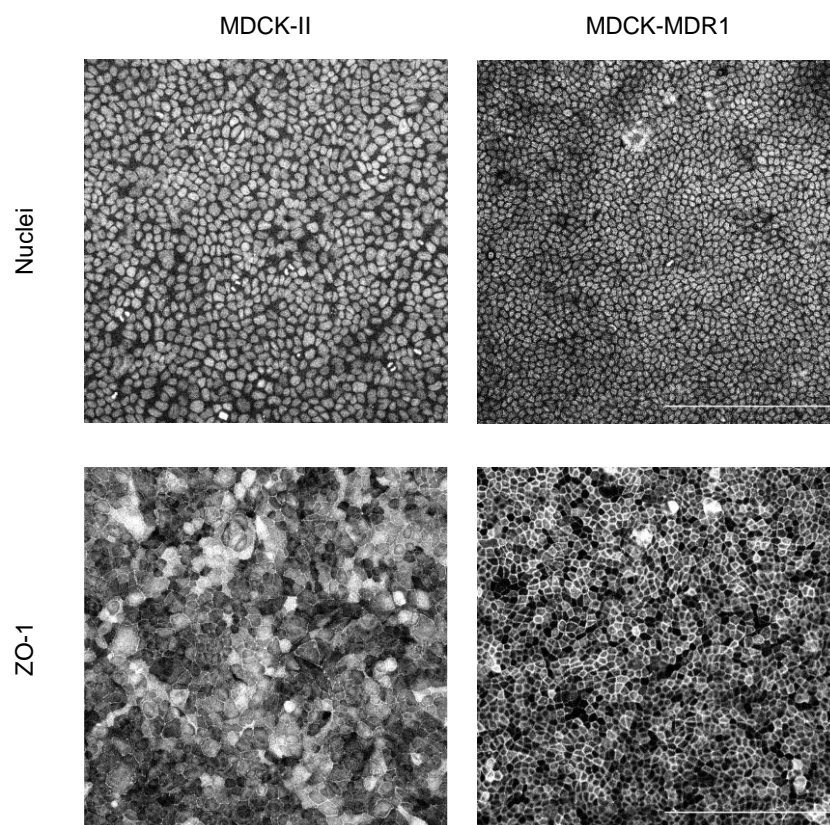


Figure VI. S1 Confocal microscopy images of MDCK-II and MDCK-MDR1 monolayers stained for nuclei and ZO-1. Representative images were obtained for cell monolayers at day 7 post-seeding after performing a multi-time permeability assay with LY. Images are a maximum intensity projection of 10-12 z-stacks, scale bar 200 μm .

Comparison MDCK-II, MDCK-MDR1 and Caco-2

Table VI. S1 Statistical analysis of LY, Flu and atenolol P_{app} values and amount transported into the acceptor compartment Q_A (% of total amount) after single time and multi-time sampling permeability assays through MDCK-II and MDCK-MDR1 monolayers. The average and the corresponding confidence intervals at 95 % confidence (CI_{95}) were obtained directly from the analysis of $\text{Log}(P_{app})$ or $\text{Log}(Q_A)$.

Cell line	Assay Conditions	Lucifer Yellow				Fluorescein				Atenolol			
		P_{app} (10^{-7} cm/s)		Q_A (%)		P_{app} (10^{-7} cm/s)		Q_A (%)		P_{app} (10^{-7} cm/s)		Q_A (%)	
	Sampling	μ	CI_{95}	μ	CI_{95}	μ	CI_{95}	μ	CI_{95}	μ	CI_{95}	μ	CI_{95}
MDCK-II	all	1.3	0.3; 5.1	0.04	0.02; 0.09	4.2	1.6; 11.3	0.13	0.06; 0.29	3.5	1.9; 6.5	0.08	0.05; 0.13
	all 1 st	1.3	0.2; 6.8	0.05	0.03; 0.10	3.6	0.8; 16.3	0.15	0.07; 0.33				
	1 st 60 min	0.7	0.5; 0.8	0.07	0.05; 0.09	2.0	1.7; 2.4	0.20	0.17; 0.24				
	1 st 10 min	2.5	1.3; 4.8	0.04	0.02; 0.08	6.6	3.1; 13.8	0.11	0.05; 0.23	5.2	4.9; 5.4	0.09	0.08; 0.09
	2 nd 10 min	2.8	0.5; 1.6	0.05	0.01; 0.26	5.7	3.5; 9.4	0.10	0.06; 0.16	4.1	3.3; 5.0	0.07	0.06; 0.08
	3 rd 10 min	1.5	0.9; 2.4	0.03	0.02; 0.04	5.2	1.3; 20.0	0.09	0.02; 0.34	3.2	2.8; 3.8	0.05	0.05; 0.06
	4 th 30 min	0.5	0.5; 0.6	0.02	0.02; 0.03	3.4	0.5; 24.6	0.17	0.02; 1.24	2.2	2.2; 2.2	0.11	0.11; 0.11
MDCK-MDR1	all	9.7	7.7; 12.3	0.29	0.07; 1.17	6.4	4.1; 10.0	0.19	0.05; 0.70	2.9	0.6; 13.5	0.06	0.02; 0.18
	all 1 st	9.3	8.5; 11.7	0.38	0.05; 3.18	5.0	3.5; 7.2	0.21	0.03; 1.53				
	1 st 60 min	8.8	3.9; 19.9	0.89	0.40; 2.01	4.6	3.8; 5.5	0.46	0.39; 0.55				
	1 st 10 min	9.7	7.2; 13.1	0.16	0.12; 0.22	5.5	2.8; 10.7	0.09	0.05; 0.18	7.5	4.4; 13.0	0.13	0.07; 0.22
	2 nd 10 min	10.1	8.2; 12.3	0.17	0.14; 0.21	7.3	4.2; 12.8	0.12	0.07; 0.22	4.6	2.4; 8.8	0.08	0.04; 0.15
	3 rd 10 min	9.7	7.0; 13.5	0.16	0.12; 0.23	7.4	7.2; 7.6	0.12	0.12; 0.13	1.9	1.0; 3.6	0.03	0.02; 0.06
	4 th 30 min	10.4	7.0; 15.5	0.53	0.36; 0.78	8.0	5.5; 11.4	0.40	0.28; 0.58	1.0	0.6; 1.7	0.05	0.03; 0.08

Comparison of MDCK-II, MDCK-MDR1 and Caco-2 monolayers

VI.6.2 – Characterization of transcellular permeability

Table VI. S2 Statistical analysis of P_{app} values of Propranolol and Salicylic Acid after multi-time sampling permeability assays through MDCK-II and MDCK-MDR1 monolayers. The average and the corresponding confidence intervals at 95 % confidence (CI_{95}), were obtained directly from the analysis of Log (P_{app}).

Cell line	Assay Conditions Sampling	P_{app} (10^{-6} cm/s)			
		Propranolol		Salicylic Acid	
		μ	CI_{95}	μ	CI_{95}
MDCK-II	all	6.0	3.0; 11.9	2.8	1.7; 4.7
	1 st 10 min	5.8	4.3; 7.8	2.6	2.5; 2.7
	2 nd 10 min	6.7	4.1; 10.8	3.2	1.4; 7.3
	3 rd 10 min	8.8	5.8; 13.4	3.6	2.1; 5.9
	4 th 30 min	3.7	1.3; 10.1	2.2	0.8; 6.3
MDCK-MDR1	all	3.8	2.0; 7.3	2.5	1.2; 5.1
	1 st 10 min	3.3	1.7; 6.2	2.7	1.6; 4.4
	2 nd 10 min	4.7	3.6; 6.2	3.4	2.7; 4.3
	3 rd 10 min	5.3	2.7; 10.5	3.1	2.5; 3.9
	4 th 30 min	2.5	1.3; 5.2	1.4	1.2; 1.6

Comparison MDCK-II, MDCK-MDR1 and Caco-2

Chapter VII

Towards reducing P_{app} variability:
understand and evaluate the effects
of distinct methodologies used in
permeability assays across cell
monolayers

VII.1 – Abstract

Permeability assays across cell monolayers are widely performed under pharmaceutical and academic context to predict the permeability of compounds. However, the application of different methodologies to perform the assays complicates the quantitative comparison and combination of the P_{app} data collected from distinct sources. In an attempt to decrease the variability in P_{app} values, the effect of some specific procedures commonly followed was systematically and quantitatively evaluated, exploring possible conversions of the measured P_{app} values into the value that would be obtained at reference conditions.

Measuring LY permeability in the same cell monolayers as the tested compounds was evaluated as a possible methodology to provide a quality control of each cell monolayer integrity. The use of this approach is especially important when mixture of compounds with unknown effects on cell monolayer integrity are applied in assays. The similarity of LY P_{app} values obtained when evaluated alone and with other compounds makes this methodology valid to help reduce the variability associated with the integrity of the cell monolayers.

The two existing sampling methods for carrying out multi-time assays, the transfer and replacement, were evaluated for their effects in the passive permeation using reference compounds. It was shown that insufficient homogenization of the acceptor solution in replacement assays prior to sample withdrawal can be a source of variability in the reported P_{app} values.

The use of BSA in the transport media is a common practice in permeability assays and its impact on the reported P_{app} was evaluated using a homologous series of amphiphiles with well-characterized properties regarding their interaction with BSA and lipid membranes. The P_{app}^{Unb} values were recalculated from the observed P_{app} using the unbound fraction of amphiphiles. The two permeability estimates were significantly different, with the calculated P_{app}^{Unb} correlating better with the compound's molecular properties.

VII.2 – Introduction

The variety of protocols used to perform permeability assays across Caco-2 monolayers has been the main factor attributed to the variability found in P_{app}

Effect of experimental methodologies

data [75,92,107,108]. In most cases, it is not possible to quantitatively compare the permeability data obtained following different approaches [103]. Attempts to establish reliable quantitative comparisons need to be developed, opening the way to the use of the large amount of P_{app} data available to develop quantitative structure-permeability relationships and gain predictive value. Normalizing P_{app} data for the change of a particular experimental parameter between studies may be a promising approach to improve the consistency of already available P_{app} values. The aim of this study is to contribute to this goal through understanding and quantitatively evaluating the effects of some common methodologies used in the permeability assays. With this knowledge it may be possible to uniform P_{app} data to standard conditions [128]. With this purpose, a systematic study was performed by the same researcher in the same laboratory, to complement the insufficient and disperse information already present in literature. Three experimental variables were evaluated i) possible effects of the tested compounds on cell monolayer integrity, through the simultaneous measurement of P_{app} for a paracellular marker; ii) the effect of using transfer or replacement as a sampling method; and iii) the effect of including BSA in the transport media.

The assessment of cell monolayer integrity is an essential methodology in permeability assays, which is often achieved using a control solute with high polarity such as LY [203,282-284]. This test is usually carried out in dedicated cell monolayer inserts prepared from the same batch of cells, or in the same monolayer insert but before or after the test compound (in the later providing additional evidence for eventual toxicity) [285]. To reduce the duration of the incubation with the transport media and the manipulations of the cell monolayers, a better approach could be to evaluate the permeability of both the control (LY) and the test compound in the same cell monolayer. This procedure has the advantage of including a quality control for each filter, thus facilitating the identification of cell monolayers with compromised integrity (outliers), and therefore decreasing the variability. This procedure has been followed before in the case of compounds with anticipated possible cytotoxicity [198], and has been used recently by us when evaluating the permeability of complex extracts from biological origin [130,286]. To validate the use of this methodology, LY permeability was evaluated alone and in the presence of reference compounds for passive (SA) and active efflux (Rho) permeation. The results obtained by us for the studies using complex mixtures of compounds with unknown effects on cell monolayer integrity are also shown. Namely for the permeability of a

cholesterol analogue in the presence of a bile salt and coffee extracts [286], and the permeability of paralytic shellfish toxins [130].

In the permeability assays across cell monolayers, the use of several time points is usually required to allow the characterization of fast permeating compounds while sink conditions are guaranteed. The sampling can be performed by two methodologies: the replacement method (removing part of the solution in the acceptor compartment and replacing it with fresh transport media), or the transfer method (where the insert is transferred to new wells containing fresh transport media). The use of the replacement approach for sampling is suggested in the reference protocol for Caco-2 permeability assays, and the steps to perform it are well detailed there [128]. This is also the sampling method used in most of the permeability studies reported in the literature. The major advantage is that the insert containing the cell monolayer is maintained in the same position during the assay. However, when carrying out this method to evaluate permeation in the apical-to-basolateral direction, the low accessibility of the basolateral compartment leads to relatively long times to withdraw the sampling solution. Consequently, in the reference protocol, the transfer approach has been proposed for the case of compounds with fast permeation [128]. This is because it only takes a few seconds to move the insert to another well in the plate. Also, the transfer method can reproduce better the physiological situation of the clearance of compounds in the capillaries. For researchers who are new in the field, the choice of the sampling method to follow may come into question. Both sampling approaches has advantages and disadvantages, as mentioned before. But what is important to know is whether the P_{app} values obtained are influenced by the sampling method followed. To our knowledge, this has never been discussed in the literature. For a better understanding of this possible source of variability, in this study we have evaluated the effect of the sampling method on the P_{app} of LY (with slow paracellular permeability) and Prop (with moderate transcellular permeability).

The incorporation of solubilizing agents in the transport media of the permeability assays is a common practice to improve the permeability assessment of poorly soluble and strongly lipophilic compounds, to increase the solubility in the transport media and to decrease sequestration in the cell monolayer, respectively [144]. BSA is the most commonly used solubilizing agent, as it has several advantages over other agents such as surfactants, amphiphilic polymers, or organic solvents. The main advantage of BSA is that its presence in

Effect of experimental methodologies

the media does not influence the properties of the cell monolayer, which is in agreement with the absence of strong interactions between the BSA and cell membranes [157]. However, the presence of BSA in the donor side of the assays will likely have an impact on the measured P_{app} values. In the case of compounds that bind moderately or strongly to BSA, a decrease in P_{app} is expected due to a reduction in the fraction of compound available for permeation (the unbound fraction) [136,138,139]. If the binding affinity for BSA is known, the P_{app} value of the compound in the absence of BSA may be obtained by reverse calculation [136,138], thus allowing a direct comparison between distinct compounds and procedures. This approach was further explored in this study using a homologous series of amphiphiles, with a polar 7-nitrobenz-2-oxa-1,3-diazol-4-yl (NBD) moiety covalently bound to an alkyl chain of varying lengths (NBD-C_n; n = 4, 6, 8). The main reason for choosing this series of compounds is the large amount of high-quality data available for all their relevant properties. Namely, i) their solubility in aqueous medium, ii) their ionization behaviour both in water and when associated with membranes, iii) the kinetics and thermodynamics of their interaction with BSA, namely the association constant (K_B), and iv) their partition coefficient (K_p) towards phosphatidylcholine (POPC) lipid bilayers mimicking the cell membranes. These properties and parameters have been previously characterized experimentally and are present in Table VII.1. Knowledge of the properties of the NBD-C_n series represent a major additional advantage in understanding and interpreting their permeation behaviour across the more complex *in vitro* systems such as Caco-2 monolayers. The measured Caco-2 P_{app} values and the recalculated P_{app} values that account for the unbound fraction (P_{app}^{Unb}) were interpreted considering the NBD-C_n interaction with BSA in the transport media as well as with the lipid membranes.

Table VII. 1 Solubility in aqueous medium and parameters for the ionization and equilibrium interaction of the amphiphiles NBD-C_n with BSA and POPC bilayers at pH=7.4. The solubility is at 25 °C, and the association constants are at 37 °C, calculated from the values at 25 °C and the temperature dependence reported in ref [173].

Amphiphile	CAC (μM)	pKa		K_B (M ⁻¹) BSA	K_p POPC membranes
		water	POPC membranes		
NBD-C4	250 ± 30			1.3 ± 0.1 × 10 ⁴	9 ± 1 × 10 ³
NBD-C6	13 ± 1	10	10.3	4.9 ± 0.3 × 10 ⁴	5 ± 1 × 10 ³
NBD-C8	0.91 ± 0.01			3.9 ± 0.3 × 10 ⁵	3.8 ± 0.3 × 10 ⁴

VII.3 – Methods

Assessment of LY permeability simultaneously with test compounds

The permeability coefficients of LY, SA and Rho across Caco-2 monolayers were evaluated individually by applying donor solutions prepared with each compound alone. In complementary assays, the permeability of the compounds was evaluated simultaneously by applying mixed solutions of LY with SA or Rho (LY+SA, LY+Rho). These solutions were prepared by adding a small aliquot of the LY stock to the final solution of SA or Rho. The same cell preparation was used to perform the assays with the compounds alone and mixed. The permeability assays were carried out in the A→B direction across Caco-2 monolayers at day 22 post-seeding, and at days 25 and 28 through the re-use of the cell monolayers, following the regeneration protocol previously established by us (Chapters IV, and V and reference [211]). In the assays with SA, LY, and LY + SA, the permeability was evaluated using either a single sampling at t_{60} and multiple samplings at t_{10} , t_{20} , t_{30} and t_{60} min. The assays with Rho, LY, and LY+Rho were performed with sampling at t_{20} , t_{40} , t_{60} , t_{80} , t_{100} , and t_{120} . The transfer of the inserts to new wells containing HBSS was used to carry out the multiple samplings. The quantification of LY, SA and Rho in the samples collected from the assays was performed by HPLC following the analytical procedures described in section III.6, Chapter III.

Solutions of the cholesterol analogue ergosta-5,7,9(11),22-tetraen-3 β -ol (DHE) emulsified by the bile salt glycocholic acid (GCA) at several concentrations and solutions of several coffee extracts (L1, L3, D1, D3) were prepared as described in Chapter III. A small aliquot of the LY stock was added to the final mixture solutions of DHE/GCA alone and in the presence of the coffee extracts. Also, a solution with LY only was applied in a dedicated cell monolayer from the same cell preparation. The permeability assays were performed across Caco-2 monolayers on day 24 after seeding in the A→B direction, with a single sampling after 6h incubation or with multiple sampling at 2, 4, and 6h. The transfer of inserts to new wells containing the acceptor transport media was used for the sampling in the multi-time assays. Although both DHE and LY are fluorescent, their spectroscopic properties are different, with DHE absorbing light and emitting fluorescence in the UV region while LY absorbs light in the blue region of the spectrum and emits fluorescence in the green. No interference of DHE in

Effect of experimental methodologies

LY fluorescence intensity was therefore observed, allowing the direct quantification of LY by fluorescence intensity using a SpectraMax iD5 Multi-Mode Microplate Reader at excitation/emission wavelengths of 435/560 nm. However, LY fluorescence interfered with the direct quantification of DHE. Accordingly, DHE was extracted from the samples using a well-defined and validated procedure and quantified by HPLC with fluorescence detection at excitation/emission wavelengths of 324/372 nm. For details on the extraction and quantification procedures see Pires et al. [286]

A crude extract of paralytic shellfish toxins was prepared at 15% (v/v) in HBSS and a solution with only the toxin Gonyautoxin-5 (GTX-5) was also prepared in HBSS as described in Rodrigues et al. [130]. A small aliquot of LY stock solution was added to both the final solutions of toxins. LY was also applied in a dedicated cell monolayer from the same cell preparation. The permeability assays were performed across Caco-2 monolayers on day 23 after seeding in the A→B direction, with a single sampling after incubation for 90 min. The quantification of GTX-5 and LY in the samples collected from the assays was determined by HPLC with fluorescence detection at excitation/emission wavelengths of 337/395 nm (for crude extract and GTX-5) and at 337/530 nm (for LY). A small interference of GTX-5 in the quantification of LY was found, leading to an apparent increase in LY P_{app} . The impact of the interference was always less than 10% (smaller than the variability in independent assays) and was therefore not considered in the values reported.

Effect of the sampling method

To compare the values obtained for P_{app} when following the transfer and the replacement sampling methods, the replacement method was also followed in the case LY and Prop, applied as a mixed solution and with the permeability evaluated in the A→B direction across Caco-2 monolayers. At the beginning of the assay, the insert was placed on a well plate containing HBSS, and the donor solution was immediately added. At the multiple time intervals of t_{10} , t_{20} , t_{30} and t_{60} min, an aliquot of the HBSS solution was removed (600 μ L) from the acceptor compartment and replaced by adding an equal volume of new HBSS. During this procedure the insert containing the cell monolayer and the donor compartment was maintained in the same position on top of the acceptor compartment. At the end of the assay, to collect the last aliquot, the insert was transferred into an

empty well, and 600 μL and 50 μL were taken from the acceptor and donor compartments, respectively. The experiments were performed on Caco-2 monolayers at day 22 post-seeding, and at days 25 and 28 through the re-use of the cell monolayers, following the regeneration protocol previously established by us (Chapters IV, and V and reference [211]). The permeabilities of LY and Prop across the same cell preparation and under the same experimental conditions but obtained with the transfer method are reported in this chapter for LY and in Chapter V for Prop.

Effect of BSA on the observed permeability

The transport of NBD-C4, NBD-C6 and NBD-C8 was evaluated in A \rightarrow B direction in the presence of BSA in both the donor and acceptor compartments. A BSA concentration of 100 μM was used, since it was sufficient to increase the solubility of the most lipophilic compound (NBD-C8) to provide enough sensitivity in its detection, and to achieve a good recovery. Also, this corresponds to the BSA concentration usually found in interstitial tissues which correspond to the acceptor compartment under *in vivo* absorptive transport conditions [287]. NBD-C8 has very low solubility in water and forms aggregates at concentrations above 0.1 μM (Table VII. 1). This concentration is not sufficient to permit its analytical quantification. However, since this compound binds to BSA with high affinity $K_B=5.2 \times 10^5$ at 25 $^\circ\text{C}$ [173], at a BSA concentration of 100 μM , the solubility of NBD-C8 in water at 25 $^\circ\text{C}$ increases to slightly above 5 μM . The higher temperature used in the assay allows for an additional small increase in solubility, allowing the use of a total concentration of NBD-C8 equal to 10 μM , which was the concentration chosen to perform the assays with all NBD-Cn amphiphiles. The donor solutions of the amphiphiles were prepared in the day before in HBSS+100 μM BSA and allowed to equilibrate overnight under orbital agitation at 100 rpm at 37 $^\circ\text{C}$. The transfer method was followed in the permeability assays, with the inserts moved to new wells containing the fresh acceptor solution of HBSS + 100 μM BSA. The permeability assays were performed with multiple samplings across monolayers derived from the Caco-2, MDCK-II and MDCK-MDR1 cell lines. The mass balance was between 90–100% for the less lipophilic amphiphile NBD-C4, 80–90% for NBD-C6 and 70–80% for the more lipophilic amphiphile NBD-C8.

Effect of experimental methodologies

The P_{app}^{Unb} of the amphiphiles was recalculated from the observed P_{app} considering that only the concentration of compound free in the aqueous medium is available for permeation and therefore acts as the driving force in Eq. III.2 (use $Q_{0\text{unbound}}^D$ rather than Q_0^D). The concentration of unbound NBD-Cn was calculated using the equilibrium association constant to the highest affinity site on BSA (K_B), according to the following Equation [138,173]:

$$\frac{[NBD - Cn]_w}{[NBD - Cn]_T} = \frac{1}{1 + K_B[BSA]} \quad \text{VII.1}$$

where $[NBD - Cn]_w$, represents the concentration of the amphiphile in the aqueous medium, $[NBD - Cn]_T$ the total concentration in the donor compartment and $[BSA]$ the concentration of BSA in the donor compartment. The K_B values at 37 °C were taken from literature [173], and are indicated in Table VII.1.

Experiments were carried out in duplicate and were independently repeated with a different cell preparation in the case of MDCK-II and MDCK-MDR1 monolayers. The statistics of the P_{app} values was analysed in terms of $\text{Log}P_{app}$ [15][28], and the average values of P_{app} and the 95% confidence intervals (CI₉₅) (Equation IV.1 in chapter IV) were calculated using the Microsoft Excel.

VII.4 – Results and discussion

VII.4.1 – Assessment of LY permeability simultaneously with test compounds

In this work, the effect of measuring the permeability of LY simultaneously with the test compounds in the same Caco-2 monolayer was evaluated as a methodology that can be used to decrease P_{app} variability due to changes in cell monolayer integrity. To validate this approach, it is first necessary to verify that the compounds do not interfere with each other in their permeation through the cell monolayer. LY is anticipated to be a good control compound in this respect because its high polarity prevents association with the cell membrane and will therefore avoid interference with membrane permeating solutes [196]. Additionally, it is not a substrate of membrane transporters (influx or efflux) [288].

It is also necessary to guarantee that the presence of LY and test compounds in the samples collected from the assays do not interfere with the analytical method for their quantification. In this section, the permeability of LY was evaluated alone and in simultaneous with test compounds and the resulting P_{app} values were compared. Possible interference in the quantification of the compounds was also evaluated.

VII.4.1.1 – Assays with reference compounds

A reference compound for the passive (SA) and active efflux (Rho) permeation routes was selected. At the assay pH, LY and SA are anionic while Rho is cationic, which introduces an additional validation assessment. Also, SA and Rho are not toxic and no effect on cell monolayer integrity is expected. Therefore, possible effects on LY P_{app} values reflect interference between the two compounds.

The permeability of LY, SA and Rho was determined in assays where each of the compounds were applied alone and as a mixture (LY+SA and LY+Rho). This evaluation was performed in assays using single and/or multi-time sampling across Caco-2 monolayers at days 22, 25 and 28 post-seeding. The P_{app} values obtained are presented in Table VII. 2.. The individual permeability of LY in the mixture with SA and Rho is similar to the P_{app} value of LY when it is evaluated as a single compound. The results obtained are independent of the day of culture of Caco-2 monolayers and whether they are acquired in single or multi-time assays. The same effect was obtained for SA and Rho, with their P_{app} values obtained in single assays being similar to those obtained when they are assessed in the presence of LY. These results indicates that no significant interactions between the compounds in the mixtures are observed. The lack of effect on LY P_{app} values of the other compounds may address LY as an ideal paracellular marker to be used as control for integrity when the permeability of more complex mixtures is evaluated across Caco-2 monolayers.

Table VII. 2 Permeability of LY when applied in the donor compartment of Caco-2 monolayers alone in solution and in simultaneous with references compounds that use passive (SA) and active efflux (Rho) pathways for permeation. The permeability of SA and Rho were also determined when each one of the compounds was applied alone and

Effect of experimental methodologies

mixture in solution with LY. The assessment of compounds P_{app} values was performed in single and/or multi-time assays in the A→B transport direction.

Assay Conditions		LY P_{app} (10^{-6} cm/s)						SA P_{app} (10^{-6} cm/s)					
		Alone			+ SA			Alone			+ LY		
Sampling	Day	N ^a	μ	CI ₉₅	N	μ	CI ₉₅	N	μ	CI ₉₅	N	μ	CI ₉₅
One time point	22	2	0.05	0.02; 0.08 ^b	3	0.03	0.02; 0.06	3	1.3	0.9; 1.6	3	0.9	0.8; 1.2
	25	2	0.06	0.03; 0.08 ^b	3	0.03	0.02; 0.07	3	1.5	1.0; 2.2	3	1.1	0.6; 1.8
	28	2	0.11	0.11; 0.12 ^b	3	0.04	0.02; 0.08	3	1.5	0.9; 2.6	3	1.2	0.8; 1.6
Multiple time points ^c	22	4	0.43	0.09; 2.2	5	0.24	0.03; 2.4	3	2.1	0.7; 6.5	5	2.8	1.4; 5.8
	25	7	0.25	0.03; 1.8	5	0.31	0.03; 2.8	3	3.2	1.3; 8.0	5	3.7	1.9; 7.2
	28	11	0.28	0.09; 0.89	5	0.32	0.08; 1.3	3	3.2	1.1; 9.7	5	3.4	1.7; 6.8

Assay Conditions		LY P_{app} (10^{-7} cm/s)						Rho P_{app} (10^{-6} cm/s)					
		Alone			+ Rho			Alone			+ LY		
Sampling	Day	N	μ	CI ₉₅	N	μ	CI ₉₅	N	μ	CI ₉₅	N	μ	CI ₉₅
Multiple time points ^d	22				2	0.92	0.49; 1.8	9	1.9	1.4; 2.6	2	2.0	1.6; 2.7
	25				3	0.53	0.30; 0.94	7	1.5	1.0; 2.1	3	1.2	0.9; 1.7
	28	2	0.13	0.07; 0.28	4	0.49	0.19; 1.3	2	1.2	1.0; 1.5	4	0.9	0.5; 1.5

^a Number of cell monolayers used in assays. ^b given the low number of experiments, the values obtained in the two experiments are shown instead of CI₉₅

For multi-time sampling assays, the value of P_{app} was calculated from the average of the instantaneous P_{app} at each time interval ^c multi-time points of 10,20,30,60 min ^d multi-time points of 20,40,60,80,100,120 min

No statistically significant differences are observed between the distinct samples.

VII.4.1.2 – Assays with mixtures of compounds having unknown effects on cell monolayer integrity

The assessment of LY permeability simultaneously with test compounds gains more importance when dealing with compounds or mixture of compounds that have unknown effects on the integrity of the cell monolayer. These effects may be caused by their properties in aqueous solution, such as aggregation or precipitation, their interaction and permeation across the cells, and possible metabolism. Before measuring their permeability across cell monolayers, it is generally first necessary to ensure that these compounds are not toxic to cells. The cytotoxicity is usually determined in assays to assess cells viability (e.g. MTT assay). However, although cytotoxicity may not have been observed, this does not guarantee that the test compounds cannot affect the integrity of the cell monolayers during the assays. This is because small changes in the cell condition may lead to large effects in the integrity of the cell monolayer and result in a

significantly higher permeability for slowly permeating compounds. Thus, the integrity control during the assays with these compounds is justified to ensure that their permeability is being properly assessed.

In this study, the effect of complex solutions containing the analogue of cholesterol DHE on the integrity of Caco-2 monolayers was evaluated in the presence of LY. The solubility of DHE in aqueous media is very low, forming aggregates in the form of crystals that can damage cells. To reduce its propensity for aggregation, DHE was previously emulsified in micelles of the bile salt glycocholic acid (GCA), for which a non-toxic concentration was selected. Solutions of DHE/GCA with increasing DHE concentrations of 10, 50 and 100 μM were incubated for 6h with Caco-2 monolayers. Its effects on the integrity of the cell monolayers were evaluated by determining the permeability of LY, which was measured simultaneously with DHE/GCA solutions. The obtained LY P_{app} values are shown in Table VII. 3. No significant effect was observed on LY permeability when evaluated alone or together with DHE (average value of $1.3 \times 10^{-7} \text{ cm s}^{-1}$). This result shows that possible DHE crystals formed did not influence the cell monolayer integrity, even at high DHE concentrations. A coffee extract, derived directly from a cup of coffee was added to the DHE/GCA mixture increasing the complexity of the solutions to be measured across Caco-2 monolayers. The coffee extract is composed of several bioactive compounds, which can have different interactions between each other and the cells. After 6 h of exposure to the Caco-2 monolayers, the presence of the coffee extract in the DHE/GCA solutions does not lead to an increase in the LY P_{app} values.

Table VII.3 Permeability of LY across Caco-2 monolayers determined when it is applied alone and in mixture with complex solutions of compounds. The evaluation include increasing concentrations of DHE in DHE/GCA solution, alone and in the presence of several types of coffee extracts. The effect on LY P_{app} values of a natural extracts of shellfish toxins and a toxin is also shown.

LY in solution	Sample	DHE [μM]	Incubation and Sampling times	LY P_{app} (10^{-7} cm/s)	
				assay 1	assay 2
Alone	LY	-	Single time at 6h	2.7	
		10		1.1	
		50		1.8	
		100		1.1	
Mixture	DHE/GCA	-	Single time at 6h	2.7	
		10		1.1	
		50		1.8	
		100		1.1	

Effect of experimental methodologies

		10		1.3	1.0
	DHE/GCA +Coffee extract	50		1.0	1.1
		100		0.51	0.80
Alone	LY			6.4	
	DHE/GCA	10	Multiple	4.7	3.3
	DHE/GCA + Coffee extract L1		sampling at 2h	5.7	2.7
Mixture	DHE/GCA + Coffee extract L3		for a total of 6h	1.8	2.0
	DHE/GCA + Coffee extract D1	10		1.7	4.3
	DHE/GCA + Coffee extract D3			4.3	1.7
Toxins					
[μM]					
Alone [130]	LY	-		1.3	4.9
	Toxin crude extract	15	Single time at	1.4	1.2
Mixture [130]	GTX-5	15	90min	1.2	1.0

No statistically significant differences are observed between the samples.

Coffee extracts obtained with different processing conditions (named D1, D3, L1, L3) have a different composition regarding the bioactive compounds. To evaluate their effects on the integrity of Caco-2 monolayers, LY was added to the solutions of DHE alone and in the presence of the several types of coffee extracts. The permeability assay had a duration of 6h, with successive samplings at 2 h of incubation. The corresponding LY P_{app} values were calculated in the last interval of 2h and are presented in Table VII. 2. The results obtained shows that LY P_{app} values varied from 0.19×10^{-6} cm/s for L3 to 0.42×10^{-6} cm/s for L1 coffee. These values are lower than the 0.5×10^{-6} cm/s, value which is indicative of cell monolayer integrity [33]. The observed LY permeability assessed alone is slightly higher (0.64×10^{-6} cm/s), although still within the expected result for cell monolayers on day 24 after seeding [31]. Overall, the results indicate that DHE, GCA, coffee extracts and samplings time points did not affect the permeability of LY in each of the cell monolayers used.

To address the advantages and utility of evaluating LY permeability in simultaneous with complex mixture of compounds, another example is provided in this work in collaboration with Rodrigues et al. [130]. Permeability assays of an extract containing different types of paralytic shellfish toxins were performed in the presence of LY. The obtained P_{app} values for LY alone does not significantly vary in relation to those obtained in simultaneous incubation with the toxins extract. The conservation of LY P_{app} values is observed when evaluated with a solution of one of the toxins present in the extract (GTX-5). The LY P_{app} values

measure in all conditions are always smaller than the threshold considered for a tight Caco-2 monolayer, confirming that the integrity of the cell monolayers remain unaffected after incubation with natural toxins.

VII.4.1.3 – Use of LY P_{app} values to reduce variability arising from changes in cell monolayer integrity

The intrinsic variability in results obtained with Caco-2 monolayers was shown to be higher for compounds that permeate paracellularly compared to other routes, pointing to the integrity of the cell monolayers as the main contributor to variability (Chapter V). After validating the simultaneous assessment of LY P_{app} with test compounds, this approach was evaluated for its potential use in reducing variability arising from changes in cell monolayer integrity. To distinguish between different cell monolayers, the P_{app} values of the compounds were plotted against LY P_{app} values in Figure VII: 1. A large variability in LY P_{app} values is observed, consistent with previous results. However, all LY P_{app} values are $\leq 10^{-6}$ cm/s, indicating that the integrity of the cell monolayers is adequate for permeability assays. This result discards the existence of outliers, decreasing the variability among the cell monolayers. Regarding the test compounds, their P_{app} values fall in distinct ranges according to their properties. In spite of that, correlations of the P_{app} of each individual compound with LY P_{app} are observed. This correlation shows that the tighter monolayers, being more impermeable to LY are also more impermeable to the other compounds. These correlations also indicate that the assay and detection method has lower uncertainty than cell monolayer variability, being able to detect the differences in monolayers tightness.

In the view of the results, LY P_{app} values can be used as a strategy to reduce variability, by applying a ratio that allows correcting for variations in paracellular permeability. Additionally, this approach may facilitate comparisons between Caco-2 monolayers used on distinct days post-seeding when correcting the P_{app} of compounds for the effect of the day. Lower LY P_{app} values will also lead to lower P_{app} values of the test compounds.

Effect of experimental methodologies

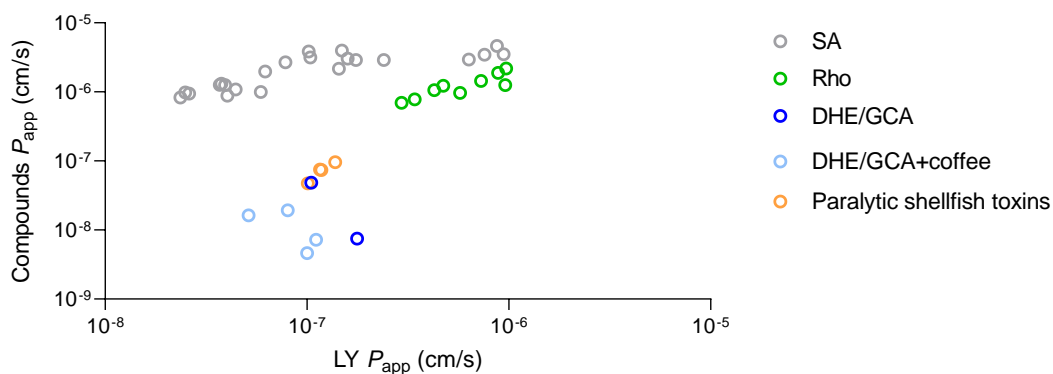


Figure VII. 1 Representation of the P_{app} values of several test compounds plotted against LY P_{app} values obtained with the same cell monolayers in the A→B transport direction. Although the correlations are stronger for compounds that permeate passively through the paracellular pathways (paralytic shellfish toxins), significant correlations are also observed for compounds that permeate through passive transcellular pathways (SA and DHE) and substrates of active efflux (Rho).

VII.4.2 – Effect of the sampling method

For permeability assays with multiple-time sampling, samples from intermediate time-points may be obtained by two methods the denominated as transfer and replacement. The transfer method was the sampling approach previously followed to perform the permeability assays of reference compounds by the distinct pathways, including the passive permeation (Chapter IV and V). The results of these assays indicated that manipulation of the insert for sampling lead to a significant amount of compound transport, with a higher impact on compounds that permeate very slowly and paracellularly, as is the case of LY. In this section we have performed permeability assays for LY and Prop with the sampling performed using the replacement method. The comparison between the results obtained with the two sampling methods will allow to evaluate if the perturbation of the cell monolayer observed was due to lifting the insert during the transfer method, and whether a smaller (or larger) perturbation is obtained when using the replacement method.

VII.4.2.1 – Slow passive permeation- Lucifer yellow

The effect of distinct sampling methods on the resulting LY P_{app} values was evaluated under identical assay conditions in the same cell preparation, changing only the method of sampling. The results obtained are presented in Figure VII. 2 and the detailed statistical analysis is provided in supplementary material – Table VII. S1.

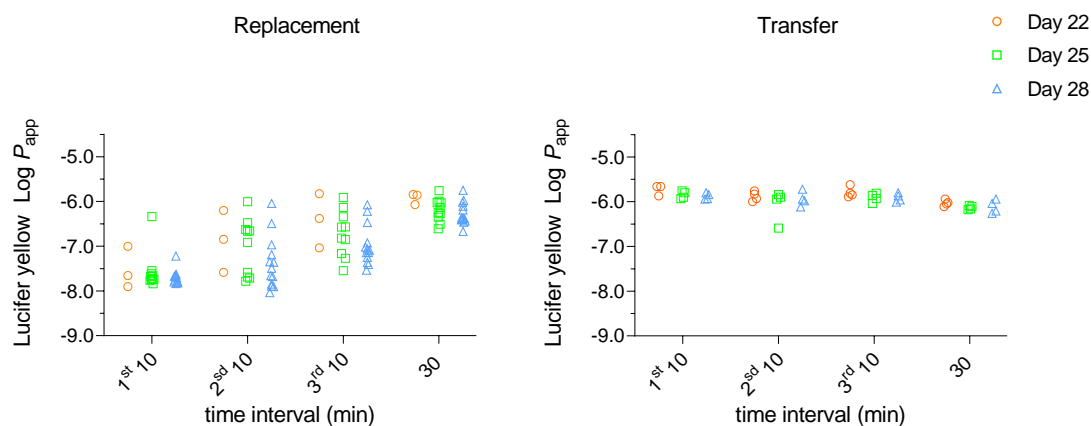


Figure VII. 2 Dependence of LY P_{app} on the sampling method and sampling time intervals. P_{app} values were obtained with replacement or transfer methods in multi-time permeability assays across Caco-2 monolayers. The results include cell monolayers used a single time at day 22 and re-used at days 25 and 28 when following the regeneration protocol previously established by us (Chapters IV, and V and reference [21]).

When following the replacement method for sampling, the values for LY permeability are always low, usually lower than for the transfer method. An increase in consecutive sampling with the same interval is obtained, as previously observed for the transfer method, suggesting that some perturbation of the cell monolayer may still be occurring. The major difference between the results obtained with the two approaches is the extremely large variability obtained with the replacement method. The variability is so large that to include all the results with the same scale for both approaches, the P_{app} values obtained with transfer appear independent on the sampling interval. Another important observation is that the values of P_{app} obtained at longer time intervals are larger than for smaller time intervals, in clear contrast with what is observed with the transfer method. This increase in P_{app} leads to an upward curvature in the cumulative amount of LY (Q_A) that reaches the acceptor compartment (supplementary material – Figure VII. S1). It is also relevant to note that the variability decreases as the sampling interval increases, and that the average P_{app} approaches that obtained with the transfer sampling method.

Effect of experimental methodologies

Another cause that may explain the sampling effect is that the solution of the residual layer formed below the insert contains a significant amount of the transported LY and that its diffusion to the acceptor solution is slow. Therefore, at the time of sample removal, the acceptor solution may not be completely homogenized in the basolateral wells. Because only the solution on the sides of the insert is accessible for sampling, the solution withdraw underestimates the total amount transported. In fact, this effect explains the lower P_{app} values obtained for short time intervals when following the replacement when compared with the transfer method. The concentration of analyte in the withdrawn solution will depend on several variables, namely the location relative to the insert, as well as the sampling time interval and the stirring efficiency. These factors may explain the large variability found for LY P_{app} values in the consecutive samplings of 10 min. For the final sampling the insert is removed and is therefore equivalent to the transfer method. It is therefore not surprising that the LY P_{app} values in the last interval are similar when using the different sampling methods.

To reduce the effect of the low diffusion of the residual layer, a stirring rate sufficient to homogenize the acceptor solution before sample removal must be implemented. However, care must be taken as the high agitation rate can damage the integrity of the cell monolayer. The agitation rate of 50 rpm used in this work, which appears to the human eye to agitate the basolateral solution, proved to be ineffective.

From the results presented in this section, it is also observed that, similar to transfer, Caco-2 monolayers can be re-used when the sampling is performed with the replacement method.

VII.4.2.2 – Fast passive permeation - Propranolol

The effect of sampling method on P_{app} values was also characterized for Prop, a compound with permeation mainly through the transcellular route. The results obtained are presented in Figure VII. 3 and the detailed statistical analysis of the data obtained using the replacement method is provided in supplementary material — Table VII. S1. As previously found for LY, an extremely large variability in Prop P_{app} values is observed when employing the replacement

instead of the transfer method. The Prop P_{app} values obtained at shorter time intervals are so small that its permeation can be confused with that of a low passive permeation compound. This result suggests that the amount of Prop transported is being underestimated in the replacement assays. The incomplete homogenization of the acceptor solution in the basolateral wells is the factor that likely contributes to the variability in collected samples. At the end of the assay, the Prop P_{app} values are comparable regardless of the sampling method used, as the samples are collected after homogenization in both cases.

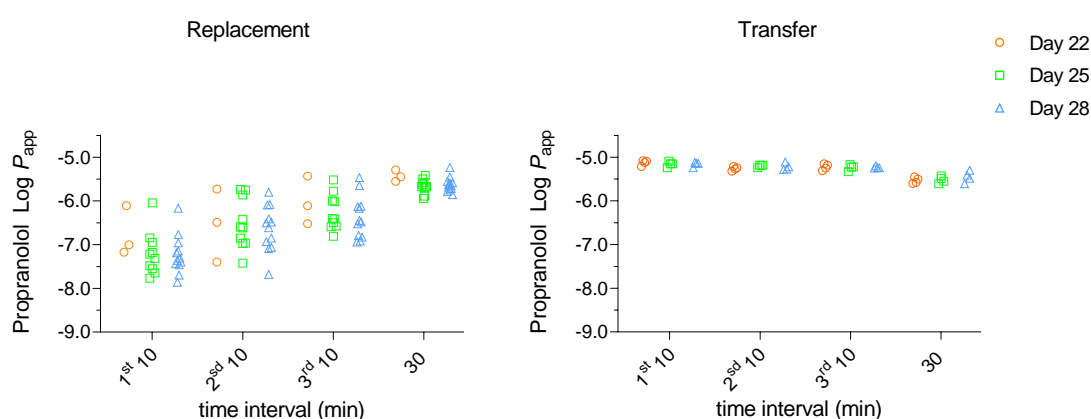


Figure VII. 3 Effect of the sampling method and sampling interval on Prop permeability in multi-time permeability assays across Caco-2 monolayers. The P_{app} values were obtained with replacement or transfer methods. The results are also shown for cell monolayers used a single time at day 22 and re-used at days 25 and 28.

Overall, the results obtained in this study suggests that an effect of the sampling method on compounds P_{app} values is inherent in multi-time permeability assays across cell monolayers, whether sampled by replacement or transfer. This leads to P_{app} values dependent on the sample time interval when distinct time intervals are used. It also leads to a non-proportionality between the amount of compound transported and the sampling time interval. In fact, the analysis of data from the literature shows that small deviations from linearity are usually observed in the cumulative amount of analyte transported (both when using the transfer and the replacement approach) [289-292]. When comparing the two sampling methods, it is clear that deviations from linearity are more pronounced for the replacement method. The variability obtained for the composition of the solution withdrawn at each sampling time was also much larger for this method, both effects supporting a better performance for the transfer sampling approach.

Effect of experimental methodologies

VII.4.3 – Effect of BSA on the observed permeability

BSA is commonly added to the transport media of permeability assays across cell monolayers as a solubilizing agent to improve the reliability of permeability assessment of poorly water-soluble and highly lipophilic compounds. The addition of BSA constitutes an experimental variation to the standard protocol, thus it is important to understand what are the implications of its use on the reported P_{app} data. Having an in-depth knowledge of the physicochemical properties and interaction of compounds with the components present in the assay media allows for a reliable evaluation of the impact of BSA on permeability assessments. In this work, to carry out this evaluation, a homologous series of small amphiphiles, the NBD-C4, NBD-C6 and NBD-C8 was used due to their well-characterized properties (Table VII.1). The affinity of these amphiphiles for lipid membranes is moderate-to-high, with partition coefficients varying from $\cong 10^3$ for NBD-C4 to 4×10^4 for NBD-C8. These amphiphiles are therefore expected to be passively transported across Caco-2 monolayers via the transcellular route. The polar moiety of the amphiphiles is the same (the NBD group), and therefore a similar rate of diffusion through the lipid membrane is expected for all amphiphiles. A faster permeation is therefore expected for the most lipophilic amphiphiles. The results for P_{app} of each NBD-Cn across Caco-2 monolayers obtained in the presence of BSA in the donor and acceptor compartments are shown in Figure VII. 4, and the detailed statistical analysis is provided in supplementary material – Table VII. S2.

The transport rates obtained for the amphiphiles are $\geq 10^{-6}$ cm/s, which are consistent with their relatively high lipophilicity and overall neutral charge. However, the rank order of Caco-2 transport among the amphiphiles in the series is inverse to the expected based on their interaction with lipid membranes, with NBD-C4 showing the larger P_{app} value while being the less lipophilic amphiphile. Additionally, the results indicate that re-using Caco-2 monolayers allows to triplicate the assessment of the effect of BSA on P_{app} of NBD-Cn, since the measured P_{app} values are not significantly different from those in single used monolayers.

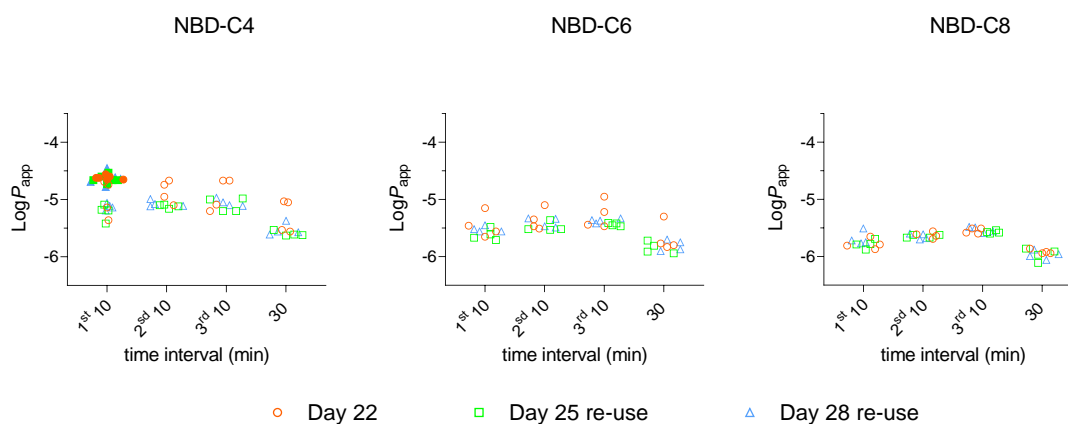


Figure VII. 4 Effect of BSA on the permeability of NBD-Cn amphiphiles across Caco-2 monolayers in multi-time sampling assays. BSA at a concentration of 100 μM was added to the donor and acceptor compartments (open symbols). For NBD-C4, a permeability assay was also performed for 10 min in the absence of BSA (filled symbols).

The P_{app} values shown do not consider the binding of the amphiphiles to the BSA present in the transport media. The amphiphiles have however a significant binding to BSA, with K_{B} determined in the order of 10^4 to 10^5 M. In these circumstances, the use of the total amount of NBD-Cn to calculate P_{app} leads to an underestimation of the P_{app} values, as has been previously observed by other authors [136,138,139]. The correct evaluation of permeability data obtained in the presence of BSA needs to consider that the amount of amphiphile available for permeation is only the fraction free in the aqueous media. This analysis of P_{app} values is shown and discussed in the next section.

VII.4.3.1 – Effect of correcting of P_{app} value for unbound fraction of NBD-Cn to BSA: calculation of the $P_{\text{app}}^{\text{Unb}}$ value

The unbound fraction of each NBD-Cn was determined using the measured K_{B} and BSA concentration (Equation VII. 1). The amount of NBD-C4, NBD-C6 and NBD-C8 free in the aqueous medium was 43 %, 17 %, and 3 % of the total amount in the donor compartment, respectively. The $P_{\text{app}}^{\text{Unb}}$ values for amphiphiles were recalculated from the observed P_{app} considering only the unbound fraction as the driving force for permeation. The results obtained are shown in Figure VII. 5 (see supplementary material — Table VII. S2 for a detailed statistical analysis). The recalculated $P_{\text{app}}^{\text{Unb}}$ values are larger than those obtained directly, now ranging from 10^{-5} to 10^{-4} cm/s, which is consistent with their relatively high lipophilicity

Effect of experimental methodologies

and neutral charge. More importantly, NBD-C8 is now the amphiphile with larger P_{app} (10×10^{-5} cm/s), followed by NBD-C6 (2.2×10^{-5} cm/s), and NBD-C4 (1.7×10^{-5} cm/s). The relative values obtained for NBD-C8 and NBD-C6 are in agreement with their respective affinities for the cell membrane. However, a more significant decrease in P_{app} was expected for NBD-C4. The maintenance of its high P_{app} in spite of the significant decrease in lipophilicity suggests that this small amphiphile may also permeate significantly through paracellular pathways.

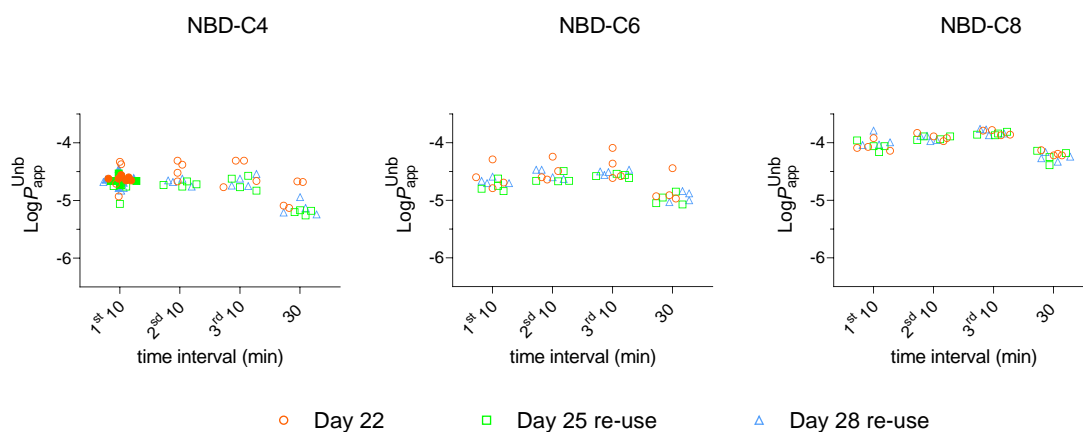


Figure VII. 5 Effect of BSA on the permeability of NBD-Cn amphiphiles through Caco-2 monolayers when the P_{app}^{Unb} values are recalculated from the observed P_{app} using the free amount of each amphiphile as the driving force for permeation. The multi-time sampling assays were performed in the presence of 100 μM BSA in the donor and acceptor compartments. For NBD-C4, a permeability assay was also performed for 10 min in the absence of BSA (filled symbols).

Table VII. 4 summarizes the effect of BSA on the permeability values and ranking order of the amphiphiles, when considering the P_{app} values measured in the Caco-2 assays and the recalculated P_{app}^{Unb} values. The presence of BSA in the donor compartment not only influences the P_{app} values measured for the amphiphiles, it can even change their permeability ranking order. To confirm that P_{app}^{Unb} is the parameter that best estimates the true permeability of amphiphiles, its value was compared to the P_{app} value obtained in the absence of BSA in the transport media. The P_{app}^{Unb} value of NBD-C4 (2.3×10^{-5} cm/s) is in good agreement with P_{app} value obtained in the absence of BSA (2.6×10^{-5} cm/s).

Table VII. 4 Summary of the effect of adding 100 μM BSA to the transport media on the permeability of a homologous NBD-Cn series across cell monolayers derived from Caco-2, MDCK-II and MDCK-MDR1 cell lines. The rank order of their permeabilities is shown when considering the P_{app} values measured in the assays and the recalculated $P_{\text{app}}^{\text{Unb}}$ values that account for the unbound fraction. The fold change between the two P_{app} values was calculated.

Cell model	Amphiphile	N ^a	With 100 μM BSA						
			P_{app} (10^{-5} cm/s)		Permeability rank order	$P_{\text{app}}^{\text{Unb}}$ (10^{-5} cm/s)		Permeability rank order	Relative variation in P_{app} value ^c
			μ	CI ₉₅		μ	CI ₉₅		
Caco-2 ^b	NBD-C4	4	0.7	0.3; 2.0	1 ^o	1.7	0.6; 4.7	3 ^o	2.4
	NBD-C6	4	0.3	0.1; 0.7	2 ^o	2.2	1.0; 5.1	2 ^o	6.3
	NBD-C8	4	0.2	0.1; 0.4	3 ^o	10.0	5.3; 19.0	1 ^o	50
MDCK-II	NBD-C4	2	1.6	0.6; 3.9	1 ^o	3.6	1.5; 9.0	3 ^o	2.3
	NBD-C6	1	0.7	0.2; 2.1	2 ^o	4.2	1.4; 12.6	2 ^o	6.0
	NBD-C8	1	0.5	0.3; 1.0	3 ^o	21.5	11.9; 38.9	1 ^o	43
MDCK-MDR1	NBD-C4	2	0.9	0.4; 1.9	1 ^o	2.0	0.9; 4.4	3 ^o	2.2
	NBD-C6	2	0.4	0.2; 0.8	2 ^o	2.2	1.0; 4.7	2 ^o	5.5
	NBD-C8	2	0.3	0.2; 0.6	3 ^o	12.5	6.2; 25.1	1 ^o	42

^a Number of cell monolayers used in assays. ^b In Caco-2 assays, the P_{app} corresponds to the mean values obtained for monolayers at 22 and re-used at 25 and 28 days post-seeding. The value of P_{app} was calculated from the average of the instantaneous permeability at each time interval of multi-sampling assays within 60 min. Statistically significant differences were found between the P_{app} values measured in the assays and the $P_{\text{app}}^{\text{Unb}}$ values for all the amphiphiles and across the distinct cell monolayers. ^c ratio between $P_{\text{app}}^{\text{Unb}}$ and P_{app} .

As an additional quantitative assessment of the impact of BSA on the observed P_{app} values, the permeability of NBD-Cn was also evaluated across cell monolayers derived from MDCK-II and MDCK-MDR1 cells. BSA is also commonly employed in permeability assays performed across these cell monolayers for the same reasons as in the Caco-2 assays. Table VII. 4 presents the results for the effect of 100 μM BSA on the permeability values and ranking order of the amphiphiles using MDCK monolayers. The NBD-Cn permeabilities estimated by the measured P_{app} values and recalculated $P_{\text{app}}^{\text{Unb}}$ values were significantly different. The two estimates affected the categorization of the transport of the amphiphiles, with the order being reversed between the shorter and the longer acyl chain NBD-Cn. The calculated $P_{\text{app}}^{\text{Unb}}$ correlating better with

Effect of experimental methodologies

the compound's molecular properties, for both MDCK cell types and as previously observed for Caco-2 monolayers.

The results presented in this work highlight the importance of correcting P_{app} values for the unbound fraction of solutes, ensuring an accurate report of their permeability for assays performed in the presence of BSA.

VII.5 – Conclusions

The systematic study present in this work allow to understand and evaluate the effects that a specific experimental methodology has on the measured P_{app} values of compounds. The quantitative characterization of the effects of the distinct methodologies used to perform the assays is important to help reduce variability in P_{app} by attempting to uniform the P_{app} values to standard conditions.

The evaluation of LY permeability in the same cell monolayer with test compounds was validated as it was shown that the simultaneously permeability assessment had no effect on the P_{app} values of either the LY or the test compounds. The use of this methodology revealed to be advantageous and useful as a quality control for each cell monolayer integrity, especially in cases where complex mixtures of compounds with unknown effects were used. This approach will avoid additional incubations with LY after a permeability assay with the test compounds and ensure that compromised cell monolayers are discarded from the analysis. In this way, this methodology can help reduce the variability associated with the integrity of the cell monolayers.

The use of transfer or replacement as sampling method influenced the measured P_{app} values of LY and Prop at distinct time intervals. The manipulation by both methods leads to the transport of a significant amount of compound, which is retained in the residual layer formed above the insert. The P_{app} values for LY and Prop were lower when obtained with replacement than transfer. This was mainly attributed to the low diffusion of the residual layer into the acceptor compartment. The sampling method may be a source of variability in the evaluation of passive permeating compounds, in particular when the agitation rate is not sufficient to homogenize the acceptor solution in replacement assays.

Another important conclusion from this work is that the addition of BSA to the transport media was shown to affect the measurement of the true P_{app} of a homologous series of amphiphiles. The direct result of this effect was observed

in the ranking order of their permeabilities across the cell monolayers, which was inverse to what was expected given their interaction with lipid membranes. Considering the unbound fraction of the amphiphiles and the BSA concentration, the P_{app}^{Unb} was recalculated from the observed P_{app} . The rationalization of permeability using the P_{app}^{Unb} values of each amphiphile showed that this parameter correlates better with the molecular properties of the amphiphiles. Thus, the presence of BSA in the assays might not necessarily introduce variability in P_{app} collected from distinct sources, regarded that the P_{app}^{Unb} values of compounds are considered. The use of a series of molecules with well-characterized properties represents a significant advancement with respect to previous studies on the effects of BSA in the transport medium. Its use allows the discrimination between the effects of the decrease in the amount of compound available to permeate (the unbound fraction), and effects on the increase in the compound solubility and/or a decrease in adsorption to the apparatus and sequestration by cell membranes.

During the execution of this study, the re-use of Caco-2 monolayers revealed to be a high-throughput approach with a great potential to be used for the quantitative characterization of the effect on P_{app} values of passive permeating compounds of the most common alterations observed in experimental protocols among literature.

VII.6 – Supplementary material

Table VII. S1 Statistical analysis of LY and Prop P_{app} values obtained when using the replacement method for sampling in multi-time permeability assays across Caco-2 monolayers. The average and the corresponding confidence intervals at 95 % confidence (CI_{95}) were obtained directly from the analysis of $\text{Log}(P_{app})$ or $\text{Log}(Q_A)$.

Day	Assay Conditions Sampling (N) ^a	Monolayer use	Lucifer Yellow				Propranolol	
			P_{app} (10^{-6} cm/s)		Q_A (%)		P_{app} (10^{-6} cm/s)	
			μ	CI_{95}	μ	CI_{95}	μ	CI_{95}
All	all (107)	Single use & re-use	0.12	0.009; 1.6	0.03	0.001; 0.69	0.4	0.03; 6.3
	1 st 10 min (26)		0.02	0.007; 0.09	0.004	0.001; 0.01	0.07	0.01; 0.5
	2 nd 10 min (26)		0.07	0.007; 0.77	0.01	0.001; 0.13	0.3	0.03; 2.8
	3 rd 10 min (26)		0.15	0.02; 1.14	0.03	0.003; 0.19	0.5	0.1; 3.3
	4 th 30 min (26)		0.63	0.23; 1.73	0.32	0.12; 0.87	2.5	1.3; 4.7
22	all (12)	Single use	0.21	0.01; 3.96	0.05	0.001; 1.55	0.7	0.04; 11.1
	1 st 10 min (3)		0.03	0.002; 0.38	0.01	0.0004; 0.06	0.2	0.008; 3.8
	2 nd 10 min (3)		0.13	0.003; 5.67	0.02	0.001; 0.95	0.3	0.003; 26.9
	3 rd 10 min (3)		0.39	0.01; 10	0.06	0.002; 1.73	0.9	0.05; 18.6
	4 th 30 min (3)		1.2	0.6; 2.4	0.6	0.3; 1.19	3.7	1.8; 7.6
25	all (40)	Re-use	0.13	0.01; 1.89	0.03	0.001; 0.72	0.4	0.03; 5.9
	1 st 10 min (10)		0.03	0.004; 0.17	0.005	0.001; 0.03	0.06	0.008; 5.1
	2 nd 10 min (10)		0.10	0.007; 1.35	0.02	0.001; 0.23	0.3	0.03; 3.4
	3 rd 10 min (10)		0.19	0.02; 1.7	0.03	0.004; 0.28	0.6	0.1; 3.1
	4 th 30 min (10)		0.64	0.64; 0.64	0.32	0.32; 0.32	2.2	2.2; 2.2
28	all (55)	Re-use	0.09	0.007; 1.10	0.02	0.001; 0.61	0.4	0.03; 6.4
	1 st 10 min (13)		0.02	0.01; 0.04	0.003	0.002; 0.01	0.06	0.01; 0.4
	2 nd 10 min (13)		0.04	0.004; 0.46	0.01	0.001; 0.08	0.3	0.03; 3.3
	3 rd 10 min (13)		0.11	0.02; 0.66	0.02	0.003; 0.11	0.5	0.07; 3.4
	4 th 30 min (13)		0.53	0.2; 1.5	0.27	0.10; 0.74	2.4	1.3; 4.7

^aNumber of time points sampled for LY + Prop permeability assays.

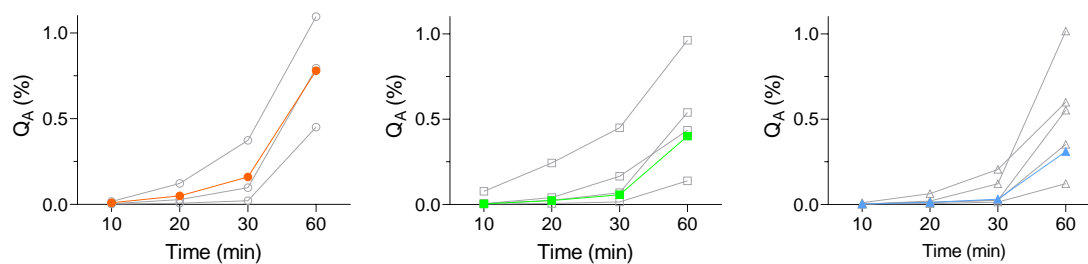


Figure VII. S1 Cumulative amount of LY that reaches the acceptor compartment for permeability experiments performed with multiple time assays following the replacement sampling method. The results are presented for cell monolayers on 22 (left), re-used on day 25 (middle) and re-used on day 28 (right) post-seeding. The average values obtained for all assays in a given condition are shown as filled and colored symbols. The open symbols are some representative results obtained for individual cell monolayers.

Effect of experimental methodologies

Table VII. S2 Statistical analysis of P_{app} values of NBD-C4, NBD-C6 and NBD-C8 after multi-time sampling permeability assays through single use and re-used Caco-2 monolayers from day 22 to 28. Their permeability across monolayers derived from MDCK-II and MDR1 cell lines were also evaluated. The average and the corresponding confidence intervals at 95 % (CI₉₅) were obtained directly from the analysis of Log (P_{app}).

Cell line	Assay Conditions		Monolayer use	P_{app} (10 ⁻⁵ cm/s)						P_{app} (10 ⁻⁵ cm/s) corrected for unbound fraction					
	Day	Sampling		NBD-C4		NBD-C6		NBD-C8		NBD-C4		NBD-C6		NBD-C8	
				μ	CI ₉₅	μ	CI ₉₅	μ	CI ₉₅	μ	CI ₉₅	μ	CI ₉₅	μ	CI ₉₅
Caco-2	All	1 st 10 min	Single use & re-use	0.8	0.3; 1.9	0.3	0.2; 0.5	0.2	0.1; 0.3	1.9	0.8; 4.5	2.2	1.2; 3.9	9.4	6.2; 14.2
		2 nd 10 min		1.0	0.5; 1.8	0.4	0.2; 0.6	0.2	0.2; 0.3	2.4	1.3; 4.4	2.8	1.7; 4.7	12.2	10.2; 14.5
		3 rd 10 min		1.0	0.5; 2.0	0.4	0.2; 0.8	0.3	0.2; 0.3	2.4	1.2; 4.8	3.2	1.8; 5.8	14.9	12.6; 17.7
		4 th 30 min		0.3	0.1; 0.8	0.2	0.08; 0.3	0.1	0.08; 0.2	0.8	0.4; 1.9	1.2	0.6; 2.4	5.9	4.4; 8.1
	22	1 st 10 min	Single use	1.0	0.2; 5.1	0.4	0.1; 1.0	0.2	0.1; 0.3	2.6	0.6; 10.6	2.6	0.9; 7.5	8.8	5.5; 14.0
		2 nd 10 min		1.4	0.5; 3.6	0.4	0.2; 1.0	0.2	0.2; 0.3	3.4	1.6; 7.5	3.2	1.3; 7.8	12.5	9.4; 16.6
		3 rd 10 min		1.2	0.3; 4.8	0.5	0.2; 1.8	0.3	0.2; 0.4	3.1	0.9; 9.9	3.9	1.2; 12.7	15.0	11.9; 18.9
		4 th 30 min		0.5	0.1; 2.2	0.2	0.06; 0.7	0.1	0.1; 0.2	1.3	0.4; 4.4	1.5	0.4; 5.3	6.4	5.3; 7.9
	25	1 st 10 min	Re-use	0.6	0.3; 1.2	0.2	0.2; 0.4	0.2	0.1; 0.2	1.5	0.7; 3.2	1.8	1.1; 2.9	8.7	5.9; 12.9
		2 nd 10 min		0.8	0.7; 0.9	0.3	0.2; 0.5	0.2	0.2; 0.3	1.9	1.6; 2.3	2.4	1.6; 3.6	12.0	10.4; 14.0
		3 rd 10 min		0.8	0.4; 1.4	0.4	0.3; 0.4	0.3	0.2; 0.3	2.0	1.1; 3.7	2.7	2.3; 3.1	14.2	12.7; 16.0
		4 th 30 min		0.3	0.2; 0.3	0.1	0.09; 0.2	0.1	0.06; 0.2	0.6	0.5; 0.8	1.1	0.6; 1.7	5.8	3.4; 9.8
	28	1 st 10 min	Re-use	0.7	0.6; 1.0	0.3	0.2; 0.4	0.2	0.1; 0.4	1.9	1.2; 2.9	2.2	1.7; 2.8	10.9	6.1; 19.3
		2 nd 10 min		0.8	0.6; 1.1	0.4	0.3; 0.6	0.2	0.2; 0.3	2.1	1.6; 2.8	2.9	1.9; 4.4	12.0	9.4; 15.2
		3 rd 10 min		0.9	0.6; 1.2	0.4	0.4; 0.5	0.3	0.2; 0.4	2.2	1.4; 3.6	3.1	2.6; 3.7	15.6	12.1; 20.1
		4 th 30 min		0.3	0.2; 0.5	0.2	0.1; 0.3	0.1	0.08; 0.2	0.7	0.4; 1.4	1.2	0.7; 1.8	5.7	4.0; 8.0
MDCK-II	7	1 st 10 min	Single use	2.1	0.8; 5.8	0.9		0.5		4.8	1.7; 13.4	5.5		19.5	
		2 nd 10 min		1.7	1.6; 1.8	1.0		0.6		3.9	3.7; 4.1	5.8		26.0	
		3 rd 10 min		2.2	1.7; 3.0	0.9		0.7		5.1	3.8; 6.9	5.1		27.8	
		4 th 30 min		0.8	0.3; 2.2	0.3		0.4		1.8	0.7; 5.0	2.0		15.2	

MDCK-MDR1	7	1 st 10 min	Single use	1.2	0.7; 2.3	0.4	0.2; 0.8	0.3	0.2; 0.4	2.9	1.5; 5.4	2.1	1.0; 4.5	11.7	8.3; 16.5
		2 nd 10 min		0.8	0.8; 0.8	0.5	0.5; 0.5	0.4	0.2; 0.8	1.8	1.8; 1.9	3.0	2.9; 3.1	16.4	8.4; 31.9
		3 rd 10 min		1.2	0.8; 1.7	0.5	0.5; 0.5	0.4	0.4; 0.4	2.7	1.8; 3.9	3.1	2.9; 3.2	16.9	16.1; 17.8
		4 th 30 min		0.5	0.3; 0.8	0.2	0.2; 0.2	0.2	0.09; 0.4	1.1	0.6; 1.9	1.2	1.1; 1.2	7.5	3.7; 15.3

The number of cell monolayers used to perform the permeability assays was 4 and 2 for monolayers derived from Caco-2 and MDCK cells, respectively.

Chapter VIII

General conclusions

The large variability in P_{app} values reported for the same compound poses challenges in the establishment of reliable QSPRs. The present work aimed to contribute to the solution of this problem through the quantitative evaluation of the effects of differences in experimental methodologies employed across laboratories.

The first approach addressed in this work focused on increasing the throughput of the permeability assays using Caco-2 monolayers. This was performed in order to enable the assessment of the effect on P_{app} values of a larger number of experimental conditions. The study presented in this thesis carried out an evaluation of two approaches aimed at improving the throughput of Caco-2 assays.

As a first alternative, a methodology was developed and implemented to allow the re-use of Caco-2 monolayers for additional permeability assessments. The assays were performed sequentially on days 22, 25 and 28 after cell seeding. The results demonstrated that the incubation period of two full days with culture media between each permeability assay was necessary and sufficient to re-establish the integrity of the cell monolayer. This allowed triplicating the throughput of the assay while following the procedure proposed in the reference protocol. The consistent P_{app} values obtained in permeability assays with compounds following the passive permeation route further supports the validity of re-using Caco-2 monolayers in subsequent assays employing this permeation pathway. Concerning the impact of re-use on carrier-mediated transport, two transporters were evaluated, glucose transporters (using the commonly used glucose derivative, NBD-G) and the efflux transporter P-gp (using rhodamine123, Rho). The results showed that although NBD-G binds efficiently to Caco-2 cell membranes, supposedly due to association with the glucose transporters, it is not transported and is thus not adequate in the evaluation of this permeation route. The results obtained for the transport of Rho were also inconclusive, mostly due to the low expression of P-gp in the Caco-2 cells at the passages used. A more comprehensive evaluation of active transport is therefore still needed for the full validation of the proposed protocol for re-use of Caco-2 monolayers in permeability assays. Although the re-use methodology has not been fully validated in this work, the overall results provided important insights. Namely, they indicated that the variability associated with the re-use approach was low compared to performing the assay with a new batch of cells, thus

General conclusions

highlighting the contribution of cell variability to the dispersion of P_{app} values in literature, and contributing to its decrease.

The second alternative evaluated in this work to increase the throughput of assays involved replacing the monolayers derived from Caco-2 cells with those of the faster-growing MDCK-II and MDCK-MDR1 cells. The quantitative comparison study between the two MDCK strains showed significant variations regarding the cell size, ZO-1 density, paracellular permeability and efflux activity. MDCK-MDR1 cells were small in size, resulting in a higher cell density within their monolayers compared to those derived of MDCK-II cells. Moreover, a larger area covered by ZO-1 staining was also observed in MDCK-MDR1 monolayers. These findings were attributed to the higher contribution of the cell-cell contacts in these monolayers due to their small size. This observation further supported the higher P_{app} values obtained for paracellular markers in MDCK-MDR1 compared to MDCK-II monolayers. The relationship between these two parameters have never been highlighted in other works.

The traditional Caco-2 model displayed the largest cell size, along with the lowest cell density and leading to the lower ZO-1 density among the three models. In spite of the lower density of tight-junctions, paracellular permeability is similar for Caco-2 and MDCK-II monolayers. This shows that the lower density of tight-junctions results from the lower contribution of cell-cell contacts due to the larger size of Caco-2 cells, and not due to a less tight cell monolayer. As previously observed in other studies, all three cell lines exhibited comparable passive transcellular permeability, further supporting the potential use of MDCK monolayers as an alternative to enhance assay throughput for transcellularly permeating compounds.

In this work we propose an innovative data analysis approach that allows a more detailed and quantitative evaluation of the contribution from active (P_{app}^{AE}) and passive (P_{app}^{PP}) transport to the overall P_{app} observed. The presence of active transport is usually evaluated through the ratio of P_{app} obtained for transport in the B→A and A→B directions, ratios higher/lower than 1 indicating active efflux/influx transport. Although providing information regarding the direction of the active transport and the relative contributions of active and passive pathways, this approach does not provide quantitative information for the rate of permeation through the distinct transport routes. In contrast, the analysis

approach proposed provides all the relevant parameters, namely i) the direction of the active transport, ii) the relative contribution of passive and active transport, and iii) a quantitative measure of P_{app} through the distinct pathways. The latter is important when comparing distinct cell lines, as a larger ratio of active/passive transport may be due to an increase in P_{app}^{AE} or a decrease in P_{app}^{PP} .

The efflux activity P_{app}^{AE} in the three cell lines studied was compared using the P-gp substrate Rho. As expected, this activity was larger in MDCK-MDR1 monolayers. However, this activity was lower than expected considering the overexpression of P-gp in these cells. This result points out to the intrinsic variability within this cell line. The efflux activity was lower in Caco-2 monolayers than in both MDCK models, in agreement with the lowest P-gp expression. The comparison of Rho P_{app}^{PP} through the different cell lines provides important information regarding the properties of the cell membranes and/or cell monolayer tightness. This parameter was similar for all cell lines, although somewhat higher for MDCK-MDR1 and lower for Caco-2 monolayers, in agreement with a significant contribution of Rho permeation by paracellular routes and the lower density of this pathway for larger cells.

The detailed work performed in the above studies also provided important insights regarding the experimental methodology and data analysis in permeability assays. The extensive number of permeability assays performed was of utmost importance in order to allow the analysis of the frequency distribution of P_{app} values. As expected, the P_{app} parameter revealed a skewed LogNormal distribution. Thus, the statistical analysis of P_{app} values should be performed from $\text{Log}P_{app}$, with the P_{app} values being then calculated from $\text{Log}P_{app}$ distribution, and described by their average and confidence intervals.

The analysis of the P_{app} values on consecutive and distinct sampling times showed that when following the transfer methodology, the manipulation of the monolayer required for sampling led to perturbations on monolayer integrity and/or that there is compound in the acceptor compartment being carried over in consecutive sampling time points. As a consequence, in multi-time assays the P_{app} values obtained were time-dependent. For this reason, it was proposed that the evaluation of monolayer integrity should be done through the amount of paracellular marker transported rather than by the instantaneous P_{app} value.

General conclusions

The second approach addressed in this work focused on contributing to the reduction of variability in P_{app} values by systematically evaluating the effect of some specific methodologies that are commonly used in the assays on the measured compounds permeability. The results showed that the inclusion of LY in the transport medium, together with the test compounds, is a promising approach to evaluate the monolayer integrity of each cell monolayer. This approach was validated for the reference compounds SA and Rho, with a global negative and positive charge, respectively. This approach was then used for test mixtures with unknown effects on cell properties (coffee and paralytic shellfish toxins extracts), highlighting its importance in helping to reduce the variability associated with the integrity of the cell monolayers.

The choice between transfer or replacement as the sampling method for performing permeability assays was also assessed. It was shown that both methods have impact on the measured P_{app} values of passive permeating compounds. The replacement approach resulted in lower P_{app} values and a much higher variability when compared to transfer. This was mainly attributed to insufficient homogenization of the acceptor solution in permeability assays performed in the A→B direction, and points towards the preferential use of the transfer sampling method.

Regarding the inclusion of BSA in the transport media, the results showed that the presence of BSA in the donor compartment not only influences the P_{app} values measured, it can even alter their permeability ranking order. The effect of BSA was evaluated using a homologous series of fluorescent amphiphiles with all the relevant parameters well known. Namely, their solubility in aqueous medium, the equilibrium association affinity for both BSA and lipid membranes, as well as the rate of permeation through the membranes. This represents a significant advancement with respect to previous studies on the effects of BSA in the transport medium, allowing the discrimination between the effects of the decrease in the amount of compound available to permeate (the unbound fraction), and effects on the increase in the compound solubility and/or a decrease in adsorption to the apparatus and sequestration by cell membranes. By considering the fraction of unbound amphiphiles, it was possible to calculate the P_{app}^{Unb} value of each amphiphile from the observed P_{app} value. The former leading to the expected permeability ranking order given their lipophilicity and interaction with lipid membranes. Therefore, if the P_{app}^{Unb} values of compounds

were considered when compiling P_{app} data from multiple sources, the presence of BSA in the assays might not necessarily introduce variability.

In the future, the effect of common alterations on Caco-2 permeability protocols could be systematically characterized in a high-throughput manner, at least for compounds following the passive permeation route. The use of a quantitative measure as a correction factor of P_{app} values to standard conditions has potential as an approach to improving the accuracy of permeability data. Its application does not require that the experimental conditions in the studies are all equal, although they must be well-described to allow the quantitative conversions. Although time-consuming, this strategy will definitely be faster than obtaining new permeability data for a large number of compounds under the same conditions.

References

1. Wunberg, T.; Hendrix, M.; Hillisch, A.; Lobell, M.; Meier, H.; Schmeck, C.; Wild, H.; Hinzen, B. Improving the hit-to-lead process: data-driven assessment of drug-like and lead-like screening hits. *Drug Discovery Today* **2006**, *11*, 175-180, doi:10.1016/s1359-6446(05)03700-1.
2. Borah, P.; Hazarika, S.; Deka, S.; Venugopala, K.N.; Nair, A.B.; Attimarad, M.; Sreeharsha, N.; Mailavaram, R.P. Application of Advanced Technologies in Natural Product Research: A Review with Special Emphasis on ADMET Profiling. *Current Drug Metabolism* **2020**, *21*, 751-767, doi:10.2174/1389200221666200714144911.
3. Fortuna, A.; Alves, G.; Falcão, A. The importance of permeability screening in drug discovery process: PAMPA, Caco-2 and rat everted gut assays. *Current Topics in Pharmacology* **2007**, *11*, 63-86.
4. Matter, H.; Schmider, W. In-Silico ADME Modeling. In *Drug Discovery and Evaluation: Safety and Pharmacokinetic Assays*, Vogel, H.G., Maas, J., Hock, F.J., Mayer, D., Eds.; Springer Berlin Heidelberg: Berlin, Heidelberg, 2013; pp. 1005-1052.
5. Harrison, R.K. Phase II and phase III failures: 2013-2015. *Nature Reviews Drug Discovery* **2016**, *15*, 817-818, doi:10.1038/nrd.2016.184.
6. Hurst, S.; Loi, C.-M.; Brodfuehrer, J.; El-Kattan, A. Impact of physiological, and biopharmaceutical factors in absorption and metabolism mechanisms on the drug oral bioavailability of rats and humans. *Expert Opinion on Drug Metabolism & Toxicology* **2007**, *3*, 469-489, doi:10.1517/17425225.3.4.469.
7. Di, L.; Artursson, P.; Avdeef, A.; Benet, L.Z.; Houston, J.B.; Kansy, M.; Kerns, E.H.; Lennernas, H.; Smith, D.A.; Sugano, K. The Critical Role of Passive Permeability in Designing Successful Drugs. *Chemmedchem* **2020**, *15*, 1862-1874, doi:10.1002/cmdc.202000419.
8. Watson, H. Biological membranes. *Understanding Biochemistry: Enzymes and Membranes* **2015**, *59*, 43-69, doi:10.1042/bse0590043.
9. Stenberg, P.; Bergstrom, C.A.S.; Luthman, K.; Artursson, P. Theoretical predictions of drug absorption in drug discovery and development. *Clinical Pharmacokinetics* **2002**, *41*, 877-899, doi:10.2165/00003088-200241110-00005.
10. Sugano, K.; Kansy, M.; Artursson, P.; Avdeef, A.; Bendels, S.; Di, L.; Ecker, G.F.; Faller, B.; Fischer, H.; Gerebtzoff, G.; et al. Coexistence of passive and carrier-mediated processes in drug transport. *Nature Reviews Drug Discovery* **2010**, *9*, 597, doi:10.1038/nrd3187 <https://www.nature.com/articles/nrd3187#supplementary-information>.
11. Krämer, S.D.; Lombardi, D.; Primorac, A.; Thomae, A.V.; Wunderli-Allenspach, H. Lipid-Bilayer Permeation of Drug-Like Compounds. *Chemistry & Biodiversity* **2009**, *6*, 1900-1916, doi:10.1002/cbdv.200900122.
12. Filipe, H.A.L.; Salvador, A.; Silvestre, J.M.; Vaz, W.L.C.; Moreno, M.J. Beyond Overton's Rule: Quantitative Modeling of Passive Permeation

References

- through Tight Cell Monolayers. *Mol. Phar*, **2014**, *11*, 3696-3706, doi:10.1021/mp500437e.
13. Paula, S.; Deamer, D.W. Membrane permeability barriers to ionic and polar solutes. *Membrane Permeability* **1999**, *48*, 77-95.
 14. Linnankoski, J.; Makela, J.; Palmgren, J.; Mauriala, T.; Vedin, C.; Ungell, A.L.; Lazorova, L.; Artursson, P.; Urtti, A.; Yliperttula, M. Paracellular Porosity and Pore Size of the Human Intestinal Epithelium in Tissue and Cell Culture Models. *Journal of Pharmaceutical Sciences* **2010**, *99*, 2166-2175, doi:10.1002/jps.21961.
 15. Leto, D.; Saltiel, A.R. Regulation of glucose transport by insulin: traffic control of GLUT4. *Nature Reviews Molecular Cell Biology* **2012**, *13*, 383-396, doi:10.1038/nrm3351.
 16. Cordoncardo, C.; O'Brien, J.P.; Boccia, J.; Casals, D.; Bertino, J.R.; Melamed, M.R. EXPRESSION OF THE MULTIDRUG RESISTANCE GENE-PRODUCT (P-GLYCOPROTEIN) IN HUMAN NORMAL AND TUMOR-TISSUES. *Journal of Histochemistry & Cytochemistry* **1990**, *38*, 1277-1287, doi:10.1177/38.9.1974900.
 17. Lin, J.H.; Yamazaki, M. Clinical relevance of P-glycoprotein in drug therapy. *Drug Metabolism Reviews* **2003**, *35*, 417-454, doi:10.1081/dmr-120026871.
 18. Sharom, F.J. The P-glycoprotein efflux pump: How does it transport drugs? *J. Membrane Biol.* **1997**, *160*, 161-175, doi:10.1007/s002329900305.
 19. Ambudkar, S.V.; Kim, I.W.; Sauna, Z.E. The power of the pump: Mechanisms of action of P-glycoprotein (ABCB1). *European Journal of Pharmaceutical Sciences* **2006**, *27*, 392-400, doi:10.1016/j.ejps.2005.10.010.
 20. Patel, B.A.; Abel, B.; Barbuti, A.M.; Velagapudi, U.K.; Chen, Z.S.; Ambudkar, S.V.; Talele, T.T. Comprehensive Synthesis of Amino Acid-Derived Thiazole Peptidomimetic Analogues to Understand the Enigmatic Drug/Substrate-Binding Site of P-Glycoprotein. *J. Med. Chem.* **2018**, *61*, 834-864, doi:10.1021/acs.jmedchem.7b01340.
 21. Egido, E.; Muller, R.; Li-Blatter, X.; Merino, G.; Seelig, A. Predicting Activators and Inhibitors of the Breast Cancer Resistance Protein (ABCG2) and P-Glycoprotein (ABCB1) Based on Mechanistic Considerations. *Mol. Phar*, **2015**, *12*, 4026-4037, doi:10.1021/acs.molpharmaceut.5b00463.
 22. Zhang, H.; Xu, H.W.; Ashby, C.R.; Assaraf, Y.G.; Chen, Z.S.; Liu, H.M. Chemical molecular-based approach to overcome multidrug resistance in cancer by targeting P-glycoprotein (P-gp). *Medicinal Research Reviews* **2021**, *41*, 525-555, doi:10.1002/med.21739.
 23. Moreno, M.J.; Filipe, H.A.L.; Cunha, S.V.P.; Ramos, C.V.; Martins, P.A.T.; Abel, B.; Loura, L.M.S.; Ambudkar, S.V. Interaction of a Homologous Series of Amphiphiles with P-glycoprotein in a Membrane Environment-

- Contributions of Polar and Non-Polar Interactions. *Pharmaceutics* **2023**, *15*, doi:10.3390/pharmaceutics15010174.
24. Okamoto, C.T. Endocytosis and transcytosis. *Adv. Drug Delivery Rev.* **1998**, *29*, 215-228, doi:10.1016/s0169-409x(97)00080-x.
 25. Zegers, M.M.P.; Hoekstra, D. Mechanisms and functional features of polarized membrane traffic in epithelial and hepatic cells. *Biochem. J.* **1998**, *336*, 257-269.
 26. Toth, A.E.; Holst, M.R.; Nielsen, M.S. Vesicular Transport Machinery in Brain Endothelial Cells: What We Know and What We Do not. *Current Pharmaceutical Design* **2020**, *26*, 1405-1416, doi:10.2174/1381612826666200212113421.
 27. Bor, G.; Hosta-Rigau, L. Next Generation of Brain Cancer Nanomedicines to Overcome the Blood-Brain Barrier (BBB): Insights on Transcytosis, Perivascular Tumor Growth, and BBB Models. *Advanced Therapeutics* **2023**, doi:10.1002/adtp.202300161.
 28. Abbott, N.J.; Rönnbäck, L.; Hansson, E. Astrocyte–endothelial interactions at the blood–brain barrier. *Nature Reviews Neuroscience* **2006**, *7*, 41-53, doi:10.1038/nrn1824.
 29. Du, W.; Fan, Y.; Zheng, N.; He, B.; Yuan, L.; Zhang, H.; Wang, X.; Wang, J.; Zhang, X.; Zhang, Q. Transferrin receptor specific nanocarriers conjugated with functional 7peptide for oral drug delivery. *Biomaterials* **2013**, *34*, 794-806, doi:<https://doi.org/10.1016/j.biomaterials.2012.10.003>.
 30. Field, F.J.; Fujiwara, D.; Born, E.; Chappell, D.A.; Mathur, S.N. Regulation of LDL receptor expression by luminal sterol flux in CaCo-2 cells. *Arteriosclerosis and thrombosis: a journal of vascular biology* **1993**, *13*, 729-737.
 31. Kramer, S.D.; Aschmann, H.E.; Hatibovic, M.; Hermann, K.F.; Neuhaus, C.S.; Brunner, C.; Belli, S. When barriers ignore the "rule-of-five". *Adv. Drug Delivery Rev.* **2016**, *101*, 62-74, doi:10.1016/j.addr.2016.02.001.
 32. Liu, Y.B.; Keib, A.; Neuber, B.; Wang, L.; Riemer, A.B.; Bonsack, M.; Hückelhoven-Krauss, A.; Schmitt, A.; Müller-Tidow, C.; Schmitt, M. Definition and Characterization of SOX11-Derived T Cell Epitopes towards Immunotherapy of Glioma. *International Journal of Molecular Sciences* **2023**, *24*, doi:10.3390/ijms24031943.
 33. Helmschrodt, C.; Hoebel, S.; Schoeniger, S.; Bauer, A.; Bonicelli, J.; Gringmuth, M.; Fietz, S.A.; Aigner, A.; Richter, A.; Richter, F. Polyethylenimine Nanoparticle-Mediated siRNA Delivery to Reduce α -Synuclein Expression in a Model of Parkinson's Disease. *Molecular Therapy-Nucleic Acids* **2017**, *9*, 57-68, doi:10.1016/j.omtn.2017.08.013.
 34. Dufés, C.; Al Robaian, M.; Somani, S. Transferrin and the transferrin receptor for the targeted delivery of therapeutic agents to the brain and cancer cells. *Therapeutic Delivery* **2013**, *4*, 629-640, doi:10.4155/tde.13.21.

References

35. Beresford, A.P.; Selick, H.E.; Tarbit, M.H. The emerging importance of predictive ADME simulation in drug discovery. *Drug Discovery Today* **2002**, *7*, 109-116.
36. van de Waterbeemd, H.; Gifford, E. ADMET in silico modelling: Towards prediction paradise? *Nature Reviews Drug Discovery* **2003**, *2*, 192-204, doi:10.1038/nrd1032.
37. Lipinski, C.A.; Lombardo, F.; Dominy, B.W.; Feeney, P.J. Experimental and computational approaches to estimate solubility and permeability in drug discovery and development settings. *Adv. Drug Delivery Rev.* **1997**, *23*, 3-25, doi:10.1016/s0169-409x(96)00423-1.
38. Wu, F.X.; Zhou, Y.Q.; Li, L.H.; Shen, X.H.; Chen, G.Y.; Wang, X.Q.; Liang, X.Y.; Tan, M.Y.; Huang, Z.N. Computational Approaches in Preclinical Studies on Drug Discovery and Development. *Frontiers in Chemistry* **2020**, *8*, doi:10.3389/fchem.2020.00726.
39. Vatansever, S.; Schlessinger, A.; Wacker, D.; Kaniskan, H.; Jin, J.; Zhou, M.M.; Zhang, B. Artificial intelligence and machine learning-aided drug discovery in central nervous system diseases: State-of-the-arts and future directions. *Medicinal Research Reviews* **2021**, *41*, 1427-1473, doi:10.1002/med.21764.
40. Tran, T.T.V.; Tayara, H.; Chong, K.T. Recent Studies of Artificial Intelligence on In Silico Drug Distribution Prediction. *International Journal of Molecular Sciences* **2023**, *24*, doi:10.3390/ijms24031815.
41. Wang, X.T.; Liu, M.; Zhang, L.; Wang, Y.; Li, Y.; Lu, T. Optimizing Pharmacokinetic Property Prediction Based on Integrated Datasets and a Deep Learning Approach. *Journal of Chemical Information and Modeling* **2020**, *60*, 4603-4613, doi:10.1021/acs.jcim.0c00568.
42. Wilson, G.; Hassan, I.F.; Dix, C.J.; Williamson, I.; Shah, R.; Mackay, M.; Artursson, P. TRANSPORT AND PERMEABILITY PROPERTIES OF HUMAN CACO-2 CELLS - AN INVITRO MODEL OF THE INTESTINAL EPITHELIAL-CELL BARRIER. *Journal of Controlled Release* **1990**, *11*, 25-40, doi:10.1016/0168-3659(90)90118-d.
43. Katritzky, A.R.; Kuanar, M.; Slavov, S.; Hall, C.D.; Karelson, M.; Kahn, I.; Dobchev, D.A. Quantitative Correlation of Physical and Chemical Properties with Chemical Structure: Utility for Prediction. *Chemical Reviews* **2010**, *110*, 5714-5789, doi:10.1021/cr900238d.
44. Wishart, D.S. Improving early drug discovery through ADME modelling: an overview. *Drugs in R&D* **2007**, *8*, 349-362.
45. Roy, K.; Das, R.N.; Ambure, P.; Aher, R.B. Be aware of error measures. Further studies on validation of predictive QSAR models. *Chemometrics and Intelligent Laboratory Systems* **2016**, *152*, 18-33, doi:10.1016/j.chemolab.2016.01.008.

46. Consonni, V.; Ballabio, D.; Todeschini, R. Comments on the Definition of the Q(2) Parameter for QSAR Validation. *Journal of Chemical Information and Modeling* **2009**, *49*, 1669-1678, doi:10.1021/ci900115y.
47. Tropsha, A.; Gramatica, P.; Gombar, V.K. The importance of being earnest: Validation is the absolute essential for successful application and interpretation of QSPR models. *Qsar & Combinatorial Science* **2003**, *22*, 69-77, doi:10.1002/qsar.200390007.
48. Sun, H.M. Predicting ADMET Properties by Projecting onto Chemical Space-Benefits and Pitfalls. *Current Computer-Aided Drug Design* **2005**, *1*, 179-193, doi:10.2174/1573409053585708.
49. Awale, M.; Visini, R.; Probst, D.; Arus-Pous, J.; Reymond, J.L. Chemical Space: Big Data Challenge for Molecular Diversity. *Chimia* **2017**, *71*, 661-666, doi:10.2533/chimia.2017.661.
50. Butina, D.; Segall, M.D.; Frankcombe, K. Predicting ADME properties in silico: methods and models. *Drug Discovery Today* **2002**, *7*, S83-S88, doi:10.1016/s1359-6446(02)02288-2.
51. Gramatica, P. Principles of QSAR models validation: internal and external. *Qsar & Combinatorial Science* **2007**, *26*, 694-701, doi:10.1002/qsar.200610151.
52. Tropsha, A. Best Practices for QSAR Model Development, Validation, and Exploitation. *Molecular Informatics* **2010**, *29*, 476-488, doi:10.1002/minf.201000061.
53. Zhu, J.Y.; Wang, J.M.; Yu, H.D.; Li, Y.Y.; Hou, T.J. Recent Developments of In Silico Predictions of Oral Bioavailability. *Combinatorial Chemistry & High Throughput Screening* **2011**, *14*, 362-374, doi:10.2174/138620711795508368.
54. Klopman, G.; Stefan, L.R.; Saiakhov, R.D. ADME evaluation 2. A computer model for the prediction of intestinal absorption in humans. *European Journal of Pharmaceutical Sciences* **2002**, *17*, 253-263, doi:10.1016/s0928-0987(02)00219-1.
55. Turner, J.V.; Glass, B.D.; Agatonovic-Kustrin, S. Prediction of drug bioavailability based on molecular structure. *Analytica Chimica Acta* **2003**, *485*, 89-102, doi:10.1016/s0003-2670(03)00406-9.
56. Sarmiento, B.; Andrade, F.; da Silva, S.B.; Rodrigues, F.; das Neves, J.; Ferreira, D. Cell-based in vitro models for predicting drug permeability. *Expert Opinion on Drug Metabolism & Toxicology* **2012**, *8*, 607-621, doi:10.1517/17425255.2012.673586.
57. Zakharova, M.; Tibbe, M.P.; Koch, L.S.; Le-The, H.; Leferink, A.M.; van den Berg, A.; van der Meer, A.D.; Broersen, K.; Segerink, L.I. Transwell-Integrated 2 μ m Thick Transparent Polydimethylsiloxane Membranes with Controlled Pore Sizes and Distribution to Model the Blood-Brain Barrier. *Advanced Materials Technologies* **2021**, *6*, doi:10.1002/admt.202100138.

References

58. Artursson, P.; Karlsson, J. Correlation Between Oral-Drug Absorption in Humans and Apparent Drug Permeability Coefficients in Human Intestinal Epithelial (Caco-2) Cells. *Biochem. Biophys. Res. Commun.* **1991**, *175*, 880-885, doi:10.1016/0006-291x(91)91647-u.
59. van Breemen, R.B.; Li, Y. Caco-2 cell permeability assays to measure drug absorption. *Expert Opinion on Drug Metabolism & Toxicology* **2005**, *1*, 175-185, doi:10.1517/17425255.1.2.175.
60. Balimane, P.V.; Chong, S. Cell culture-based models for intestinal permeability: A critique. *Drug Discovery Today* **2005**, *10*, 335-343, doi:[https://doi.org/10.1016/S1359-6446\(04\)03354-9](https://doi.org/10.1016/S1359-6446(04)03354-9).
61. Volpe, D.A. Advances in cell-based permeability assays to screen drugs for intestinal absorption. *Expert Opinion on Drug Discovery* **2020**, *15*, 539-549, doi:10.1080/17460441.2020.1735347.
62. Grasset, E.; Pinto, M.; Dussaulx, E.; Zweibaum, A.; Desjeux, J.F. EPITHELIAL PROPERTIES OF HUMAN COLONIC-CARCINOMA CELL-LINE CACO-2 - ELECTRICAL PARAMETERS. *American Journal of Physiology* **1984**, *247*, C260-C267, doi:10.1152/ajpcell.1984.247.3.C260.
63. Hidalgo, I.J.; Raub, T.J.; Borchardt, R.T. Characterization of the human colon carcinoma cell line (Caco-2) as a model system for intestinal epithelial permeability. *Gastroenterology* **1989**, *96*, 736-749.
64. Pinto, M.; Robineleon, S.; Appay, M.D.; Kedinger, M.; Triadou, N.; Dussaulx, E.; Lacroix, B.; Simonassmann, P.; Haffen, K.; Fogh, J.; et al. ENTEROCYTE-LIKE DIFFERENTIATION AND POLARIZATION OF THE HUMAN-COLON CARCINOMA CELL-LINE CACO-2 IN CULTURE. *Biology of the Cell* **1983**, *47*, 323-330.
65. Vachon, P.H.; Beaulieu, J.F. Transient mosaic patterns of morphological and functional-differentiation in the Caco-2 cell-line. *Gastroenterology* **1992**, *103*, 414-423, doi:10.1016/0016-5085(92)90829-n.
66. Hilgers, A.R.; Conradi, R.A.; Burton, P.S. Caco-2 cell monolayers as a model for drug transport across the intestinal-mucosa. *Pharmaceutical Research* **1990**, *7*, 902-910, doi:10.1023/a:1015937605100.
67. Angelis, I.D.; Turco, L. Caco-2 cells as a model for intestinal absorption. *Current protocols in toxicology* **2011**, *Chapter 20*, Unit20.26-Unit20.26, doi:10.1002/0471140856.tx2006s47.
68. Fedi, A.; Vitale, C.; Ponschin, G.; Ayehunie, S.; Fato, M.; Scaglione, S. In vitro models replicating the human intestinal epithelium for absorption and metabolism studies: A systematic review. *Journal of Controlled Release* **2021**, *335*, 247-268, doi:10.1016/j.jconrel.2021.05.028.
69. Sjöberg, Å.; Lutz, M.; Tannergren, C.; Wingolf, C.; Borde, A.; Ungell, A.L. Comprehensive study on regional human intestinal permeability and prediction of fraction absorbed of drugs using the Ussing chamber

- technique. *European Journal of Pharmaceutical Sciences* **2013**, *48*, 166-180, doi:10.1016/j.ejps.2012.10.007.
70. Maher, S.; Kennelly, R.; Bzik, V.A.; Baird, A.W.; Wang, X.X.; Winter, D.; Brayden, D.J. Evaluation of intestinal absorption enhancement and local mucosal toxicity of two promoters. I. Studies in isolated rat and human colonic mucosae. *European Journal of Pharmaceutical Sciences* **2009**, *38*, 291-300, doi:10.1016/j.ejps.2009.09.001.
71. Fortuna, A.; Alves, G.; Falcao, A.; Soares-da-Silva, P. Evaluation of the permeability and P-glycoprotein efflux of carbamazepine and several derivatives across mouse small intestine by the Ussing chamber technique. *Epilepsia* **2012**, *53*, 529-538, doi:10.1111/j.1528-1167.2012.03409.x.
72. Spring, K.R. Routes and mechanism of fluid transport by epithelia. *Annual Review of Physiology* **1998**, *60*, 105-119, doi:10.1146/annurev.physiol.60.1.105.
73. Konsoula, R.; Barile, F.A. Correlation of in vitro cytotoxicity with paracellular permeability in Caco-2 cells. *Toxicology in Vitro* **2005**, *19*, 675-684, doi:10.1016/j.tiv.2005.03.006.
74. Antonescu, I.E.; Rasmussen, K.F.; Neuhoff, S.; Frette, X.; Karlgren, M.; Bergstrom, C.A.S.; Nielsen, C.U.; Steffansen, B. The Permeation of Acamprostate Is Predominantly Caused by Paracellular Diffusion across Caco-2 Cell Monolayers: A Paracellular Modeling Approach. *Molecular Pharmaceutics* **2019**, *16*, 4636-4650, doi:10.1021/acs.molpharmaceut.9b00733.
75. Delie, F.; Rubas, W. A human colonic cell line sharing similarities with enterocytes as a model to examine oral absorption: advantages and limitations of the Caco-2 model. *Critical Reviews™ in Therapeutic Drug Carrier Systems* **1997**, *14*.
76. Sun, H.; Chow, E.C.Y.; Liu, S.; Du, Y.; Pang, K.S. The Caco-2 cell monolayer: usefulness and limitations. *Expert Opinion on Drug Metabolism & Toxicology* **2008**, *4*, 395-411, doi:10.1517/17425255.4.4.395.
77. Artursson, P. EPITHELIAL TRANSPORT OF DRUGS IN CELL-CULTURE .1. A MODEL FOR STUDYING THE PASSIVE DIFFUSION OF DRUGS OVER INTESTINAL ABSORPTIVE (CACO-2) CELLS. *Journal of Pharmaceutical Sciences* **1990**, *79*, 476-482, doi:10.1002/jps.2600790604.
78. Gres, M.C.; Julian, B.; Bourrie, M.; Meunier, V.; Roques, C.; Berger, M.; Boulenc, X.; Berger, Y.; Fabre, G. Correlation between oral drug absorption in humans, and apparent drug permeability in TC-7 cells, a human epithelial intestinal cell line: Comparison with the parental Caco-2 cell line. *Pharmaceutical Research* **1998**, *15*, 726-733, doi:10.1023/a:1011919003030.
79. Hou, T.J.; Wang, J.M.; Zhang, W.; Xu, X.J. ADME evaluation in drug discovery. 7. Prediction of oral absorption by correlation and

References

- classification. *Journal of Chemical Information and Modeling* **2007**, *47*, 208-218, doi:10.1021/ci600343x.
80. Lennernas, H.; Palm, K.; Fagerholm, U.; Artursson, P. Comparison between active and passive drug transport in human intestinal epithelial (Caco-2) cells in vitro and human jejunum in vivo. *International Journal of Pharmaceutics* **1996**, *127*, 103-107, doi:10.1016/0378-5173(95)04204-0.
81. Hellinger, E.; Veszelka, S.; Toth, A.E.; Walter, F.; Kittel, A.; Bakk, M.L.; Tihanyi, K.; Hada, V.; Nakagawa, S.; Thuy, D.H.D.; et al. Comparison of brain capillary endothelial cell-based and epithelial (MDCK-MDR1, Caco-2, and VB-Caco-2) cell-based surrogate blood-brain barrier penetration models. *European Journal of Pharmaceutics and Biopharmaceutics* **2012**, *82*, 340-351, doi:10.1016/j.ejpb.2012.07.020.
82. Veszelka, S.; Tóth, A.; Walter, F.R.; Tóth, A.E.; Gróf, I.; Mészáros, M.; Bocsik, A.; Hellinger, É.; Vastag, M.; Rákhely, G.; et al. Comparison of a Rat Primary Cell-Based Blood-Brain Barrier Model With Epithelial and Brain Endothelial Cell Lines: Gene Expression and Drug Transport. *Frontiers in Molecular Neuroscience* **2018**, *11*, doi:10.3389/fnmol.2018.00166.
83. Plaza-Oliver, M.; Santander-Ortega, M.J.; Lozano, M.V. Current approaches in lipid-based nanocarriers for oral drug delivery. *Drug Delivery and Translational Research* **2021**, *11*, 471-497, doi:10.1007/s13346-021-00908-7.
84. Ontawong, A.; Duangjai, A.; Srimaroeng, C. Coffea arabica bean extract inhibits glucose transport and disaccharidase activity in Caco-2 cells. *Biomedical Reports* **2021**, *15*, doi:10.3892/br.2021.1449.
85. vandeWaterbeemd, H.; Camenisch, G.; Folkers, G.; Raevsky, O.A. Estimation of Caco-2 cell permeability using calculated molecular descriptors. *Quantitative Structure-Activity Relationships* **1996**, *15*, 480-490, doi:10.1002/qsar.19960150604.
86. Sherer, E.C.; Verras, A.; Madeira, M.; Hagmann, W.K.; Sheridan, R.P.; Roberts, D.; Bleasby, K.; Cornell, W.D. QSAR Prediction of Passive Permeability in the LLC-PK1 Cell Line: Trends in Molecular Properties and Cross-Prediction of Caco-2 Permeabilities. *Molecular Informatics* **2012**, *31*, 231-245, doi:10.1002/minf.201100157.
87. Singh, K.P.; Gupta, S.; Basant, N. In silico prediction of cellular permeability of diverse chemicals using qualitative and quantitative SAR modeling approaches. *Chemometrics and Intelligent Laboratory Systems* **2015**, *140*, 61-72, doi:10.1016/j.chemolab.2014.10.005.
88. Wang, N.N.; Dong, J.; Deng, Y.H.; Zhu, M.F.; Wen, M.; Yao, Z.J.; Lu, A.P.; Wang, J.B.; Cao, D.S. ADME Properties Evaluation in Drug Discovery: Prediction of Caco-2 Cell Permeability Using a Combination of NSGA-II and Boosting. *Journal of Chemical Information and Modeling* **2016**, *56*, 763-773, doi:10.1021/acs.jcim.5b00642.

89. Wang, Y.K.; Chen, X.B. QSPR model for Caco-2 cell permeability prediction using a combination of HQPSO and dual-RBF neural network. *Rsc Advances* **2020**, *10*, 42938-42952, doi:10.1039/d0ra08209k.
90. Artursson, P.; Palm, K.; Luthman, K. Caco-2 monolayers in experimental and theoretical predictions of drug transport. *Adv. Drug Delivery Rev.* **1996**, *22*, 67-84.
91. Press, B.; Di Grandi, D. Permeability for Intestinal Absorption: Caco-2 Assay and Related Issues. *Current Drug Metabolism* **2008**, *9*, 893-900, doi:10.2174/138920008786485119.
92. Volpe, D.A. Variability in Caco-2 and MDCK cell-based intestinal permeability assays. *Journal of Pharmaceutical Sciences* **2008**, *97*, 712-725, doi:10.1002/jps.21010.
93. Subramanian, G.; Kitchen, D.B. Computational approaches for modeling human intestinal absorption and permeability. *Journal of Molecular Modeling* **2006**, *12*, 577-589, doi:10.1007/s00894-005-0065-z.
94. Clark, R.D.; Daga, P.R. Building a Quantitative Structure-Property Relationship (QSPR) Model. *Bioinformatics and Drug Discovery* **2019**, *1939*, 139-159, doi:10.1007/978-1-4939-9089-4_8.
95. Lomize, A.L.; Hage, J.M.; Schnitzer, K.; Golobokov, K.; LaFaive, M.B.; Forsyth, A.C.; Pogozheva, I.D. PerMM: A Web Tool and Database for Analysis of Passive Membrane Permeability and Translocation Pathways of Bioactive Molecules. *Journal of Chemical Information and Modeling* **2019**, *59*, 3094-3099, doi:10.1021/acs.jcim.9b00225.
96. Juracka, J.; Srejber, M.; Melikova, M.; Bazgier, V.; Berka, K. MolMeDB: Molecules on Membranes Database. *Database-the Journal of Biological Databases and Curation* **2019**, doi:10.1093/database/baz078.
97. Avdeef, A. *Permeability: Caco-2/MDCK*; John Wiley & Sons, Inc.: Hoboken, 2012; p. 499-574.
98. Egan, W.J.; Merz, K.M.; Baldwin, J.J. Prediction of drug absorption using multivariate statistics. *Journal of Medicinal Chemistry* **2000**, *43*, 3867-3877, doi:10.1021/jm000292e.
99. Irvine, J.D.; Takahashi, L.; Lockhart, K.; Cheong, J.; Tolan, J.W.; Selick, H.E.; Grove, J.R. MDCK (Madin-Darby canine kidney) cells: A tool for membrane permeability screening. *Journal of pharmaceutical sciences* **1999**, *88*, 28-33.
100. Yazdanian, M.; Glynn, S.L.; Wright, J.L.; Hawi, A. Correlating partitioning and Caco-2 cell permeability of structurally diverse small molecular weight compounds. *Pharmaceutical Research* **1998**, *15*, 1490-1494, doi:10.1023/a:1011930411574.
101. Chong, S.H.; Dando, S.A.; Soucek, K.M.; Morrison, R.A. In vitro permeability through Caco-2 cells is not quantitatively predictive of in vivo absorption for peptide-like drugs absorbed via the dipeptide

References

- transporter system. *Pharmaceutical Research* **1996**, *13*, 120-123, doi:10.1023/a:1016045820933.
102. Pade, V.; Stavchansky, S. Link between drug absorption solubility and permeability measurements in Caco-2 cells. *Journal of Pharmaceutical Sciences* **1998**, *87*, 1604-1607, doi:10.1021/js980111k.
103. Lee, J.B.; Zgair, A.; Taha, D.A.; Zang, X.W.; Kagan, L.; Kim, T.H.; Kim, M.G.; Yun, H.Y.; Fischer, P.M.; Gershkovich, P. Quantitative analysis of lab-to-lab variability in Caco-2 permeability assays. *European Journal of Pharmaceutics and Biopharmaceutics* **2017**, *114*, 38-42, doi:10.1016/j.ejpb.2016.12.027.
104. Jung, S.J.; Choi, S.O.; Um, S.Y.; Kim, J.I.; Choo, H.Y.P.; Choi, S.Y.; Chung, S.Y. Prediction of the permeability of drugs through study on quantitative structure-permeability relationship. *Journal of Pharmaceutical and Biomedical Analysis* **2006**, *41*, 469-475, doi:10.1016/j.jpba.2005.12.020.
105. Kerns, E.H.; Di, L.; Petusky, S.; Farris, M.; Ley, R.; Jupp, P. Combined application of parallel artificial membrane permeability assay and Caco-2 permeability assays in drug discovery. *Journal of Pharmaceutical Sciences* **2004**, *93*, 1440-1453, doi:10.1002/jps.20075.
106. Larregieu, C.A.; Benet, L.Z. Drug Discovery and Regulatory Considerations for Improving In Silico and In Vitro Predictions that Use Caco-2 as a Surrogate for Human Intestinal Permeability Measurements. *Aaps J.* **2013**, *15*, 483-497, doi:10.1208/s12248-013-9456-8.
107. Sambuy, Y.; De Angelis, I.; Ranaldi, G.; Scarino, M.L.; Stamatii, A.; Zucco, F. The Caco-2 cell line as a model of the intestinal barrier: influence of cell and culture-related factors on Caco-2 cell functional characteristics. *Cell Biology and Toxicology* **2005**, *21*, 1-26, doi:10.1007/s10565-005-0085-6.
108. Oltra-Noguera, D.; Mangas-Sanjuan, V.; Centelles-Sangüesa, A.; Gonzalez-Garcia, I.; Sanchez-Castaño, G.; Gonzalez-Alvarez, M.; Casabo, V.-G.; Merino, V.; Gonzalez-Alvarez, I.; Bermejo, M. Variability of permeability estimation from different protocols of subculture and transport experiments in cell monolayers. *Journal of Pharmacological and Toxicological Methods* **2015**, *71*, 21-32, doi:<https://doi.org/10.1016/j.vascn.2014.11.004>.
109. Walter, E.; Kissel, T. Heterogeneity in the human intestinal cell line Caco-2 leads to differences in transepithelial transport. *European Journal of Pharmaceutical Sciences* **1995**, *3*, 215-230, doi:[https://doi.org/10.1016/0928-0987\(95\)00010-B](https://doi.org/10.1016/0928-0987(95)00010-B).
110. Behrens, I.; Kamm, W.; Dantzig, A.H.; Kissel, T. Variation of peptide transporter (PepT1 expression in Caco-2 cells as a function and HPT1) of cell origin. *Journal of Pharmaceutical Sciences* **2004**, *93*, 1743-1754, doi:10.1002/jps.20062.

111. Yu, H.S.; Cook, T.J.; Sinko, P.J. Evidence for diminished functional expression of intestinal transporters in Caco-2 cell monolayers at high passages. *Pharmaceutical Research* **1997**, *14*, 757-762, doi:10.1023/a:1012150405949.
112. Lu, S.; Gough, A.W.; Bobrowski, W.F.; Stewart, B.H. Transport properties are not altered across Caco-2 cells with heightened TEER despite underlying physiological and ultrastructural changes. *Journal of Pharmaceutical Sciences* **1996**, *85*, 270-273, doi:10.1021/js950269u.
113. Briske-Anderson, M.J.; Finley, J.W.; Newman, S.M. The influence of culture time and passage number on the morphological and physiological development of Caco-2 cells. *Proceedings of the society for experimental biology and medicine* **1997**, *214*, 248-257.
114. Chantret, I.; Rodolosse, A.; Barbat, A.; Dussaulx, E.; Brotlaroche, E.; Zweibaum, A.; Rousset, M. DIFFERENTIAL EXPRESSION OF SUCRASE-ISOMALTASE IN CLONES ISOLATED FROM EARLY AND LATE PASSAGES OF THE CELL-LINE CACO-2 - EVIDENCE FOR GLUCOSE-DEPENDENT NEGATIVE REGULATION. *Journal of Cell Science* **1994**, *107*, 213-225.
115. Behrens, I.; Kissel, T. Do cell culture conditions influence the carrier-mediated transport of peptides in Caco-2 cell monolayers? *European Journal of Pharmaceutical Sciences* **2003**, *19*, 433-442, doi:10.1016/s0928-0987(03)00146-5.
116. Hosoya, K.; Kim, K.J.; Lee, V.H.L. Age-dependent expression of P-glycoprotein gp170 in Caco-2 cell monolayers. *Pharmaceutical Research* **1996**, *13*, 885-890, doi:10.1023/a:1016005212640.
117. Markowska, M.; Oberle, R.; Juzwin, S.; Hsu, C.P.; Gryszkiewicz, M.; Streeter, A.J. Optimizing Caco-2 cell monolayers to increase throughput in drug intestinal absorption analysis. *Journal of Pharmacological and Toxicological Methods* **2001**, *46*, 51-55, doi:10.1016/s1056-8719(01)00161-7.
118. D'Souza, V.M.; Shertzer, H.G.; Menon, A.G.; Pauletti, G.M. High glucose concentration in isotonic media alters Caco-2 cell permeability. *Aaps Pharmsci* **2003**, *5*.
119. DeMarco, V.G.; Li, N.; Thomas, J.; West, C.M.; Neu, J. Glutamine and barrier function in cultured Caco-2 epithelial cell monolayers. *Journal of Nutrition* **2003**, *133*, 2176-2179, doi:10.1093/jn/133.7.2176.
120. Ranaldi, G.; Consalvo, R.; Sambuy, Y.; Scarino, M.L. Permeability characteristics of parental and clonal human intestinal Caco-2 cell lines differentiated in serum-supplemented and serum-free media. *Toxicology in Vitro* **2003**, *17*, 761-767, doi:10.1016/s0887-2333(03)00095-x.
121. Herold, G.; Rogler, D.; Rogler, G.; Stange, E.F. MORPHOLOGY OF CACO-2 CELLS VARIES IN DIFFERENT CELL BATCHES. *In Vitro Cellular & Developmental Biology-Animal* **1994**, *30A*, 289-291.

References

122. Horie, K.; Tang, F.X.; Borchardt, R.T. Isolation and characterization of Caco-2 subclones expressing high levels of multidrug resistance protein efflux transporter. *Pharmaceutical Research* **2003**, *20*, 161-168, doi:10.1023/a:1022359300826.
123. Santos, A.; Rodrigues, A.M.; Sobral, A.J.F.N.; Monsanto, P.V.; Vaz, W.L.C.; Moreno, M.J. Early Events in Photodynamic Therapy: Chemical and Physical Changes in a POPC:Cholesterol Bilayer due to Hematoporphyrin IX-mediated Photosensitization. *Photochemistry and Photobiology* **2009**, *85*, 1409-1417, doi:10.1111/j.1751-1097.2009.00606.x.
124. Jovanovic, O.; Skulj, S.; Pohl, E.E.; Vazdar, M. Covalent modification of phosphatidylethanolamine by 4-hydroxy-2-nonenal increases sodium permeability across phospholipid bilayer membranes. *Free Radical Biology and Medicine* **2019**, *143*, 433-440, doi:10.1016/j.freeradbiomed.2019.08.027.
125. Meyer, T.N.; Schwesinger, C.; Ye, J.M.; Denker, B.M.; Nigam, S.K. Reassembly of the tight junction after oxidative stress depends on tyrosine kinase activity. *Journal of Biological Chemistry* **2001**, *276*, 22048-22055, doi:10.1074/jbc.M011477200.
126. Dubois, N.; Muñoz-Garcia, J.; Heymann, D.; Renodon-Cornière, A. High glucose exposure drives intestinal barrier dysfunction by altering its morphological, structural and functional properties. *Biochemical Pharmacology* **2023**, *216*, doi:10.1016/j.bcp.2023.115765.
127. Morresi, C.; Cianfruglia, L.; Sartini, D.; Cecati, M.; Fumarola, S.; Emanuelli, M.; Armeni, T.; Ferretti, G.; Bacchetti, T. Effect of High Glucose-Induced Oxidative Stress on Paraoxonase 2 Expression and Activity in Caco-2 Cells. *Cells* **2019**, *8*, doi:10.3390/cells8121616.
128. Hubatsch, I.; Ragnarsson, E.G.E.; Artursson, P. Determination of drug permeability and prediction of drug absorption in Caco-2 monolayers. *Nature Protocols* **2007**, *2*, 2111, doi:10.1038/nprot.2007.303.
129. Moreira, L.N.; Feltrin, C.; Gonçalves, J.E.; de Castro, W.V.; Simoes, C.M.O.; de Pádua, R.M.; Cortes, S.F.; Braga, F.C. Determination of L-(+)-bornesitol, the hypotensive constituent of *Hancornia speciosa*, in rat plasma by LC-MS/MS and its application on a pharmacokinetic study. *Biomedicine & Pharmacotherapy* **2020**, *132*, doi:10.1016/j.biopha.2020.110900.
130. Rodrigues, E.T.; Nascimento, S.F.; Pires, C.L.; Godinho, L.P.; Churro, C.; Moreno, M.J.; Pardal, M.A. Determination of intestinal absorption of the paralytic shellfish toxin GTX-5 using the Caco-2 human cell model. *Environmental Science and Pollution Research* **2021**, doi:10.1007/s11356-021-15342-y.
131. Lechanteur, A.; Almeida, A.; Sarmiento, B. Elucidation of the impact of cell culture conditions of Caco-2 cell monolayer on barrier integrity and intestinal permeability. *European Journal of Pharmaceutics and Biopharmaceutics* **2017**, *119*, 137-141, doi:10.1016/j.ejpb.2017.06.013.

132. DiMarco, R.L.; Hunt, D.R.; Dewi, R.E.; Heilshorn, S.C. Improvement of paracellular transport in the Caco-2 drug screening model using protein-engineered substrates. *Biomaterials* **2017**, *129*, 152-162, doi:10.1016/j.biomaterials.2017.03.023.
133. Yamashita, S.; Furubayashi, T.; Kataoka, M.; Sakane, T.; Sezaki, H.; Tokuda, H. Optimized conditions for prediction of intestinal drug permeability using Caco-2 cells. *European Journal of Pharmaceutical Sciences* **2000**, *10*, 195-204, doi:10.1016/s0928-0987(00)00076-2.
134. Saha, P.; Kou, J.H. Effect of solubilizing excipients on permeation of poorly water-soluble compounds across Caco-2 cell monolayers. *European Journal of Pharmaceutics and Biopharmaceutics* **2000**, *50*, 403-411, doi:10.1016/s0939-6411(00)00113-2.
135. Aungst, B.J.; Nguyen, N.H.; Bulgarelli, J.P.; Oates-Lenz, K. The influence of donor and reservoir additives on Caco-2 permeability and secretory transport of HIV protease inhibitors and other lipophilic compounds. *Pharmaceutical Research* **2000**, *17*, 1175-1180, doi:10.1023/a:1026402410783.
136. Neuhoff, S.; Artursson, P.; Zamora, I.; Ungell, A.L. Impact of extracellular protein binding on passive and active drug transport across Caco-2 cells. *Pharmaceutical Research* **2006**, *23*, 350-359, doi:10.1007/s11095-005-9304-3.
137. Krishna, G.; Chen, K.-j.; Lin, C.-c.; Nomeir, A.A. Permeability of lipophilic compounds in drug discovery using in-vitro human absorption model, Caco-2. *International journal of pharmaceutics* **2001**, *222*, 77-89.
138. Katneni, K.; Charman, S.A.; Porter, C.J.H. Use of plasma proteins as solubilizing agents in in vitro permeability experiments: Correction for unbound drug concentration using the reciprocal permeability approach. *Journal of Pharmaceutical Sciences* **2008**, *97*, 209-224, doi:10.1002/jps.20877.
139. Yu, H.L.; Huang, Q.R. Investigation of the Absorption Mechanism of Solubilized Curcumin Using Caco-2 Cell Monolayers. *Journal of Agricultural and Food Chemistry* **2011**, *59*, 9120-9126, doi:10.1021/jf201451m.
140. Neuhoff, S.; Ungell, A.-L.; Zamora, I.; Artursson, P. pH-Dependent Bidirectional Transport of Weakly Basic Drugs Across Caco-2 Monolayers: Implications for Drug-Drug Interactions. *Pharmaceutical Research* **2003**, *20*, 1141-1148, doi:10.1023/a:1025032511040.
141. Karlsson, J.; Artursson, P. A method for the determination of cellular permeability coefficients and aqueous boundary layer thickness in monolayers of intestinal epithelial (Caco-2) cells grown in permeable filter chambers. *International journal of pharmaceutics* **1991**, *71*, 55-64.
142. Korjamo, T.; Heikkinen, A.T.; Waltari, P.; Mönkkönen, J. The Asymmetry of the Unstirred Water Layer in Permeability Experiments. *Pharmaceutical Research* **2008**, *25*, 1714, doi:10.1007/s11095-008-9573-8.
143. Ingels, F.; Deferme, S.; Destexhe, E.; Oth, M.; Van den Mooter, G.; Augustijns, P. Simulated intestinal fluid as transport medium in the Caco-

References

- 2 cell culture model. *International Journal of Pharmaceutics* **2002**, *232*, 183-192, doi:10.1016/s0378-5173(01)00897-3.
144. Buckley, S.T.; Fischer, S.M.; Fricker, G.; Brandl, M. In vitro models to evaluate the permeability of poorly soluble drug entities: Challenges and perspectives. *European Journal of Pharmaceutical Sciences* **2012**, *45*, 235-250, doi:10.1016/j.ejps.2011.12.007.
145. Gomes, F.M.C.; Geraldles, C.F.G.; Vaz, W.L.C.; Moreno, M.J. Emulsification of Cholesterol in Bile Salt Micelles: relevance For Cholesterol Absorption. *Biophys. J.* **2010**, *98*, 80A-80A, doi:10.1016/j.bpj.2009.12.450.
146. Moreno, M.J.; Bastos, M.; Velazquez-Campoy, A. Partition of amphiphilic molecules to lipid bilayers by isothermal titration calorimetry. *Analytical Biochemistry* **2010**, *399*, 44-47, doi:10.1016/j.ab.2009.11.015.
147. Delamaza, A.; Parra, J.L. VESICLE-MICELLE STRUCTURAL TRANSITIONS OF PHOSPHOLIPID-BILAYERS AND SODIUM DODECYL-SULFATE. *Langmuir* **1995**, *11*, 2435-2441, doi:10.1021/la00007a021.
148. Bogman, K.; Erne-Brand, F.; Alsenz, J.; Drewe, J. The role of surfactants in the reversal of active transport mediated by multidrug resistance proteins. *Journal of Pharmaceutical Sciences* **2003**, *92*, 1250-1261, doi:10.1002/jps.10395.
149. Coreta-Gomes, F.M.; Martins, P.A.T.; Velazquez-Campoy, A.; Vaz, W.L.C.; Geraldles, C.F.G.; Moreno, M.J. Interaction of Bile Salts with Model Membranes Mimicking the Gastrointestinal Epithelium: A Study by Isothermal Titration Calorimetry. *Langmuir* **2015**, *31*, 9097-9104, doi:10.1021/acs.langmuir.5b01810.
150. Ollila, F.; Slotte, J.P. A thermodynamic study of bile salt interactions with phosphatidylcholine and sphingomyelin unilamellar vesicles. *Langmuir* **2001**, *17*, 2835-2840, doi:10.1021/la0014196.
151. Schuldes, H.; Dolderer, J.H.; Zimmer, G.; Knobloch, J.; Bickeböllner, R.; Jonas, D.; Woodcock, B.G. Reversal of multidrug resistance and increase in plasma membrane fluidity in CHO cells with R-verapamil and bile salts. *European Journal of Cancer* **2001**, *37*, 660-667, doi:10.1016/s0959-8049(00)00450-0.
152. Laitinen, L.; Takala, E.; Vuorela, H.; Vuorela, P.; Kaukonen, A.M.; Marvola, M. Anthranoid laxatives influence the absorption of poorly permeable drugs in human intestinal cell culture model (Caco-2). *European Journal of Pharmaceutics and Biopharmaceutics* **2007**, *66*, 135-145, doi:10.1016/j.ejpb.2006.09.006.
153. Da Violante, G.; Zerrouk, N.; Richard, I.; Provot, G.; Chaumeil, J.C.; Arnaud, P. Evaluation of the cytotoxicity effect of dimethyl sulfoxide (DMSO) on Caco-2/TC7 colon tumor cell cultures. *Biological & Pharmaceutical Bulletin* **2002**, *25*, 1600-1603, doi:10.1248/bpb.25.1600.

154. Bohnert, T.; Gan, L.S. Plasma Protein Binding: From Discovery to Development. *Journal of Pharmaceutical Sciences* **2013**, *102*, 2953-2994, doi:10.1002/jps.23614.
155. Rafols, C.; Amezqueta, S.; Fuguet, E.; Bosch, E. Molecular interactions between warfarin and human (HSA) or bovine (BSA) serum albumin evaluated by isothermal titration calorimetry (ITC), fluorescence spectrometry (FS) and frontal analysis capillary electrophoresis (FA/CE). *Journal of Pharmaceutical and Biomedical Analysis* **2018**, *150*, 452-459, doi:10.1016/j.jpba.2017.12.008.
156. Zhuo, W.L.; Peng, X.L.; Lin, X. Insights into the interaction mechanism between tiagabine hydrochloride and two serum albumins. *RSC Adv.* **2018**, *8*, 24953-24960, doi:10.1039/c8ra04153a.
157. Pantusa, M.; Sportelli, L.; Bartucci, R. Spectroscopic and calorimetric studies on the interaction of human serum albumin with DPPC/PEG:2000-DPPE membranes. *European Biophysics Journal with Biophysics Letters* **2008**, *37*, 961-973, doi:10.1007/s00249-008-0314-z.
158. Reddy, A.C.P.; Sudharshan, E.; Rao, A.G.A.; Lokesh, B.R. Interaction of curcumin with human serum albumin - A spectroscopic study. *Lipids* **1999**, *34*, 1025-1029, doi:10.1007/s11745-999-0453-x.
159. Thomae, A.V.; Wunderli-Allenspach, H.; Kramer, S.D. Permeation of aromatic carboxylic acids across lipid bilayers: The pH-partition hypothesis revisited. *Biophysical Journal* **2005**, *89*, 1802-1811, doi:10.1529/biophysj.105.060871.
160. Bretschneider, B.; Brandsch, M.; Neubert, R. Intestinal transport of beta-lactam antibiotics: Analysis of the affinity at the H⁺/peptide symporter (PEPT1), the uptake into Caco-2 cell monolayers and the transepithelial flux. *Pharmaceutical Research* **1999**, *16*, 55-61, doi:10.1023/a:1018814627484.
161. Lennernäs, H. Human intestinal permeability. *Journal of Pharmaceutical Sciences* **1998**, *87*, 403-410, doi:10.1021/js970332a.
162. Volpe, D.A. Application of Method Suitability for Drug Permeability Classification. *The AAPS Journal* **2010**, *12*, 670-678, doi:10.1208/s12248-010-9227-8.
163. Natoli, M.; Leoni, B.D.; D'Agnano, I.; Zucco, F.; Felsani, A. Good Caco-2 cell culture practices. *Toxicology in Vitro* **2012**, *26*, 1243-1246, doi:10.1016/j.tiv.2012.03.009.
164. Gao, J.; Hugger, E.D.; Beck-Westermeyer, M.S.; Borchardt, R.T. Estimating intestinal mucosal permeation of compounds using Caco-2 cell monolayers. *Current protocols in pharmacology* **2001**, *Chapter 7*, Unit 7.2-Unit 7.2, doi:10.1002/0471141755.ph0702s08.
165. Paixao, P.; Gouveia, L.F.; Morais, J.A.G. Prediction of the in vitro permeability determined in Caco-2 cells by using artificial neural

References

- networks. *European Journal of Pharmaceutical Sciences* **2010**, *41*, 107-117, doi:10.1016/j.ejps.2010.05.014.
166. Hidalgo, I.J. Assessing the absorption of new pharmaceuticals. *Current topics in medicinal chemistry* **2001**, *1*, 385-401, doi:10.2174/1568026013395010.
167. Cho, M.J.; Thompson, D.P.; Cramer, C.T.; Vidmar, T.J.; Scieszka, J.F. The Madin Darby Canine Kidney (MDCK) Epithelial Cell Monolayer as a Model Cellular Transport Barrier. *Pharmaceutical Research* **1989**, *6*, 71-77, doi:10.1023/a:1015807904558.
168. Dukes, J.D.; Whitley, P.; Chalmers, A.D. The MDCK variety pack: choosing the right strain. *Bmc Cell Biology* **2011**, *12*, doi:10.1186/1471-2121-12-43.
169. Bicker, J.; Alves, G.; Fortuna, A.; Soares-da-Silva, P.; Falcão, A. In vitro assessment of the interactions of dopamine β -hydroxylase inhibitors with human P-glycoprotein and Breast Cancer Resistance Protein. *European Journal of Pharmaceutical Sciences* **2018**, *117*, 35-40, doi:<https://doi.org/10.1016/j.ejps.2018.02.006>.
170. Harwood, M.D.; Zettl, K.; Weinheimer, M.; Pilla-Reddy, V.; Shen, H.; Jacobs, F.; Chu, X.Y.; Huth, F.; Nakakariya, M.; Chothe, P.P.; et al. Interlaboratory Variability in the Madin-Darby Canine Kidney Cell Proteome. *Molecular Pharmaceutics* **2023**, *20*, 3505-3518, doi:10.1021/acs.molpharmaceut.3c00108.
171. Volpe, D.A. Drug-permeability and transporter assays in Caco-2 and MDCK cell lines. *Future Medicinal Chemistry* **2011**, *3*, 2063-2077, doi:10.4155/fmc.11.149.
172. Jin, X.; Thu-Lan, L.; Reese, N.; Gaona, H.; Collazo-Velez, V.; Chau, V.; Potter, B.; Sousa, J.C.; Olmeda, R.; Li, Q.; et al. Comparison of MDCK-MDR1 and Caco-2 cell based permeability assays for anti-malarial drug screening and drug investigations. *Journal of Pharmacological and Toxicological Methods* **2014**, *70*, 188-194, doi:10.1016/j.vascn.2014.08.002.
173. Cardoso, R.M.S.; Filipe, H.A.L.; Gomes, F.; Moreira, N.D.; Vaz, W.L.C.; Moreno, M.J. Chain length effect on the binding of amphiphiles to serum albumin and to POPC bilayers. *The Journal of Physical Chemistry B* **2010**, *114*, 16337-16346.
174. Lavis, L.D.; Rutkoski, T.J.; Raines, R.T. Tuning the pK(a) of fluorescein to optimize binding assays. *Analytical Chemistry* **2007**, *79*, 6775-6782, doi:10.1021/ac070907g.
175. Matsushita, Y.; Takahashi, M.; Moriguchi, I. BINDING OF FLUORESCENT 7-AMINO-4-NITROBENZOXADIAZOLE DERIVATIVES TO BOVINE SERUM-ALBUMIN. *Chemical & Pharmaceutical Bulletin* **1986**, *34*, 333-339.

176. Balimane, P.V.; Chong, S. Cell culture-based models for intestinal permeability: a critique. *Drug Discovery Today* **2005**, *10*, 335-343, doi:10.1016/s1359-6446(04)03354-9.
177. Volpe, D.A. Advances in cell-based permeability assays to screen drugs for intestinal absorption. *Expert Opinion on Drug Discovery* **2020**, *15*, 539-549, doi:10.1080/17460441.2020.1735347.
178. Hidalgo, I.J.; Raub, T.J.; Borchardt, R.T. Characterization of the Human-Colon Carcinoma Cell-Line (Caco-2) as a Model System for Intestinal Epithelial Permeability. *Gastroenterology* **1989**, *96*, 736-749.
179. Hilgers, A.R.; Conradi, R.A.; Burton, P.S. Caco-2 Cell Monolayers as a Model for Drug Transport Across the Intestinal-Mucosa. *Pharmaceutical Research* **1990**, *7*, 902-910, doi:10.1023/a:1015937605100.
180. van Breemen, R.B.; Li, Y. Caco-2 cell permeability assays to measure drug absorption. *Expert Opin. Drug Metab. Toxicol.* **2005**, *1*, 175-185, doi:10.1517/17425255.1.2.175.
181. Artursson, P.; Palm, K.; Luthman, K. Caco-2 monolayers in experimental and theoretical predictions of drug transport. *Adv. Drug Deliv. Rev.* **2012**, *64*, 280-289, doi:10.1016/j.addr.2012.09.005.
182. Hubatsch, I.; Ragnarsson, E.G.E.; Artursson, P. Determination of drug permeability and prediction of drug absorption in Caco-2 monolayers. *Nat. Protoc.* **2007**, *2*, 2111-2119, doi:10.1038/nprot.2007.303.
183. BriskeAnderson, M.J.; Finley, J.W.; Newman, S.M. The influence of culture time and passage number on the morphological and physiological development of Caco-2 cells. *Proceedings of the Society for Experimental Biology and Medicine* **1997**, *214*, 248-257.
184. Lu, S.; Gough, A.W.; Bobrowski, W.F.; Stewart, B.H. Transport properties are not altered across Caco-2 cells with heightened TEER despite underlying physiological and ultrastructural changes. *J. Pharm. Sci.* **1996**, *85*, 270-273, doi:10.1021/js950269u.
185. Liang, E.; Chessic, K.; Yazdanian, M. Evaluation of an accelerated Caco-2 cell permeability model. *J. Pharm. Sci.* **2000**, *89*, 336-345, doi:10.1002/(sici)1520-6017(200003)89:3<336::aid-jps5>3.3.co;2-d.
186. Yamashita, S.; Konishi, K.; Yamazaki, Y.; Taki, Y.; Sakane, T.; Sezaki, H.; Furuyama, Y. New and better protocols for a short-term Caco-2 cell culture system. *J. Pharm. Sci.* **2002**, *91*, 669-679, doi:10.1002/jps.10050.
187. Sevin, E.; Dehouck, L.; Fabulas-da Costa, A.; Cecchelli, R.; Dehouck, M.P.; Lundquist, S.; Culot, M. Accelerated Caco-2 cell permeability model for drug discovery. *J. Pharmacol. Toxicol. Methods* **2013**, *68*, 334-339, doi:10.1016/j.vascn.2013.07.004.
188. Cai, Y.K.; Xu, C.S.; Chen, P.Y.; Hu, J.Q.; Hu, R.; Huang, M.; Bi, H.C. Development, validation, and application of a novel 7-day Caco-2 cell

References

- culture system. *J. Pharmacol. Toxicol. Methods* **2014**, *70*, 175-181, doi:10.1016/j.vascn.2014.07.001.
189. Marino, A.M.; Yarde, M.; Patel, H.; Chong, S.H.; Balimane, P.V. Validation of the 96 well Caco-2 cell culture model for high throughput permeability assessment of discovery compounds. *Int. J. Pharmaceut.* **2005**, *297*, 235-241, doi:10.1016/j.ijpharm.2005.03.008.
190. Balimane, P.V.; Patel, K.; Marino, A.; Chong, S.H. Utility of 96 well Caco-2 cell system for increased throughput of P-gp screening in drug discovery. *European Journal of Pharmaceutics and Biopharmaceutics* **2004**, *58*, 99-105, doi:10.1016/j.ejpb.2004.02.014.
191. Sevin, E.; Dehouck, L.; Versele, R.; Culot, M.; Gosselet, F. A Miniaturized Pump Out Method for Characterizing Molecule Interaction with ABC Transporters. *Int. J. Mol. Sci.* **2019**, *20*, 15, doi:10.3390/ijms20225529.
192. Alsenz, J.; Haenel, E. Development of a 7-day, 96-well Caco-2 permeability assay with high-throughput direct UV compound analysis. *Pharmaceutical Research* **2003**, *20*, 1961-1969, doi:10.1023/b:pham.0000008043.71001.43.
193. Bu, H.Z.; Poglod, M.; Micetich, R.G.; Khan, J.K. High-throughput Caco-2 cell permeability screening by cassette dosing and sample pooling approaches using direct injection/on-line guard cartridge extraction/tandem mass spectrometry. *Rapid Communications in Mass Spectrometry* **2000**, *14*, 523-528, doi:10.1002/(sici)1097-0231(20000331)14:6<523::aid-rcm906>3.3.co;2-k.
194. Laitinen, L.; Kangas, H.; Kaukonen, A.M.; Hakala, K.; Kotiaho, T.; Kostiainen, R.; Hirvonen, J. N-in-one permeability studies of heterogeneous sets of compounds across Caco-2 cell monolayers. *Pharmaceutical Research* **2003**, *20*, 187-197, doi:10.1023/a:1022262818573.
195. Tannergren, C.; Langguth, P.; Hoffmann, K.J. Compound mixtures in Caco-2 cell permeability screens as a means to increase screening capacity. *Pharmazie* **2001**, *56*, 337-342.
196. Konsoula, R.; Barile, F.A. Correlation of in vitro cytotoxicity with paracellular permeability in Caco-2 cells. *Toxicology in Vitro* **2005**, *19*, 675-684, doi:10.1016/j.tiv.2005.03.006.
197. Vachon, P.H.; Beaulieu, J.F. Transient Mosaic Patterns of Morphological and Functional-Differentiation in the Caco-2 Cell-Line. *Gastroenterology* **1992**, *103*, 414-423, doi:10.1016/0016-5085(92)90829-n.
198. Ujhelyi, Z.; Fenyvesi, F.; Varadi, J.; Feher, P.; Kiss, T.; Veszelka, S.; Deli, M.; Vecsernyes, M.; Bacskay, I. Evaluation of cytotoxicity of surfactants used in self-micro emulsifying drug delivery systems and their effects on paracellular transport in Caco-2 cell monolayer. *European Journal of Pharmaceutical Sciences* **2012**, *47*, 564-573, doi:10.1016/j.ejps.2012.07.005.
199. Corazza, F.G.; Ernesto, J.V.; Nambu, F.A.N.; de Carvalho, L.R.; Leite-Silva, V.R.; Varca, G.H.C.; Calixto, L.A.; Vieira, D.P.; Andreo-Filho, N.; Lopes,

- P.S. Papain-cyclodextrin complexes as an intestinal permeation enhancer: Permeability and in vitro safety evaluation. *Journal of Drug Delivery Science and Technology* **2020**, *55*, doi:10.1016/j.jddst.2019.101413.
200. Paketuryte, V.; Petrauskas, V.; Zubriene, A.; Abian, O.; Bastos, M.; Chen, W.-Y.; Moreno, M.J.; Krainer, G.; Linkuviene, V.; Sedivy, A.; et al. Uncertainty in protein-ligand binding constants: asymmetric confidence intervals versus standard errors. *European Biophysics Journal with Biophysics Letters* **2021**, *50*, 661-670, doi:10.1007/s00249-021-01518-4.
201. Kemmer, G.; Keller, S. Nonlinear least-squares data fitting in Excel spreadsheets. *Nat. Protoc.* **2010**, *5*, 267-281, doi:10.1038/nprot.2009.182.
202. Delie, F.; Rubas, W. A human colonic cell line sharing similarities with enterocytes as a model to examine oral absorption: Advantages and limitations of the Caco-2 model. *Critical Reviews in Therapeutic Drug Carrier Systems* **1997**, *14*, 221-286.
203. Hidalgo, I.J. Assessing the absorption of new pharmaceuticals. *Current topics in medicinal chemistry* **2001**, *1*, 385-401, doi:10.2174/1568026013395010.
204. Madara, J.L. Regulation of the movement of solutes across tight junctions. *Annu. Rev. Physiol.* **1998**, *60*, 143-159, doi:10.1146/annurev.physiol.60.1.143.
205. Hellinger, E.; Veszelka, S.; Toth, A.E.; Walter, F.; Kittel, A.; Bakk, M.L.; Tihanyi, K.; Hada, V.; Nakagawa, S.; Thuy, D.H.D.; et al. Comparison of brain capillary endothelial cell-based and epithelial (MDCK-MDR1, Caco-2, and VB-Caco-2) cell-based surrogate blood-brain barrier penetration models. *European Journal of Pharmaceutics and Biopharmaceutics* **2012**, *82*, 340-351, doi:10.1016/j.ejpb.2012.07.020.
206. Tervonen, A.; Ihalainen, T.O.; Nymark, S.; Hyttinen, J. Structural dynamics of tight junctions modulate the properties of the epithelial barrier. *PLoS One* **2019**, *14*, 26, doi:10.1371/journal.pone.0214876.
207. Adson, A.; Raub, T.J.; Burton, P.S.; Barsuhn, C.L.; Hilgers, A.R.; Audus, K.L.; Ho, N.F.H. Quantitative Approaches to Delineate Paracellular Diffusion in Cultured Epithelial-Cell Monolayers. *J. Pharm. Sci.* **1994**, *83*, 1529-1536, doi:10.1002/jps.2600831103.
208. Yee, S.Y. In vitro permeability across Caco-2 cells (colonic) can predict in vivo (small intestinal) absorption in man - Fact or myth. *Pharmaceutical Research* **1997**, *14*, 763-766, doi:10.1023/a:1012102522787.
209. Saitoh, R.; Sugano, K.; Takata, N.; Tachibana, T.; Higashida, A.; Nabuchi, Y.; Aso, Y. Correction of permeability with pore radius of tight junctions in Caco-2 monolayers improves the prediction of the dose fraction of hydrophilic drugs absorbed by humans. *Pharmaceutical Research* **2004**, *21*, 749-755, doi:10.1023/B:PHAM.0000026423.48583.e2.

References

210. Linnankoski, J.; Makela, J.; Palmgren, J.; Mauriala, T.; Vedin, C.; Ungell, A.L.; Lazorova, L.; Artursson, P.; Urtili, A.; Yliperttula, M. Paracellular Porosity and Pore Size of the Human Intestinal Epithelium in Tissue and Cell Culture Models. *J. Pharm. Sci.* **2010**, *99*, 2166-2175, doi:10.1002/jps.21961.
211. Pires, C.L.; Praca, C.; Martins, P.A.T.; de Carvalho, A.; Ferreira, L.; Marques, M.P.M.; Moreno, M.J. Re-Use of Caco-2 Monolayers in Permeability Assays-Validation Regarding Cell Monolayer Integrity. *Pharmaceutics* **2021**, *13*, doi:10.3390/pharmaceutics13101563.
212. Seithel, A.; Karlsson, J.; Hilgendorf, C.; Bjorquist, A.; Ungell, A.L. Variability in mRNA expression of ABC- and SLC-transporters in human intestinal cells: Comparison between human segments and Caco-2 cells. *European Journal of Pharmaceutical Sciences* **2006**, *28*, 291-299, doi:10.1016/j.ejps.2006.03.003.
213. Xu, X.Q.; Wang, P.Y.; Wang, B.G.; Wang, M.K.; Wang, S.Y.; Liu, Z.H.; Zhang, Y.; Kang, W.Y. Glucose absorption regulation and mechanism of the compounds in *Lilium lancifolium* Thunb on Caco-2 cells. *Food and Chemical Toxicology* **2021**, *149*, doi:10.1016/j.fct.2021.112010.
214. Blodgett, A.B.; Kothinti, R.K.; Kamyshko, I.; Petering, D.H.; Kumar, S.; Tabatabai, N.M. A Fluorescence Method for Measurement of Glucose Transport in Kidney Cells. *Diabetes Technology & Therapeutics* **2011**, *13*, 743-751, doi:10.1089/dia.2011.0041.
215. Wu, P.P.; He, P.; Zhao, S.Q.; Huang, T.M.; Lu, Y.J.; Zhang, K. Effects of Ursolic Acid Derivatives on Caco-2 Cells and Their Alleviating Role in Streptozocin-Induced Type 2 Diabetic Rats. *Molecules* **2014**, *19*, 12559-12576, doi:10.3390/molecules190812559.
216. Alzaid, F.; Cheung, H.M.; Preedy, V.R.; Sharp, P.A. Regulation of Glucose Transporter Expression in Human Intestinal Caco-2 Cells following Exposure to an Anthocyanin-Rich Berry Extract. *Plos One* **2013**, *8*, doi:10.1371/journal.pone.0078932.
217. Yamada, K.; Nakata, M.; Horimoto, N.; Saito, M.; Matsuoka, H.; Inagaki, N. Measurement of Glucose Uptake and Intracellular Calcium Concentration in Single, Living Pancreatic β -Cells. *Journal of Biological Chemistry* **2000**, *275*, 22278-22283, doi:10.1074/jbc.M908048199.
218. Román, Y.; Alfonso, A.; Louzao, M.C.; Vieytes, M.R.; Botana, L.M. Confocal microscopy study of the different patterns of 2-NBDG uptake in rabbit enterocytes in the apical and basal zone. *Pflugers Archiv-European Journal of Physiology* **2001**, *443*, 234-239, doi:10.1007/s004240100677.
219. Ambudkar, S.V.; Dey, S.; Hrycyna, C.A.; Ramachandra, M.; Pastan, I.; Gottesman, M.M. Biochemical, cellular, and pharmacological aspects of the multidrug transporter. *Annual Review of Pharmacology and Toxicology* **1999**, *39*, 361-398, doi:10.1146/annurev.pharmtox.39.1.361.

220. Yumoto, R.; Murakami, T.; Nakamoto, Y.; Hasegawa, R.; Nagai, J.; Takano, M. Transport of rhodamine 123, a P-glycoprotein substrate, across rat intestine and Caco-2 cell monolayers in the presence of cytochrome P-450 3A-related compounds. *Journal of Pharmacology and Experimental Therapeutics* **1999**, *289*, 149-155.
221. Szewczyk, P.; Tao, H.C.; McGrath, A.P.; Villaluz, M.; Rees, S.D.; Lee, S.C.; Doshi, R.; Urbatsch, I.L.; Zhang, Q.H.; Chang, G. Snapshots of ligand entry, malleable binding and induced helical movement in P-glycoprotein. *Acta Crystallographica Section D-Structural Biology* **2015**, *71*, 732-741, doi:10.1107/s1399004715000978.
222. Lusvardi, S.; Robey, R.W.; Gottesman, M.M.; Ambudkar, S.V. Multidrug transporters: recent insights from cryo-electron microscopy-derived atomic structures and animal models. *F1000Research* **2020**, *9*, doi:10.12688/f1000research.21295.1.
223. Fu, Q.X.; Wang, H.Z.; Xia, M.X.; Deng, B.; Shen, H.Y.; Ji, G.; Li, G.W.; Xie, Y. The effect of phytic acid on tight junctions in the human intestinal Caco-2 cell line and its mechanism. *European Journal of Pharmaceutical Sciences* **2015**, *80*, 1-8, doi:10.1016/j.ejps.2015.09.009.
224. Batistela, V.R.; Cedran, J.D.; de Oliveira, H.P.M.; Scarminio, I.S.; Ueno, L.T.; Machado, A.E.H.; Hioka, N. Protolytic fluorescein species evaluated using chemometry and DFT studies. *Dyes and Pigments* **2010**, *86*, 15-24, doi:10.1016/j.dyepig.2009.11.002.
225. Yamamoto, N.; Ueda-Wakagi, M.; Sato, T.; Kawasaki, K.; Sawada, K.; Kawabata, K.; Akagawa, M.; Ashida, H. Measurement of Glucose Uptake in Cultured Cells. *Current protocols in pharmacology* **2015**, *71*, 12.14.11-12.14.26, doi:10.1002/0471141755.ph1214s71.
226. Zou, C.; Wang, Y.; Shen, Z. 2-NBDG as a fluorescent indicator for direct glucose uptake measurement. *Journal of Biochemical and Biophysical Methods* **2005**, *64*, 207-215, doi:<https://doi.org/10.1016/j.jbbm.2005.08.001>.
227. D'Souza, L.J.; Wright, S.H.; Bhattacharya, D. Genetic evidence that uptake of the fluorescent analog 2NBDG occurs independently of known glucose transporters. *Plos One* **2022**, *17*, doi:10.1371/journal.pone.0261801.
228. Hamilton, K.E.; Bouwer, M.F.; Louters, L.L.; Looyenga, B.D. Cellular binding and uptake of fluorescent glucose analogs 2-NBDG and 6-NBDG occurs independent of membrane glucose transporters. *Biochimie* **2021**, *190*, 1-11, doi:10.1016/j.biochi.2021.06.017.
229. Sinclair, L.V.; Barthelemy, C.; Cantrell, D.A. Single Cell Glucose Uptake Assays: A Cautionary Tale. *Immunometabolism* **2020**, *2*, e200029, doi:10.20900/immunometab20200029.
230. Dahlgren, D.; Lennernas, H. Intestinal Permeability and Drug Absorption: Predictive Experimental, Computational and In Vivo Approaches. *Pharmaceutics* **2019**, *11*, doi:10.3390/pharmaceutics11080411.

References

231. Lin, J.H.; Yamazaki, M. Role of P-glycoprotein in pharmacokinetics - Clinical implications. *Clinical Pharmacokinetics* **2003**, *42*, 59-98, doi:10.2165/00003088-200342010-00003.
232. del Amo, E.M.; Heikkinen, A.T.; Monkkonen, J. In vitro-in vivo correlation in p-glycoprotein mediated transport in intestinal absorption. *European Journal of Pharmaceutical Sciences* **2009**, *36*, 200-211, doi:10.1016/j.ejps.2008.11.005.
233. Hayeshi, R.; Hilgendorf, C.; Artursson, P.; Augustijns, P.; Brodin, B.; Dehertogh, P.; Fisher, K.; Fossati, L.; Hovenkamp, E.; Korjamo, T.; et al. Comparison of drug transporter gene expression and functionality in Caco-2 cells from 10 different laboratories. *European Journal of Pharmaceutical Sciences* **2008**, *35*, 383-396, doi:<https://doi.org/10.1016/j.ejps.2008.08.004>.
234. Anderle, P.; Niederer, E.; Rubas, W.; Hilgendorf, C.; Spahn-Langguth, H.; Wunderli-Allenspach, H.; Merkle, H.P.; Langguth, P. P-glycoprotein (P-gp) mediated efflux in Caco-2 cell monolayers: The influence of culturing conditions and drug exposure on P-gp expression levels. *Journal of pharmaceutical sciences* **1998**, *87*, 757-762.
235. Troutman, M.D.; Thakker, D.R. Rhodamine 123 requires carrier-mediated influx for its activity as a P-glycoprotein substrate in Caco-2 cells. *Pharmaceutical Research* **2003**, *20*, 1192-1199, doi:10.1023/a:1025096930604.
236. Magalhaes, N.; Simoes, G.M.; Ramos, C.; Samelo, J.; Oliveira, A.C.; Filipe, H.A.L.; Ramalho, J.P.P.; Moreno, M.J.; Loura, L.M.S. Interactions between Rhodamine Dyes and Model Membrane Systems-Insights from Molecular Dynamics Simulations. *Molecules* **2022**, *27*, doi:10.3390/molecules27041420.
237. Noack, A.; Noack, S.; Hoffmann, A.; Maalouf, K.; Buettner, M.; Couraud, P.O.; Romero, I.A.; Weksler, B.; Alms, D.; Römermann, K.; et al. Drug-Induced Trafficking of P-Glycoprotein in Human Brain Capillary Endothelial Cells as Demonstrated by Exposure to Mitomycin C. *Plos One* **2014**, *9*, doi:10.1371/journal.pone.0088154.
238. Miao, Q.; Wang, Z.Y.; Zhang, Y.Y.; Miao, P.P.; Zhao, Y.Y.; Zhang, Y.J.; Ma, S.C. In vitro potential modulation of baicalin and baicalein on P-glycoprotein activity and expression in Caco-2 cells and rat gut sacs. *Pharmaceutical Biology* **2016**, *54*, 1548-1556, doi:10.3109/13880209.2015.1107744.
239. Estronca, L.M.B.B.; Filipe, H.A.L.; Salvador, A.; Moreno, M.J.; Vaz, W.L.C. Homeostasis of Free Cholesterol in the Blood – A Preliminary Evaluation and Modeling of Its Passive Transport. *J. Lipid Res.* **2014**, *55*, 1033-1043, doi:10.1194/jlr.M043067.
240. Lu, Y.; Ruan, G.T.; Du, W.; Li, J.; Yang, N.D.; Wu, Q.; Lu, L.; Zhang, C.W.; Li, L. Recent progress in rational design of fluorescent probes for Fe²⁺ and

- bioapplication. *Dyes and Pigments* **2021**, *190*, doi:10.1016/j.dyepig.2021.109337.
241. Moser, S.; Lim, J.; Chegeni, M.; Wightman, J.D.; Hamaker, B.R.; Ferruzzi, M.G. Concord and Niagara Grape Juice and Their Phenolics Modify Intestinal Glucose Transport in a Coupled in Vitro Digestion/Caco-2 Human Intestinal Model. *Nutrients* **2016**, *8*, doi:10.3390/nu8070414.
 242. Liang, E.; Chessic, K.; Yazdanian, M. Evaluation of an accelerated Caco-2 cell permeability model. *Journal of Pharmaceutical Sciences* **2000**, *89*, 336-345, doi:10.1002/(sici)1520-6017(200003)89:3<336::aid-jps5>3.3.co;2-d.
 243. Alsenz, J.; Haenel, E. Development of a 7-day, 96-well Caco-2 permeability assay with high-throughput direct UV compound analysis. *Pharmaceutical Research* **2003**, *20*, 1961-1969, doi:10.1023/b:pham.0000008043.71001.43.
 244. Sevin, E.; Dehouck, L.; Fabulas-da Costa, A.; Cecchelli, R.; Dehouck, M.P.; Lundquist, S.; Culot, M. Accelerated Caco-2 cell permeability model for drug discovery. *Journal of Pharmacological and Toxicological Methods* **2013**, *68*, 334-339, doi:10.1016/j.vascn.2013.07.004.
 245. Gartzke, D.; Fricker, G. Establishment of Optimized MDCK Cell Lines for Reliable Efflux Transport Studies. *Journal of Pharmaceutical Sciences* **2014**, *103*, 1298-1304, doi:10.1002/jps.23901.
 246. Richardson, J.C.W.; Scalera, V.; Simmons, N.L. IDENTIFICATION OF 2 STRAINS OF MDCK CELLS WHICH RESEMBLE SEPARATE NEPHRON TUBULE SEGMENTS. *Biochimica Et Biophysica Acta* **1981**, *673*, 26-36, doi:10.1016/0304-4165(81)90307-x.
 247. Chu, X.Y.; Bleasby, K.; Evers, R. Species differences in drug transporters and implications for translating preclinical findings to humans. *Expert Opinion on Drug Metabolism & Toxicology* **2013**, *9*, 237-252, doi:10.1517/17425255.2013.741589.
 248. Mease, K.; Sane, R.; Podila, L.; Taub, M.E. Differential Selectivity of Efflux Transporter Inhibitors in Caco-2 and MDCK-MDR1 Monolayers: A Strategy to Assess the Interaction of a New Chemical Entity with P-gp, BCRP, and MRP2. *Journal of Pharmaceutical Sciences* **2012**, *101*, 1888-1897, doi:10.1002/jps.23069.
 249. Tang, F.X.; Horie, K.; Borchardt, R.T. Are MDCK cells transfected with the Human *MDR1* gene a good model of the human intestinal mucosa? *Pharmaceutical Research* **2002**, *19*, 765-772, doi:10.1023/a:1016140429238.
 250. Putnam, W.S.; Ramanathan, S.; Pan, L.; Takahashi, L.H.; Benet, L.Z. Functional characterization of monocarboxylic acid, large neutral amino acid, bile acid and peptide transporters, and P-glycoprotein in MDCK and Caco-2 cells. *Journal of Pharmaceutical Sciences* **2002**, *91*, 2622-2635, doi:10.1002/jps.10264.
 251. Pastan, I.; Gottesman, M.M.; Ueda, K.; Lovelace, E.; Rutherford, A.V.; Willingham, M.C. A RETROVIRUS CARRYING AN MDR1 CDNA

References

- CONFERS MULTIDRUG RESISTANCE AND POLARIZED EXPRESSION OF P-GLYCOPROTEIN IN MDCK CELLS. *Proceedings of the National Academy of Sciences of the United States of America* **1988**, *85*, 4486-4490, doi:10.1073/pnas.85.12.4486.
252. Hämmerle, S.P.; Rothen-Rutishauser, B.; Krämer, S.D.; Günthert, M.; Wunderli-Allenspach, H. P-glycoprotein in cell cultures:: a combined approach to study expression, localisation, and functionality in the confocal microscope. *European Journal of Pharmaceutical Sciences* **2000**, *12*, 69-77, doi:10.1016/s0928-0987(00)00142-1.
253. De Souza, J.; Benet, L.Z.; Huang, Y.; Storpirtis, S. Comparison of Bidirectional Lamivudine and Zidovudine Transport Using MDCK, MDCK-MDR1, and Caco-2 Cell Monolayers. *Journal of Pharmaceutical Sciences* **2009**, *98*, 4413-4419, doi:10.1002/jps.21744.
254. Ranaldi, G.; Islam, K.; Sambuy, Y. EPITHELIAL-CELLS IN CULTURE AS A MODEL FOR THE INTESTINAL TRANSPORT OF ANTIMICROBIAL AGENTS. *Antimicrobial Agents and Chemotherapy* **1992**, *36*, 1374-1381, doi:10.1128/aac.36.7.1374.
255. Tang, F.X.; Hui, O.Y.; Yang, J.Z.; Borchardt, R.T. Bidirectional transport of rhodamine 123 and Hoechst 33342, fluorescence probes of the binding sites on P-glycoprotein, across MDCK-MDR1 cell monolayers. *Journal of Pharmaceutical Sciences* **2004**, *93*, 1185-1194, doi:10.1002/jps.20046.
256. Powell, D.W. BARRIER FUNCTION OF EPITHELIA. *American Journal of Physiology* **1981**, *241*, G275-G288, doi:10.1152/ajpgi.1981.241.4.G275.
257. Tokuda, S.; Furuse, M. Claudin-2 Knockout by TALEN-Mediated Gene Targeting in MDCK Cells: Claudin-2 Independently Determines the Leaky Property of Tight Junctions in MDCK Cells. *Plos One* **2015**, *10*, doi:10.1371/journal.pone.0119869.
258. Saaby, L.; Helms, H.C.C.; Brodin, B. IPEC-J2 MDR1, a Novel High-Resistance Cell Line with Functional Expression of Human P-glycoprotein (ABCB1) for Drug Screening Studies. *Molecular Pharmaceutics* **2016**, *13*, 640-652, doi:10.1021/acs.molpharmaceut.5b00874.
259. Chen, X.M.; Slättengren, T.; de Lange, E.C.M.; Smith, D.E.; Hammarlund-Udenaes, M. Revisiting atenolol as a low passive permeability marker. *Fluids and Barriers of the Cns* **2017**, *14*, doi:10.1186/s12987-017-0078-x.
260. Kopecka, J.; Trouillas, P.; Gasparovic, A.C.; Gazzano, E.; Assaraf, Y.G.; Riganti, C. Phospholipids and cholesterol: Inducers of cancer multidrug resistance and therapeutic targets. *Drug Resistance Updates* **2020**, *49*, doi:10.1016/j.drug.2019.100670.
261. Hendrich, A.B.; Michalak, K. Lipids as a target for drugs modulating multidrug resistance of cancer cells. *Current Drug Targets* **2003**, *4*, 23-30, doi:10.2174/1389450033347172.

262. Peetla, C.; Bhave, R.; Vijayaraghavalu, S.; Stine, A.; Kooijman, E.; Labhasetwar, V. Drug Resistance in Breast Cancer Cells: Biophysical Characterization of and Doxorubicin Interactions with Membrane Lipids. *Molecular Pharmaceutics* **2010**, *7*, 2334-2348, doi:10.1021/mp100308n.
263. Vijayaraghavalu, S.; Peetla, C.; Lu, S.; Labhasetwar, V. Epigenetic Modulation of the Biophysical Properties of Drug-Resistant Cell Lipids to Restore Drug Transport and Endocytic Functions. *Molecular Pharmaceutics* **2012**, *9*, 2730-2742, doi:10.1021/mp300281t.
264. Callaghan, R.; Vangorkom, L.C.M.; Epan, R.M. A COMPARISON OF MEMBRANE-PROPERTIES AND COMPOSITION BETWEEN CELL-LINES SELECTED AND TRANSFECTED FOR MULTIDRUG RESISTANCE. *British Journal of Cancer* **1992**, *66*, 781-786, doi:10.1038/bjc.1992.360.
265. Kok, J.W.; Veldman, R.J.; Klappe, K.; Koning, H.; Filipeanu, C.M.; Müller, M. Differential expression of sphingolipids in MRP1 overexpressing HT29 cells. *International Journal of Cancer* **2000**, *87*, 172-178, doi:10.1002/1097-0215(20000715)87:2<172::aid-ijc3>3.0.co;2-k.
266. Moreno, M.J.; Martins, P.A.T.; Bernardino, E.F.; Abel, B.; Ambudkar, S.V. Characterization of the Lipidome and Biophysical Properties of Membranes from High Five Insect Cells Expressing Mouse P-Glycoprotein. *Biomolecules* **2021**, *11*, 426, doi:10.3390/biom11030426.
267. Eytan, G.D.; Regev, R.; Oren, G.; Assaraf, Y.G. The role of passive transbilayer drug movement in multidrug resistance and its modulation. *Journal of Biological Chemistry* **1996**, *271*, 12897-12902, doi:10.1074/jbc.271.22.12897.
268. Ramstedt, B.; Slotte, J.P. Sphingolipids and the formation of sterol-enriched ordered membrane domains. *Biochimica Et Biophysica Acta-Biomembranes* **2006**, *1758*, 1945-1956, doi:10.1016/j.bbamem.2006.05.020.
269. Moreno, M.J.; Estronca, L.; Vaz, W.L.C. Translocation of phospholipids and dithionite permeability in liquid-ordered and liquid-disordered membranes. *Biophysical Journal* **2006**, *91*, 873-881, doi:10.1529/biophysj.106.082115.
270. Shang, H.H.; Wang, Z.; Ma, H.; Sun, Y.H.; Ci, X.Y.; Gu, Y.; Liu, C.X.; Si, D.Y. Influence of verapamil on the pharmacokinetics of rotundic acid in rats and its potential mechanism. *Pharmaceutical Biology* **2021**, *59*, 200-208, doi:10.1080/13880209.2021.1871634.
271. Collection, A.T.C. Passage number effects in cell lines. Available online: <https://www.atcc.org/resources/technical-documents/passage-number-effects-in-cell-lines> (accessed on 29 April 2024).
272. Jia, Y.L.; Guo, X.; Lu, J.T.; Wang, X.Y.; Qiu, L.L.; Wang, T.Y. CRISPR/Cas9-mediated gene knockout for DNA methyltransferase Dnmt3a in CHO cells displays enhanced transgenic expression and long-term stability.

References

- Journal of Cellular and Molecular Medicine* **2018**, *22*, 4106-4116, doi:10.1111/jcmm.13687.
273. Belli, S.; Elsener, P.M.; Wunderli-Allenspach, H.; Krämer, S.D. Cholesterol-Mediated Activation of P-Glycoprotein: Distinct Effects on Basal and Drug-Induced ATPase Activities. *Journal of Pharmaceutical Sciences* **2009**, *98*, 1905-1918, doi:10.1002/jps.21558.
274. Martins, P.T.; Velazquez-Campoy, A.; Vaz, W.L.C.; Cardoso, R.M.S.; Valerio, J.; Moreno, M.J. Kinetics and Thermodynamics of Chlorpromazine Interaction with Lipid Bilayers: Effect of Charge and Cholesterol. *Journal Of The American Chemical Society* **2012**, *134*, 4184-4195, doi:10.1021/ja209917q.
275. Pohl, E.E.; Krylov, A.V.; Block, M.; Pohl, P. Changes of the membrane potential profile induced by verapamil and propranolol. *Biochimica Et Biophysica Acta-Biomembranes* **1998**, *1373*, 170-178, doi:10.1016/s0005-2736(98)00098-4.
276. Yang, Y.F.; Xu, W.; Song, W.; Ye, M.; Yang, X.W. Transport of Twelve Coumarins from *Angelicae Pubescentis Radix* across a MDCK-pHaMDR Cell Monolayer-An *in Vitro* Model for Blood-Brain Barrier Permeability. *Molecules* **2015**, *20*, 11719-11732, doi:10.3390/molecules200711719.
277. Weidner, L.D.; Fung, K.L.; Kannan, P.; Moen, J.K.; Kumar, J.S.; Mulder, J.; Innis, R.B.; Gottesman, M.M.; Hall, M.D. Tariquidar Is an Inhibitor and Not a Substrate of Human and Mouse P-glycoprotein. *Drug Metabolism and Disposition* **2016**, *44*, 275-282, doi:10.1124/dmd.115.067785.
278. Shukla, S.; Abel, B.; Chufan, E.E.; Ambudkar, S.V. Effects of a detergent micelle environment on P-glycoprotein (ABCB1)-ligand interactions. *Journal of Biological Chemistry* **2017**, *292*, 7066-7076, doi:10.1074/jbc.M116.771634.
279. Balda, M.S.; Matter, K. The tight junction protein ZO-1 and an interacting transcription factor regulate ErbB-2 expression. *Embo Journal* **2000**, *19*, 2024-2033, doi:10.1093/emboj/19.9.2024.
280. Gumbiner, B.; Lowenkopf, T.; Apatira, D. IDENTIFICATION OF A 160-KDA POLYPEPTIDE THAT BINDS TO THE TIGHT JUNCTION PROTEIN-ZO-1. *Proceedings of the National Academy of Sciences of the United States of America* **1991**, *88*, 3460-3464, doi:10.1073/pnas.88.8.3460.
281. Ali, M.M.; Agha, F.G.; El-Sammad, N.M.; Hassan, S.K. Modulation of Anticancer Drug-Induced P-Glycoprotein Expression by Naringin. *Zeitschrift Fur Naturforschung Section C-a Journal of Biosciences* **2009**, *64*, 109-116.
282. Press, B.; Di Grandi, D. Permeability for Intestinal Absorption: Caco-2 Assay and Related Issues. *Current Drug Metabolism* **2008**, *9*, 893-900, doi:10.2174/138920008786485119.

283. Bohets, H.; Annaert, P.; Mannens, G.; Van Beijsterveldt, L.; Anciaux, K.; Verboven, P.; Meuldermans, W.; Lavrijsen, K. Strategies for absorption screening in drug discovery and development. *Current topics in medicinal chemistry* **2001**, *1*, 367-383, doi:10.2174/1568026013394886.
284. Volpe, D.A. Application of Method Suitability for Drug Permeability Classification. *Aaps Journal* **2010**, *12*, 670-678, doi:10.1208/s12248-010-9227-8.
285. Antonescu, I.E.; Rasmussen, K.F.; Neuhoff, S.; Frette, X.; Karlgren, M.; Bergstrom, C.A.S.; Nielsen, C.U.; Steffansen, B. The Permeation of Acamprostate Is Predominantly Caused by Paracellular Diffusion across Caco-2 Cell Monolayers: A Paracellular Modeling Approach. *Mol. Phar*, **2019**, *16*, 4636-4650, doi:10.1021/acs.molpharmaceut.9b00733.
286. Pires, C.L.; Silva, I.M.V.; Coimbra, M.A.; Moreno, M.J.; Coreta-Gomes, F. Effect of Coffee on the Bioavailability of Sterols. *Foods* **2022**, *11*, doi:10.3390/foods11192935.
287. Smith, E.B.; Staples, E.M. Plasma-Protein Concentrations in Interstitial Fluid From Human Aortas. *Proc. Royal Soc. B* **1982**, *217*, 59-75, doi:10.1098/rspb.1982.0094.
288. Shimizu, M.; Tsunogai, M.; Arai, S. Transepithelial transport of oligopeptides in the human intestinal cell, Caco-2. *Peptides* **1997**, *18*, 681-687, doi:10.1016/s0196-9781(97)00002-8.
289. Artursson, P. Epithelial transport of drugs in cell culture. I: A model for studying the passive diffusion of drugs over intestinal absorptive (Caco-2) cells. *J. Pharm. Sci.* **1990**, *79*, 476-482, doi:10.1002/jps.2600790604.
290. Broeders, J.J.W.; van Eijkeren, J.C.H.; Blaauboer, B.J.; Hermens, J.L.M. Transport of Chlorpromazine in the Caco-2 Cell Permeability Assay: A Kinetic Study. *Chemical Research in Toxicology* **2012**, *25*, 1442-1451, doi:10.1021/tx300221k.
291. Hidalgo, I.J.; Borchardt, R.T. Transport of Bile-Acids In a Human Intestinal Epithelial-Cell Line, Caco-2. *Biochim. Biophys. Acta* **1990**, *1035*, 97-103, doi:10.1016/0304-4165(90)90179-z.
292. Hosoya, K.; Kim, K.J.; Lee, V.H.L. Age-dependent expression of P-glycoprotein gp170 in Caco-2 cell monolayers. *Pharmaceutical Research* **1996**, *13*, 885-890, doi:10.1023/a:1016005212640.

Indexes

Index of figures

Figure I. 1 Mechanisms of drugs permeation through a cell monolayer, exemplified for the case of the intestinal epithelium: (1) Passive diffusion (2) Carrier-mediated transport (3) Transcytosis.	7
Figure I. 2 Schematic representation of the experimental procedure for the use of cell monolayers to assess the permeability of compounds, consisting of three major steps: cell culture, permeability assay, and data analysis.	20
Figure I. 3 Variability in Caco-2 P_{app} values obtained in experiments carried out in 7 different laboratories... ..	32
Figure III. 1 Typical HPLC chromatograms with fluorescence detection, for the compounds used in the permeability assays.....	80
Figure IV. 1 Evaluation of the Caco-2 monolayer integrity when used for a single permeability assay at distinct days after seeding (22, 25, and 28). The TEER values obtained before are shown in Plot A, and after the permeability assay in Plot B.	97
Figure IV. 2 Evaluation of the re-establishment of Caco-2 monolayer integrity when incubated in culture media for two full days after being used for a permeability assay by TEER measurements.....	98
Figure IV. 3 Dependence of LY P_{app} (one sampling at 60 min) on the day post-seeding and on the re-use of the monolayer for additional permeability assays after incubation with culture media for two full days.. ..	99
Figure IV. 4 Effect of the sampling time interval on the paracellular permeability of LY through Caco-2 monolayers at days 22, 25, or 28, post-seeding. The LY Log P_{app} and LogQA are shown for a sampling interval of 10 min or 60 min.	102
Figure IV. 5 Effect of multiple time sampling on the paracellular permeability of LY through Caco-2 monolayers at days 22, 25, or 28, post-seeding. The LY LogQA is shown for 3 consecutive 10 min sampling intervals at 10, 20, and 30 min....	104
Figure IV. 6 Immunofluorescence ZO-1 staining in representative images of Caco-2 monolayers at days 22, 25, and 28 under distinct conditions.	105
Figure IV. 7 Staining of ZO-1 and nuclei for Caco-2 monolayers at day 28 post-seeding under distinct conditions. The representation of z-stacks at the cross section is indicated by a yellow triangle.	106
Figure V. 1 Dependence of LY P_{app} on the sampling interval, day post-seeding and re-use of the cell monolayers in multi-time and single-time sampling permeability assays.. ..	143
Figure V. 2 Effect of re-use and day post-seeding on Flu and Atenolol passive permeability through Caco-2 monolayers after multi-time and single-time sampling assays.	144

Figure V. 3 Effect of re-use and day post-seeding on Prop and SA passive permeability through Caco-2 monolayers after multi-time and single-time sampling assays.	145
Figure V. 4 Effect of re-use and day post-seeding on the cumulative amount of 2-NBDG that reaches the acceptor compartment during multi-time sampling permeability assays.	146
Figure V. 5 Confocal microscopy images of Caco-2 monolayers obtained with λ_{ex} = 458 nm and λ_{em} = 459–551 nm for (A) cell monolayers not used in permeability assays and for cell monolayers exposed to 250 μ M of 2-NBDG for 60 min during permeability assays in the A→B (B) and in the B→A (C) directions.	147
Figure V. 6 Effect of re-use and day post-seeding on Rho permeability and P-gp expression across Caco-2 monolayers. Plot A: $\text{Log}P_{app}$ values measured in the A→B and B→A directions and efflux ratios. Plot B: contribution of passive permeation (P_{app}^{PP}) and active efflux (P_{app}^{AE}) to the measured Rho P_{app} values. Comparison of efflux activity P_{app}^{AE} and P-gp expression.	149
Figure V. 7 Effect of re-use and day post-seeding on Rho permeability across Caco-2 monolayers after the pre-incubation with Verapamil at 100 μ M. Plot A: $\text{Log}P_{app}$ values measured in the A→B and B→A directions and efflux ratios. Plot B: contribution of passive permeation (P_{app}^{PP}) and active efflux (P_{app}^{AE}) ..	151
Figure VI. 1 Representative images of MDCK-II and MDCK-MDR1 monolayers observed at the confocal microscope.....	176
Figure VI. 2 Staining of ZO-1 protein and nuclei for MDCK-II and MDCK-MDR1 monolayers. The localization of ZO-1 is shown for the corresponding z-stacks at the cross section indicated by the yellow line.	177
Figure VI. 3 Dependence of LY P_{app} values on the sampling interval in either MDCK-II and MDCK-MDR1 monolayers after multi-time and single-time sampling permeability assays.	178
Figure VI. 4 Dependence of Flu and Atenolol P_{app} values on the sampling interval for permeability assays performed across MDCK-II and MDCK-MDR1 monolayers.....	179
Figure VI. 5 Propranolol and Salicylic acid P_{app} values after a multi-time sampling permeability assay across MDCK-II and MDCK-MDR1 monolayers.	180
Figure VI. 6 Rho permeability across MDCK-II and MDCK-MDR1 monolayers. Plot A: Instantaneous $\text{Log}P_{app}$ values measured as a function of the incubation time in the A→B and B→A directions. Plot B and C: instantaneous efflux ratio and contributions of passive (P_{app}^{PP}) and active efflux (P_{app}^{AE}) to the measured P_{app} values.....	181
Figure VI. 7 Rho permeability across MDCK-II and MDCK-MDR1 monolayers after pre-incubation with 100 μ M Verapamil for P-gp efflux inhibition. Plot A: Instantaneous $\text{Log}P_{app}$ values measured as a function of the incubation time in	

the A→B and B→A direction. Plot B and C: instantaneous efflux ratio and contributions of passive (P_{app}^{PP}) and active efflux (P_{app}^{AE}) to the measured P_{app} values. 184

Figure VII. 1 Representation of the P_{app} values of several test compounds plotted against LY P_{app} values obtained with the same cell monolayers.. 214

Figure VII. 2 Dependence of LY P_{app} on the sampling method and sampling time intervals. P_{app} values were obtained with replacement or transfer methods in multi-time permeability assays across Caco-2 monolayers..... 215

Figure VII. 3 Effect of the sampling method and sampling interval on Prop permeability in multi-time permeability assays across Caco-2 monolayers..... 217

Figure VII. 4 Effect of BSA on the permeability of NBD-Cn amphiphiles across Caco-2 monolayers in multi-time sampling assays. 219

Figure VII. 5 Effect of BSA on the permeability of NBD-Cn amphiphiles through Caco-2 monolayers when the P_{app}^{Unb} values are recalculated from the observed P_{app} using the free amount of each amphiphile.. 220

Index of figures in Supplementary Material

Figure IV. S1 Representative results obtained for individual cell monolayers in days 22, 25 and 28 post-seeding, for the variation of their TEER values and P_{app} values obtained for LY with a single-time sampling at 60 min. 112

Figure IV. S2 Cumulative amount of LY that reaches the acceptor compartment for permeability experiments performed with single and multi-time sampling on cell monolayers at day 22, 25 and 28 post-seeding. 117

Figure IV. S3 Confocal microscopy images of Caco-2 monolayers stained for ZO-1 and nuclei. Maximum intensity projections of 8-9 z-stacks are shown for cell monolayers at day 22, 25 and 28 under distinct conditions. 119

Figure IV. S4 Distribution of $\text{Log}P_{app}$ obtained on permeability assays with a 60 min sampling for cell monolayers from different batches and passages. 121

Figure IV. S5 Correlation between the TEER value (left plot) and normalized nuclei area (right plot), with the cell density for monolayers on day 22 before and after the execution of a LY permeability assay..... 125

Figure V. S1 Confocal microscopy images of Caco-2 monolayers obtained with excitation light at 458 nm and emission detection from 459–551 nm. Maximum intensity projections of z-stacks are shown for (A) cell monolayers not used for any permeability assay and for cell monolayers exposed to 250 μM of 2-NBDG in the A→B direction (B) and in the B→A direction (C) during the permeability assays at day 28 post-seeding.. 160

Figure V. S2 Effect of re-use and day post-seeding on Rho permeability. The instantaneous $\text{Log}P_{app}$ values in the A→B and B→A direction, and instantaneous efflux ratio are shown as a function of the incubation time. 161

Figure V. S3 Effect of re-use and day post-seeding on Rho permeability after pre-inhibition of P-gp efflux with 100 μ M of Verapamil. The instantaneous LogPapp values in the A→B and B→A direction, and instantaneous efflux ratio are shown as a function of the incubation time..... 162

Figure V. S4 Representative histograms overlay of flow cytometric analysis to determine expression of P-gp in Caco-2 cells. 165

Figure VI. S1 Confocal microscopy images of MDCK-II and MDCK-MDR1 monolayers stained for nuclei and ZO-1. Maximum intensity projections of 10-12 z-stacks are shown for cell monolayers at day 7 post-seeding after a multi-time permeability assay with LY..... 195

Figure VII. S1 Cumulative amount of LY that reaches the acceptor compartment for permeability experiments performed with multiple time assays following the replacement sampling method. 225

Index of tables

Table I. 1 Overview of some examples of <i>in silico</i> contributions to the quantitative prediction of P_{app} values across Caco-2 monolayers.....	25
Table I. 2 Performance comparison of two online databases containing experimental data of drug permeability across Caco-2 monolayers: PerMM and MolMeDB.	29
Table I. 3 Magnitude of the variability in Caco-2 P_{app} values obtained in experiments carried out in the same laboratory.....	31
Table I. 4 Analysis of the experimental factors related with cell culture that are potential causes of variability in Caco-2 permeability data, obtained from a survey of the literature published between 2015 and 2020 (221 papers).....	34
Table I. 5 Analysis of the impact of several sources of variability related with cell culture protocols (pre- and post-seeding in the Transwell™ inserts) on the P_{app} values across Caco-2 monolayers.....	35
Table I. 6 Analysis of the impact of different protocols for the permeability assays on the P_{app} values of reference compounds across Caco-2 monolayers.....	45
Table III. 1 Molecular structure and some molecular descriptors calculated using the MarvinSketch software for the compounds used in this work.....	73
Table III. 2 Preparation of the donor solutions of test compounds evaluated in permeability assays.....	75
Table VI. 1 Paracellular tightness of the distinct cell monolayers assessed by TEER measurements and permeability of model compounds that use the paracellular route.	188
Table VI. 2 Permeability of model compounds that use the transcellular route measured across the distinct cell monolayers.	189
Table VI. 3 Permeability of Rho across the distinct cell monolayers. The results are presented as the values of P_{app} obtained in both the transport directions and the values for the components of passive and active efflux processes. The analysis was also performed after the inhibition of P-gp efflux with Verapamil.	190
Table VII. 1 Solubility in aqueous medium and parameters for the ionization and equilibrium interaction of the amphiphiles NBD-Cn with BSA and POPC bilayers at pH=7.4.	204
Table VII. 2 Permeability of LY when applied in the donor compartment of Caco-2 monolayers alone in solution and in simultaneous with references compounds that use passive (SA) and active efflux (Rho) pathways for permeation.....	209
Table VII.3 Permeability of LY across Caco-2 monolayers determined when it is applied alone and in mixture with complex solutions of compounds. The evaluation include increasing concentrations of DHE in DHE/GCA solution, alone and in the presence of	

several types of coffee extracts. The effect on LY P_{app} values of a natural extracts of shellfish toxins and a toxin is also shown..... 211

Table VII. 4 Summary of the effect of adding 100 μ M BSA to the transport media on the permeability of a homologous NBD-Cn series across cell monolayers derived from Caco-2, MDCK-II and MDCK-MDR1 cell lines. The rank order of their permeabilities is shown when considering the P_{app} values measured in the assays and the recalculate P_{app}^{Unb} values that account for the unbound fraction. 221

Index of tables in Supplementary Material

Table IV. S1 Characteristic TEER values and confidence intervals for the different cell monolayers before and after LY permeability assays of 60 min..... 111

Table IV. S2 Characteristic TEER values and confidence intervals for the different cell monolayers before and after LY permeability assays with a single or multi-time sampling. 113

Table IV. S3 Characteristic LY P_{app} values and confidence intervals at 95 % confidence (CI_{95}) obtained directly from the results and from the best fit of a Normal distribution to the frequency distribution of the P_{app} or $\text{Log}(P_{app})$ values..... 115

Table IV. S4 Statistical analysis of LY Permeability (P_{app}) and amount of LY transported into the acceptor compartment (Q_A (%)) for all the conditions tested. 115

Table IV. S5 Inter-variability between cell batches and passages regarding TEER values before the permeability assay and amount of LY transported during the first sampling interval. 120

Table IV. S6 Multivariate analysis (MVA) to evaluate the correlation between the variables TEER or the amount of LY transported into the acceptor compartment (Q_A) with the distinct experimental variables..... 122

Table IV. S7 Cell density and fractional area occupied by nuclei and by tight junctions for images obtained by confocal microscopy ($428 \times 428 \mu\text{m}^2$) of cell monolayers in different conditions. 130

Table IV. S8 Multivariate analysis of the cell monolayers whose morphological characteristics have been characterized by confocal microscopy..... 131

Table V. S1 Statistical analysis of LY, Flu and atenolol P_{app} and amount transported into the acceptor compartment Q_A after single time and multi-time sampling permeability assays through single use (day 22) and re-use (day 25 and 28) Caco-2 monolayers.... 154

Table V. S2 Statistical analysis of P_{app} values of Propranolol and Salicylic Acid after single time and multi-time sampling permeability assays through single use and re-used Caco-2 monolayers from day 22 to 28. 157

Table V. S3 Statistical analysis of P_{app} values of 2-NBDG in A→B and B→A directions and the resulting influx ratio.	159
Table V. S4 Statistical analysis of the P_{app} values of Rho in A→B and B→A directions, efflux ratio and the contribution of passive permeation (P_{app}^{PP}) and active efflux (P_{app}^{AE}) to the measured Rho P_{app} values.....	163
Table VI. S1 Statistical analysis of LY, Flu and atenolol P_{app} values and amount transported into the acceptor compartment Q_A after single time and multi-time sampling permeability assays through MDCK-II and MDCK-MDR1 monolayers..	196
Table VI. S2 Statistical analysis of P_{app} values of Propranolol and Salicylic Acid after multi-time sampling permeability assays through MDCK-II and MDCK-MDR1 monolayers.....	196
Table VII. S1 Statistical analysis of LY and Prop P_{app} values obtained when using the replacement method for sampling in multi-time permeability assays across Caco-2 monolayers.....	224
Table VII. S2 Statistical analysis of P_{app} values of NBD-C4, NBD-C6 and NBD-C8 after multi-time sampling permeability assays through single use and re-used Caco-2 monolayers from day 22 to 28. Their permeability across monolayers derived from MDCK-II and MDR1 cell lines were also evaluated.....	226

